Rôle des récepteurs nicotiniques des circuits de l'addiction à la nicotine : une manipulation originale des récepteurs grâce à la lumière

Sarah Mondoloni

Thèse de doctorat de Sorbonne Université

Spécialité Neurosciences
École doctorale Cerveau – Cognition – Comportement

Présentée par
Sarah Mondoloni

Pour obtenir le grade de
Docteur de Sorbonne Université

Sujet de thèse :

Rôle des récepteurs nicotiniques des circuits de l'addiction à la nicotine : une manipulation originale des récepteurs grâce à la lumière

Soutenue le 20 Novembre 2020

Devant le jury composé de :

Dr. Stéphanie Caillé-Garnier	Rapporteure
Dr. Manuel Mameli	Rapporteur
Dr. Véronique Deroche-Gamonet	Examinatrice
Dr. Guillaume Dugué	Examinateur
Dr. Jean-Antoine Girault	Président
Dr. Alexandre Mourot	Directeur de thèse
Dr. Philippe Faure	Invité

Sorbonne Université
Bureau d'accueil des doctorants
Institut de formation doctorale
Escalier G, 2ème étage
15 rue de l'école de médecine
75270 - PARIS CEDEX 06

Secrétariat : 01 42 34 68 35
Fax : 01 42 34 68 40
pour les étudiants de A à EL : 01 42 34 68 41
pour les étudiants de EM à MON : 01 42 34 68 41
pour les étudiants de MOO à Z : 01 42 34 68 51
e-mail : scolarite.doctorat@sorbonne-universite.fr

Table des matières

Résumé

L'accroissement mondial des maladies liées au tabac reste un problème majeur de santé publique. La nicotine, principale substance active du tabac, agit exclusivement sur les récepteurs nicotiniques de l'acétylcholine (nAChR). Dans le système nerveux central, il existe douze sous-unités nicotiniques (α2-10 et β2-4) qui s'assemblent en pentamères selon diverses combinaisons, ce qui génère une grande diversité de récepteurs ayant des propriétés pharmacologiques, des localisations et des fonctions différentes. Outre son rôle indéniable et très bien décrit dans le renforcement, la nicotine peut également déclencher une aversion chez les individus. Ces effets opposés pourraient reposer sur l'activation de nAChR au sein de circuits neuronaux distincts, et sont prédicteurs, lors de la première expérience d'inhalation de tabac, des risques de développer une addiction à la nicotine. Comprendre le rôle des différents isoformes de nAChR et des circuits dans lesquels ils sont exprimés a été un défi majeur dans ce domaine, et un des questionnements de ce travail.

Lors de la première partie de ma thèse, nous avons mis au point des nAChR contrôlables par la lumière (LinAChR) qui fonctionnent normalement dans l'obscurité ou sous une lumière verte (500 nm) et sont rapidement inhibés sous une lumière violette (380 nm). Nous avons implémenté cette technologie *in vivo*, dans l'aire tegmentale ventrale, un noyau dopaminergique qui joue un rôle clé dans le renforcement et la dépendance. Le blocage des LinAChR β2 par la lumière a révélé l'impact du tonus cholinergique endogène sur l'activité spontanée des neurones dopaminergiques, et a permis d'abolir le renforcement à la nicotine chez les souris.

Lors de la seconde partie de ma thèse, je me suis intéressée aux mécanismes moléculaires et cellulaires qui sont impliqués dans la régulation de la consommation de nicotine. Pour cela, j'ai mis en place une tâche qui repose sur la consommation volontaire de nicotine, et développé une méthode d'analyse qui rend compte de la variabilité comportementale des souris. J'ai ainsi observé qu'une partie des souris développe une aversion spontanée et dose-dépendante à la nicotine. J'ai pu montrer qu'un traitement chronique à la nicotine diminue l'expression fonctionnelle des nAChR β4 dans le noyau interpédonculaire, et que cette régulation à la baisse impacte à la fois l'aversion à la nicotine et sa consommation.

Les travaux que j'ai menés suggèrent que la récompense et l'aversion à la nicotine impliquent à la fois des récepteurs et des circuits neuronaux distincts. Mes travaux mettent aussi l'accent sur le développement de nouvelles technologies optiques pour comprendre comment la dynamique d'activation des récepteurs conduit à des modifications d'activité dans des circuits spécifiques, et à des comportements liés à la dépendance.

Abstract

The global increase in tobacco-related diseases remains a major public health problem. Nicotine, the main active substance in tobacco, acts exclusively on nicotinic acetylcholine receptors (nAChRs). Twelve nAChR subunits (α2-10 and β2-4) are expressed in the central nervous system, and assemble into pentamers of various combinations, generating a wide variety of receptors with different pharmacological properties, locations and functions. In addition to its undeniable and well-described role in reinforcement, nicotine can also trigger aversion in individuals. These opposing effects may rely on the activation of nAChRs expressed within distinct neural circuits, and are predictive of the risk to develop habitual tobacco use in first time smokers. Understanding the role of the different nAChR isoforms and the circuits in which they are expressed has been a major challenge in the field, and one main aim of this work.

In the first part of my thesis, we developed light-controllable nAChRs (LinAChRs) that function normally in darkness or under green light (500 nm) and are rapidly inhibited under violet light (380 nm). We implemented this technology in vivo, in the ventral tegmental area, a dopaminergic nucleus that plays a key role in reinforcement and addiction. Blocking β2-containing nAChRs revealed that the endogenous acetylcholine tone sets the activity of dopaminergic neurons, and abolished nicotine reinforcement in mice.

In the second part of my thesis, I was interested in the molecular and cellular mechanisms involved in the regulation of nicotine consumption. To this aim, I set up a task based on voluntary nicotine consumption and developed an analytical method that accounts for the behavioral variability of mice. I observed that a significant fraction of the mice developed spontaneous and dose-dependent aversion to nicotine. I could show that chronic nicotine treatment decreases the functional expression of β4 nAChRs in the interpeduncular nucleus, and that such downregulation, in turn, impacts both nicotine aversion and nicotine consumption.

My work suggests that nicotine reward and aversion involve distinct receptors and circuits. My work also focuses on the development of new optical technologies to understand how the dynamics of receptor activation lead to changes in neuronal activity in specific circuits, and to addictive behaviors.

Listes des publications

Ce travail a été effectué à Sorbonne Université (Campus Pierre et Marie Curie), au sein du laboratoire Neuroscience Paris-Seine (UMR 8246) dirigé par le Dr. Hervé Chneiweiss, dans l'équipe Neurophysiologie et Comportements (Dr. Philippe Faure et Dr. Alexandre Mourot). Ce travail devrait donner lieu à huit publications, dont trois en premier ou co-premier auteur :

- **Mondoloni, S.**, Nguyen, C., Durand-de Cuttoli, R., Torquet, N., Jehl, J., Tolu, S., Pons, S., Maskos, U., Marti, F., Faure, P.**, and Mourot, A**. The sensitivity of the interpeduncular nucleus determines the threshold dose of nicotine that triggers persistent aversion. *En préparation*

- Dongelmans, M.*, Durand-de Cuttoli, R.*, Nguyen, C., Come, M., Ahmed Yahia, T., Lemoine, D., Duranté, E.K., Britto, R., **Mondoloni, S.,** Didienne, S., Bousseyrol, E., Hanesse, B., Torquet, N., Dalkara D., Naudé, J., Marti, F., Mourot, A., Faure, P. Chronic nicotine alters decision-making strategies in mice by increasing midbrain dopamine neuron activity. *En préparation*

- Lemoine, D., **Mondoloni, S.,** Tange, J., Lambolez, B., Faure, P., Taly, A.**, Tricoire, L.**, and Mourot, A**. Probing the ionotropic activity of the orphan glutamate delta 2 receptor with genetically-engineered photopharmacology. *bioRxiv (2020).*

- Nguyen, C., **Mondoloni, S.,** Centeno, I., Durand-de Cuttoli, R., Tolu, S., Valverde, S., Le Borgne, T., Hannesse, B., Pons, S., Maskos, U., Dalkara, D., Hardelin, JP., Mourot, A., Marti, F.**, Faure, P**. Distinct dopamine circuits transmit the reinforcing and anxiogenic effects of nicotine. *bioRxiv (2020).*

- **Mondoloni, S.***, Durand-de Cuttoli, R.*, and Mourot, A*. Cell-Specific Neuropharmacology. *Trends in Pharmacological Sciences (2019).*

- Durand-de Cuttoli, R.*, **Mondoloni, S.***, Marti, F., Lemoine, D., Nguyen, C., Naudé, J., d'Izarny-Gargas, T., Pons, S., Maskos, U., Trauner, D., Kramer, RH., Faure, P.**, and Mourot, A**. Manipulating midbrain dopamine neurons and reward-related behaviors with light-controllable nicotinic acetylcholine receptors. *eLife (2018).* * co-premier auteur.

- Forget, B., Scholze, P., Langa, F., Morel, C., Pons, S., **Mondoloni, S.,** Besson, M., Durand-de Cuttoli, R., Hay, A., Tricoire, L., Lambolez, B., Mourot, A., Faure, P., Maskos., U. A Human Polymorphism in CHRNA5 Is Linked to Relapse to Nicotine Seeking in Transgenic Rats. *Current Biology (2018).*

- Durand-de Cuttoli, R., **Mondoloni, S.,** and Mourot, A. Dissection optique du rôle des récepteurs nicotiniques neuronaux à l'aide de récepteurs photo-contrôlables. *Biologie Aujourd'hui (2017).*

Listes des abréviations

AAV	Virus adéno-associé
ACh	Acétylcholine
AChBP	Acetylcholine binding protein
AChE	Acétylcholinestérase
BAC	Bed nucleus of the anterior commissure
BLA	Amygdale basolatérale
CeA	Amygdale centrale
CGPn	Central gray of the pons
Ch	Choline
ChT	Transporteur de la choline
ChAT	Choline-Acétyltransférase
CLi	Noyau linéaire caudal
CNS	Système nerveux central
CPP	Préférence de Place Conditionée
Cre	Cre-recombinase
DA	Dopamine
DAT	Transporteur de la dopamine
DOPA	Dihydroxyphénylalalanine
DTg	Tegmentum dorsal
eGFP	enhanced Green Fluorescent Protein
EPSC	Courants post-synaptiques excitateurs
ERK	Extracellular signal-regulated kinases
FR	Fasciculus retroflexus
GABA	Acide γ-amino-butyrique
GABAAR	Récepteur GABA de type A
GAD	Glutamate décarboxylase
GLP-1	Glucagon-like peptide-1
GluN	Récepteur glutamate type NMDA
GlyR	Récepteur de la glycine
HCN	Hyperpolarisation-activated Cyclic-Nucleotid modulated Cation Non-selective Channel
IF	Noyau interfasciculaire
IPA	IPN apical
IPC	IPN caudal
IPDL	IPN dorsolatéral
IPDM	IPN dorsomédial
IPI	IPN intermédiaire
IPL	IPN latéral
IPN	Noyau interpédonculaire
IPR	IPN rostral
Kv	Canal potassique voltage-dépendant
LDTg	Tegmentum latérodorsal
LGIC	Ligand-gated ion channel
LHb	Habénula latérale
LinAChR	Récepteur nicotinique photo-contrôlable
LTP	Potentialisation à long terme
MAHoCh	Maléimide Azobenzène Homocholine
MEC	Mécamylamine

MFB	Faisceau médian du télencéphale
MHb	Habénula médiale
MHbD	MHb dorsale
MHbVc	MHb ventrocentrale
MHbVl	MHb ventrolatérale
MHbVm	MHb ventromédiale
MLA	Méthyllycaconitine
MS	Septum médian
NAcc	Noyau accumbens (striatum ventral)
nAChR	Récepteur nicotinique de l'acétylcholine
NTS	Nucleus tractus solitarus
PA	Potentiel d'action
PBP	Noyau parabrachial pigmentosus
PFC	Cortex préfrontal
PN	Noyau latéral paranigral
PPTg	Noyau pédonculopontin
RLi	Noyau linéaire rostral
RMTg	Rostromedial tegmental nucleus (tail of the VTA)
RPE	Erreur de prédiction de la récompense
SC	Stimulus conditionné
SFi	septofimbrial nucleus
shRNA	Short hairpin RNA
SI	Stimulus inconditionné
SK	small conductance calcium-activated potassium channels
SN	Stimulus neutre
SNP	Single nucleotide polymorphism
SPN	Spiny projecting neurons
SST	Somatostatin
TH	Tyrosine-3-Hydroxylase
TS	Triangular septum
VAChT	Transporteur vésiculaire de l'ACh
VGCC	Canaux calciques voltage-dépendants
VGLUT	Transporteur vésiculaire du glutamate
VMAT	Transporteur vésiculaire des monoamines
VTA	Aire tegmentale ventrale
WT	Wild-type
5HT	Sérotonine (5-hydroxy tryptamine)

Introduction générale

A long terme, le tabagisme induit des effets nocifs sur le système cardiovasculaire et pulmonaire en augmentant le risque de développer des cancers. Malgré les politiques de préventions et l'augmentation du coût à l'achat, la consommation de tabac constitue, encore aujourd'hui, la première cause de mortalité évitable en France.

Depuis l'introduction du tabac en Europe au 16ème siècle, son mode de consommation a fluctué, au fil du temps et des modes, entre fumer, mâcher ou « sniffer ». Aujourd'hui, la consommation de tabac est majoritairement orale *via* les cigarettes à rouler ou industrielles. Parmi les 4000 composés chimiques retrouvés dans une cigarette, au moins 50 sont cancérigènes (Comité National Contre le Tabagisme), tandis qu'une partie pourrait présenter des propriétés addictives. Cependant, c'est bien la nicotine, un alcaloïde toxique, qui contribue majoritairement aux propriétés « addictives » du tabac. Malgré la quasi absence d'effets psychotropes (euphorie, hallucination, ivresse), la nicotine est l'une des substances les plus addictives (Nutt et al., 2007, Observatoire français des drogues et des toxicomanies). Ces propriétés addictives sont clairement mises en évidence dès lors qu'on s'intéresse à l'initiation, à la prévalence des consommateurs et aux échecs auxquels ils font face pour arrêter de fumer. En effet, près d'un tiers des personnes qui ont essayé de fumer deviennent des consommateurs réguliers ; près d'un milliard de personnes dans le monde fument quotidiennement (OMS) et seuls 7% des fumeurs qui veulent arrêter arrivent à se sevrer complétement de la nicotine (Centers for Disease Control and Prevention (US) et al., 2010).

Les définitions liées à la consommation de drogue d'abus ont évolué et se sont affinées. Aujourd'hui le terme « troubles liés à une substance » est préféré aux termes « addiction » ou « dépendance », qui sont par ailleurs souvent confondus (*Manuel diagnostique et statistique des troubles mentaux*, DSM-V 2013). Le terme dépendance est également utilisé lorsque la prise médicamenteuse induit des réponses normales de tolérance et de sevrage. Au contraire du DSM-IV qui avait une approche plutôt catégorielle, le DSM-V propose une approche qui permet d'évaluer la gravité de l'addiction en fonction du nombre de symptômes présents chez les individus, et ainsi de mieux saisir la complexité de cette pathologie (Traité d'addictologie, Reynaud, 2016).

Dans le contexte des drogues, la prise répétée, persistante voire compulsive de substance addictive pourrait être le résultat d'un équilibre dynamique entre des effets positifs et des effets émotionnels négatifs (Koob and Le Moal, 1997), et/ou de la mise en place d'habitude pathologique (Everitt, 2014). Ces concepts sous-tendent que l'initiation de l'addiction et la compulsion découleraient de la mise en place d'un renforcement positif à la drogue d'abus et des apprentissages aberrants, tandis que l'évitement des états émotionnels négatifs produit par le retrait de la nicotine et le manque favoriserait la poursuite de la consommation et la rechute après l'arrêt du tabac. Le schéma classique de l'addiction à la nicotine prend en compte ces mécanismes à la fois positifs et négatifs qui contribuent à la mise en place de la pathologie et aux échecs de tentatives de sevrage (Dani and De Biasi, 2013; Gutkin et al., 2006; Hall et al., 2015; Kenny and Markou, 2001).

Les effets de la nicotine passent par son action sur les récepteurs nicotiniques de l'acétylcholine (nAChR). Dans le système nerveux central, il existe douze sous-unités nicotiniques différentes (α2-10 et β2-4) qui s'assemblent en pentamères selon diverses combinaisons, ce qui produit une grande diversité de nAChR qui se distinguent par leurs propriétés pharmacologiques, leurs localisations et leurs fonctions (Changeux, 2010a, Chapitre I). De par son action sur ces récepteurs, la nicotine produit des effets récompensant (De Biasi and Dani, 2011; Faure et al., 2014) mais aussi aversifs, très bien observés aux fortes doses (Fowler and Kenny, 2014; Picciotto, 2003).

Deux systèmes neuronaux, riches en nAChR, ont été en particulier impliqués dans les différentes étapes de l'addiction à la nicotine (Chapitre II) et dans la genèse des effets renforçants ou aversifs. Le premier est la voie mésocorticolimbique qui est constituée des neurones dopaminergiques de l'aire tegmentale ventrale, qui projettent vers les cortex et le système limbique. L'action de la nicotine sur l'aire tegmentale ventrale induit une augmentation de l'activité des neurones dopaminergiques et conduit au renforcement à la nicotine (Chapitre III). Le second système est la voie habénulo-interpédonculaire, qui est un circuit qui fait le pont entre les structures du cerveau antérieur et les noyaux monoaminergiques et cholinergiques. Cette voie est impliquée dans la régulation des réponses à un stimulus aversif. La voie habénulo-interpédonculaire a gagné en notoriété lorsqu'elle a été impliquée dans la transmission des effets négatifs de la nicotine. En effet, l'activation de cette voie par la nicotine est à l'origine de la transmission des effets aversifs de la nicotine, tandis que la suractivité de celle-ci lors d'un sevrage conduit à l'émergence de symptômes de manque (Chapitre IV).

L'objectif au cours de ma thèse a été de comprendre comment les processus de renforcement et d'aversion interagissent ou s'opposent pour aboutir à l'initiation et au maintien de l'addiction à la nicotine. Notamment, j'ai cherché à comprendre quels sont les dynamiques d'activation et de désensibilisation des récepteurs nicotiniques au sein de circuit spécifiques qui favorisent la signalisation des effets positifs ou négatifs de la nicotine. Pour étudier l'impact de la nicotine sur des nAChR spécifiques et dans des voies neuronales données, nous avons mis en place une technique innovante, appelée pharmacologie optogénétique. Cette nanotechnologie permet de contrôler optiquement, et donc de manière réversible et ciblée, l'activité de nAChR avec une spécificité pharmacologique absolue. Dans un premier temps, je me suis focalisée sur l'étude du rôle des récepteurs nicotiniques de type β2 de l'aire tegmentale ventrale dans le renforcement à la nicotine. Ensuite, j'ai travaillé sur le noyau interpédonculaire et le récepteur de type β4 afin de mieux comprendre le rôle de ce noyau dans la régulation de la consommation de nicotine.

Dans ce manuscrit je présenterai tout d'abord le système nicotinique et ses récepteurs ainsi que l'action de la nicotine sur ce système. Cette description précèdera une description plus approfondie des systèmes dopaminergique et habénulo-interpédonculaire, ainsi que de leur rôle dans l'addiction à la nicotine. Enfin, avant de décrire les résultats j'introduirai les techniques de pharmacologie optogénétique (Chapitre V).

Introduction

1. Chapitre 1 : La transmission nicotinique dans le système nerveux central

1.1. L'acétylcholine

L'acétylcholine (ACh) est un neurotransmetteur important des systèmes nerveux périphérique, notamment végétatif, ainsi que dans le système nerveux central (SNC). L'ACh est l'acteur moléculaire qui a permis, grâce aux expériences de Otto Loewi sur le nerf vague, de démontrer que la communication électrique entre les neurones peut passer par un signal chimique (Loewi, 1922). Ce neurotransmetteur endogène est synthétisé par la choline acétyltransférase des neurones cholinergiques (**Box 1.1**). Dans le SNC, l'ACh agit sur deux grandes familles de récepteurs, les récepteurs muscariniques et nicotiniques, qui tirent leurs noms de leurs agonistes spécifiques la nicotine et la muscarine (Dale, 1914). Les récepteurs muscariniques sont des récepteurs métabotropes à sept domaines transmembranaires. Il existe cinq types de récepteurs muscariniques (M1 à M5) qui vont transmettre une signalisation intracellulaire de type excitatrice ou inhibitrice en fonction de la voie de signalisation associée (Kruse et al., 2014; Picciotto, 2003; Scarr, 2012). Dans cette thèse nous n'aborderons pas la fonction des récepteurs muscariniques.

Box 1.1 | Métabolisme de l'ACh

La choline acétyltransférase (ChAT) est une enzyme située dans le cytosol des neurones cholinergiques qui permet le transfert du groupement acétyl, de l'acétyl-coenzyme A, sur la choline. L'ACh est ensuite transportée et stockée dans les vésicules synaptiques par le transporteur vésiculaire de l'ACh (VAChT). Lorsque l'ACh est libérée dans le milieu extracellulaire, elle est rapidement dégradée par l'acétylcholinestérase (AChE) en choline qui est ensuite recapturée au niveau des terminaisons des neurones pré-synaptiques par le transporteur de la choline (ChT).

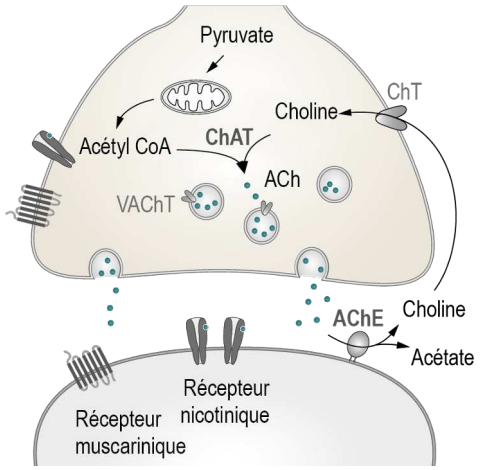

Bien que les preuves soient incontestables en ce qui concerne l'existence d'une transmission synaptique cholinergique neuromusculaire, l'existence de ce mode de la transmission dans le cerveau a été un sujet très controversé. Malgré quelques travaux princeps qui suggèrent l'existence d'une transmission synaptique rapide dans le cerveau (Hay et al., 2016; Zhang et al., 2016), les démonstrations de la littérature vont plutôt dans le sens d'une transmission cholinergique de type volumique (Dani and Bertrand, 2007; Sarter et al., 2009). En effet, il a été montré que les connexions cholinergiques sont diffuses dans le cerveau, et les sites de relargage de l'acétylcholine sont topographiquement éloignés des récepteurs nicotiniques post-synaptiques (Kawaja et al., 1990; Picciotto et al., 2012). L'ACh dans le cerveau jouerait donc plutôt le rôle d'un neuromodulateur, et a été associée à des fonctions cérébrales telles que le niveau d'éveil, le sommeil, l'attention, l'intégration sensorielle ou l'agression (Lewis and Picciotto, 2020; Picciotto et al., 2012).

1.2. Les récepteurs nicotiniques de l'acétylcholine

Les récepteurs nicotiniques (nAChR) sont des récepteurs ionotropes (LGIC, *ligand-gated ion channel*), à savoir des protéines membranaires dont l'activation par un ligand permet le passage d'ions à travers la membrane plasmique (**Fig1.1a**). Il existe trois superfamilles de récepteurs ionotropes : Les récepteurs à « boucle cystéine » (*cys-loop*) pentamériques, les récepteurs du glutamate tétramériques, et les récepteurs trimériques (Lemoine et al., 2012). Les récepteurs ionotropes participent à la communication entre cellules distinctes en transformant une information moléculaire chimique (neurotransmetteur ou messager chimique), en une information électrique générée par le passage passif d'ions à travers la membrane (Hille, 2001; Karpen and Ruiz, 2002). La superfamille des récepteurs pentamériques *cys-loop* comprend les nAChR, les récepteurs de la sérotonine ($5HT_3R$), de l'acide ɣ-aminobutyrique ($GABA_AR$) et de la glycine (GlyR) (Figure 1a). Ces récepteurs sont composés de cinq sous-unités, et présentent une perméabilité soit cationique (nAChR, $5HT_3R$) soit anionique ($GABA_AR$, GlyR). Les sous-unités des récepteurs *cys-loop* ont toutes une architecture moléculaire semblable (Lynagh and Pless, 2014; Sparling and DiMauro, 2017; Thompson et al., 2010, **Fig1.1b**) caractérisée par:

- Un large domaine extracellulaire (N-terminal) qui comprend le site agoniste, ainsi qu'une boucle caractéristique d'approximativement 13 résidus et bordée par deux cystéines formant un pont disulfure. Cette boucle a donné son nom à la superfamille des « cys-loop ».
- Quatre domaines transmembranaires (M1-M4), qui forment le canal ionique.
- Un domaine intracellulaire entre les domaines transmembranaires M3 et M4.

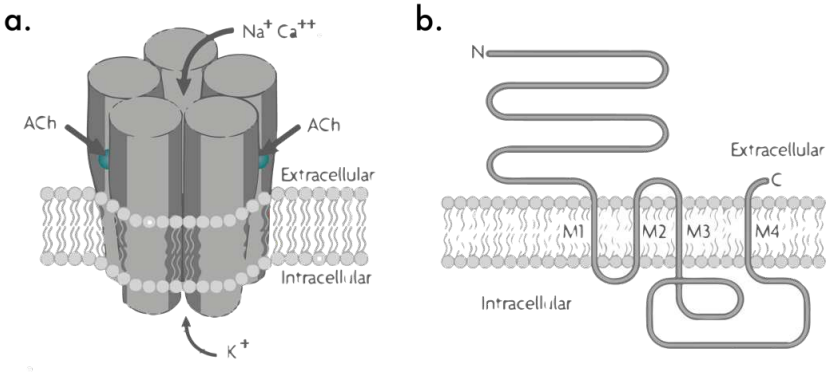

Figure 1.1 | Représentation schématique du récepteur nicotinique : a. Le récepteur nicotinique est une protéine membranaire perméable aux cations et constituée de cinq sous-unités. **b.** Chaque sous-unité comprend une large partie extracellulaire, 4 domaines transmembranaires et un domaine cytosolique. *Figure adaptée de Changeux, 2010.*

Les nAChR sont les récepteurs qui ont été les plus étudiés d'un point de vue structural, biophysique et pharmacologique (Taly et al., 2009). Il existe deux types de récepteurs nicotiniques : les récepteurs nicotiniques musculaires qui participent à la transmission électrique à l'origine de la contraction musculaire, et les récepteurs nicotiniques neuronaux. On dénombre cinq sous-unités musculaires α1, β1, ɣ, δ et ε et douze sous-unités neuronales, avec neuf sous-unités α (α2-α10) et trois sous-unités β (β2-β4). Par la suite, nous discuterons seulement de la fonction des nAChR neuronaux.

Le dysfonctionnement de la neurotransmission nicotinique est impliqué dans des maladies psychiatriques (addiction, schizophrénie, trouble du déficit de l'attention...) et neurodégénératives (maladie d'Alzheimer, maladie de Parkinson...Taly et al., 2009). De nombreuses recherches se sont efforcées d'identifier ou de développer des traitements pharmacologiques qui ciblent les substrats moléculaires de la transmission nicotiniques. La description de la structure quaternaire des récepteurs a permis de compléter les connaissances sur l'état des récepteurs et ainsi de mieux comprendre comment un agent pharmacologique peut moduler son fonctionnement.

1.3. Structure du récepteur nicotinique

Les protéines membranaires sont particulièrement difficiles à étudier d'un point de vue structural, à cause de leur caractère amphiphile, à la fois hydrophile et hydrophobe. Les premiers modèles structuraux du nAChR se sont surtout basés sur l'*acetylcholine binding protein* (AChBP, Brejc et al., 2001; Smit et al., 2003), une protéine soluble homologue au domaine N-terminal du nAChR présente chez la grande limnée (*Lymnaea stagnalis*), ainsi que sur le nAChR type musculaire retrouvé à la jonction neuromusculaire chez la torpille marbrée (*Torpedo mamorta*) (Miyazawa et al., 2003; Unwin, 2005). Ces modèles ont plus récemment été complétés par la résolution de la structure atomique du nAChR α4β2, qui est le sous-type majoritairement exprimé au niveau du SNC (Morales-Perez, 2016).

Les sous-unités α et β présentent une architecture tridimensionnelle similaire (**Fig1.2a**). Les cinq sous-unités du récepteur s'arrangent de manière pseudo-symétrique autour d'un axe, ce qui permet la formation d'un canal ionique et de sites de liaison du ligand (**Fig1.2b**). La partie extracellulaire hydrophile N-terminale qui est constituée d'environ 210 acides aminés (Arias, 1997; Taly et al., 2009), forme le site de liaison orthostérique de l'ACh (**Box 1.2**). Le site de liaison du ligand est à l'interface entre deux sous-unités nicotiniques (**Fig1.2**) : la majorité du site est portée par une sous-unité dite principale (α), tandis que le reste est porté par une sous-unité dite complémentaire (α ou β). Certaines sous-unités (α5 et β3) sont quant à elles nommées accessoires car elles ne possèdent pas les caractéristiques nécessaires à la formation d'un site de liaison.

Box 1.2 | Site orthostérique vs. allostérique :

Un site orthostérique est le principal site actif de la protéine, où un ligand apparenté va agir pour modifier directement l'état de la protéine. Un site allostérique, est un site de liaison non compétitif où les modulateurs allostériques peuvent agir de manière non compétitive pour moduler positivement ou négativement l'état du récepteur. Un modulateur allostérique (positif ou négatif) a un effet actif sur une protéine uniquement lorsque celle-ci est activée au niveau du site orthostérique, et donc, par définition, ne peut pas agir seul sur l'état du récepteur.

La partie extracellulaire hydrophile N-terminale est constituée d'une hélice terminale et de dix brins β qui s'enroulent vers l'intérieur pour former un sandwich (Morales-Perez et al., 2016). Six boucles extracellulaires sont intercalées dans ces feuillets β et forment à elles seules le site orthostérique avec trois boucles (A, B et C) qui sont situées sur la sous-unité principale et trois autres boucles (D, E et F) sur la sous-unité complémentaire. Bien que leurs architectures soit similaires, les sous-unités α se distinguent par la présence de deux

cystéines (192 et 193 sur le récepteur de torpille) dites « vicinales » (Kotzyba-Hibert et al., 1997) situées dans le site agoniste sur la boucle C. Les acides aminés qui participent à la liaison de l'ACh sont principalement des résidus aromatiques (tryptophane, W et tyrosine, Y) et sont situés sur les boucles A, B, C et D (**Fig1.2c**). L'interaction ligand-récepteur repose sur une interaction électrostatique nommée cation-π, où l'ammonium de l'ACh (cation) interagit avec le système π riche en électrons des résidus aromatiques (Zhong et al., 1998).

Les résidus identifiés sur les boucles A, B et C sont très conservés et présents sur toutes les sous-unités α, à l'exception de la sous-unité α5, qui ne possède pas les résidus tyrosines aux positions homologues 93 et 190 (Arias, 1997). Par conséquent, cette sous-unité ne permet pas la formation de site orthostérique, et est donc insensible à l'ACh. Les cystéines vicinales sont absentes dans les sous-unités β, mais les sous-unités β2 et β4 contiennent un résidu tryptophane (boucle D) qui permet de former la partie complémentaire du site de liaison de l'agoniste. La sous-unité β3 quant à elle ne présente pas ce résidu tryptophane nécessaire à la formation du site ACh, et est donc, comme α5, une sous-unité accessoire. Par conséquent, à l'exception d'α5 le nombre de sites de liaison de l'ACh peut varier de deux à cinq en fonction du nombre de sous-unités α présentes dans le récepteur.

Chaque sous-unité nicotinique possède quatre domaines transmembranaires nommés M1, M2, M3 et M4, qui présentent une structure secondaire en hélice α à caractère hydrophobe (Miyazawa et al., 2003; Morales-Perez et al., 2016; Unwin, 1992, **Fig1.1b**). Des homologues radioactifs des bloqueurs non compétitifs du canal ont permis de cartographier, à l'aide de marquages par photo-affinité, les résidus impliqués dans la formation du canal ionique (Arias, 1997), localisés au niveau du domaine M2. Ces résidus définissent les propriétés de perméabilité ionique, de sélectivité ionique et de conductance du canal du récepteur. D'un point de vue structural, les hélices M2 qui bordent le canal ionique sont entourées par les domaines M1 et M3 qui forment le deuxième anneau. Les domaines M4 sont au niveau de la face externe du canal.

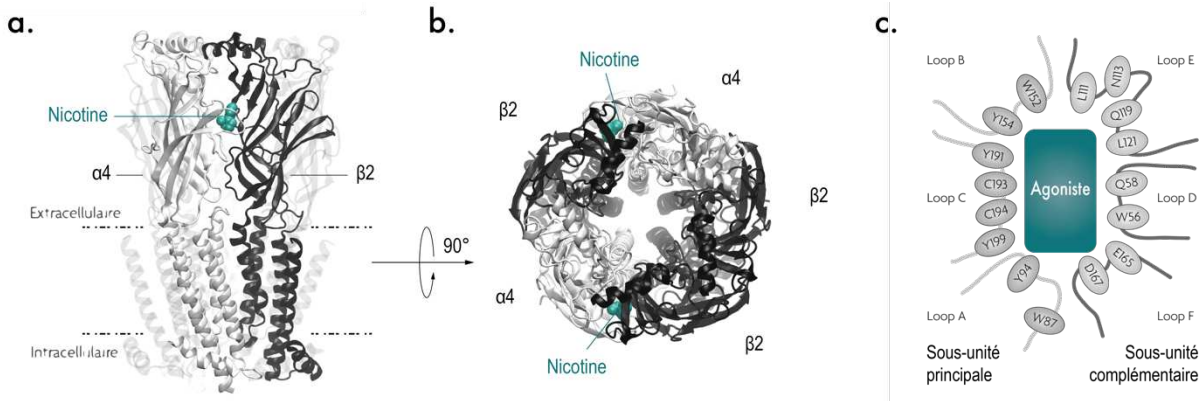

Figure 1.2 | Architecture du récepteur α4β2 et site de liaison du ligand : a. Structure du récepteur de profil (**a.**) ou de haut (**b.**) avec les sous-unités α4 en gris, β2 en noir et la nicotine en vert émeraude (images réalisées sur *Visual molecular dynamics* à partir du fichier PDB 5kxi). **c.** Schéma qui illustre les acides aminés des boucles A, B et C (sous-unité principale) et D, E, F (complémentaire) qui participent à la formation du site de liaison du ligand *Figure adaptée de Taly et al., 2009*.

Le domaine intracellulaire est un segment hydrophile formé entre les segments transmembranaires M3 et M4 dont la structure n'est pas décrite puisqu'il qu'il n'a jamais pu être cristallisé (Stokes et al., 2015, Fig1.1b). La partie cytosolique est de loin la moins décrite et le rôle fonctionnel de celle-ci reste encore à déterminer. La fonction du domaine cytosolique du récepteur nicotinique musculaire a été impliquée, de par son interaction avec la protéine d'échafaudage rapsyne, dans la formation et le maintien d'un *pool* post-synaptique de nAChR. Malheureusement, la séquence de la partie intracellulaire présente une faible homologie entre espèces mais aussi entre les différentes sous-unités d'une même espèce. Il est donc difficile de transposer la fonction du segment musculaire à celle des sous-unités neuronales. Il semble que le domaine intracellulaire cytosolique puisse jouer un rôle de filtre ionique, ajuster les propriétés de désensibilisation (Kuo et al., 2005; Liu et al., 2015), être impliqué dans l'organisation de la localisation subcellulaire/synaptique des récepteurs (Williams et al., 1998) et être la cible de modifications post-traductionnelles.

Des études génomiques chez l'homme ont mis en évidence un polymorphisme nucléotidique de la sous-unité α5 (SNP-α5 D398N). Ce polymorphisme a été associé à une vulnérabilité à la dépendance à la nicotine. Cette substitution est localisée au niveau de la boucle intracellulaire, et de manière intrigante, la perturbation fonctionnelle de ce variant n'a jamais été associée au rôle de ce domaine. Cette mutation ponctuelle semble altérer la fonction des récepteurs qui contiennent la sous-unité α5, en diminuant l'efficacité de certains agonistes et en perturbant les cinétiques de désensibilisation. La désensibilisation sera abordée dans le chapitre suivant. Il semble ainsi, que la boucle intracellulaire ajuste les propriétés fonctionnelles du nAChR (George et al., 2012; Tammimäki et al., 2012).

1.4. Allostérie des nAChR

En absence de ligand, le récepteur est dans un état de repos où le canal est fermé, non conducteur. Cet état forme une barrière physique qui empêche le passage des ions à travers la membrane. La liaison d'agoniste sur le récepteur précipite le passage d'un état de repos à un état activé qui correspond à l'ouverture du canal ionique. L'application prolongée d'un agoniste sur le récepteur fait apparaitre un troisième état non conducteur, l'état désensibilisé (Katz and Thesleff, 1957, Fig1.3a). Néanmoins, bien que ces trois états englobent les formes prédominantes du récepteur au niveau de la membrane, certains modèles allostériques suggèrent la présence d'un continuum entre ces trois états, laissant place à une large palette de conformations biophysiques du récepteur (Karpen and Ruiz, 2002).

Le concept d'allostérie a été défini dans les années soixante, lorsque l'activité des enzymes bactériennes a révélé des interactions ligand-protéine différentes des mécanismes classiques d'inhibition par compétition (Changeux, 2010b). L'allostérie correspond à l'interaction indirecte d'effecteurs sur différents sites de liaison topographiquement éloignés au sein d'un oligomère, dont résultent une modification structurale et réversible de la protéine. Le modèle a été établi en premier lieu sur les enzymes puis il a ensuite été transposé aux récepteurs membranaires, dont le nAChR. Les études sur le récepteur nicotinique ont permis de l'inclure dans la famille des protéines allostériques.

Le modèle allostérique de Monod–Wyman–Changeux repose sur les hypothèses suivantes (Changeux, 2010b):

- Les protéines allostériques sont organisées à partir d'un nombre fini de sous-unités identiques (protomères) disposées de manière équivalente. Par conséquent, la structure de la protéine possède au moins un axe de symétrie, et forme une machinerie coopérative.
- Les oligomères existent dans quelques conformations discrètes et interconvertibles. Il existe au moins deux conformations T (*tight*) et R (*relaxed*) qui sont à l'équilibre en absence de régulateur, et qui présentent des affinités différentes pour l'effecteur et le modulateur allostérique.
- Les ligands régulateurs ne font que déplacer l'équilibre entre les conformations, en stabilisant sélectivement celle pour laquelle ils présentent la plus grande affinité.
- Les transitions conformationnelles se font de manière concertée, du tout ou rien pour toutes les sous-unités et donc avec conservation de la symétrie.

Les récepteurs nicotiniques possèdent tous les critères d'une machinerie allostérique : la structure du récepteur nicotinique a mis en évidence la présence de cinq sous-unités identiques (ou homologues) arrangées autour d'un axe pseudo-symétrique perpendiculaire à la membrane plasmique. Les sites de liaison, de 2 à 5, sont éloignés d'au moins 40 Å, et se situent à l'interface des sous-unités (Morales-Perez et al., 2016; Unwin, 1992). De plus, les sites de liaison de l'ACh et le canal ionique sont topographiquement distincts (60 Å) : l'action de l'ACh sur son site de liaison fait intervenir une interaction allostérique, à distance, qui est à l'origine de l'ouverture indirecte du canal ionique. Finalement, la coopérativité positive (coefficient de Hill > 1) observée dans les courbes dose-réponse de liaison et d'activation du récepteur est une autre indication du caractère allostérique des nAChR.

Le développement des enregistrements électrophysiologiques de canal unique en patch-clamp a permis d'affiner les connaissances sur les probabilités d'ouverture du canal. Ces enregistrements ont révélé la présence de courants unitaires spontanés (Auerbach, 2012). Bien que surprenant, mais en adéquation avec le modèle Monod–Wyman–Changeux, les récepteurs nicotiniques, même sans agoniste, coexistent à l'équilibre sous deux états distincts : un état fermé, non conducteur et un état ouvert, conducteur. L'efficacité d'ouverture spontanée du canal demeure un évènement rare en absence d'agoniste (~10^{-5} à 10^{-6}, Jackson, 1986; Neubig et al., 1982).

Des études d'affinité de ligand sur le récepteur ont permis de mettre en évidence qu'un ligand orthostérique présente une affinité non-équivalente en fonction de l'état de récepteur. Les récepteurs nicotiniques dans l'état désensibilisé présentent une affinité pour les agonistes de l'ordre du nanomolaire, plus forte que dans l'état de repos qui est plutôt de l'ordre du micromolaire (Changeux, 2018; Weber et al., 1975). De plus, les antagonistes compétitifs stabilisent non pas l'état désensibilisé mais l'état de repos, fermé des récepteurs nicotiniques. Il apparait ainsi que la proportion de récepteurs dans un état donné peut dépendre du type de ligand (antagoniste ou agoniste) et de son affinité pour le récepteur, et

que le ligand va au final stabiliser l'état du récepteur pour lequel il a la plus forte affinité (Changeux, 2018).

Le récepteur nicotinique possède de multiples sites de modulation allostérique sensibles à différents composés, notamment dans les domaines extracellulaire (par exemple, Ca^{2+}) et transmembranaire (par exemple, ivermectine, anesthésique général). Ces sites sont distincts des sites orthostériques, et permettent ainsi de mettre en évidence la complexité de cette machine allostérique qu'est le récepteur nicotinique.

1.5. Les sous-types de récepteurs nicotiniques neuronaux

Dans le SNC, il existe 12 sous-unités nicotiniques avec neuf sous-unités α (α2-α10) et trois sous-unités β (β2-β4), dont les combinaisons en pentamère constituent une grande variété de sous-types de récepteurs nicotiniques. Il existe les récepteurs homopentamériques constitués de cinq sous-unités α identiques, et hétéropentamériques qui sont constitués à la fois de sous-unités α et β (**Fig1.3b**). Les hétéropentamères sont constitués de deux paires α-β qui forment deux sites de liaison primaires, et d'une sous-unité α ou β en cinquième position. Les sous-unités α3, α4, α5, β2, β3 et β4 sont susceptibles d'occuper la cinquième position, mais seules les sous-unités α3 et α4 permettent de former un troisième site de liaison à l'agoniste (Zoli et al., 2015). Ces différents sous-types des nAChR diffèrent dans leurs propriétés pharmacologiques, leur perméabilité calcique, et leur distribution neuronale (préterminale, pré- et post-synaptique, extrasynaptique ou somato-dendritique).

Les homopentamères α7 ont des cinétiques d'activation et de désensibilisation rapides et présentent la plus grande perméabilité pour le calcium. De plus, ils peuvent être activés par la choline qui est le produit de dégradation de l'ACh (Alkondon et al., 1997). Les hétéropentamères quant à eux présentent des cinétiques de désensibilisation plus faibles que les récepteurs α7, néanmoins leur sensibilité à l'ACh et à la nicotine est plus élevée. La sous-unité α, qui forme le site principal de liaison du ligand, détermine généralement la sensibilité à l'agoniste du récepteur. Par exemple, les récepteurs α4β2 et α4β4 présentent une affinité apparente à l'ACh comparable (EC_{50}~10 µM), tandis que les affinités des récepteurs α3β2 et α3β4 sont de 60 et 120 µM respectivement. La sous-unité β va ajuster les propriétés de désensibilisation des récepteurs : la sous-unité β4 présente une désensibilisation faible voire inexistante en fonction des conditions d'études (Fenster et al., 1997).

Bien que les propriétés de chaque sous-type de récepteur nicotinique soient uniques, la forte homologie de séquence entre sous-unités (i.e. α2 et α4) limite fortement la distinction pharmacologique des récepteurs nicotiniques. Les ligands sont généralement utilisés dans une fenêtre de concentrations sélectives qui permet d'atténuer l'action d'agents pharmacologiques sur un autre sous-type de récepteur. Les ligands des récepteurs hétéropentamériques présentent une pharmacologie modestement « sélective ». En revanche, puisque le récepteur α7 est le seul représentant des récepteurs homopentamériques dans le SNC adulte mammifère, l'utilisation d'une pharmacologie sélective (i.e. méthyllycaconitine, MLA) des récepteurs homopentamériques aura un impact négligeable sur les hétéropentamères.

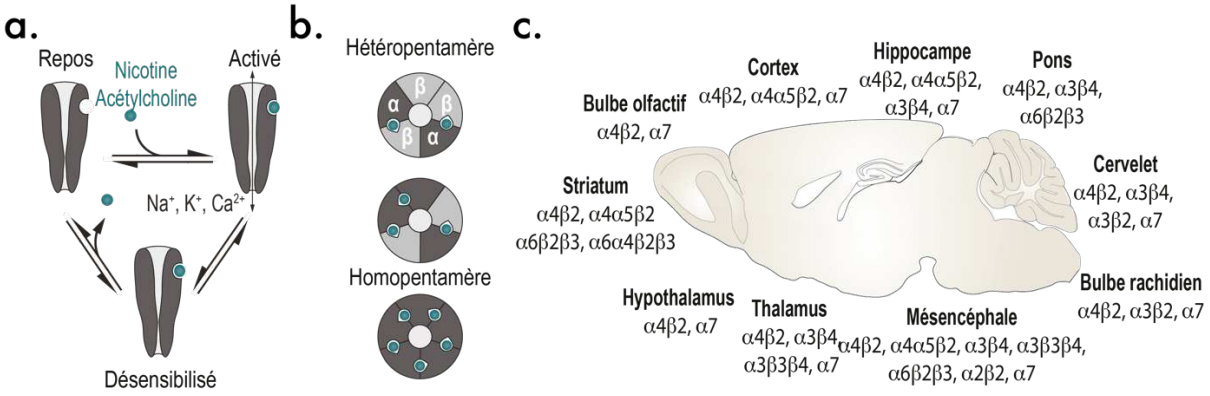

Figure 1.3 | Allostérie, diversité et localisation des nAChR neuronaux : a. Allostérie des nAChR **b.** Assemblages hétéropentamériques et homopentamériques des nAChR. **c.** Distribution des différents sous-types de nAChR dans le cerveau de la souris.

1.6. Localisation des nAChR du système nerveux central

La distribution de protéines dans le cerveau est souvent analysée par immunohistochimie grâce à l'utilisation d'anticorps qui détectent un antigène spécifique de la protéine. Puisqu'il n'existe toujours pas d'anticorps spécifique des sous-unités nicotiniques, la carte de leur distribution a été réalisée dans un premier temps par des stratégies de marquage radioactif couplées à l'utilisation de souris invalidées pour une sous-unité nicotinique et/ou l'utilisation de ligand froid, puis par l'utilisation de protéines fluorescentes rapportrices (Baddick and Marks, 2011; Zoli, 1998).

Ces marquages utilisent des ligands radioactifs basés soit sur des toxines soit sur des molécules pharmacologiques telles que la nicotine. Les toxines ont la particularité de présenter une affinité quasi-spécifique pour certaines populations de nAChR. Les toxines principalement utilisées sont : l'α-bungarotoxine, qui agit dans le SNC sur les récepteurs α7; l'épibatidine qui est sélective des récepteurs hétéropentamériques, et l'α-conotoxine MII qui agit au niveau des sites α3β2 et α6β2 (Zoli et al., 2015). La présence de marquage chez des souris invalidées pour une sous-unité nicotinique particulière permet, par déduction, de mettre en évidence la localisation des récepteurs nicotiniques (**Fig 1.3c**). L'utilisation de souris génétiquement modifiées pour exprimer une protéine rapportrice (i.e. GFP) a permis de compléter la cartographie des récepteurs. Ces souris sont basées soit sur l'expression de la GFP cytosolique sous le contrôle du promoteur d'une sous-unité nicotinique, sans altération fonctionnelle du récepteur (Hsu et al., 2013), soit sur des protéines de fusion entre nAChR et protéine rapportrice (Shih et al., 2015). Par exemple, la localisation dans le cerveau de la sous-unité accessoire α5, qui ne présente pas de site de liaison du ligand, a été mise en évidence grâce à une lignée de souris BAC α5_EGFP (*bacterial artificial chromosome*), chez lesquelles l'expression de la sous-unité α5 est cytosolique. Les modèles de fusions de la protéine d'intérêt sont utiles pour identifier les neurones qui l'expriment, mais peu compatibles avec l'étude fonctionnelle du récepteur car cela altère leur fonctionnalité (Shih et al., 2015).

Chez les souris de type sauvage, le marquage des récepteurs hétéropentamériques est largement distribué dans tout le cerveau, néanmoins, l'utilisation de cytisine (ligand froid, non radioactif) dont la sensibilité est majoritaire sur les récepteurs α4β2 – et pas α6β2 ou α3β4 – a permis de déduire la localisation des récepteurs α3β4. Cela a notamment pu être confirmé d'abord par l'utilisation de souris délétées, comme par exemple les souris $\beta4^{-/-}$ puis avec l'utilisation des souris α3-GFP et β4-GFP (Shih et al., 2015; Zoli, 1998; Zoli et al., 2015).

Ces études ont permis de mettre en évidence la co-expression de différentes sous-unités : l'expression de la sous-unité β2 coïncide avec l'expression des sous-unités α4, α6 et α5, tandis que pour la sous-unité β4 est co-exprimée avec les sous-unités α3, α4 et α5 (Zoli, 2011). Il existe donc des sous-types particuliers dans le cerveau, dont la majorité sont les récepteurs α4β2* et α3β4* (*, qui contiennent la sous-unité), qui peuvent être représentés soit dans la stœchiométrie la plus classique $(\alpha4)_3(\beta2)_2$ ou $(\alpha3)_3(\beta4)_2$, soit à combinaison plus exotique comme α6α4β2β3. A l'inverse des récepteurs β2* et α7 qui sont représentés dans tout le cerveau, les récepteurs β4* sont principalement exprimés au niveau de la voie habénulo-interpédonculaire (MHb-IPN), de la glande pinéale, du tractus solitaire, de *l'area postrema* et de la rétine (**Fig1.3c**)

2. Chapitre 2 : Action de la nicotine sur le cerveau et dépendance à la nicotine

2.1. Pharmacocinétique et consommation de nicotine chez l'humain

Lorsqu'elle est inhalée (Fig2.1a), la nicotine est rapidement acheminée vers le système sanguin. La concentration sanguine de nicotine atteint rapidement un pic (Benowitz et al., 1984, 2009; Foulds, 2003) qui coïncide avec la fin de la consommation de la cigarette (~5min), puis diminue lentement, la demi-vie de la nicotine dans l'organisme étant d'environ deux heures (Benowitz et al., 2009). Des prises répétées de nicotine au cours de la journée vont augmenter ponctuellement, au rythme des cigarettes consommées, la concentration sanguine de nicotine (Benowitz et al., 1984; Foulds, 2003; Henningfield, 1993, Fig2.1b). On considère néanmoins que la quantité moyenne de nicotine dans le sang au cours de la journée atteint un plateau (Benowitz et al., 1984, Fig2.1c), qui est dépendent de la concentration de nicotine dans la cigarette et reflète une capacité de titration des individus. Chez les fumeurs la concentration moyenne de nicotine dans le sang va dépendre du niveau de consommation de tabac et du métabolisme de la personne.

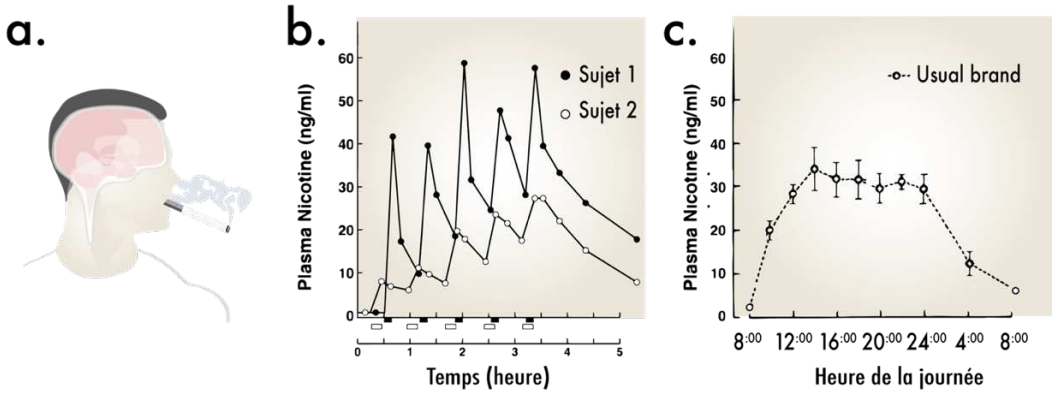

Figure 2.1 | La consommation de tabac chez l'homme : a. Schéma d'un fumeur de cigarette **b.** Effet de la consommation consécutive de 5 cigarettes sur la concentration de nicotine dans le sang chez deux individus. Les rectangles blanc et noir représentent le moment et la durée de la prise de tabac *Figure adaptée de Isaac and Rand, 1972*. **c.** Concentration moyenne de nicotine dans le sang en fonction du type de cigarette. En journée, la concentration sanguine de nicotine atteint un plateau *Figure adaptée de Benowitz et al., 1984*.

2.2. Effet aigu de la nicotine

Une fois dans le sang, la nicotine traverse la barrière hémato-encéphalique et atteint le SNC (Lester et al., 2009) où elle va agir au niveau des nAChR et va perturber l'activité des neurones en modulant la balance des entrées excitatrices et inhibitrices synaptiques. Les nAChR ont une localisation membranaire variable en fonction des sous-types de récepteurs et des types neuronaux où ils sont exprimés (Changeux, 2010a; Laviolette and van der Kooy, 2004). L'activation des nAChR somato-dendritiques agit sur le potentiel de repos, le seuil de déclenchement des potentiels d'action et/ou la fréquence de décharge des neurones, tandis que l'activation de nAChR sur les terminaisons axonales va induire une augmentation de la libération de neurotransmetteurs excitateurs ou inhibiteurs.

Le renforcement à la nicotine repose sur l'activation du système mésocorticolimbique (Faure et al., 2014; Maskos et al., 2005, Chapitre III) qui est notamment impliqué dans l'apprentissage par renforcement, l'encodage de la valeur, et la prédiction de la récompense (Schultz et al., 1997). Lorsque les neurones dopaminergiques sont activés, cela produit un relargage massif de dopamine (DA) dans les structures cibles, notamment dans le striatum ventral, dit noyau accumbens (NAcc, Dani, 2003). Ces effets, qui se traduisent par une sensation positive et récompensante, à l'origine de la mise en place de la dépendance à la nicotine.

Outre son rôle indéniable dans les multiples facettes de la dépendance, la prise aiguë de nicotine peut également déclencher de l'aversion chez les individus. Les effets aversifs de la nicotine seraient induits par l'activation de la voie habénulo-interpédonculaire, qui est impliquée dans les mécanismes d'aversion, de peur et d'anxiété (Fowler and Kenny, 2014; McLaughlin et al., 2017; Molas et al., 2017b, Chapitre IV). L'activation simultanée de ces deux circuits neuronaux riches en nAChR serait à l'origine des effets opposés de la nicotine. Ces concepts de renforcement et d'aversion seront abordés plus en détail dans les chapitres III et IV. La question encore aujourd'hui est de comprendre si ces effets distincts jouent un rôle dans l'initiation de la dépendance à la nicotine et son maintien.

2.3. Les effets d'une exposition à long terme de nicotine sur les nAChR

Une exposition prolongée à la nicotine va induire une régulation homéostatique des nAChR (Dani, 2003). Dans un premier temps, la nicotine va stabiliser les récepteurs dans un état désensibilisé (régulation « négative »). A plus long terme, des mécanismes d'*up-regulation* des nAChR vont permettre d'augmenter le nombre de récepteurs exprimés à la surface des neurones. Cette *uprégulation* peut être vue comme une réponse à la désensibilisation, permettant de rétablir une transmission nicotinique neuronale « normale ». Si ces mécanismes d'adaptation cellulaire sont très bien décrits en système hétérologue, ils restent difficiles à mettre en évidence dans le SNC chez l'animal.

La désensibilisation serait une adaptation permettant de limiter une activation prolongée aberrante des récepteurs canaux, et ainsi de bloquer le passage d'ions à travers la cellule. Ce mécanisme est plus fréquemment répandu dans la famille des canaux ioniques cationiques par rapport aux canaux anioniques puisque l'entrée de cations, notamment de calcium, est toxique pour les cellules (Lester, 2009). Au contraire de l'ACh qui est hydrolysée par l'acétylcholine estérase, la nicotine n'est pas dégradée au niveau du cerveau, par conséquent le temps de résidence de cette molécule dans le cerveau va favoriser la désensibilisation des nAChR (Brody et al., 2006; De Biasi and Dani, 2011; Lester et al., 2009). La désensibilisation induite par la nicotine concerne principalement les récepteurs hétéropentamériques à haute affinité, à savoir les récepteurs α4β2* (Brody et al., 2006; Fenster et al., 1999).

À plus long terme, la nicotine va également altérer la régulation de l'expression des nAChR. En effet, la nicotine, lorsqu'elle est non ionisée, est capable de traverser le milieu membranaire inhospitalier (Henderson and Lester, 2015, Fig2.2), et d'agir directement sur les processus de régulation d'expression des récepteurs à la membrane. La nicotine présente

en effet des propriétés de chaperonne moléculaire et son action intracellulaire conduit à l'augmentation du nombre de récepteurs exprimés à la membrane. Il a été montré que la nicotine peut stabiliser l'assemblage des sous-unités entre elles, faciliter la maturation et la migration à la membrane des récepteurs et ainsi diminuer le taux de *turn-over* des nAChR (Colombo et al., 2013; Corringer et al., 2006; Lester et al., 2009, Fig 2.2).

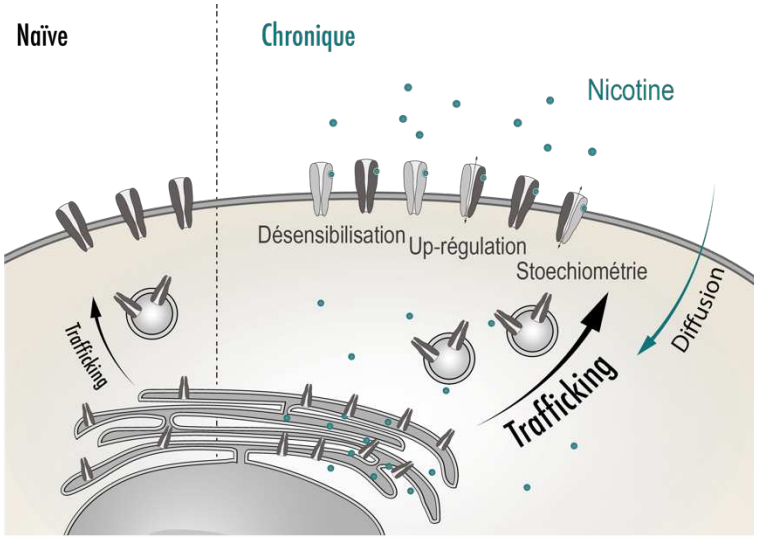

Figure 2.2 | Effets d'une exposition à long terme de nicotine sur le nAChR :

A long terme la nicotine va induire une désensibilisation des nAChR et en agissant au niveau intracellulaire, va augmenter le nombre de récepteurs exprimés. Par conséquent, la stœchiométrie est altérée avec une expression prédominance de récepteur avec 2 sous-unités α et 3 sous-unités β. Les récepteurs (α β)2 α sont représentés en gris foncé et les récepteurs (αβ)2β en gris clair.

Les mécanismes d'*uprégulation*, en système hétérologue, se produisent en quelques heures sur les récepteurs α7, α3β2*, α4β2*, α6β2* and α3β4*, et sont dépendants de la concentration de nicotine. Les récepteurs α4β2*, qui présentent la plus haute affinité apparente pour la nicotine, sont les récepteurs les plus sensibles aux mécanismes d'*uprégulation* (Corringer et al., 2006; Fenster et al., 1999; Srinivasan et al., 2011). Au sein même de cette sous-population de récepteurs, ceux dont la stœchiométrie est $(\alpha4)_2(\beta2)_3$ sont majoritairement *uprégulés* (Colombo et al., 2013; Nelson et al., 2003; Sallette et al., 2005). Ainsi, les mécanismes sous-jacents vont impacter à la fois la quantité de récepteurs exprimés, mais aussi leur stœchiométrie. Au contraire des sous-unités α4 ou β2, la production *de novo* des sous-unités α3 et β4 est nécessaire pour qu'il y ait de l'*uprégulation* (Colombo et al., 2013; Mazzo et al., 2013). Ces études suggèrent que les proportions de récepteurs $(\alpha4\beta2)_2\beta2$ et $(\alpha3\beta4)_2\beta4$ vont être augmentées par rapport aux récepteurs $(\alpha4\beta2)_2\alpha4$ et $(\alpha3\beta4)_2\alpha3$ suite à une exposition à long terme de nicotine. D'un point de vue fonctionnel, le récepteur $(\alpha4\beta2)_2\beta2$ est 100 fois plus affin pour les agonistes que $(\alpha4\beta2)_2\alpha4$ mais possède une perméabilité calcique et une conductance plus faibles (Nelson et al., 2003; Tapia et al., 2006), tandis que $(\alpha3\beta4)_2\beta4$ à la même affinité que son confère $(\alpha3\beta4)_2\alpha3$ mais possède des cinétiques d'ouvertures et une conductance différentes (Krashia et al., 2010).

Ces mécanismes d'adaptation semblent être généralisés, et certains ont pu être mis en évidence chez l'homme. Des prélèvements *post-mortem* de tissus neuronaux ont permis de révéler une quantité plus importante de nAChR dans le cerveau des fumeurs (Benwell et al., 1988). La démonstration de la désensibilisation chez l'homme est indirecte, mais fortement suggérée puisque des études en imagerie fonctionnelle ont mis en évidence que la consommation de cigarettes conduit à une occupation presque complète des récepteurs α4β2* (Brody et al., 2006).

2.4. Diagnostic des troubles d'utilisation du tabac

L'addiction à la nicotine est une maladie psychiatrique qui est définie par la mise en place de comportements aberrants aboutissant à une consommation régulière de tabac, malgré ses conséquences négatives sur la santé et le coût financier. C'est un trouble chronique récurrent dont le diagnostic est posé lorsque les individus présentent une motivation accrue pour rechercher et s'administrer la drogue d'abus, perdent le contrôle de leur consommation et présentent des effets émotionnels négatifs lorsque l'accès à la drogue est contraint ou prohibé (Koob and Le Moal, 2006; Reynaud, 2016). Cette pathologie a été redéfinie en « trouble de d'utilisation du tabac » dans la cinquième version du DSM-V.

L'initiation à la consommation de tabac découle principalement de l'action de la nicotine sur le système dopaminergique, qui est impliqué dans le renforcement d'un comportement aboutissant à l'obtention d'une récompense (De Biasi and Dani, 2011; Faure et al., 2014; Maskos et al., 2005). L'activation du système dopaminergique par la nicotine conduit à la mise en place d'un renforcement à la nicotine. La consommation de tabac est souvent associée à un contexte particulier, par exemple lorsque les individus accompagnent leur café d'une cigarette. L'association d'un contexte avec la prise de tabac contribue fortement au maintien de la consommation à la nicotine, où les individus, dès lors qu'ils se retrouvent dans ces contextes, vont avoir la sensation et le besoin irrépressible de fumer. Progressivement, des mécanismes de tolérance ou d'accoutumance se mettent en place, c'est-à-dire que les individus vont augmenter leur consommation pour atteindre les effets désirés (Dani and Heinemann, 1996; De Biasi and Dani, 2011).

La consommation à long terme de nicotine va mettre en place des mécanismes d'adaptation moléculaires et cellulaires qui permettent d'atteindre un nouvel état homéostatique. Ce nouvel équilibre atteint en présence de nicotine aboutit à la mise en place d'un état émotionnel négatif qui s'exprime particulièrement lorsque la nicotine devient absente (De Biasi and Dani, 2011; Koob and Volkow, 2010). Chez l'homme, les effets de manque à la nicotine se manifestent par une collection de symptômes affectifs, tels que l'anxiété, les troubles de la concentration, la recherche compulsive du produit, l'irritabilité, et l'état dépressif ; et physiques, tels que la bradycardie, des problèmes digestifs ou prise de poids (Antolin-Fontes et al., 2015; De Biasi and Dani, 2011; Hughes, 1992; Hughes et al., 1984; Kenny and Markou, 2001). La durée des symptômes de manque chez les individus est très variable, mais est généralement de quelques semaines, avec un pic des symptômes de manque à sept jours (Hughes, 1992). Cela coïncide notamment avec le temps nécessaire pour retrouver un équilibre d'expression et d'état non désensibilisé des nAChR chez l'humain (Staley, 2006). Même après des années d'abstinence, l'envie de fumer peut quant à elle persister. Les symptômes de manque et le *craving* participent aux échecs de tentative de sevrage et augmentent ainsi les risques de rechute.

2.5. Régulation des nAChR : un écho moléculaire de la pathologie

Les mécanismes d'adaptation moléculaire induits par la nicotine pourraient faire miroir au cercle vicieux de l'addiction à la nicotine. Les chercheurs Dani et Heinemann ont conceptualisé cela et proposent que l'état allostérique et la densité de nAChR pourraient

participer à la mise en place et surtout au maintien de l'addiction à la nicotine (Dani and Heinemann, 1996).

Dans leur modèle (**Fig 2.3**), l'activation des récepteurs nicotiniques du système de la récompense conduit à un relargage massif de dopamine, et la réitération de ces processus serait à l'origine de la mise en place du renforcement à la nicotine. La prise de nicotine va induire une désensibilisation des nAChR et sera à l'origine de la mise en place d'une tolérance : pour atteindre les mêmes niveaux d'activation, les individus doivent augmenter leur prise de nicotine. A plus long terme, le nombre de nAChR augmente mais n'altère pas la transmission nicotinique parce que la désensibilisation permet de compenser cette *uprégulation*. Par contre, en période d'abstinence, les circuits neuronaux soumis à une modulation cholinergique seraient alors sollicités de manière aberrante, puisqu'il y aurait depuis eu une resensibilisation des nAChR désensibilisés. Cette hypercholinergie des circuits serait à l'origine de l'apparition de sensations de mal-être et d'agitation, qui peuvent faire partie des symptômes de manque. Ces effets négatifs favoriseraient les individus à retomber dans le cercle vicieux de la consommation de nicotine, afin de rétablir un équilibre neuronal, pourtant pathologique.

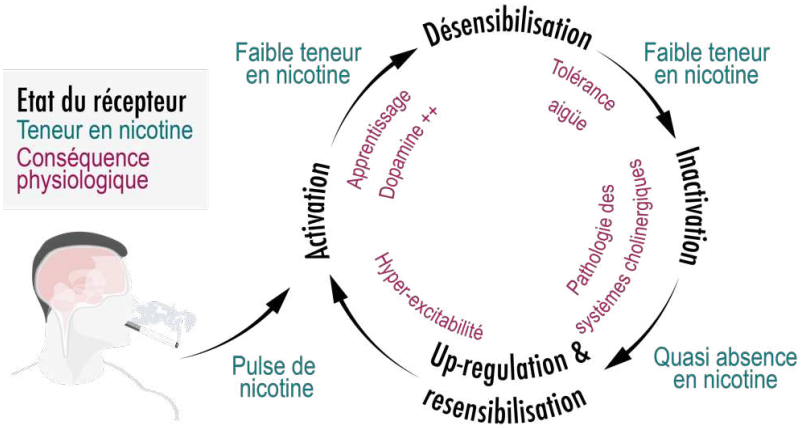

Figure 2.3 | Cercle vicieux de l'addiction et états des nAChR : Schéma récapitulatif de l'impact de l'état des récepteurs nicotiniques sur l'état des circuits neuronaux et par conséquent les symptômes associés *Figure adaptée et revisitée de Dani and Heinemann, 1996*.

Ce modèle n'implique un seul système, celui de la récompense, car une grande partie des travaux sur la dépendance aux drogues d'abus était focalisée sur les mécanismes moléculaires et synaptiques qui sous-tendent le renforcement positif et négatif (Dani and Heinemann, 1996; Mathis and Kenny, 2019, **Chapitre III**). Par conséquent, ce modèle ne traite pas des altérations d'autres circuits, qui sont au centre de la régulation des effets émotionnels négatifs. Depuis, plusieurs études ont mis en évidence le rôle déterminant des structures neuronales connectées à l'habénula dans l'anxiété, l'aversion et la mise en place de symptômes de manque. Notamment, les récepteurs nicotiniques de la voie habénulo-interpédonculaire ont été impliqués dans les effets négatifs de la nicotine (Antolin-Fontes et al., 2015; Fowler and Kenny, 2014). Ainsi, concernant la mise en place de symptômes de manque suite à une période de sevrage à cause d'une hypercholinergie, il semblerait que ces mécanismes puissent découler d'une dérégulation de l'équilibre nicotinique de la voie

habénulo-interpédonculaire (Chapitre IV). Le rôle prépondérant de l'état des nAChR dans l'addiction à la nicotine est toujours d'actualité. Il est nécessaire aujourd'hui de prendre en compte les altérations synaptiques et nicotiniques afin de comprendre comment des perturbations au sein de circuits neuronaux spécifiques aboutissent à la mise en place de la dépendance à la nicotine et à la régulation de la consommation de nicotine.

2.6. Effets opposés de la nicotine et impact sur la consommation

La nicotine, chez l'homme tout comme chez les rongeurs, engendre des effets positifs mais aussi négatifs. En fonction du test expérimental ou de la dose de nicotine utilisée, les études comportementales montrent souvent des résultats contradictoires. Par exemple, lors de l'utilisation de paradigme de préférence/aversion de place conditionnée, la nicotine peut induire un renforcement ou, à l'inverse, une aversion pour le compartiment associé à la nicotine (Grieder et al., 2010; Walters et al., 2006; Wolfman et al., 2018). De la même manière, la nicotine peut induire des effets parfois anxiolytiques ou au contraire anxiogènes (Kutlu and Gould, 2015; Nguyen et al., 2020; Ouagazzal et al., 1999; Varani and Balerio, 2012). La courbe dose réponse en U-inversé a été introduite dans le cadre de l'addiction à la nicotine afin d'expliciter l'absence d'effet comportemental lors d'utilisation de doses sous-seuil, des effets positifs pour une gamme de dose relativement faible, et des effets absents voire négatifs à forte dose (Ashton et al., 1980; Picciotto, 2003, Fig2.4a).

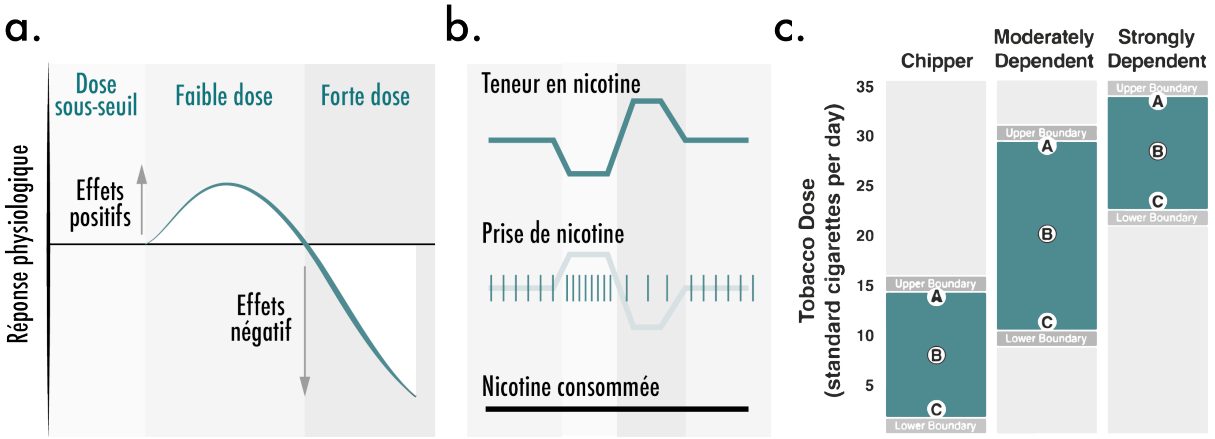

Figure 2.4 | Effets de la nicotine et consommation de nicotine : a. Représentation de la courbe dose-réponse en U-inversé classiquement décrite. **b.** Illustration d'une stratégie de prise de nicotine en fonction de la teneur en nicotine. **c.** Le « Boundary Model » de l'utilisation du tabac extrait de *Kozlowski and Herman, 1984*. Ce modèle de titration repose sur trois zones, celles en gris qui incitent les individus à consommer un niveau de cigarette stable dans le temps, et une zone verte dite zone avec les meilleurs effets psychosociaux. La zone gris clair du dessous représente les effets émotionnels négatifs dus au manque tandis que la zone supérieure représenterait les effets aversifs nocifs dû à une dose trop élevée de nicotine.

De ces études comportementales a émergé un consensus ; il est ainsi décrit encore aujourd'hui que la nicotine à faible dose conduit à des effets perçus comme positifs et récompensants, tandis qu'à fortes doses elle induit des effets négatifs voire aversifs (Fowler and Kenny, 2014, Fig2.4a). Ces effets opposés reposeraient en partie sur l'activation de nAChRs exprimés dans des circuits neuronaux distincts (Chapitre III et IV). Une des hypothèses serait que l'activation des récepteurs à haute affinité (type β2) de la voie

mésocorticolimbique soit impliquée dans les effets positifs de la nicotine aux faibles doses, tandis que l'activation des nAChR de basse affinité (type β4) de la voie habénulo-interpédonculaire signalerait des effets négatifs. Cette dichotomie des faibles et fortes doses de nicotine est particulière et doit être nuancée, en fonction des conditions, des questions posées et des différences interindividuelles. Contrairement aux idées reçues, la voie habénulo-interpédonculaire exprime aussi des récepteurs nicotiniques à haute affinité (Beiranvand et al., 2014; Grady et al., 2009, Chapitre IV). Savoir si de faibles doses pourraient à la fois solliciter le circuit de la récompense et la voie aversive a été une des questions auxquelles je me suis intéressée au cours de ma thèse.

La courbe dose-réponse en U-inversé est également retrouvée lors d'expériences de consommation volontaire de nicotine chez l'homme ou chez les rongeurs (Corrigall and Coen, 1989; Fowler and Kenny, 2014; Henningfield et al., 1983; Isaac and Rand, 1972; Woodward and Tunstall-Pedoe, 1993). Néanmoins, la diminution du nombre de prises conséquentes à l'augmentation de la concentration de nicotine reflète la capacité des individus à titrer leur consommation, par exemple en espaçant les prises de nicotine pour consommer une dose finale identique (Fig2.4b). Chez les rongeurs, la consommation volontaire de nicotine peut se faire dans des paradigmes d'auto-administration ou de libre choix entre deux bouteilles (Box 2.1). Dans ce cadre, pour réguler sa consommation face à une dose deux fois plus élevée que celle délivrée auparavant, l'animal peut alors soit appuyer deux fois moins sur le levier ou boire deux fois moins souvent au biberon qui contient de la nicotine (Corrigall and Coen, 1989; Fowler and Kenny, 2014; Morel et al., 2014). Ces variations dans le comportement de titration observées chez les rongeurs rappellent les observations faites chez l'homme. En effet, des sujets humains confrontés à des cigarettes en faible teneur de nicotine, ou dans le cadre d'auto-administration intraveineuse, sont capables de développer une large palette de stratégies de titration, allant d'une augmentation du nombre de bouffées par cigarette à l'augmentation du temps d'inhalation de celles-ci (Ashton et al., 1980; Maron and Fortmann, 1987; Russell et al., 1980; Schachter et al., 1977).

Box 2.1 | Paradigme de consommation active de nicotine :

Les expériences d'auto-administration chez le rongeur reposent sur l'implantation d'un cathéter intraveineux qui permet de délivrer de la nicotine en soluté. Pour s'administrer la drogue, les animaux peuvent par exemple appuyer sur un levier ou positionner leur museau dans une ouverture (*nose-poke*). La concentration de nicotine est choisie par les expérimentateurs et l'injection de nicotine peut nécessiter un nombre variable d'appuis-levier ou de *nose-pokes*, permettant aussi d'évaluer l'état de motivation de l'animal.

Les expériences de choix à deux bouteilles reposent généralement sur la présentation d'une bouteille d'eau et une de nicotine dans l'environnement. Les souris peuvent librement aller consommer de la nicotine dissoute dans l'eau de boisson, sans l'intervention de l'expérimentateur. La concentration de nicotine est imposée par les expérimentateurs.

Les processus qui permettent aux individus de maintenir activement une consommation apparente stable sont complexes. Le modèle de Kozlowski et Herman est un modèle qui intègre une majorité des notions clés liées à la consommation de nicotine, telles que le renfocement, l'aversion aux fortes doses ou le manque (De Biasi and Dani, 2011; Fowler and Kenny, 2014; Kenny and Markou, 2001). Ce modèle repose sur deux zones

aversives qui délimitent une troisième zone de « sastisfaction générale » (Fig.2.4c). Ici, la réponse comportementale des individus est donc un point d'équilibre qui permet d'éviter ces deux zones extrêmes. Si la dose de nicotine est insuffisante, l'état de manque pousse à augmenter sa consommation, alors que si la consommation de nicotine est excessive, elle entraine une réponse aversive et nocive qui incite à la réduire. Un point d'equilibre entre ces deux limites est donc trouvé. Dans ce modèle la zone centrale représente une zone dite « d'indifférences biologiques avec les meilleurs effets psychosociaux » qui reflète l'absence d'une réponse comportementale face à une variation de la consommation dans cette gamme. Pour les pharmacologistes, cette zone correspondrait à la « gamme de dose efficace » qui produirait les « meilleurs » effets. Bien qu'incontestablement nécessaires pour l'initiation de la dépendance à la nicotine, les effets récompensants de la nicotine seraient selon ce modèle peu déterminants dans la régulation de la consommation de nicotine, au profit des effets aversifs. Cette zone permet de prendre en compte l'importance des systèmes liés à la récompense ou à la motivation en fonction de la pression psychosociale.

Il s'agit de surcroît d'un modèle dynamique, les zones aversives évoluant positivement ou négativement en importance en fonction de la gravité de la dépendance à la nicotine. Les effets aversifs observés aux fortes doses peuvent ainsi s'atténuer au fur et à mesure de la répétition des prises, tandis que la zone correspondant à l'état de manque lié à une sous-consommation s'amplifie. Par conséquent, la zone de satisfaction centrale est décalée vers des besoins de consommation de nicotine plus élevés, faisant écho aux processus de tolérance qui font partie du diagnostic de l'addiction à la nicotine (DSM-V, 2013). Lorsqu'on se focalise sur l'évolution de l'importance des effets positifs et l'état émotionnel négatif, ce modèle présente des similitudes avec les hypothèses homéostatiques et allostatiques développées par Koob et Le Moal (Koob and Le Moal, 1997, 2008). Le modèle de Koob et Le Moal est généralisé aux drogues d'abus, et est souvent utilisé pour proposer une hypothèse qui justifie la transition d'une consommation régulée vers une consommation compulsive. Les processus neuronaux qui sous-tendent de tels comportements de régulation de la consommation de nicotine sont élaborés, résultants de l'action conjointe de plusieurs systèmes en équilibre dynamique, et un seul modèle ne serait probablement pas suffisant pour prendre en compte leur complexité.

Une des problématiques qui m'a intéressée au cours de ma thèse était de comprendre si les effets aversifs classiquement décrits aux fortes doses existent lors de consommations régulières de nicotine, et s'ils sont au centre des processus impliqués dans le contrôle de la consommation.

3. Chapitre 3 : Système dopaminergique et renforcement à la nicotine

Dans les années 50, James Olds et Peter Milner ont été les premiers à démontrer que les rats étaient capables de travailler vigoureusement pour obtenir une stimulation électrique des composants du faisceau médian du télencéphale (MFB), qui contient notamment les projections dopaminergiques. Cette étude pionnière a permis de mettre en évidence que la stimulation des fibres dopaminergiques peut être intrinsèquement récompensante (Olds and Milner, 1954). Par la suite, il a été montré que l'activation du système dopaminergique mésocorticostriatal par un stimulus récompensant sert de substrat majeur pour l'acquisition d'un comportement (Schultz et al., 1997; Wise, 1998; Wise and Koob, 2014) et il est aujourd'hui proposé que les neurones dopaminergiques codent pour l'utilité de nos actions, de nos buts.

Les concepts qui décrivent l'initiation de la dépendance mettent l'accent sur le détournement du système dopaminergique par les drogues d'abus. La nicotine va, comme toutes les drogues d'abus, induire un relargage massif de dopamine (DA) dans le cerveau (Di Chiara and Imperato, 1988). Cette augmentation répétée de DA dans les structures cibles du système dopaminergique va moduler l'excitabilité des neurones et conduire à la mise en place de plasticités synaptiques au sein de circuits spécifiques (Luscher, 2013; Mameli et al., 2009; Pascoli et al., 2015; Reynolds et al., 2001; Robbins and Everitt, 1999; Schultz and Dickinson, 2000; Tritsch and Sabatini, 2012). Ces altérations sous-tendraient les troubles liés à la consommation de tabac (De Biasi and Dani, 2011; Laviolette and van der Kooy, 2004) et une surévaluation des effets positifs des drogues au dépens des récompenses naturelles (Keiflin and Janak, 2015; Redish, 2004).

3.1. La dopamine

La dopamine (DA) est un neuromodulateur impliqué dans des fonctions cérébrales telles que le contrôle moteur, l'apprentissage par renforcement, la prise de décision et la motivation dirigée vers un but. La DA est, comme la noradrénaline et l'adrénaline, issue de la voie de biosynthèse des catécholamines, composés organiques synthétisés à partir de la tyrosine (**Box 3.1**). Par conséquent la présence de l'enzyme tyrosine hydroxylase (TH) dans les neurones permet d'identifier les neurones DA, noradrénergiques et adrénergiques. La DA agit sur les récepteurs dopaminergiques qui font partie de la super famille des récepteurs à sept domaines transmembranaires couplés à des protéines G. C'est un neuromodulateur puisque qu'il n'existe pas de synapse dopaminergique à proprement parler et que la transmission du signal résulte de l'activation de récepteurs métabotropes qui engagent une signalisation intracellulaire lente.

Les premières études de la transmission dopaminergique ont permis d'identifier le rôle la DA sur la voie de signalisation de l'adénylate cyclase. Il existe deux types de récepteurs dopaminergiques, les récepteurs de type D1 et ceux de type D2, qui activent et inhibent respectivement l'adénylate cyclase (Creese et al., 1976; Kebabian and Greengard, 1971). Les récepteurs de type D1 (D1 et D5) sont majoritairement associés à Gαs/olf, et mènent à

une augmentation de l'excitabilité neuronale; tandis que les récepteurs de type D2 (D2, D3 et D4) sont associés à Gαi/o et sont inhibiteurs (Girault and Greengard, 2004). Les récepteurs dopaminergiques peuvent également être couplés à la protéine Gαq ou Gβɣ dont l'activation par la DA induit une cascade de signalisation intracellulaire de la phospholipase C ou module les canaux cationiques (Andrianarivelo et al., 2019; Girault and Greengard, 2004; Klein et al., 2019; Tritsch and Sabatini, 2012).

Box 3.1 | La signalisation dopaminergique

La dopamine est synthétisée à partir de la L-tyrosine grâce à deux enzymes, la tyrosine hydroxylase (TH) et la dopamine décarboxylase. La dihydroxyphénylalalanine (DOPA) issu de l'hydratation de la tyrosine est décarboxylée pour former la dopamine. La dopamine synthétisée dans le cytoplasme est chargée dans les vésicules synaptiques par le transporteur vésiculaire des monoamines (VMAT, vesicular monoamine transporter). Une fois libérée dans le milieu extracellulaire, elle agit sur les récepteurs dopaminergiques. La dopamine est ensuite recapturée par le transporteur de la dopamine (DAT).

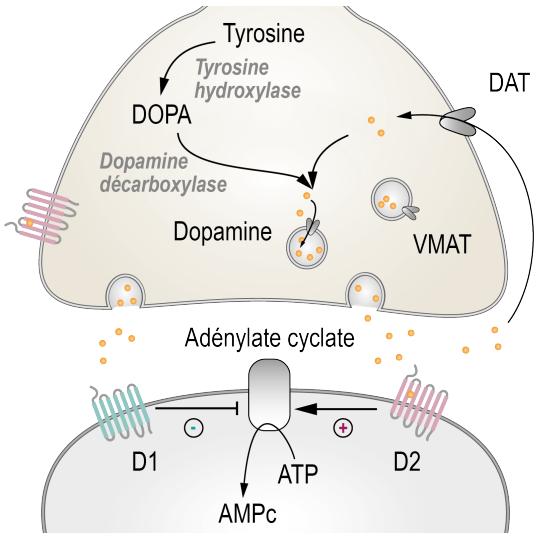

3.2. L'aire tegmentale ventrale et les circuits dopaminergiques

La signalisation dopaminergique repose principalement sur deux noyaux mésencéphaliques : la substance noire *pars compacta* (A9) et l'aire tegmentale ventrale (VTA, *ventral tegmental area*, A10, **Fig3.1a**). La substance noire *pars compacta*, qui fait partie intégrante des circuits des ganglions de la base, projette principalement sur le striatum dorsal, les cortex, et dans une moindre mesure sur le striatum ventral, l'amygdale et les noyaux sous-thalamiques (Yetnikoff et al., 2014). La substance noire *pars compacta* a largement été étudiée dans le contexte de la maladie de Parkinson qui entraine la dégénérescence des neurones dopaminergiques de cette structure. Différentes études ont permis de mettre en évidence le rôle de la DA dans le contrôle moteur, la mémoire procédurale et l'erreur de prédiction de la récompense (Chevalier and Deniau, 1990; Haber et al., 2000; Klaus et al., 2019; Schultz et al., 1997). Au cours de ma thèse, je me suis focalisée seulement sur le rôle des neurones dopaminergiques de la VTA dans l'initiation et le maintien de l'addiction à la nicotine.

La VTA est une structure du mésencéphale qui est constituée de cinq noyaux (**Fig3.1b**) : le noyau parabrachial pigmentosus (PBP), le noyau latéral paranigral (PN), le noyau interfasciculaire (IF), le noyau linéaire rostral (RLi) et le noyau linéaire caudal (CLi). Les noyaux les plus médians (IF, RLi et CLi) présentent une faible proportion de neurones DA. Les expériences histologiques et de traçages anatomiques ont permis de cartographier et de quantifier les types neuronaux ainsi que de décrire les premiers circuit de la VTA (Beier et al., 2015; Margolis et al., 2006; Nair-Roberts et al., 2008). Le développement des stratégies virales couplées à l'utilisation de souris transgéniques exprimant l'enzyme Cre

recombinase (i.e. DAT-Cre, VGlut2-Cre, GAD-Cre etc), en combinaison avec l'optogénétique et les enregistrements électrophysiologiques, ont permis de compléter ces études en y ajoutant une description fonctionnelle (Morales and Margolis, 2017). Il est estimé que la VTA est constituée d'une majorité de neurones dopaminergiques (60%), d'environ 30% de neurones GABAergiques de projection ou interneurones, et d'une minorité de neurones glutamatergiques (<10%) (Margolis et al., 2006; Nair-Roberts et al., 2008). Certains neurones présentent une co-libération de ces neurotransmetteurs (Morales and Margolis, 2017; Root et al., 2014; Stuber et al., 2010; Tecuapetla et al., 2010; Yoo et al., 2016; Zhang et al., 2015).

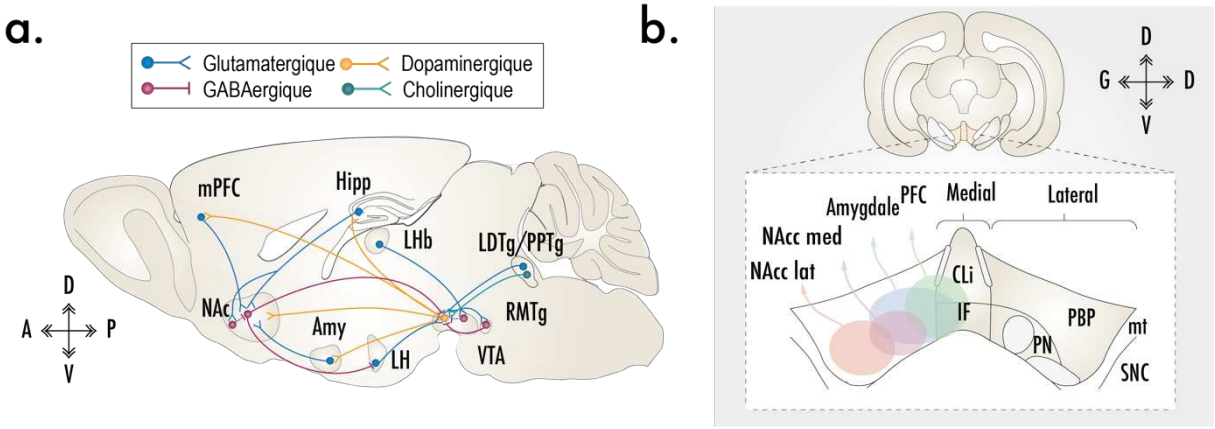

Figure 3.1 | Système dopaminergique de l'aire tegmentale ventrale : a. Afférences et efférences sur système dopaminergique de la VTA. *Figure adaptée de Russo and Nestler, 2013* **b.** Représentation répartition anatomique des neurones dopaminergiques en fonction de leur projection sur les structures cibles. *Figure adaptée de Beier et al., 2015; Morales and Margolis, 2017*

La VTA est une structure qui, avec ces afférences et efférences (**Fig3.1**), forme un réseau complexe impliqué dans différentes fonctions cérébrales. Elle peut être découpée en sous-circuits en fonction des projections.

La voie mesocorticale est formée par les neurones de la VTA qui projettent vers les cortex. Cette voie est impliquée dans des fonctions cognitives, telles que les processus attentionnels, la flexibilité comportementale, la planification (Chudasama and Robbins, 2004; Floresco, 2013) et la motivation (Bromberg-Martin et al., 2010; Westbrook and Braver, 2016). Les cortex préfrontaux et orbitofrontaux font partie des principales régions de projection des neurones de la VTA avec des afférences dopaminergiques, GABAergiques et glutamatergiques (Fields et al., 2007; Lammel et al., 2008; Margolis et al., 2006). En retour, une importante proportion des entrées glutamatergiques sur les neurones DA de la VTA est de nature corticale (Beier et al., 2015; Ikemoto, 2007; Tong et al., 1996; Watabe-Uchida et al., 2012) et pourrait participer à l'activité en bouffée des neurones DA (voir Partie 3.3, Tong et al., 1996).

La projection des neurones DA vers le NAcc, qui constitue la voie mésostriatale, présente une ségrégation anatomique bien définie (de Jong et al., 2019; Lammel et al., 2008; Moore and Bloom, 1978) avec les neurones DA de la VTA médiale qui projettent sur le NAcc médial (*core et shell*), et ceux de la VTA latérale qui projettent vers le NAcc latéral (Beier

et al., 2015; Lammel et al., 2008, 2011). L'activation de cette voie a longtemps été associée aux processus d'anticipation des récompenses et des effets de renforcement de récompense naturelle (Cox and Witten, 2019; Salamone and Correa, 2002). La libération de dopamine est associée à une potentiation des entrées corticales sur les *spiny projecting neurons* (SPN) (Reynolds et al., 2001; Robbins and Everitt, 1999). Depuis, il a été montré que ces faisceaux dopaminergiques pouvaient aussi s'activer lors de la présentation de stimuli aversifs (de Jong et al., 2019). En retour, les SPN du NAcc constituent une source d'inhibition des neurones de la VTA (Beier et al., 2015; Yang et al., 2018). Les neurones du NAcc latéral semblent cibler majoritairement les neurones GABAergiques de la VTA, conduisant à une désinhibition des neurones DA de la VTA latérale alors que le NAcc médial produirait une inhibition directe des neurones dopaminergiques de la VTA médiale (Yang et al., 2018). Le NAcc est aussi la cible de projections glutamatergiques et GABAergiques de la VTA (Brown et al., 2012; Hnasko et al., 2012; Qi et al., 2016; Tecuapetla et al., 2010; Yamaguchi et al., 2011; Yoo et al., 2016; Zhang et al., 2015).

Une partie des projections dopaminergiques cible également l'amygdale basolatérale (BLA) et centrale (CeA) (Lammel et al., 2008; Stamatakis et al., 2014; Tang et al., 2020). La prédiction de la récompense à une drogue conduit à une augmentation de la libération de dopamine au sein de la BLA (Weiss et al., 2000). Les projections de la VTA vers l'amygdale pourraient moduler les processus tels que l'apprentissage de valeur émotionnelle et l'addiction (Stamatakis et al., 2014).

Enfin, il existe des connexions réciproques entre la VTA et l'habenula latérale (LHb) ou « *l'anti-reward system* » car les neurones de l'habenula latérale signalent la valence d'un stimulus négatif contribuant à des comportements aversifs (Hu et al., 2020; Matsumoto and Hikosaka, 2007). L'activation des neurones glutamatergiques de la VTA projetant sur la LHb mène à des comportements de type aversif (Lammel et al., 2015; Lecca et al., 2017; Root et al., 2014). En retour, les neurones excitateurs de la LHb projettent massivement sur le RMTg, *the tail of the VTA,* et sur les neurones de la VTA médiale (Balcita-Pedicino et al., 2011; Lammel et al., 2012; Maroteaux and Mameli, 2012). Le RMTg, noyau GABAergique, est l'une des sources majeures d'inhibition de la VTA (Jhou et al., 2009). Par conséquent, l'activation de la LHb va favoriser la voie « aversive » de la VTA (i.e. VTA médiale) et induire une inhibition indirecte de la VTA latérale *via* l'activation des neurones GABAergiques du RMTg (Lammel et al., 2012). D'autres régions reçoivent également des projections dopaminergiques de la VTA comme le tubercule olfactif, l'hippocampe dorsal, le pallidum ventral, le septum latéral ou encore le cortex entorhinal (Fields et al., 2007; Gasbarri et al., 1997; Gruber et al., 2007; McBride et al., 1999; Swanson', 1982).

3.3. Activité des neurones dopaminergiques

La caractérisation *in vivo* de l'activité électrique des neurones dopaminergiques a été réalisée chez le rongeur anesthésié (Grace and Bunney, 1984a, 1984b) et éveillé (Hyland et al., 2002), et chez le primate éveillé (Schultz, 1986; Schultz et al., 1997). Bien qu'une partie des neurones dopaminergiques soient silencieux (Grace and Bunney, 1984b), une majorité d'entre eux présentent une activité spontanée. Les neurones DA ont un potentiel d'action (PA) large dont la taille est supérieure à 2,2 ms, et présentent un patron de décharge lent et

régulier qui peut être interrompu par une activité en bouffées (ou *bursts*). Une grande majorité des neurones DA expriment les autorécepteurs D2 inhibiteurs (Grace and Bunney, 1984a, 1984b; Paladini and Roeper, 2014; Schultz et al., 1997).

La caractérisation électrophysiologique des neurones DA a été par la suite complétée grâce à des études *in vitro*, en électrophysiologie patch-clamp (Kitai et al., 1999; Shi, 2009). Il ressort de ces études que les neurones dopaminergiques ont une empreinte électrophysiologique conservée qui repose sur deux types de patrons de décharge (**Fig3.2**) :

- **Un patron de décharge régulier,** dit *pacemaker,* qui est à relativement basse fréquence (1– 5 Hz). L'activité régulière spontanée a aussi été observée lors d'enregistrements *in vitro,* et ce même lorsque les entrées synaptiques sont complètement interrompues, indiquant qu'il s'agit d'une activité intrinsèque spontanée (Roeper, 2013; Shi, 2009). Plusieurs canaux ioniques sont mis en jeu dans ce type de décharge. De manière générale, il est considéré que le PA induit l'ouverture des canaux calciques voltage-dépendants (*voltage-gated calcium channels*, VGCC). Les entrées calciques activent les *small conductance calcium-activated K+ channels* (canaux SK) (Shepard and Bunney, 1988). L'ouverture des canaux SK conduit à une hyperpolarisation du neurone et par conséquent à l'activation de canaux HCN (*Hyperpolarisation-activated Cyclic-Nucleotid modulated Cation Non-selective Channel*). Le courant entrant, dit Ih, induit une rectification entrante permettant une dépolarisation lente du potentiel de membrane (Grace and Bunney, 1983). Cette repolarisation est ralentie par l'activation de canaux potassiques voltages dépendant (Kv) (Grace and Onn, 1989) mais elle est accentuée par les VGCC ce qui permet d'atteindre à nouveau le seuil de déclenchement d'un nouveau PA.

- **Un patron de décharge en bouffées** dit « *burstant* » qui est transitoire et à haute fréquence supérieure à 15 Hz (Grace and Bunney, 1984a; Schultz et al., 1997). Cette activé est absente des enregistrements *in vitro* et, par conséquent il est considéré que l'activité en bouffée repose sur des propriétés émergeantes du réseau *via* les entrées synaptiques excitatrices et inhibitrices (Kitai et al., 1999). Grace et Bunney ont ainsi défini les *bursts*: l'entrée dans un *burst* est caractérisée par un intervalle inter-spike (ISI) inférieur à 80 ms, tandis que la fin de la bouffée est marquée par une longue pause déterminée par un ISI supérieur à 160 ms (Grace and Bunney, 1984a).

Les neurones dopaminergiques peuvent donc être caractérisés par leur fréquence de décharge régulière et le nombre de PA dans le *burst* (**Fig3.2a**). Cela permet de classifier les neurones dopaminergiques en quatre profils qui sont les neurones : (1) à faible fréquence et peu de *bursts*, (2) à faible fréquence et beaucoup de *bursts*, (3) à forte fréquence et peu de *bursts* et (4) à forte fréquence et beaucoup de *bursts* (Hyland et al., 2002; Mameli-Engvall et al., 2006).

Le type de décharge lent et régulier a été associé à une libération de DA faible et constante, dite tonique (Grace, 1995, **Fig3.2b-c**). Une altération de ce tonus dopaminergique est associée à des pathologies neuronales, telles que les addictions (Melis et al., 2005), la schizophrénie (Sekiguchi et al., 2019) ou la maladies de Parkinson (Degos et al., 2013;

Deniau et al., 2010). Ces constats reflètent l'importance de ce tonus dans la régulation de l'activité des structures cibles. L'activité en bouffées entraîne un pic massif et transitoire de relargage de DA (Gonon, 1988; Tsai et al., 2009, Fig3.2b–c). Il est supposé que les pics de relargage dits « phasiques » de DA émergent non seulement de l'activité en *burst* des neurones individuels, mais surtout de la synchronie des bursts sur une population de neurones dopaminergiques. Cette activité en *bursts* est déterminante pour l'apprentissage par renforcement et dans la prédiction de la récompense (Tolu et al., 2013; Tsai et al., 2009).

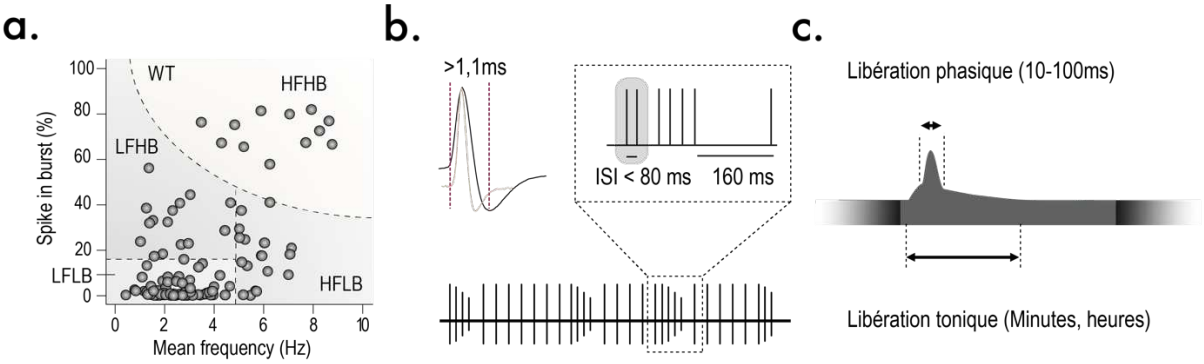

Figure 3.2 | Activité spontanée des neurones DA de la VTA : a. Représentation des neurones DA en fonction de leur patron de décharge régulier et en bouffée. LFLB : Low firing, low burst ; LFHB : Low firing, high burst, HFLB : High firing, low burst ; HFHB : High firing, high burst. *Figure adaptée de Changeux, 2010a* **b.** Représentation d'un potentiel d'action de neurone DA (noir) par rapport à un neurone GABA (gris). Illustration d'un neurone qui présente une activité régulière et en burst. **c.** Schéma des différents modes, tonique et phasique, de libération de dopamine dans les structures cibles.

3.4. Apprentissage par renforcement et dopamine

Les études pionnières d'enregistrement *in vivo* des neurones dopaminergiques chez le primate (Flg3.3a) par Wolfram Schultz *et al* n'ont pas seulement permis de générer une base électrophysiologique solide sur les patrons de décharge des neurones dopaminergiques (Paladini and Roeper, 2014), elles ont également permis de fournir des éléments capitaux sur les bases neuronales des mécanismes d'apprentissage par renforcement (Dayan and Balleine, 2002; Schultz, 2017; Schultz et al., 1997). Ces expériences montrent que les neurones dopaminergiques répondent par une activité en bouffées a des stimuli appétitifs ou récompensants (Fig3.3). Notamment, cette activité en bouffées a été observée soit lors de l'obtention d'une récompense inattendue soit, après apprentissage au moment de la prédiction de l'obtention d'une récompense (Schultz et al., 1993, 1997). Le paradigme comportemental réalisé dans ces expériences repose sur une tâche de conditionnement pavlovien classique, à savoir l'association de deux éléments présentés à l'animal :

- Un stimulus arbitraire, neutre (SN), sans valeur récompensante ou aversive intrinsèque et qui n'évoque pas initialement de réponse comportementale. Ce stimulus est visuel ou auditif.

- Un stimulus inconditionné (SI) qui peut être appétitif ou aversif, dont l'obtention va induire une réponse positive ou négative. Le SI peut être une récompense telle qu'une goutte de jus d'orange, ou une punition telle qu'un choc électrique.

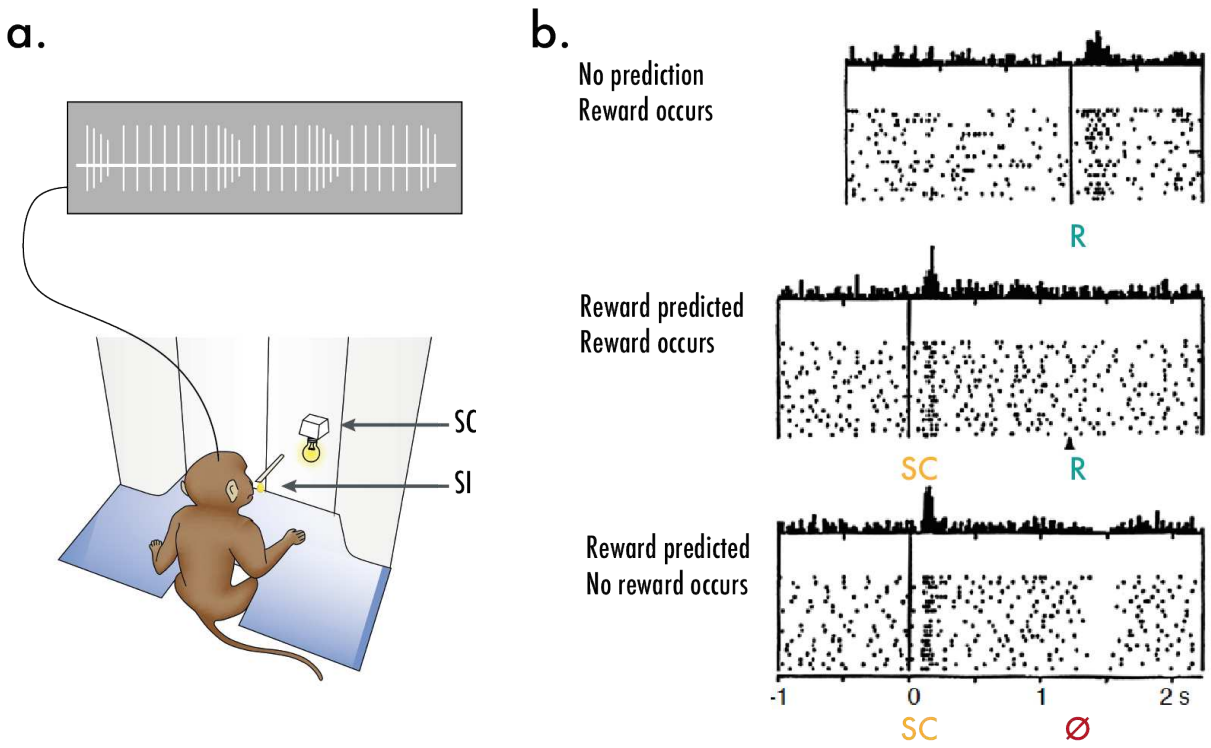

Figure 3.3 | Encodage de l'erreur de prédiction de récompense : a. Représentation d'un primate dans une tâche de conditionnement Pavlovien. Le stimulus lumineux, initialement neutre devient un stimulus conditionné (SC) au cours de l'apprentissage. La goûte de jus d'orange est un stimulus inconditionné. Au cours de la tâche les neurones putatifs DA sont enregistrés chez l'animal. *Figure adaptée de Schultz, 2000* **b.** Rasterplot des neurones enregistrés au cours de la tâche en fonction des différentes conditions *Figure adaptée de Schultz, 1997*. R : récompense ; Ø : omission de la récompense.

La répétition de la présentation du SN quelques secondes avant le SI va permettre l'association du stimulus initialement neutre au SI, et par conséquent le SN devient un stimulus conditionné (SC). Le premier résultat remarquable du travail de Wolfram Schultz a été de montrer que les neurones DA adaptent leur réponse au SC et au SI au cours de l'association (Fig3.3b). Au début de la tâche, avant apprentissage, les neurones dopaminergiques vont augmenter leur activité, principalement en bouffées, lors de l'obtention d'une récompense (SI) qui dans ce contexte est inattendue (Mirenowicz and Schultz, 1996; Schultz et al., 1993, 1997). Au fur et à mesure de l'apprentissage, le pic d'activité des neurones dopaminergiques se décale dans le temps pour ne plus apparaitre lors du SI mais au moment du stimulus prédicteur, le SC. Il a notamment été montré que l'amplitude du signal permet de prédire la valeur subjective de la récompense ; c'est-à-dire que plus cette dernière est importante, plus l'augmentation de l'activité des neurones DA sera grande (Coddington and Dudman, 2018; Fiorillo et al., 2003; Lak et al., 2014; Naudé et al., 2018; Roesch, 2004). De plus, si la récompense n'est pas délivrée, l'activité des neurones dopaminergiques diminue (ou fait une pause) au moment de l'omission. De ces expériences, il apparait que les neurones dopaminergiques ne prédisent pas seulement les stimuli à venir, mais encoderaient l'erreur de prédiction de la récompense (RPE, *reward prediction error*) qui est définie par la différence entre la valeur attendue et la valeur perçue. L'activité au moment du SI refléterait un calcul instantané de cette différence.

Dans le cadre des théories de renforcement de l'apprentissage, les RPE négatives et positives agissent comme un signal d'apprentissage pour actualiser la valeur des récompenses attendues. Ce signal joue un rôle clé dans les mécanismes d'apprentissage, puisque la variation du niveau de libération de DA dans le striatum permettrait de modifier les poids synaptiques de circuits spécifiques, notamment des connexions cortico-striatales. Ces processus d'apprentissage résultent en la sélection des actions qui mènent à des stimuli appétitifs et en l'évitement des comportements à effets négatifs.

Des stimulations optogénétiques des neurones DA ou électriques du faisceau médian du télencéphale (MFB, *medial forebrain bundle*) qui miment une activité phasique des neurones DA, sont suffisantes pour induire un apprentissage par renforcement dans des paradigmes de conditionnement classique ou instrumental (Coddington and Dudman, 2018; Corbett and Wise, 1980; Kim et al., 2012; Olds and Milner, 1954; Pascoli et al., 2018; Steinberg et al., 2013; Tsai et al., 2009). En revanche, l'inhibition optogénétique ou pharmacologique conduit à une inhibition comportementale ou un évitement, même lorsque celle-ci est brève et mime une pause (Chang et al., 2016, 2018; Tan et al., 2012; Tolu et al., 2013). Ces études ont permis de faire un lien causal entre les dynamiques d'activation et d'inhibition des neurones DA et les RPE négatives et positives, et confirment le rôle de la DA dans l'apprentissage de la récompense naturelle. Bien que les drogues d'abus induisent une libération massive de dopamine dans le striatum ventral (Di Chiara and Imperato, 1988), une altération du principe computationnel de la RPE dans le contexte des addictions n'a pas été explicitement testée (Keiflin and Janak, 2015; Redish, 2004).

3.5. Modulation cholinergique du système dopaminergique

Les entrées excitatrices et inhibitrices de la VTA vont orchestrer les dynamiques d'activation des neurones et influencer le devenir des connexions synaptiques (Kitai et al., 1999). De nombreuses recherches se sont focalisées sur le rôle de la modulation cholinergique du système dopaminergique (Corrigall et al., 2002; Faure et al., 2014; Mansvelder et al., 2003; Maskos, 2009; Picciotto et al., 2012), principalement parce que l'initiation de la dépendance à la nicotine résulte d'une activation des nAChR du système DA (Drenan et al., 2008; Exley et al., 2011; Maskos et al., 2005; Picciotto et al., 1998; Tapper, 2004; Tolu et al., 2013). La modulation cholinergique de la VTA provient principalement des noyaux du pont, dont font partie le tegmentum latérodorsal (LDTg) et le noyau pédonculopontin (PPTg) (Grace et al., 2007; Lodge and Grace, 2006; Maskos, 2009; Picciotto et al., 2012). Les noyaux cholinergiques du pont jouent un rôle dans les cycles éveil-sommeil (Kroeger et al., 2017; Van Dort et al., 2015), les mouvements et l'orientation visuels (Garcia-Rill, 1991) ainsi que la locomotion et l'acquisition de récompenses (Datta and Siwek, 2002; Norton et al., 2011; Xiao et al., 2016). Sachant que les noyaux du pont projettent sur la VTA, il est suggéré que ceux-ci pourraient réguler les informations sensorielles importantes associées à une récompense et/ou nécessitant un mouvement volontaire (Norton et al., 2011). Au niveau des terminaisons, la libération de DA dans les structures cibles peut être modulée par les interneurones cholinergiques du striatum ou des cortex (Mansvelder et al., 2009).

Une inactivation pharmacologique ou une lésion des noyaux du pons altèrent l'activité en *burst* des neurones dopaminergiques (Lodge and Grace, 2006), et diminuent le relargage de DA dans le striatum (Blaha et al., 1996). Bien que ces structures contiennent des neurones cholinergiques, glutamatergiques et/ou GABAergiques du LDTg et PPTg, des études ont mis en évidence l'importance de la modulation cholinergique dans l'activité des neurones DA. Notamment, l'activation et l'inactivation pharmacologique des récepteurs cholinergiques de la VTA conduisent respectivement à une augmentation et une diminution de la libération de DA dans le striatum (Miller and Blaha, 2005). De plus, l'activation optogénétique des neurones cholinergiques du pont va principalement activer les neurones DA (Dautan et al., 2016; Xiao et al., 2016). Malgré l'importance de l'activation des mAChR, il existe un faisceau d'évidence qui pointe le rôle clé du contrôle nicotinique sur les neurones de la VTA (Durand-de Cuttoli et al., 2018; Faure et al., 2014; Marti et al., 2011; Maskos et al., 2005; Naudé et al., 2016; Picciotto et al., 1998; Tolu et al., 2013). Lors de ma thèse, j'ai utilisé un nAChR photo-contrôlable pour sonder, en temps réel et *in vivo*, l'impact de la modulation nicotinique endogène sur l'activité spontanée des neurones DA de la VTA (Durand-de Cuttoli et al., 2018).

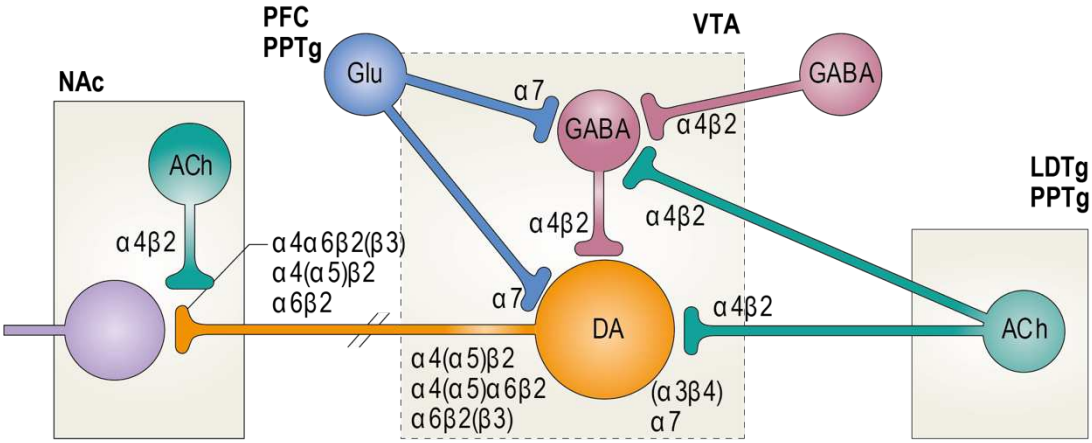

Figure 3.4 | Répartition des nAChR de la VTA : Les récepteurs majoritaires de la VTA sont les récepteurs α4β2. Les neurones DA sont soumis à une régulation nicotinique importantes. *Figure adaptée de Changeux, 2010a*

Les récepteurs nicotiniques sont largement distribués dans la VTA. En effet, ils sont exprimés sur les neurones dopaminergiques et GABAergiques et sur les terminaisons axonales des afférences de la VTA. Le récepteur majoritaire est le récepteur α4β2* qui peut être associé aux sous-unités α5 et/ou α6, tandis que les récepteurs α7 sont plutôt exprimés au niveau présynaptique des afférences de la VTA (**Fig3.4**). Chez l'animal anesthésié, les neurones dopaminergiques de la VTA des souris $\beta2^{-/-}$ (Mameli-Engvall et al., 2006; Maskos et al., 2005) ont une fréquence de décharge faible et ne présentent pas de *burst*. Chez les souris $\alpha4^{-/-}$, la structure du *burst* est également altérée (Exley et al., 2011). Des expériences de réexpression locale (dans la VTA) des sous-unités β2 ou α4 permettent de rétablir ces phénotypes, ce qui met en lumière le rôle de l'ACh et des récepteurs α4β2* dans l'activité régulière et en bouffée des neurones DA. Chez les autres modèles *knock-out* $\alpha7^{-/-}$, $\alpha5^{-/-}$, $\alpha6^{-/-}$ et $\beta4^{-/-}$, l'activité spontanée des neurones DA n'est pas altérée, ce qui suggère que ces récepteurs ne contribuent pas à l'activité spontanée des neurones dopaminergiques (Exley et

al., 2011; Harrington et al., 2016; Mameli-Engvall et al., 2006; Morel et al., 2014). Les récepteurs α6* de la VTA sont surtout localisés au niveau des terminaisons axonales des neurones DA, par conséquent le rôle de ces récepteurs a plutôt été attribué à la modulation de la libération de DA au niveau du striatum (Exley et al., 2013; Threlfell et al., 2012).

Comment se traduisent ces altérations électrophysiologiques au niveau comportemental ? Les neurones DA des souris $\beta2^{-/-}$ ne montrent pas d'activité en bouffée lorsque l'animal est anesthésié, ce qui pourrait suggérer un impact majeur au niveau comportemental, étant donné le rôle clé des *bursts* dans des processus aussi fondamentaux que l'apprentissage par renforcement. Néanmoins, il est important de noter que, chez les souris éveillées, les neurones DA de la souris $\beta2^{-/-}$ présentent une activité quasi-identique à ceux de la souris de type sauvage, mais ne montrent pas le même niveau de synchronisation (Naudé et al., 2018). La présence de *bursts* chez la souris $\beta2^{-/-}$ est en accord avec le fait que les *bursts* ne sont pas juste sous contrôle nicotinique (Kitai et al., 1999). L'utilisation du modèle de la souris $\beta2^{-/-}$ couplé à de la réexpression locale dans la VTA a permis de mettre en évidence le rôle des β2* nAChR dans la locomotion spontanée ou l'exploration (Avale et al., 2008; Maskos et al., 2005) et dans l'exploration de récompenses incertaines (Naudé et al., 2016). De plus, l'activation optogénétique des afférences cholinergiques dans la VTA conduit à un renforcement positif et promeut la locomotion (Dautan et al., 2016, Xiao et al., 2016).

3.6. Renforcement à la nicotine

Comme nous l'avons vu, les dynamiques de décharge des neurones dopaminergiques sont au centre des processus d'apprentissage par renforcement (Schultz, 2007). L'activation pharmacologique du système DA par la nicotine perturbe l'activité des neurones dopaminergiques, modifie le poids synaptique dans les circuits de la récompense et conduit à la mise en place de comportements de consommation aberrants. La nicotine induit des comportements d'auto-administration chez les humains, les primates et les rongeurs (Ashton et al., 1980; Corrigall and Coen, 1989; Goldberg et al., 1981; Henningfield et al., 1983). La propriété appétitive de la nicotine dépend principalement de son action sur la VTA, car les comportements d'auto-administration sont reproduits lors d'injection locale de nicotine dans la VTA ou que le renforcement à la nicotine est bloqué lors du blocage pharmacologique de la VTA (Corrigall et al., 1994; Durand-de Cuttoli et al., 2018; Exley et al., 2011; Harrington et al., 2016; Maskos et al., 2005; Tolu et al., 2013).

De nombreuses études ont permis de mettre en évidence les mécanismes moléculaires et cellulaires qui sous-tendent l'action de la nicotine sur les neurones de la VTA et le renforcement. L'application de nicotine sur les neurones DA de la VTA lors d'enregistrements *ex vivo* évoque un courant entrant en condition voltage-imposé, principalement au niveau de la VTA postérieure (Zhao-Shea et al., 2011), et conduit à une augmentation de la décharge des neurones en mode courant-imposé. Ces réponses sont diminuée lors de l'utilisation d'antagoniste de α4β2* ou α7 (Durand-de Cuttoli et al., 2018; Klink et al., 2001; Pidoplichko et al., 1997; Tapper, 2004). La réponse à la nicotine des neurones dopaminergiques est relativement longue (plusieurs minutes). Il est suggéré que cette réponse persistante dépend des cinétiques d'activation et de désensibilisation des

nAChR α4β2* et α7 au niveau somatique des neurones DA et GABA de la VTA et des nAChR pré-synaptiques des afférences glutamatergiques et GABAergiques (Lecca et al., 2011; Mansvelder et al., 2002; Wooltorton et al., 2003).

La stimulation des nAChR α7 sur les terminaisons glutamatergiques dans la VTA peut induire une potentialisation à long terme (LTP) des entrées excitatrices sur les neurones DA (Mansvelder and McGehee, 2000). Au niveau des terminaisons dopaminergiques dans le striatum, la nicotine va faciliter la libération de DA lors de stimulations phasiques, mais pas toniques, des fibres DA (Rice and Cragg, 2004) et cela dépend des récepteurs α4α6β2β3 (Drenan et al., 2008; Exley et al., 2012).

Box 3.2 | Modèle génétique

Les approches génétiques ont permis de faire une avancée considérable dans l'évaluation du rôle des différents sous-types de récepteurs au sein de circuits spécifiques. Une des approches de choix pour les récepteurs nicotiniques repose sur l'utilisation de modèles *knock-out*, couplée à de la réexpression locale du gène en question. Le principe repose sur la caractérisation cellulaire (i.e. caractéristiques électrophysiologiques basales ou en réponse à la nicotine) et comportementales des souris invalidées pour le gène d'intérêt, comparée à celle souris de type sauvage. Les études sont complétées grâce à l'utilisation de vecteur viraux, qui permettent la réexpression du gène d'intérêt dans une structure cible, ou de manière cellule spécifique afin d'évaluer le sauvetage ou non du phénotype. Les stratégies qui permettent de diminuer l'expression du gène d'intérêt et qui reposent sur l'utilisation de shRNA par exemple ne sont pas assez efficaces avec les récepteurs nicotiniques.

Ces études *ex vivo* sont à mettre en parallèle d'études *in vivo* qui permettent d'évaluer la réponse à la nicotine des neurones dopaminergiques et la libération de la DA dans les structures cibles, tout en conservant les afférences et efférences des circuits dopaminergiques. Les neurones DA de la VTA répondent à une injection intraveineuse de nicotine par une augmentation de la fréquence de décharge régulière et en *bursts* (Eddine et al., 2015; Forget et al., 2018; Mameli-Engvall et al., 2006; Schilström et al., 2003). Notamment, les neurones dopaminergiques répondent à partir d'une dose classiquement renforçante dans des paradigmes d'auto-administration (Forget et al., 2018; Fowler et al., 2011; Harrington et al., 2016; Morel et al., 2014) et l'amplitude de la réponse est dose-dépendante (Eddine et al., 2015; Forget et al., 2018; Morel et al., 2014). Cette réponse est associée à une augmentation de libération de DA dans les structures cibles (Blaha et al., 1996) qui conduit à l'activation des voies de signalisation (ERK) des récepteurs D1 (Valjent et al., 2004). Plus récemment, le laboratoire a montré que les neurones DA qui projettent vers l'amygdale répondent par une inhibition suite à une injection de nicotine, ce qui conduit à une augmentation de l'anxiété (Eddine et al., 2015; Nguyen et al., 2020, **Annexes**). L'implication du système dopaminergique dans les effets négatifs sera discutée dans la dernière partie de ce manuscrit.

D'un point de vue mécanistique, des études basées sur la réexpression de sous-unités nicotiniques (**Box 3.2**) dans la VTA ont permis de faire le lien entre les théories d'apprentissages par renforcement et la réponse à la nicotine des neurones DA. La réponse à la nicotine en fréquence et en *burst* des neurones DA est absente chez la souris $\beta2^{-/-}$, et cette altération est associée à une absence des comportements d'auto-administration de

nicotine (Maskos et al., 2005; Pons et al., 2008; Tolu et al., 2013). La réexpression de la sous-unité β2 seulement dans les neurones DA de la VTA (KOβ2^{DA}) est suffisante pour rétablir la réponse en fréquence, mais pas en *burst,* et ces souris ne présentent pas d'activation de la voie de signalisation des récepteurs D1 suite à une injection de nicotine (Tolu et al., 2013). Les souris KOβ2^{DA} s'auto-administrent transitoirement de la nicotine ; ce comportement ne persiste pas dans le temps, au contraire des souris de type sauvage. Les souris α4$^{-/-}$ présentent le même profil que ces souris KOβ2^{DA}, c'est-à-dire une absence de réponse en *burst* et une préférence transitoire pour le bras renforcé (Exley et al., 2011; Pons et al., 2008). La réexpression de la sous-unité β 2 à la fois dans les neurones DA et GABAergiques est suffisante pour rétablir la réponse en fréquence et en *burst* des neurones DA, et pour activer la voie de signalisation ERK dans le NAcc. Ces souris sont capables de renforcer des comportements de consommation de nicotine (Maskos et al., 2005; Pons et al., 2008; Tolu et al., 2013). De la même manière, le comportement est rétabli chez les souris α4$^{-/-}$ après la réexpression de la sous-unité α4 dans la VTA (Pons et al., 2008).

Les sous-unités α5 et α6 qui peuvent être inclues dans les récepteurs α4β2 jouent un rôle dans la sensibilité des réponses à la nicotine des neurones DA ou dans la libération terminale de dopamine dans le NAcc, ce qui n'altère pas dramatiquement les comportements d'auto-administration (Exley et al., 2011, 2013; Morel et al., 2014).

L'action de la nicotine au sein de la VTA est incontestablement l'élément le plus déterminant pour l'initiation de la dépendance à la nicotine. Les mécanismes moléculaires et cellulaires impliqués sont complexes, et il est important de prendre en compte les dynamiques d'activation et de désensibilisation des récepteurs. Pour cela, nous avons développé une stratégie de pharmacologie optogénétique, qui confère l'avantage de pouvoir agir sur un sous-type de nAChR, avec des résolutions temporelle et spatiale compatibles avec les cinétiques de la transmission neuronale (Chapitre V). L'étude que nous avons réalisée apporte des éléments de réponse sur l'implication des dynamiques d'activation des récepteurs, et permet d'étudier le rôle des nAChR dans le renforcement à la nicotine et dans les processus d'apprentissage par renforcement.

4. Chapitre 4 : La voie habénulo-interpédonculaire et nicotine

Les drogues d'abus induisent également des effets aversifs ou encore nocifs qui s'opposent à leurs effets récompensants. Les effets aversifs sont induits soit directement lors de la prise de drogue, soit lors des périodes d'abstinence (Jhou et al., 2013; Kenny and Markou, 2001; Riley, 2011). Relativement peu étudiés en comparaison aux mécanismes sous-tendant le renforcement, ces effets aversifs pourraient pourtant jouer un rôle clé dans les comportements de consommation de drogue d'abus (Fowler and Kenny, 2014; Koob and Le Moal, 2008; Kozlowski and Herman, 1984).

Les effets aversifs associés à la consommation de nicotine vont être principalement transmis par la voie habénulo-interpédonculaire (Antolin-Fontes et al., 2015; Dani and De Biasi, 2013; Fowler and Kenny, 2014; Molas et al., 2017a). Elle joue en effet un rôle central dans l'aversion à la nicotine, dans l'émergence de symptômes de manque consécutifs à une période d'abstinence (Frahm et al., 2011; Salas et al., 2009; Zhao-Shea et al., 2013) et dans la régulation de la consommation de nicotine (Ables et al., 2017; Antolin-Fontes et al., 2020; Fowler et al., 2011; Tuesta et al., 2017). Anatomiquement, cette voie permet de faire le lien entre le cerveau antérieur qui exerce les fonctions exécutives, et les structures postérieures impliquées dans les processus liés à la récompense ou aux états émotionnels. D'un point de vue de la dépendance à la nicotine, le rôle des signaux aversifs de la voie habénulo-interpédonculaire dans la régulation de la prise de nicotine, et les acteurs moléculaires et cellulaires impliqués dans ce processus, sont encore aujourd'hui mal connus.

4.1. La voie habénulo-interpédonculaire

L'habénula est une structure épithalamique très conservée phylogénétiquement et présente chez pratiquement tous les vertébrés (Aizawa et al., 2011, **Fig 4.1**). Elle contribue à l'apprentissage par renforcement, au contrôle d'états aversifs (Hikosaka, 2010; Matsumoto and Hikosaka, 2007; Molas et al., 2017a), et joue un rôle central dans la régulation des effets négatifs des drogues d'abus (Fowler and Kenny, 2014; Hu et al., 2020; Meye et al., 2017). L'habénula est un noyau asymétrique chez certaines espèces (les poissons, les amphibiens et les reptiles), mais symétrique chez les mammifères et les oiseaux. Le point commun entre toutes les espèces est la présence du *fasciculus retroflexus* (FR) qui est la voie de sortie des neurones de l'habénula, et qui longe l'épithalamus jusqu'au mésencéphale (**Fig 4.2**). Chez les mammifères, l'habénula est située au niveau dorso-médial du thalamus postérieur, de manière adjacente au 3ème ventricule. Ce noyau est divisé en deux structures : l'habénula latérale (LHb) et l'habénula médiale (MHb) (Aizawa et al., 2011; Andres et al., 1999, **Fig 4.1b**) qui se distinguent par leurs localisations anatomiques, leurs identités moléculaires et leurs afférences et efférences (Aizawa et al., 2011; Hikosaka, 2010).

La LHb est constituée majoritairement de neurones glutamatergiques (Aizawa et al., 2011; Herzog et al., 2004; Lammel et al., 2012) et dans une moindre mesure d'interneurones GABAergiques (Flanigan et al., 2020; Webster et al., 2020). Les neurones glutamatergiques de la LHb projettent sur les noyaux sérotoninergiques, DA et sur le RMTg (**Chapitre III**). La LHb, en régulant les systèmes monoaminergiques, joue un rôle central dans les processus

motivationnels, la prise de décision, et est impliquée dans des maladies psychiatriques (Hikosaka, 2010; Hu et al., 2020; Lecca et al., 2014; Nuno-Perez et al., 2018).

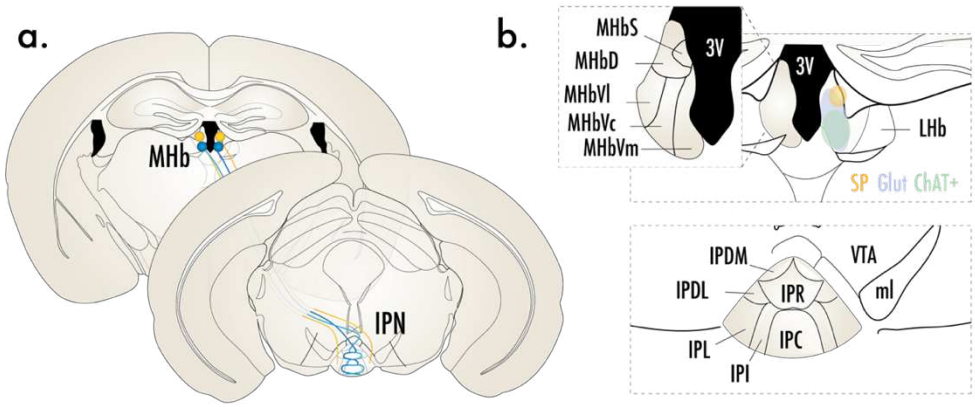

Figure 4.1 | La voie habénulo-interpédonculaire : a. Représentation de la voie habénulo-interpédonculaire sur des coupes coronales. Les neurones de la MHb dorsale projettent sur l'IPN latéral et les neurones de la MHb ventrale projettent sur l'IPN médial en croisant plusieurs fois la ligne médiale. **b.** Les sous-noyaux de la MHb et de l'IPN.

La voie habénulo-interpédonculaire est composée des neurones de la MHb qui projettent sur l'IPN (**Fig 4.1a**). La MHb est située proche du 3ème ventricule chez le rongeur tandis qu'elle est plus dorsale et entoure la LHb chez l'homme (Aizawa et al., 2011; Antolin-Fontes et al., 2015; Hu et al., 2020). Elle est subdivisée en cinq noyaux (Aizawa et al., 2012; Wagner et al., 2014, **Fig 4.1b**), deux au niveau dorsal et trois au niveau ventral (chez le rongeur) qui ont été définis notamment selon les projections distinctes au sein de l'IPN. Les neurones glutamatergiques sont ubiquitaires dans la MHb, mais les parties ventrale et dorsale se distinguent par leurs types neuronaux : la MHb dorsale (MHbD) est constituée de neurones à substance P, tandis la MHb ventrale, qui regroupe les noyaux ventrolatéral (MHbVl), ventrocentral (MHbVc) et ventromédial (MHbVm), est constituée de neurones cholinergiques et de neurones qui co-libèrent de l'ACh et du glutamate (Aizawa et al., 2012; Ren et al., 2011). La MHb projette quasiment exclusivement sur l'IPN, via le FR.

L'IPN est un noyau impair du mésencéphale qui est subdivisé en 3 noyaux impairs et 4 paires (Hemmendinger and Moore, 1984). Les noyaux impairs sont localisés sur la ligne médiane et comprennent l'IPN apical, caudal et rostral (IPA, IPC, IPR) alors que les structures paires sont les noyaux dorsomédial, dorsolatéral, intermédiaire et latéral (IPDM, IPDL, IPI et IPL). L'IPN est constitué principalement de neurones de projection et d'interneurones GABAergiques. Il existe une proportion de neurones à somatostatine ou à parvalbumine qui sont localisés dans l'IPN dorsal, tandis que les neurones glutamatergiques, bien qu'en faible proportion, sont localisés dans l'IPL (Hsu et al., 2013; Quina et al., 2017). La projection des neurones de la MHb respecte la topographie des sous-noyaux de l'IPN, suivant une rotation à 90° où la MHb dorsale contacte l'IPN latéral, la MHb médiale connecte l'IPN ventral et la MHb latérale contacte l'IPN dorsal (Herkenham and Nauta, 1979). Les projections cholinergiques croisent plusieurs fois la ligne médiane au niveau de L'IPR et de l'IPC, tandis que les projections des neurones SP+ sont ipsilaterales et projettent sur l'IPL (Molas et al., 2017a, **Flg 4.1**).

4.2. Afférences et efférences

La MHb fait le pont entre les structures du télencéphale, notamment des noyaux sous-corticaux, et les systèmes de neuromodulation (ACh, sérotonine) grâce au relais principal de l'IPN (**Fig 4.2**). Les afférences majoritaires de la MHb proviennent du septum. Les projections du septum médial (MS, *medial septum*) et du *nucleus of diagonal band* (NBD) sont principalement GABAergiques tandis que les afférences en provenance du septum postérieur sont majoritairement glutamatergiques (Otsu et al., 2018; Yamaguchi et al., 2013) et potentiellement purinergiques (Robertson and Edwards, 1998). Les afférences GABAergiques sont cependant excitatrices dans la MHb (Choi et al., 2016; Kim and Chung, 2007; Zhang et al., 2016). Le septum postérieur, qui est formé du *septofimbrial nucleus* (SFi), du *triangular septum* (TS) et le *bed nucleus of the anterior commissure* (BAC), présente une ségrégation anatomique de ces projections. Notamment, le TS projette vers la MHb ventrale tandis que la BAC projette sur la MHb dorsale (Yamaguchi et al., 2013). D'autres structures projettent vers la MHb comme la VTA, le locus cœruleus et le raphé (Antolin-Fontes et al., 2015; McLaughlin et al., 2017).

L'IPN contacte les systèmes neuromodulateurs tels que les noyaux sérotoninergiques du raphé, les noyaux cholinergiques du pont, et indirectement le système dopaminergique (**Fig 4.2**). Les connexions entre l'IPN et la VTA ne sont pas réciproques et seules les projections des neurones DA de la VTA vers l'IPN ont été mises en évidence fonctionnellement (DeGroot et al., 2020; Molas et al., 2017b; Zhao-Shea et al., 2015). Les neurones de l'IPN projettent principalement sur le raphé médian et dorsal ainsi que sur le tegmentum laterodorsale (LDTg) et dorsal (DTg). L'IPN peut alors agir sur le système dopaminergique grâce au relais des noyaux du pont et du raphé (Hsu et al., 2013; Morales and Margolis, 2017; Quina et al., 2017; Wolfman et al., 2018). L'IPN exerce également un contrôle inhibiteur sur le *nucleus incertus*, le *central gray of the pont* (CGPn) et la partie médiale de la LHb (Lima et al., 2017; Quina et al., 2017). En plus des afférences massives de la MHb, l'IPN reçoit des projections du raphé, du LDTg, du nucleus incertus, de la LHb, et du *nucleus tractus solitarus* (NTS). (Lima et al., 2017; Quina et al., 2017).

Une étude a récemment montré que les projections vers l'hippocampe et le septum proviennent de l'IPA, un noyau sérotoninergique et glutamatergique de l'IPN qui est en continuité du raphé médian. Les auteurs de cette étude proposent que, de par les types neuronaux et les efférences de l'IPA, ce sous-noyau ferait plutôt partie du raphé que de l'IPN (Quina et al., 2017), ce qui remet en question les projections de l'IPN vers le cerveau antérieur, étant donné que c'est principalement l'IPA qui projette de manière antérieure.

4.3. La transmission nicotinique de la voie habénulo-interpédonculaire

La voie habénulo-interpédonculaire présente une des densités les plus importantes en récepteurs nicotiniques du SNC et une des plus fortes diversités en nAChR puisque, à l'exception de α9 et α10, toutes les sous-unités nicotiniques y sont exprimées (Beiranvand et al., 2014; Hsu et al., 2013; Shih et al., 2014). Les nAChR sont principalement exprimés au niveau de la MHb ventrale et au niveau de l'IPN médial (IPR, IPC, IPDL, IPDM), qui corresponds à l'axe cholinergique de cette voie. Dans l'habénula médiale, les sous-unités

les plus abondamment exprimées sont les sous-unités α3 et β4, et dans une moindre mesure α4, α6, β2 et β3. En addition de ces sous-unités, les neurones de l'IPN expriment aussi les sous-unités α5 et α7 (Hsu et al., 2013; Zhao-Shea et al., 2013). Bien que précédemment débattue, la présence de la sous-unités α5 dans la voie MHb-IPN chez la souris est en fait circonscrite aux neurones de l'IPN rostral, d'après les marquages obtenus chez la souris transgénique exprimant la GFP sous le contrôle du promoteur α5 (Hsu et al., 2013; Morton et al., 2018), mais elle est présente dans la MHb des rats.

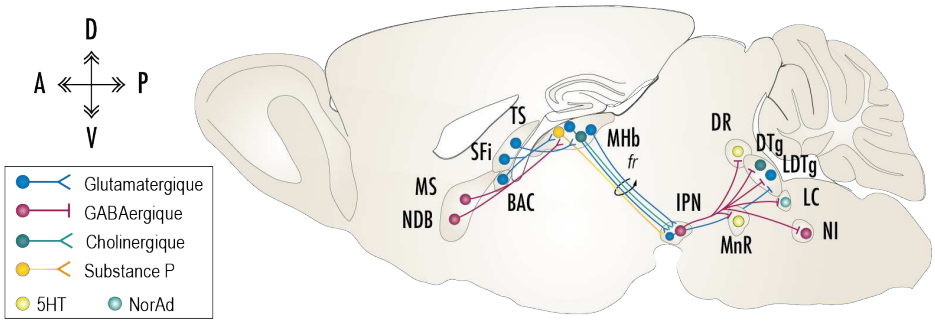

Figure 4.2 | Afférences et efférences : Représentation des afférences et éfferences principales de la voie habénulo-interpédonculaire. *NDB : nucleus of diagonal band, MS : medial septum, SFi : septofimbrial nucleus, TS : triangular septum, BAC : bed nucleus of the anterior commissure, MHb : habénula médiale, IPN : noyaux interpédonculaire, MnR : raphé médian, DR : dorsal raphé, DTg : dorsal tegmentum, LDTg : laterodorsal tegmentum, LC : locus coeruleus, NI : nucleus incertus.*

Les neurones cholinergiques de la MHb expriment des transporteurs vésiculaires glutamatergiques, notamment VGlut1 et VGlut2 (Aizawa et al., 2012), et l'activation optogénétique de ces neurones induit une co-libération d'ACh et de glutamate (Ren et al., 2011; Soria-Gómez et al., 2015; Zhang et al., 2016). Une fois libérée dans l'IPN, l'ACh va agir sur les nAChRs somatodendritiques des neurones de l'IPN et au niveau des terminaisons axonales, en provenance de la MHb ou des interneurones, et induire respectivement une augmentation de l'excitabilité des neurones et une facilitation de la libération de neurotransmetteur (Grady et al., 2009; Léna et al., 1993). Notamment, il a été montré que la facilitation de libération de neurotransmetteur passe uniquement par les récepteurs α3β4* des neurones cholinergiques (Grady et al., 2009). La MHb possède une forte densité de nAChRs mais la source d'ACh et les mécanismes qui permettent l'activation des nAChR somatodendritiques sont à ce jour inconnus.

De manière intéressante d'un point de vue de l'addiction à la nicotine, on retrouve dans cette voie une forte densité des sous-unités α5, α3 et β4 (Beiranvand et al., 2014; Grady et al., 2009; Shih et al., 2014). Ces trois sous-unités sont codées par le cluster de gènes CHRNA5-A3-B4 du chromosome humain 15q25. Des études de génétique humaine ont montré une association forte entre ce locus, la dépendance à la nicotine – en terme de nombre de cigarettes fumées par jour, et de sévérité de dépendance en fonction de l'âge d'initiation – et la survenue du cancer du poumon (Bierut et al., 2008; Keskitalo et al., 2009; Wang et al., 2009). La présence non négligeable des sous-unités α5, α3 et β4 au niveau de la voie habénulo-interpédonculaire, couplée aux études génétiques réalisées chez l'humain et aux études physiologiques réalisées sur des modèles animaux, suggère que cette voie joue un rôle clé dans les mécanismes d'aversion, de manque et de rechute.

4.4. Rôles physiologiques de la voie habénulo-interpédonculaire

Plusieurs études se sont efforcées à déterminer le rôle physiologique de cette voie et ont permis de mettre en évidence son implication dans la régulation des états émotionnels négatifs tels que la peur, l'anxiété, ou l'aversion. Chez la souris, des études princeps de lésions électriques/pharmacologiques de l'habénula ou de l'IPN ont mis en évidence des altérations des comportements d'évitement (Vale-Martínez et al., 1997; Wirtshafter, 1980) et du niveau d'anxiété (Murphy et al., 1996). Ces résultats ont été confirmés avec des stratégies plus spécifiques qui permettent d'inactiver les neurones de la MHb sans altérer la LHb. Notamment, le blocage de la transmission neuronale grâce à la toxine tétanique, ou la lésion à la nitroréductase dans une population spécifique de l'habénula dorsale du zebrafish, l'orthologue de la MHb, ont révélé un déficit d'apprentissage des conditionnements de peur et une anxiété anormale (Agetsuma et al., 2010; Lee et al., 2010; Mathuru and Jesuthasan, 2013). Des altérations fonctionnelles similaires ont été retrouvées chez le rongeur dans une étude qui inactive sélectivement les neurones de la MHb (Kobayashi et al., 2013, **Box 4.1**).

Box 4.1 | Peur et anxiété :

La peur et l'anxiété sont des réactions comportementales défensives innées qui ont évolué pour permettre à l'organisme de réduire ou éviter les préjudices physiques ou psychiques et ainsi assurer sa survie. **L'anxiété** est induite par une menace potentielle non identifiable et non localisable, et incite l'animal à suspendre ses comportements en cours et à augmenter son niveau d'éveil en vue de l'évaluation du danger potentiel. Les tests en *open field* et *elevated plus maze* sont largement utilisés et ont été validés pharmacologiquement. **La peur** est induite par une menace imminente et identifiable, et suscite des comportements tels que la fuite, le « *freezing* » et le combat (attaque défensive) en fonction de l'imminence de la menace entrante et de la possibilité de fuite (distance défensive). Chez les rongeurs elle est évaluée en réponse à un stimulus aversive (i.e. choc électrique) et lors de conditionnement de peur.

Les mécanismes neuronaux qui sous-tendent une anxiété exacerbée ou la peur en réponse à un stimulus aversif ont souvent été associés aux circuits de l'amygdale (Tovote et al., 2015), mais des études plus récentes semblent impliquer également la voie MHb-IPN. Longtemps décrites comme étant purinergiques, les afférences du septum postérieur seraient exclusivement glutamatergiques et l'activation optogénétique de cette voie conduit à une diminution de l'anxiété (Otsu et al., 2018). Deux circuits distincts de la voie septo-habénulaire, dont l'un émerge du *triangular septum* et l'autre du *bed nucleus of the anterior commissure*, auraient des rôles respectifs dans l'anxiété et la peur. L'utilisation d'une immunotoxine a permis d'inactiver spécifiquement chacune des deux voies chez la souris. L'inactivation de la voie TS-MHbv, qui projette vers l'IPN médial, induit une diminution de l'anxiété, tandis que l'inactivation de la voie BAC-MHbd qui projette vers l'IPN latéral induit une augmentation des réponses de peur induites par un choc électrique et un déficit de l'association négative dans un paradigme de conditionnement de peur (Yamaguchi et al., 2013). La séparation anatomo-fonctionnelle décrite dans (Yamaguchi et al., 2013) est intéressante mais ne corrobore pas les données de la littérature, qui montrent que la signalisation présynaptique des neurones cholinergiques de la MHb ventrale – supposée signaler l'anxiété seulement –, est déterminante pour le conditionnement de peur, tandis qu'une lésion des neurones de la MHb dorsale n'aurait quant à elle pas d'effet sur le conditionnement de peur (Hsu et al., 2016; Soria-Gómez et al., 2015; Zhang et al., 2016).

La voie habénulo-interpédonculaire est également impliquée dans l'apprentissage par renforcement de stimuli appétitifs et aversifs. Une signalisation glycinergique excitatrice, qui est régulée par la libération de glycine gliale, a été mise en évidence dans la MHb. Cette signalisation est inhabituelle parce qu'elle passe par l'activation de récepteurs NMDA non conventionnels, constitués des sous-unités GluN1/GluN3A, et activables uniquement par la glycine. Une réduction de l'expression des récepteurs GluN1/GluN3A bloque l'acquisition d'un conditionnement aversif (Otsu et al., 2019), mais n'a aucun effet sur le conditionnement de peur. De plus, une activation optogénétique des neurones de l'IPN, ou des afférences GABAergiques de l'IPN sur le LDTg, induit une aversion de place dans un paradigme de conditionnement de place en temps réel (Wolfman et al., 2018). Lorsque la stimulation optogénétique est spécifique des neurones de l'IPN qui expriment la sous-unité α5, les effets négatifs se mettent en place seulement lorsque la tâche est répétée le lendemain, ou suite à une pré-stimulation optogénétique (Morton et al., 2018). Cela suggère que l'activation répétée des neurones de l'IPN jouerait un rôle dans la consolidation d'une mémoire aversive. De manière paradoxale, les animaux sont capables de travailler pour activer la voie habénulo-interpédonculaire *via* une stimulation électrique intra-crâniale de l'habénula ou du *fasciculus retroflexus* ou par activation optogénétique des neurones de la MHb dorsale (Hsu et al., 2016; Sutherland and Nakajima, 1981).

Finalement, l'activation ou l'inhibition optogénétique des neurones de l'IPN ou des afférences de la MHb / VTA sur l'IPN altèrent les comportements exploratoires des animaux face à un stimulus nouveau ou familier. Cette étude a mis en évidence que les afférences excitatrices de la MHb et dopaminergiques de la VTA sur l'IPN, en régulant l'activité des neurones GABAergiques de l'IPN, déterminent les réactions comportementale en assignant une saillance motivationnelle aux informations nouvelles par rapport aux informations familières (Molas et al., 2017b).

Ces différentes études décrivent des résultats contradictoires, parfois surprenants, avec des effets opposés sur l'anxiété ou la signalisation de stimulus appétitifs et aversifs. Cela pourrait s'expliquer par l'existence d'afférences synaptiques complexes, de sous-circuits distincts ou par l'état des animaux. Globalement, la voie habénulo-interpédonculaire permettrait d'une part de moduler directement l'état émotionnel d'un individu ou de percevoir la saillance d'un stimulus, et d'autre part de contribuer à la consolidation d'un souvenir aversif.

De par sa densité en nAChR, la voie habénulo-interpédonculaire est particulièrement sensible à l'action de la nicotine. Puisque cette voie est impliquée à la fois dans la mémoire aversive, et dans les états émotionnels négatifs, plusieurs études ont cherché à comprendre quels sont, au niveau de cette voie, les mécanismes moléculaires et cellulaires qui sous-tendent l'expression de comportement aversif à la nicotine.

4.5. Les effets négatifs dans le contexte de la dépendance à la nicotine

Comme nous l'avons rappelé précédemment, la prise de nicotine conduit à des effets aversifs qui sont induits soit directement par l'action pharmacologique de la nicotine, soit par le manque de nicotine. Ces deux types d'effets négatifs de la nicotine pourraient en partie passer par la voie MHb-IPN.

L'aversion pharmacologique induite par la nicotine a été décrite lors d'analyses des réponses comportementales en dose-réponse, qui ont révélé la présence d'effets négatifs aux fortes doses de nicotine (**Chapitre II**). Dans un paradigme de préférence de place, la dose classiquement utilisée pour induire du renforcement à la nicotine est de 0,5 mg/kg (Durand-de Cuttoli et al., 2018; Walters et al., 2006) tandis que celle utilisée pour faire de l'aversion est généralement supérieure à 1,5 mg/kg (Grieder et al., 2010; Wolfman et al., 2018). De telles doses aversives de nicotine (1,5 mg/kg) induisent dans l'IPN une augmentation du marquage *cfos,* un facteur de transcription immédiat précoce qui reflète l'activation neuronale (Fowler et al., 2011), avec une absence de marquage aux doses renforçantes. Les doses de nicotine qui induisent une aversion sont largement diminuées chez des souris transgéniques (souris TABAC) qui surexpriment la sous-unité β4 aux sites endogènes, c'est-à-dire principalement dans la voie MHb-IPN (Frahm et al., 2011). Cette altération comportementale est restaurée lorsque la sous-unité α5 est exprimée dans la MHb, *via* une réduction supposée la transmission nicotinique. Cependant, l'expression de la sous-unité α5 est complètement ectopique puisque celle-ci n'est pas présente de manière endogène dans la MHb chez la souris (Hsu et al., 2013), mais serait présente chez le rat. Ces études suggèrent néanmoins que l'activation par la nicotine de la voie habénulo-interpédonculaire induit de l'aversion. En accord avec cette hypothèse, l'inhibition optogénétique des terminaisons axonales de l'IPN dans le LDTg abolit l'aversion à la nicotine (injection systémique), mettant en lumière le rôle de l'activation de l'IPN dans la traduction des effets aversifs de la nicotine (Wolfman et al., 2018).

Des symptômes de manque peuvent apparaître suite à un arrêt brusque de consommation de nicotine. Un rongeur soumis à une exposition chronique de nicotine présente des symptômes de manque lors d'une période d'abstinence ou suite à une injection intrapéritonéale de mécamylamine, qui est un bloqueur du canal des nAChR (Grieder et al., 2010; Perez et al., 2015; Salas, 2004). L'induction des symptômes de manque par la mécamylamine chez la souris induit une augmentation du nombre de neurones *cfos*+ dans l'IPN et la MHb (Shih et al., 2014; Zhao-Shea et al., 2013, 2015), et une augmentation de la fréquence des courants post-synaptiques excitateurs (EPSCs) dans l'IPN (Zhao-Shea et al., 2013), ce qui suppose que la voie MHb-IPN s'active lorsque les animaux présentent des symptômes de manque. Lorsque que les nAChR de la voie Hb-IPN sont inhibés par une injection locale de mécamylamine dans la MHb ou dans l'IPN, les souris présentent des symptômes de manque physiques et affectifs (Salas et al., 2009; Zhao-Shea et al., 2013, 2015), ce qui suggère que l'altération de la transmission nicotinique joue un rôle déterminant dans le manque. Depuis, il a été montré que ces effets sont médiés par les nAChR β4*. En effet, les souris $\beta4^{-/-}$ ne présentent pas de symptômes de manque physique à la nicotine, et surtout, l'inhibition des nAChR β4* de la MHb ou de l'IPN, *via* une injection locale d'un antagoniste sélectif des récepteurs α3β4*, est suffisante pour induire des symptômes de manque (Salas et al., 2009; Zhao-Shea et al., 2013, 2015).

La voie habénulo-interpédonculaire est donc impliquée dans les effets aversifs aigus induits par la nicotine, qui ont tendance à limiter la consommation, et les effets négatifs en réponse à un manque d'apport de nicotine, qui incitent les individus à re-consommer ou consommer plus.

4.6. Rôle de la voie MHb-IPN dans la régulation de la prise de nicotine

La voie habénulo-interpédonculaire a également été impliquée dans la régulation de la prise de nicotine. Une avancée majeure a été faite dans la compréhension des récepteurs et circuits impliqués dans le contrôle de la consommation, par la découverte de variations alléliques qui augmentent les risques d'addiction, notamment dans le cluster de gènes codant les sous-unités α5, β4 et α3 qui sont largement exprimées dans la voie Mhb-IPN. Par exemple, la présence chez l'homme, en un ou deux exemplaires, du polymorphisme nucléotidique (single nucleotide polymorphism, ou SNP) α5 D398N conduit à une consommation de tabac de deux à trois fois plus importante (Bierut et al., 2008). Ce polymorphisme nucléotidique diminue la fonction des récepteurs contenant α5 (George et al., 2012; Kuryatov et al., 2011). Les souris $\alpha5^{-/-}$ montrent une consommation de nicotine nettement supérieure aux souris de type sauvage et, de manière importante, une sensibilité diminuée au niveau de l'IPN, comme le suggère la baisse de la densité des cellules marquées *cfos* dans l'IPN après une injection de nicotine (Fowler et al., 2011). L'expression virale d'α5 dans la MHb chez la souris $\alpha5^{-/-}$ restaure un profil de consommation WT (malgré l'absence de cette sous-unité dans la Mhb de souris), et le knockdown d'α5 dans la MHb de rat récapitule le profil knock-out souris, pointant vers un rôle de cette voie dans la régulation de la consommation.

Afin d'étudier l'effet du polymorphisme nucléotidique α5 D398N, l'équipe d'Uwe Maskos a généré des rats transgéniques α5 D398N. Ces rats s'auto-administrent plus de nicotine que les rats de type sauvage. De plus, ils montrent un taux de rechute induite par la nicotine bien supérieur aux animaux de type sauvage Cette rechute est associée à une hypoactivation des neurones de l'IPN et une altération des courants nicotiniques de l'IPN (Forget et al., 2018, Annexes). Cette étude, en accord avec les études précédentes (Fowler et al., 2011), confirme qu'une diminution fonctionnelle des récepteurs α5* conduit à une consommation plus élevée, et implique pour la première fois l'IPN dans la rechute. Les récepteurs β4* de l'IPN jouent aussi un rôle déterminant dans la régulation de la consommation. Comme nous l'avons vu plus haut, les souris TABAC qui surexpriment β4 présente une aversion à la nicotine plus forte que les souris WT, et donc consomment très peu de nicotine (Frahm et al., 2011; Ślimak et al., 2014). D'une manière générale, les manipulations des niveaux d'expression de la sous-unité β4 dans la MHb et l'IPN résultent en une altération de la régulation de la consommation de nicotine, même si les résultats sont parfois contradictoires (Frahm et al., 2011; Gallego et al., 2012; Harrington et al., 2016; Husson et al., 2020; Ślimak et al., 2014).

Par ailleurs, un lien vient d'être établi entre le circuit MHb-IPN, la consommation de nicotine et le diabète. La nicotine peut augmenter le taux de sucre dans le sang chez l'homme, et les fumeurs ont un risque beaucoup plus élevé de diabète que les non-fumeurs. Les antidiabétiques, qui stimulent la production de glucagon-like peptide-1 (GLP-1), diminuent la consommation de nicotine chez les souris. Il a été montré que l'activation optogénétique des neurones GLP-1 du *nucleus tractus solitarus* (NTS) excite les projections de la MHb sur l'IPN, et diminue la consommation de nicotine (Tuesta et al., 2017). De plus, les rats ayant un dérèglement dans leur facteur de transcription 7-like 2 (Tcf7l2), qui est

fortement exprimé dans la MHb, montrent une consommation en nicotine nettement plus importante que les rats témoins, et une augmentation de sucre dans le sang en réponse à la nicotine réduite (Duncan et al., 2019). Les rats ayant une activité réduite de Tcf7l2 n'ont donc pas subi les effets de la nicotine qui favorisent le diabète.

La régulation de la consommation de nicotine fait aussi intervenir d'autres circuits que la voie MHb-IPN, et notamment la VTA. En effet, la VTA des souris $\alpha5^{-/-}$ ou α5D398N montre une diminution de la sensibilité à la nicotine, ce qui pourrait également expliquer pourquoi ces souris ont besoin de doses plus fortes pour activer le système de renforcement à cette drogue. La réexpression d'α5 dans la VTA permet de restaurer le phénotype sauvage. De manière assez inattendue, les neurones DA de la VTA répondent à des doses plus faibles de nicotine chez la souris $\beta4^{-/-}$, malgré la faible expression de cette sous-unité dans cette région du cerveau. Pour autant, ces souris s'auto-administrent moins que les souris WT (Harrington et al., 2016), sauf à forte dose (Husson et al., 2020). Cette fois ci ce n'est pas la réexpression dans la VTA qui permet de restaurer le phénotype observé mais la réexpression de la sous-unité β4 dans l'IPN. Malgré l'absence de connexion directe des neurones de l'IPN sur la VTA, il semblerait que l'IPN puisse moduler la transmission nicotinique des neurones DA.

Plusieurs hypothèses permettraient d'expliquer comment la voie habénulo-interpédonculaire est impliquée dans la régulation de la consommation de nicotine. La première, qui est discutée dans les articles de Paul Kenny, serait que cette voie joue un rôle de « senseur de satiété », qui permettrait aux individus de réguler leur consommation (Fowler and Kenny, 2014). Dans ce cas, la question serait de savoir quels sont les partenaires moléculaires et cellulaires qui jouent le rôle de senseur. Sachant le rôle crucial de cette voie dans la signalisation et la consolidation de stimuli aversifs, la seconde possibilité serait que la voie MHb-IPN viendrait s'opposer aux effets appétitifs de la nicotine en induisant de l'aversion. Cette hypothèse est alléchante, mais considérant que la même voie est impliquée dans l'émergence de symptôme de manque, il est nécessaire de comprendre, s'ils existent, quels sont les mécanismes/sous-circuits qui permettent à la fois de réduire la consommation de nicotine en signalisant des effets aversifs, et à la fois d'augmenter (ou ré-initier) la prise de nicotine en déclenchant des symptômes de manque.

5. Chapitre 5 : Stratégies de pharmacologie cellule-spécifique

L'addiction à la nicotine est un phénomène complexe qui implique d'une part des voies neuronales variées, et d'autre part des substrats moléculaires spécifiques tels que les récepteurs nicotiniques. Les régulations allostériques et les niveaux d'expression des nAChR sont au centre des mécanismes d'adaptations moléculaires qui sous-tendent la dépendance à la nicotine. Comprendre comment ces dynamiques d'activation, de désensibilisation et d'*uprégulation* des nAChR au sein de circuits spécifiques sont impactées au cours de la dépendance à la nicotine est encore aujourd'hui un défi. Les outils actuels, génétiques ou pharmacologiques, présentent certaines limites. Les outils génétiques ont une spécificité moléculaire et potentiellement neuronale, mais ont une pauvre résolution temporelle et peuvent induire des phénomènes compensatoires. Les agents pharmacologiques ne permettent pas le ciblage cellulaire, manquent en général de spécificité, et ont des pharmacocinétiques beaucoup plus lentes que les mécanismes neuronaux mis en jeu.

L'optogénétique a fourni une boite à outils puissante qui permet de manipuler optiquement des circuits spécifiques avec une précision temporelle et génétique inégalable (Deisseroth, 2015). La découverte d'opsines microbiennes a été une opportunité pour les neurosciences. Au contraire de la rhodopsine des vertébrés, dont l'activation déclenche une cascade intracellulaire, les opsines microbiennes transforment directement les photons en courant électrique (Nagel et al., 2003). Les opsines microbiennes sont des canaux ioniques ou des transporteurs dont l'expression exogène permet d'activer ou d'inhiber une population neuronale spécifique (Boyden et al., 2005; Zhang et al., 2007). Le contrôle optogénétique de l'activité électrique des neurones a permis de faire un lien causal entre circuits et comportements. Il demeure néanmoins crucial de comprendre quels sont les acteurs moléculaires qui pilotent les circuits neuronaux. Obtenir une vision de la dynamique d'activation des canaux ioniques ou des récepteurs nécessite le développement d'outils à haute résolution temporelle et spatiale pour perturber leurs fonctions.

Afin de surmonter ces limites, j'ai mis en place une technique innovante, la pharmacologie optogénétique, qui permet de contrôler optiquement, localement et de manière réversible, un sous-type de nAChR, chez la souris en comportement. Le principe de cette technique repose sur l'attachement covalent d'un ligand photosensible sur un récepteur natif modifié génétiquement, afin de permettre la photo-inhibition rapide et réversible du récepteur modifié (Pour revue du contrôle optique des nAChR, Durand-de Cuttoli et al., 2017). La pharmacologie optogénétique, de par son ciblage génétique, permet en théorie de manipuler un récepteur dans un type de cellule spécifique. Il est ainsi possible de cibler les récepteurs postsynaptiques, en laissant les récepteurs présynaptiques intacts par exemple, ce qui est chose impossible à faire avec la pharmacologie classique. D'autres stratégies de pharmacologie cellule-spécifique ont été développées au cours des années précédentes. Dans la revue suivante, nous décrivons ces différentes stratégies, et discutons de la pertinence du ciblage cellulaire pour la pharmacologie expérimentale et clinique.

Trends in Pharmacological Sciences

CellPress
REVIEWS

Review

Cell-Specific Neuropharmacology

Sarah Mondoloni,[1,3] Romain Durand-de Cuttoli,[1,2,3] and Alexandre Mourot[1,3,*]

Neuronal communication involves a multitude of neurotransmitters and an outstanding diversity of receptors and ion channels. Linking the activity of cell surface receptors and ion channels in defined neural circuits to brain states and behaviors has been a key challenge in neuroscience, since cell targeting is not possible with traditional neuropharmacology. We review here recent technologies that enable the effect of drugs to be restricted to specific cell types, thereby allowing acute manipulation of the brain's own proteins with circuit specificity. We highlight the importance of developing cell-specific neuropharmacology strategies for decoding the nervous system with molecular and circuit precision, and for developing future therapeutics with reduced side effects.

Highlights

Targeting drugs to specific neuronal types usually requires genetic manipulation of either the target protein or the target cell.

Chemogenetic technologies that combine the speed of pharmacology with the cellular precision of genetics are emerging, enabling acute control of neuronal receptors with circuit specificity.

In vivo implementation of these technologies allows unprecedented control of brain circuits at the molecular level, and helps to unambiguously link the activity of specific receptors to behavioral functions.

Probing the Nervous System With Cell-Targeted Drugs

Investigating the function of neurotransmitter receptors and ion channels has greatly benefited from both pharmacological and genetic techniques. Conditional mutagenesis and virally-delivered **short hairpin RNAs** (**shRNAs**, see Glossary) enable the manipulation of proteins with molecular specificity in targeted brain circuits, notably through the use of **cre/lox recombination**. Yet, these techniques do not have sufficient temporal resolution to establish a direct link between the activation of receptors and the modulation of circuits and behavior. In addition, they can lead to developmental alterations that compensate for those induced by the deletion/mutation of the receptor. In contrast, conventional pharmacology offers acute and often reversible control of endogenous proteins, enables graded alterations by varying drug concentration, and can be applied at any time in development. Nevertheless, pharmacology suffers from lack of functional selectivity, since small chemicals affect all types of neurons and cannot be cell targeted. This is especially an issue considering the wide distribution of ion channels and receptors in the brain, and the various functions they have in different cells or networks. Local distribution of drugs to precise brain regions may afford anatomical specificity, but has major drawbacks, such as the difficulty to control dosage and diffusion, and the inability to target specific neuronal types. Making small chemicals photocontrollable using caged compounds or photoswitches permits cellular or even subcellular optical targeting at the single cell level, and improves spatiotemporal control *in vivo* [1,2]. Yet, even with the most sophisticated light source, controlling receptors located on different cell types within the same circuit in an intact brain is elusive with optical techniques alone. The ability to acutely control signaling proteins in a complex environment such as the nervous system in a cellular- and circuit-specific manner and in the behaving animal should accelerate progress in our molecular understanding of brain function (Figure 1A, Key Figure).

The idea behind cell-specific pharmacology is to combine the acute onset of pharmacology with the cellular and molecular precision of genetics, to achieve acute control of signaling proteins in a cell-specific fashion. To this aim, several chemogenetic strategies have recently been developed, which we classify here in three categories (Figure 1 and Table 1). The receptor–ligand pair approach (Figure 1B) consists of re-engineering proteins to make them sensitive to synthetic ligands. The key outcome is an increase in potency of the synthetic ligand compared with the natural one (Figure 1C). The **tethered**-ligand approach (Figure 1D) relies on the anchoring of a ligand to the cell surface and results in an increased local concentration of the ligand. Anchoring

[1]Neuroscience Paris Seine – Institut de Biologie Paris Seine (NPS – IBPS), CNRS, INSERM, Sorbonne Université, Paris, France
[2]Nash Family Department of Neuroscience, Center for Affective Neuroscience, and Friedman Brain Institute, Icahn School of Medicine at Mount Sinai, New York, NY, USA
[3]All the authors contributed equally to the work.

*Correspondence:
alexandre.mourot@upmc.fr (A. Mourot).

can be performed either to a membrane-embedded element (membrane-tethered) or to a genetically modified receptor (receptor-tethered). Finally, the last approach is to selectively deliver drugs to the cytoplasm of targeted cells, either using enzyme–prodrug pairs or facilitated diffusion through large ion channels (Figure 1E). Cell-specific neuropharmacology approaches provide the ability to test the function of receptors on specific types of neurons with unprecedented cellular precision (e.g., pre- vs postsynaptic cells, or two different cell types within the same circuit) [3,4]. They also offer a unique opportunity to test the benefits of cell-targeted drugs for neurological and neuropsychiatric disorders. We review here these techniques, with a special focus on surface receptors and ion channels, highlighting their potentials and pitfalls, and the challenges they meet for *in vivo* use in rodents and for clinical applications.

The Receptor–Ligand Pair Approach

One central problem of traditional pharmacology is to identify small molecules that interact with a desired protein target with high specificity. This is especially challenging for proteins that belong to large protein families and therefore share a high degree of homology with other proteins in the cell. To address this shortcoming, a chemogenetic strategy named **bump-hole** was developed, allowing inhibition of specific alleles of protein kinases [5]. The idea is to genetically create a hole on the catalytic active site of the protein, and to chemically modify the inhibitor, with a corresponding bump (Figure 1B). The synthetic ligand is **orthogonal**: it confers high specificity to the engineered enzyme, without affecting wild-type (WT) kinases. Importantly, the engineered kinase is a nonorthogonal mutant protein; that is, it can still phosphorylate endogenous substrates. A wide range of kinase–inhibitor pairs were generated, displaying incomparable potency and specificity compared with known inhibitors [5].

Inspired by this approach, neuroscientists developed orthogonal receptor–ligand pairs, the most widely used being the **designer receptors exclusively activated by designer drugs (DREADDs)** [6,7]. DREADDs are modified G-protein-coupled receptors (GPCRs) engineered through directed molecular evolution that are insensitive to their natural ligands but sensitive to synthetic agonists (Figure 2A). The original DREADDs (hM3Dq and hM4Di) are based on human M3 and M4 muscarinic receptors, which couple to Gq and Gi, respectively [6]. hM3Dq and hM4Di are made insensitive to acetylcholine (ACh), sensitive to the synthetic ligand clozapine-N-oxide (CNO), and importantly, show minimal basal activity in the absence of chemical activation (but see [8]). hM3Dq is classically used for enhancing neuronal activity, while hM4Di is used for neuronal inhibition. Newer DREADDs include GsD that couples to Gs, hM4D^{nrxn} that is axonally targeted and affords presynaptic inhibition, and a κ-opioid-derived DREADD (KORD) that operates with salvinorin B [9], a compound distinct from CNO, thus allowing multiplexed and bidirectional modulation of neuronal activity and behavior.

Receptor–ligand pairs have also been developed for ligand gated ion channels (LGICs, Figure 2B). The ligand-binding domain (LBD) of the α7 nicotinic acetylcholine receptor (nAChR), referred to as **pharmacologically selective actuator module (PSAM)**, was engineered to respond solely to synthetic molecules called **pharmacological selective effector molecules (PSEMs)** [10,11]. Activation of PSAM by PSEMs induces either cation, calcium, or chloride influx, depending on the ion pore domain (IPD) spliced onto the LBD (serotonin 5HT3, α7-nAChR or glycine receptor IPD, respectively). Hence PSAMs can be used to either drive or suppress neuronal activity, or to increase intracellular calcium, in genetically targeted neurons. DREADDS, and to a lesser extent PSAMs, have proven valuable tools for the manipulation of circuits with cellular specificity, providing crucial information as to how circuits shape behavior [7,12]. However, because they are no longer sensitive to their cognate ligands, DREADDs and PSAMs are constrained to decode the nervous system at the circuit level, and cannot be used for the

Glossary

Azobenzene: a chemical photoswitch that can be reversibly isomerized between an elongated *trans* state and a twisted *cis* isomer with short (classically near-UV) and long (blue-green) wavelengths of light, respectively.
BOLT, bio-orthogonal ligand tethering: ligand is conjugated to an UAA through click chemistry.
Bump-hole: strategy based on the enlargement of binding sites (holes) in proteins (initially enzymes) to make them selective to complementary 'bumped' ligands.
Click chemistry: orthogonal bioconjugation reaction that is rapid, biocompatible, and high yielding.
CM, cyclopropylmethyl carboxyl: masking group cleaved selectively by PLE.
Cre/lox recombination: genetic manipulation based on an enzyme, Cre recombinase, and its recognition site, lox P, used for tissue-specific gene expression.
DART, drugs acutely restricted by tethering: method for capturing drugs at the cell surface using a HaloTag.
DREADDs, designer receptors exclusively activated by designer drugs: engineered GPCRs that exclusively respond to synthetic ligands.
GPI (glycosylphosphatidylinositol) anchor: glycolipid that can be attached to the C terminus of a protein.
His-tag: tag made of 4–9 histidine residues (4 in the MAC technology) classically used for purification of recombinant proteins.
LOV domain, light-oxygen-voltage domain: blue light sensor from algae, plants, bacteria, and fungi, used to control cellular responses with light.
MAC, metal complex–agonist conjugate: bifunctional ligand containing a Ni^{2+}-nitrilotriacetic acid (Ni-NTA) moiety for selective coordination tethering to His-tagged receptors.
Maleimide, 1H-pyrrole-2,5-dione: cysteine-reactive chemical group.
NM, 2-nitro-N-methylimidazolyl: Masking group selectively unmasked with NTR.
NTR, nitroreductase: from *E. coli* used for selective reduction of NM groups.
Opto-XR: chimeric photocontrollable receptor engineered using opsins and the intracellular loops or N-terminal tail of mammalian GPCRs.

molecular dissection of the role of endogenous GPCR or LGIC signaling in the modulation of circuits and behaviors.

With the advent of optogenetics [13], light-based strategies for controlling brain proteins have emerged, affording improved spatiotemporal resolution over chemical approaches [1]. Notably, light-controllable adrenergic, opioid, serotoninergic, and glutamatergic GPCRs (**Opto-XRs**) have been engineered [14,15]. Opto-XRs are chimeric proteins, usually engineered with a mammalian opsin (e.g., rhodopsin or melanopsin) and the intracellular loops and C-terminal tail of endogenous GPCRs (Figure 2C). In addition to trafficking and signaling like their native counterparts, OptoXRs are photoactivatable, offering the possibility to mimic the spatiotemporal dynamics of neuromodulator signaling *in vivo*. Nevertheless, Opto-XRs bind retinal and therefore lack responsiveness to endogenous ligands, restricting their use, as with DREADDS, to a circuit-level understanding of brain function.

Dissecting the role of endogenous receptors and channels in behaviors requires maintaining their natural pharmacology and signaling properties. To this aim, two receptor–ligand pair-like approaches have been developed for $GABA_A$ receptors ($GABA_ARs$) and nAChRs. $GABA_AR$ signaling is potentiated by the allosteric modulator zolpidem, yet only when the γ2 subunit is present in the receptor. A single mutation (phenylalanine to isoleucine) at position 77 on the γ2 subunit is sufficient to convert a zolpidem-sensitive into a zolpidem-insensitive receptor (Figure 2D) [16]. In transgenic mice expressing γ2(Ile77), sensitivity to zolpidem can be restored in a tissue-specific fashion using Cre-recombinases that switch γ2(Ile77) to γ2(Phe77). Zolpidem sensitivity was notably restricted to cerebellar Purkinje neurons, to show that potentiation of GABAergic inhibition in these cells induces motor deficits [17]. Even though motor deficits have been observed after zolpidem administration in WT mice, interpretation is ambiguous considering the profound sedative effects of this compound. Furthermore, mice with a deletion of γ2 in Purkinje cells show no motor deficit, emphasizing the importance of developing cell-specific pharmacology approaches for acute interventions. Nevertheless, it should be noted that this strategy requires triple crosses of mouse lines, making it technologically demanding.

In nAChRs, the strategy is referred to as gain-of-function mutations [18]. The idea is to increase agonist sensitivity in a subtype-specific fashion using site-directed mutagenesis, and to use subthreshold doses of nicotine for isoform-selective activation (Figure 2E). The leucine residue in position 9′ on the transmembrane (TM) segment M2 is a conserved residue that, when mutated to alanine, serine, or threonine in the α subunit, considerably reduces the energy required to open the channel, resulting in a hypersensitive mutant with increased agonist sensitivity [18]. Using the Cre-lox technology, expression of such hypersensitive mutants could be restricted to specific neurons such as GABAergic cells of the ventral tegmental area or cholinergic neurons of the medial habenula, unveiling new roles for α4 nAChRs in reward and anxiety, respectively [19,20]. However, it should be noted that these mutant receptors are also more sensitive to endogenous ACh, which may result in unintended neuronal adaptations.

The Tethered-Ligand Approach

The overall strategy is to increase local concentration of the drug at the cell surface through covalent attachment [21]. One major advantage of this approach is that once bioconjugation is achieved, there is no need for reapplication of the drug.

Membrane-Tethered Ligands

A first example is based on genetically encoded ligands that are self-embedded in cell membranes. The fusion construct is composed of a peptide linked by a flexible linker to the

Orthogonal: which does not interfere with native biological processes.
PEG, polyethylene glycol: flexible polymer that is highly water soluble.
PLE, porcine liver esterase: exogenous enzyme that efficiently and selectively hydrolyses CM ester substrates.
PORTL, photoswitchable orthogonal remotely tethered ligand: photoswitchable ligand tethered to a protein or nanobody through SNAP- or CLIP-tag conjugation.
PSAM/PSEM: synthetic protein (pharmacologically selective actuator module, PSAM) that is selectively activated by synthetic ligands (pharmacologically selective effector molecules, PSEMs).
PTL, photoswitchable tethered ligand: thiol-reactive ligand incorporating a chemical photoswitch, that photosensitizes cysteine-substituted receptors and ion channels.
QAQ, Quaternary-ammonium azobenzene quaternary-ammonium: light-sensitive blocker of voltage-gated potassium and sodium channels, used as a photoreversible local anesthetics.
shRNAs: short (or small) hairpin RNA used to silence gene expression.
SNAP-, CLIP- and Halo-tags: protein-based self-labeling tags, catalyzing the formation of a specific, covalent bond between a labeling molecule and a tag-fused protein of interest.
Tethered: covalently (irreversibly) anchored.
Tet-on/off system: tetracycline (Tet) approach for precise and reversible spatiotemporal control of gene expression.
Thiol: side chain of the amino acid cysteine, which imparts reactivity to maleimides for ligand tethering.
UAA, unnatural amino acid: synthetic amino acid that can be incorporated into proteins using the Amber stop codon technology.

Key Figure

Cell-Specific Neuropharmacology Strategies

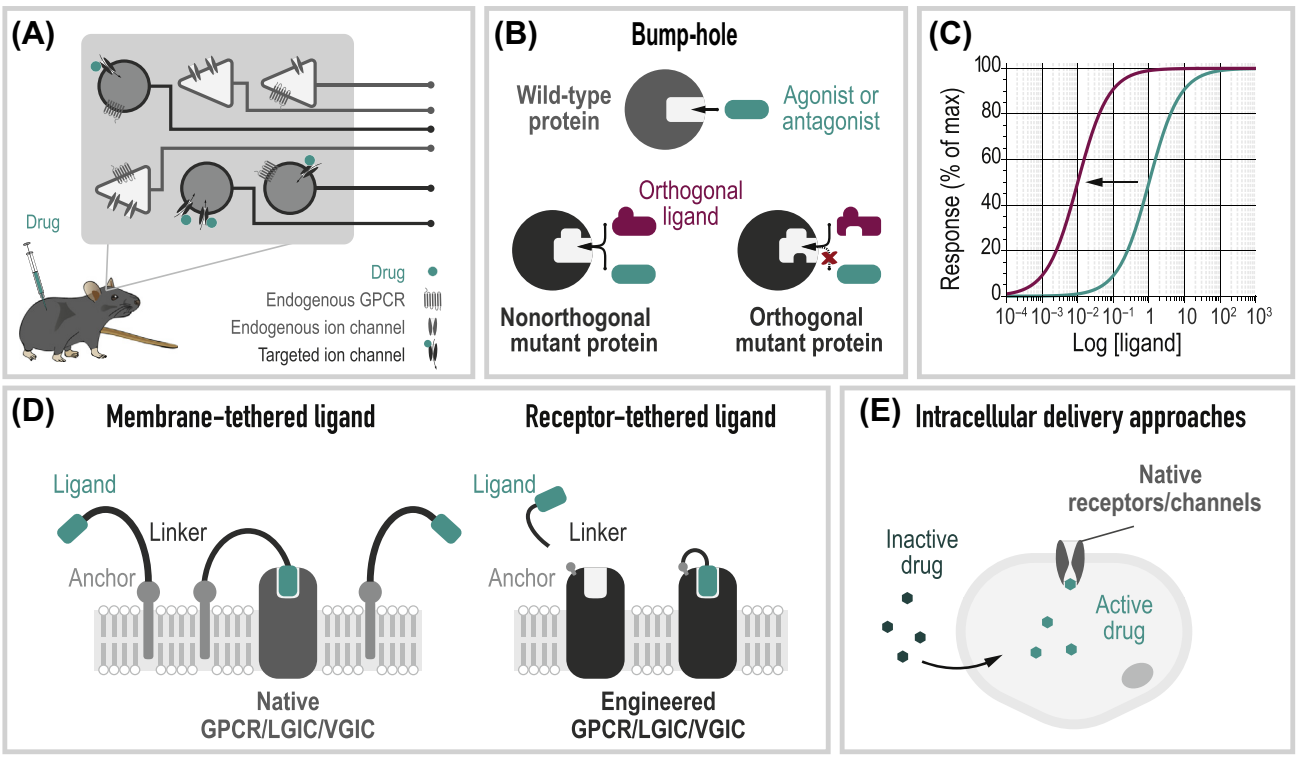

Figure 1. (A) Cell-specific pharmacology concept. A drug (green) is delivered to the whole organism but targets only specific types of neurons in the brain. The approach allows one to evaluate the neurophysiological and behavioral consequences of the manipulation of receptors in discrete circuits of the brain. (B) Bump-hole strategy. (Top) The ligand (agonist or antagonist, green) acts on wild-type proteins. (Bottom left) The engineered protein contains a hole in the binding pocket, while the synthetic ligand (purple) contains a corresponding bump. The mutant protein is nonorthogonal because it remains sensitive to the endogenous ligand (green). The orthogonal ligand acts specifically and exclusively on the engineered protein. (Bottom right) Both the modified protein and the synthetic ligand are orthogonal. (C) Leftward shift in the concentration–response curve for the synthetic ligand (purple) compared with the natural agonist or antagonist (green). (D) Tethered-ligand approaches developed for G-protein-coupled receptors (GPCRs), ligand-gated ion channels (LGIC), and voltage-gated ion channels (VGICs). (Left) The ligand is either embedded in the cell membrane (membrane-tethered) or tethered to the receptor itself (receptor-tethered). (E) Intracellular delivery approaches. The drug is inactive in the extracellular space, and becomes active only after it has entered targeted cells. Color coding throughout A–E: native proteins are shown in light grey and engineered ones in dark grey.

extracellular side of the membrane, either through a TM segment or a **glycosyl-phosphatidyl-inositol (GPI)** anchor (Figure 3A) [22–27]. The peptide ligand can either be an agonist (t-peptide) or an antagonist (t-toxin). This versatile approach has been successfully applied to activate class B GPCRs [22] and to inhibit specific voltage-gated sodium (Na_v) and calcium (Ca_v) channels as well as nAChRs [24–27]. Toxins can be extremely specific for a particular type of ion channel, enabling blockade of $NA_v1.7$ without affecting $Na_v1.8$ for instance [28]. However, since the ligand is permanently expressed at the membrane, the action of t-peptides and t-toxins is irreversible. T-toxin expression can be placed under the control of a **Tet-on/Tet-off system**, allowing antagonism to be triggered on and off, yet still with slow kinetics (days) [24]. Consequently, these tools have been used for chronic inhibition of neuronal activity and genetic dissection of neurophysiological circuits rather than for acute, cell-specific pharmacology. T-toxins were notably

Table 1. Cell-Specific Neuropharmacology Approaches

Tool name	Receptor	Ligand	On timescale	Off timescale	Therapeutic window (fold)	Application	*In vivo* application	Refs
Receptor–ligand pairs								
DREADDS	Synthetic GPCR	Synthetic (CNO, perlapine…)	s–min	min–h	100–10 000	On/off control of neuronal activity	*Drosophila*, mice, rats, monkeys	[6,7]
PSAM/PSEM	Synthetic LGIC	Synthetic (22S, 89S…)	s–min	min–h	30->10 000	On/off control of neuronal activity	Mice	[10,11]
Opto-XR	Opsin–GPCR chimera	Retinal + blue light	ms–s	ms–s	Fully orthogonal (light)	Activation of G protein signaling	Mice	[14,15]
Zolpidem-insensitive $GABA_AR$	Mutant $GABA_AR$	Synthetic (Zolpidem)	s–min	min–h	>600	Modulation of $GABA_ARs$	Mice	[17]
Gain of function nAChRs	Mutant nAChR	Exogenous (Nicotine) and endogenous (ACh)	s–min	min–h	10–100	Activation of nAChR subtypes	Mice	[19,20]
Membrane-tethered ligands								
t-toxins and t-peptides	Native receptors and ion channels	Genetically encoded toxins or peptides	Always on (days with Tet-on system)	Irreversible (days with Tet-off system)	N.A.[a] (constitutive)	Genetic dissection of circuits	*Drosophila*, zebrafish, mice	[22–27]
Lumitoxin	Native receptors and ion channels	Genetically encoded toxins + blue light	min	s	Fully orthogonal (light)	Block of ion channel subtypes	N.R.	[29]
DART	Native AMPA receptors	HaloTag-reactive ligand	s–min	days	30–300	Antagonism of AMPARs and mAChRs	Mice	[3]
Receptor-tethered ligands								
RECON	SNAP-tagged GPCR	SNAP-reactive ligand	s–min	Irreversible (min with redox agent)	N.A.	Activation and internalization of GPCRs	N.R.	[30]
MAC	His-tagged GPCR	Metal complex-agonist conjugate	s–min	min	10–100	Activation of GPCRs	N.R.	[31]
PTL	Cysteine-substituted receptor	Thiol-reactive ligand + UV-visible light	ms–s	ms–s	N.A. (orthogonal after attachment)	On/off control of receptors and ion channels	Zebrafish, mice	[4,32–43]
PORTL	SNAP- or CLIP-tagged GPCR or nanobody	SNAP- or CLIP- reactive ligand + UV-visible light	ms–s	ms–s	N.A. (orthogonal after attachment)	On/off control of receptors	Mice	[46–48]
iBOLT (and photoBOLT)	Receptor mutated with unnatural aminoacid	Click chemistry-reactive ligand (+ UV light)	min–h	Irreversible (min with light)	N.A.	Inhibition of protein activity (reversible with light)	N.R.	[50]

Table 1. (continued)

Tool name	Receptor	Ligand	On timescale	Off timescale	Therapeutic window (fold)	Application	*In vivo* application	Refs
Intracellular delivery								
Enzyme–prodrug pair	Native proteins	Masked drug	min	Irreversible	N.A.	Control of protein activity	N.R.	[53–55]
Facilitated diffusion through large ion channels	Native proteins	Membrane-impermeant and cationic (+UV-visible light)	Min (ms–s with light)	Days (ms–s with light)	N.A.	Block of ion channels (on/off with light)	Mice, rats	[58–60,62,63,65,66]

[a]Abbreviations: N.A., not applicable; N.R., not reported.

used in freely moving mice, where chronic inhibition of $Ca_v2.1$ and $Ca_v2.2$ allowed probing the role of thalamostriatal excitatory synaptic transmission in the susceptibility to social stress [27].

An extension of this approach is to include in the construct a photosensitive group to afford reversibility. Notably, the **light-oxygen-voltage (LOV)** protein domain from plants was used to produce lumitoxins, light-controllable membrane-tethered toxins (Figure 2B) [29]. LOV domains incorporate a flavin chromophore, ubiquitously present in mammalian cells, and changes conformation upon illumination with blue light. In darkness, lumitoxins produce sustained block of voltage-gated potassium (Kv) channels, while illumination results in rapid (seconds) channel unblocking. The LOV domain returns to its resting state slowly in darkness, restoring blockade within minutes. Specific Kv homologs such as Kv1.1, Kv1.2, or Shaker can be photosensitized using appropriate membrane-tethered toxins. However, this technique has not yet been extended to other protein families and has not been deployed *in vivo*.

Another strategy, called **drug acutely restricted by tethering (DART)**, relies on a bacterial enzyme called **HaloTag** for capturing drugs at the cell surface [3]. HaloTag is a self-labeling enzyme that catalyzes the covalent attachment of synthetic molecules containing a HaloTag ligand (HTL) with high efficiency and specificity (Box 1). In DART, the HaloTag is expressed at the cell surface through a TM domain. The synthetic ligand is composed of an active drug linked to the HTL through a **polyethylene glycol (PEG)** flexible linker. Once infused, it attaches to the HaloTag, resulting in a 100-fold elevation of drug concentration at the cell surface. This strategy is unique in that it offers acute pharmacological manipulation (seconds to minutes) of native receptors with cellular specificity. However, the effect is only slowly reversible (days). DART has been applied to AMPA receptors (AMPARs) and metabotropic muscarinic receptors (mAChRs), showing that the method can be applied to different receptor types. Specific inhibition of AMPARs in distinct neuronal populations of the dorsal striatum (D1 vs D2 neurons) reveals that activity of these receptors is causally linked with the akinesia observed in a mouse model of Parkinson's disease. Moreover, antagonism of AMPARs expressed on D2 but not D1 neurons has therapeutic effects on motor dysfunction, illustrating the power of targeting drugs to specific cell types.

Receptor-Tethered Ligands

Various strategies have been developed to tether ligands directly to their receptors. In the RECON (REductively Cleavable agONist) approach, a GPCR is N-terminally fused to a **SNAP-tag** [30], another type of self-labeling tag. The tethered ligand combines a peptide agonist for either class A or B GPCR, a central PEG linker bearing a disulfide bridge, and a SNAP-tag substrate. This synthetic ligand covalently and specifically attaches to the SNAP-tag, resulting in permanent

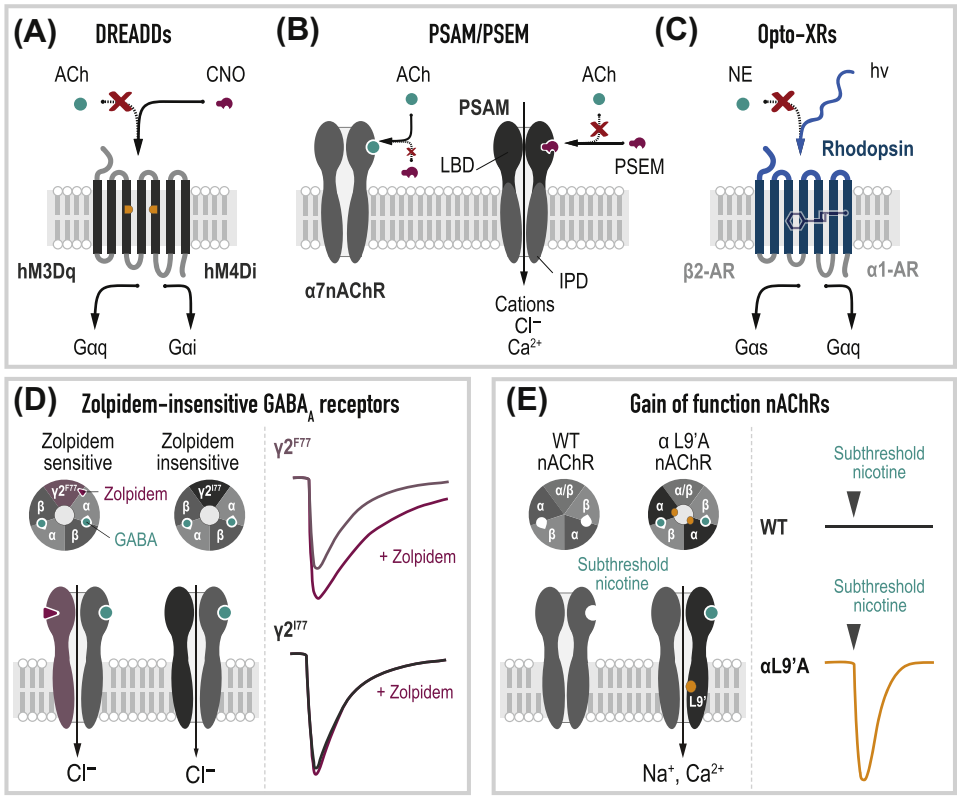

Figure 2. Receptor-Ligand Pair Approach. (A) Designer receptors exclusively activated by designer drugs (DREADDs) are orthologous receptor–ligand pairs made of a modified human muscarinic receptor (hM), with mutations in transmembrane domains (orange), that is insensitive to its natural agonist acetylcholine (ACh), but is exclusively activated by a synthetic ligand [e.g., clozapine-N-oxide (CNO)]. (B) Pharmacologically selective actuator module (PSAM)/PSEM (pharmacologically selective effector molecule) strategy: PSAM is an orthogonal, engineered ligand-binding domain (LBD) of the homopentameric α7 nicotinic acetylcholine receptor (α7-nAChR) that is solely activated by PSEM (and not ACh). Different ion pore domain (IPDs) can be spliced on the PSAM allowing calcium, cation, or chloride permeation. (C) Opto-XR approach: opsin–GPCR chimeras are made of the intracellular domains of mammalian GPCRs (such as β2- and α1-adrenergic receptors, grey) swapped on the transmembrane domain of mammalian opsin (e.g., rhodopsin, blue). Opto-XRs are not sensitive to endogenous ligands [e.g., norepinephrine (NE)]. They contain a retinal chromophore (blue) and enable the optical control of intracellular signaling transduction. (D) Zolpidem (pink) potentiates GABA signaling by binding to $GABA_A$Rs that contain the γ2 subunit. Substitution of phenylalanine (F) 77 by isoleucine (I) on γ2 induces a loss of response to zolpidem. (E) Mutation of the leucine residue in position 9' (L9'), for instance to alanine (A), leads to a hypersensitive nAChR that is activated with subthreshold concentrations of the agonist nicotine.

receptor activation. The disulfide bridge can be cleaved with redox agents, resulting in slow agonist dissociation. This method should be especially useful for studying GPCR activation and internalization *in vitro*; however, its use for neuropharmacology is elusive.

Increasing local agonist concentration at the receptor surface does not necessarily require covalent attachment. Another design is to install a **His-tag** on a GPCR, and to use a **metal-complex agonist conjugate (MAC)** that binds with high affinity to the His-tag through coordination tethering (Figure 3D) [31]. Affinity of the synthetic ligand is 10–100 times higher for the engineered than for the WT receptor. Interaction between MAC and the His-tag is not covalent; hence activation is reversible. The MAC strategy was used for cell-specific control of class A GPCRs (β2 adrenoreceptors and mAChRs), but its efficacy *in vivo* has not been reported yet.

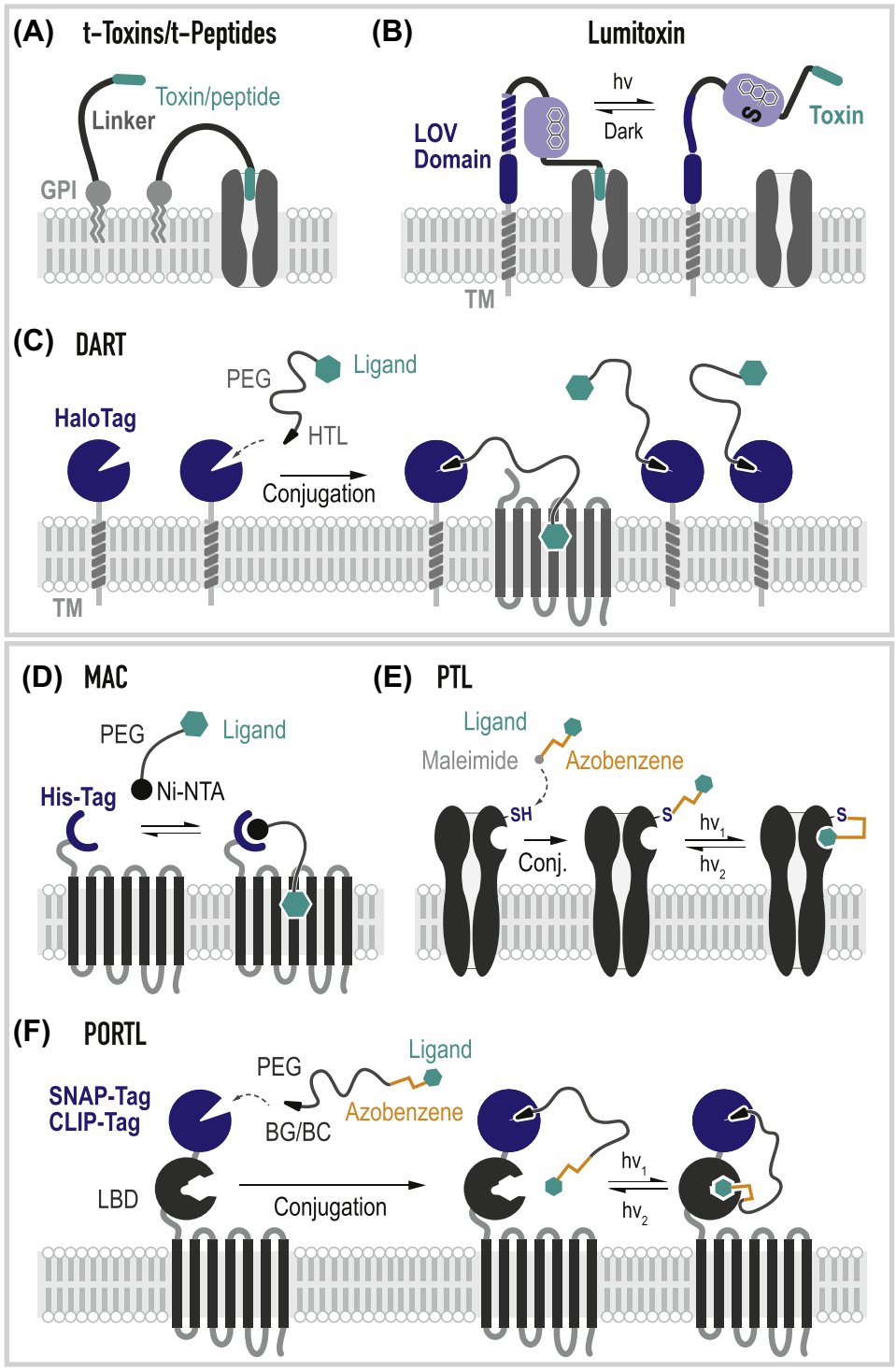

Figure 3. Tethered Ligand Approach. (A) t-toxins and t-peptides are genetically encoded ligands permanently tethered to the cell surface through either a glycosylphosphatidylinositol (GPI) anchor (depicted here) or a transmembrane (TM)

(Figure legend continued at the bottom of the next page.)

One major drawback of tethered ligands is irreversibility of action. One solution to this issue is to incorporate a chemical photoswitch in the ligand, and use light to trigger binding/unbinding. This can be achieved by anchoring a **photoswitchable tethered ligand (PTL)** onto a cysteine-substituted receptor (Figure 3E). The cysteine mutation is incorporated in proximity to a ligand-binding site. The PTL is made of three elements: a **maleimide** moiety, which is a **thiol**-reactive group for attachment to cysteines; a central **azobenzene** photoswitch; and a bioactive ligand (agonist, antagonist, or pore blocker). Light is used to reversibly change the geometry of the photoswitch from elongated to twisted, which triggers binding/unbinding. This opto-chemogenetic strategy allows reversible control of receptors with high spatial and temporal precision. The PTL approach has proven to be highly versatile. It has been applied to potassium channels [32–34], ionotropic [35–37] and metabotropic [38] glutamate receptors, nAChRs [4,39], $GABA_A$Rs [40,41], dopamine receptors [42], as well as P2X receptors [43]. It has been used to probe neurotransmission in various neuronal settings, both *ex vivo* and *in vivo* in zebrafish and mice [1]. In zebrafish, the photoswitch can simply be added to the swimming water, but in mice it has to be locally delivered. Despite this drawback, the PTL approach has been applied to the living mouse, notably for restoring vision to blind mice [44], for manipulating action potential firing [45] and GABAergic inhibition [41] in the visual cortex, or for controlling nicotinic transmission in the ventral tegmental area and addiction-related behaviors [4]. One potential shortcoming of PTLs is their nonselective attachment to endogenous cysteines, even though no adverse effect has been observed so far [4,41].

More specific bioconjugation (Box 1) can be achieved with the **photoswitchable orthogonal remotely tethered ligand (PORTL)** approach, which uses self-labeling enzymes such as **SNAP-** or **CLIP-tags** (Figure 3F) [46–48]. These self-labeling tags can be fused directly to receptors [46,47] or alternatively to nanobodies [48]; an interesting alternative for proteins for which incorporation of the tag is prohibited. Light is used to change the geometry of the ligand, and thereby its affinity for the protein. This technology has so far only been applied to metabotropic glutamate receptors, and was used to restore patterned vision in a blind mouse model [49].

Another alternative for site-specific bioconjugation is the **bio-orthogonal ligand tethering (BOLT)** technique, which is based on the incorporation of **unnatural amino acids (UAAs)** in proteins [50]. The UAA is used as a biorthogonal handle for attachment of a synthetic ligand through **click chemistry**. BOLT demonstrates selective inhibition of kinases in mammalian cells, and can be made photoreversible by introducing a photo-isomerizable group to the ligand (photoBOLT). Expansion of the genetic code in the mouse is technically challenging [51], but the recent generation of transgenic animals carrying a tRNA synthetase/tRNA pair into their genome should facilitate future use [52].

domain. (B) Lumitoxins are chimeric proteins composed of a TM, a light-oxygen-voltage (LOV) domain, a linker, and a toxin (green). In darkness, lumitoxin blocks endogenous potassium channels at the cell surface, while illumination with blue light unfolds LOV and relieves blockade. (C) The drug acutely restricted by tethering (DART) strategy is based on the expression of a TM anchor linked to a specific self-labeling protein tag (e.g., HaloTag), allowing the capture of a specific ligand to the cell surface. The ligand is composed of a HaloTag ligand (HTL), a flexible linker polyethylene glycol (PEG) and a ligand (green). Conjugation results in a 100-fold increased concentration of the ligand at the cell surface. (D) Specific binding of a metal complex–agonist conjugate (MAC) to a His-Tagged G-protein-coupled receptor (GPCR), through coordination between the Ni^{2+}–nitrilotriacetic acid (Ni–NTA) group of the ligand and the His-Tag. (E) Photoswitchable tethered ligands (PTLs) are composed of a cysteine reactive group (maleimide, grey), a photosensitive azobenzene core (orange), and a ligand (green). PTLs covalently attach to an engineered receptor that contains a single cysteine substitution, near the ligand binding site, thereby affording reversible photocontrol. (F) Photoswitchable orthogonal remotely tethered ligands (PORTLs) are composed of a ligand, a photoswitchable azobenzene molecule, a flexible linker and a benzylguanine (BG) or benzylcytosine (BC) group for conjugation to SNAP- or CLIP-tags, respectively.

Intracellular Delivery Approaches

Intracellular, cell-specific delivery can also be achieved, allowing targeting not only cell-surface receptors but also enzymes and signaling pathways (Figure 1E). Two different approaches have been described.

The Enzyme–Prodrug Pair Approach

This approach relies on selective enzyme–substrate pairs to convert an inert prodrug into an active molecule (Figures 1E and 4) [53]. The drug is masked by a disposable blocking group that is hydrolyzed specifically by an exogenous enzyme, but not by native ones. Expression of the specific enzyme in genetically targeted cells allows unmasking the drug in a cell-specific fashion. The challenges were to develop an ester-masking group with high stability toward hydrolysis by endogenous esterases, and to find an esterase that would hydrolyze this ester bond with high efficiency. Screening resulted in the discovery of **porcine liver esterase (PLE)**, an enzyme that efficiently hydrolyzes the **cyclopropylmethyl carboxyl (CM)** ester-masking group [53]. More recently, another selective enzyme–substrate pair was developed, based on engineered variants of *E. coli* **nitroreductase (NTR)** and a **nitroimidazol (NM)** masking group [54]. This strategy has proven generalizable to various masked small molecules such as fluorophores, calcium indicators, enzyme inhibitors, cAMP analogs, or ion-channel blockers [53–55]. Notably, the masked compound CM-MK801 has been used to confirm, in brain slices, the role of dopamine-neuron-expressed N-methyl-d-aspartic acid (NMDA) receptors in cocaine-induced plasticity [55]. Both the CM and NM groups were shown to be highly stable in neurons, an important requirement for cell specificity. That said, care must be taken because drugs that are too membrane permeable may diffuse out of the target neuron and affect nearby cells nonselectively. This limitation can be circumvented, for instance, by increasing polarity of the compound [54]. The biggest challenge for future applications remains to use this technology *in vivo*. So far, the limited aqueous solubility of the masked compounds precludes direct brain delivery. In addition, systemic application of CM-masked drugs is prohibited as well because CM is not resistant to esterases expressed in the periphery.

Box 1. Bioconjugation Technologies

Bioconjugation reagents are used to link together a small chemical molecule (e.g., a ligand) and a protein of interest (POI). Chemically tagging a protein with low toxicity and high specificity in a complex cellular environment is a challenge. It requires genetic modification of the POI, in order to incorporate a reactive group that will serve as a biorthogonal handle for conjugation. Multiple strategies exist [75]. The smallest and least disruptive genetic modification is the incorporation of a cysteine amino acid on the protein surface through site-directed mutagenesis. Cysteines contain a thiol group that reacts efficiently, rapidly (minutes), and with high selectivity with maleimide groups (Figure I) to form stable, covalent adducts [75]. Cysteine has become the primary choice for site-specific modification of membrane proteins because it is relatively lowly abundant, often engaged in disulfide bridges, and highly nucleophilic at neutral pH [21]. Importantly, due the strong reductive environment of the cytoplasm, cysteine–maleimide conjugation chemistry is restricted to extracellularly accessible sites on membrane proteins [21]. In addition, because cysteines are naturally present on many endogenous proteins, novel bioconjugation techniques that work inside cells and that are fully bio-orthogonal have been developed. This includes the use of unnatural amino acids (UAAs) that contain a double (alkene) or triple bond (alkyne) for bioconjugation with tetrazine-containing ligands through click chemistry [50] (Figure I). Click chemistry is popular for protein bioconjugation because it relies on chemical groups that are highly selective toward each other, yet remain inert otherwise, exhibits fast reaction kinetics in aqueous media (minutes), and produces adducts that are stable [75]. However, UAAs must be incorporated into proteins through Amber codon suppression technology, which remains challenging *in vivo* [52]. The other approaches for orthogonal labeling rely on larger modifications of the POI, such as the incorporation of polypeptide tags. For instance, metal chelation methods using poly-histidine tags (His-tag), which are classically used for protein purification, have been used for noncovalent labeling with Ni-NTA ligands [31]. His-tags are small (4–9 residues), conferring minimal disturbance to the protein, and label probes with high efficiency and selectivity. Nevertheless, labeling is reversible and Ni is toxic to cells, hampering *in vivo* use [75]. Finally, self-labeling domains such as SNAP-, CLIP- or HALO-tags use enzyme-catalyzed reactions for irreversible conjugation of ligands to POI in live cells. The reaction is highly biorthogonal, rapid, irreversible, and works intracellularly with low concentration of substrate (nanomolar range) [75], but requires fusion of the POI with a large protein domain (>20 kDa) at the N or C terminus, which either is prohibited (as with nAChRs or $GABA_A$Rs for instance) or may affect POI function.

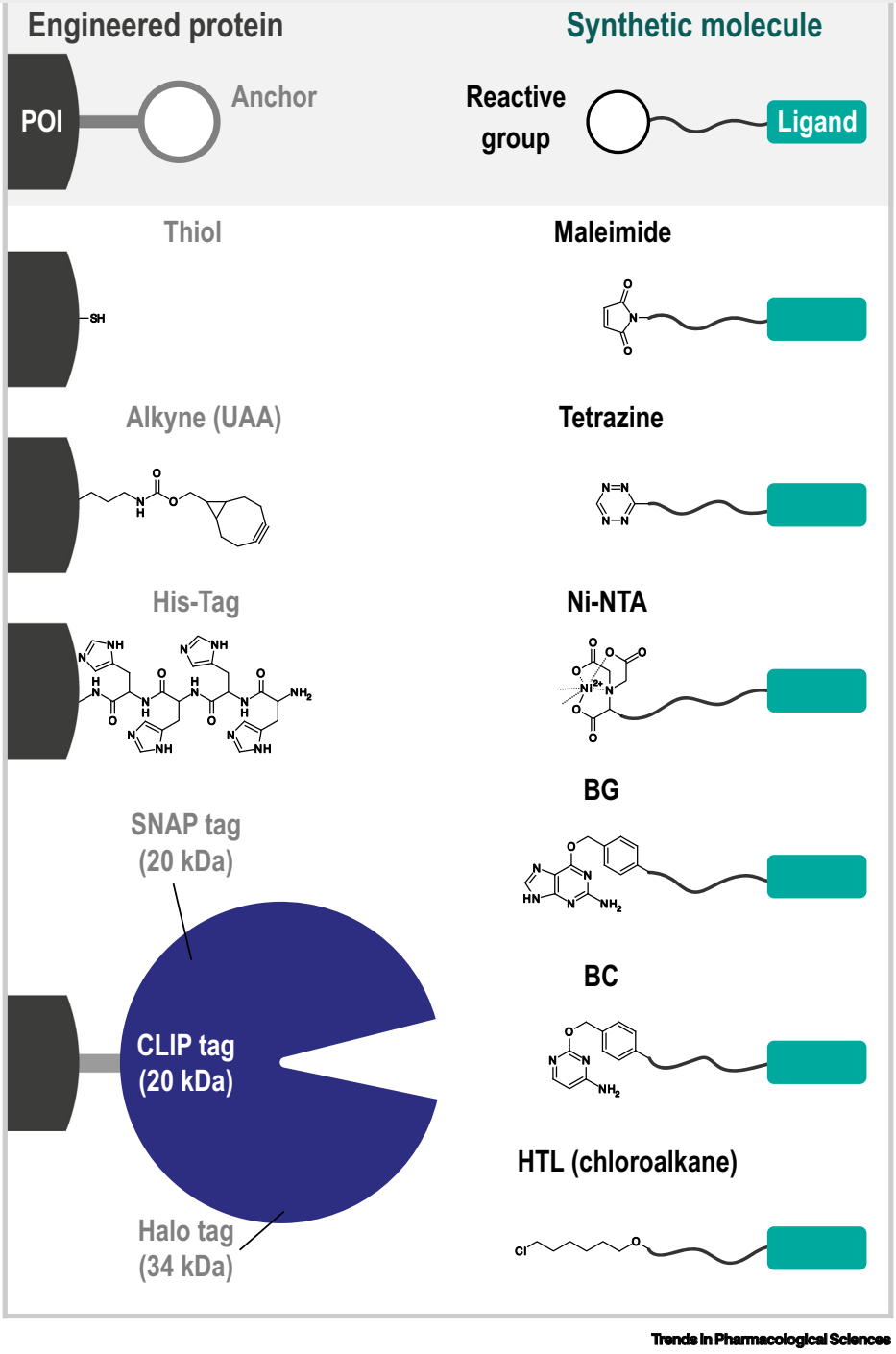

Figure I. Representative Reactive Groups for Protein–Ligand Bioconjugation. Abbreviations: BC, benzylcytosine; BG, benzylguanine; HTL, HaloTag ligand, Ni-NTA, Ni^{2+}–nitrilotriacetic acid; POI, protein of interest; UAA, unnatural amino acid.

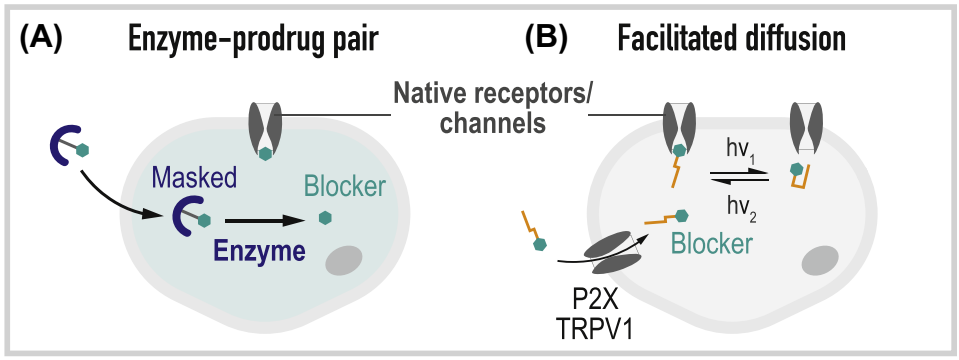

Figure 4. Intracellular Delivery Approaches. (A) The enzyme–prodrug pair approach relies on the use of a masked prodrug, and an exogenous enzyme that coverts the prodrug into an active drug. (B) The facilitated diffusion approach uses large ion channels such as TRPV1 or P2X receptors for the selective entry of membrane-impermeant drugs. Here, the drug is photocontrollable, enabling on and off action at the target protein with two distinct wavelengths of light.

Outstanding Questions

Is multiplexing of the methods for concurrent delivery of two or more drugs to distinct cellular populations, possible?

As one of the current limitations of DART technology is its slow reversal, can it be made photo-reversible?

Can fully bio-orthogonal groups be developed for tethered ligands?

Facilitated Diffusion through Large Ion-Channel Pores

Another approach is based on the selective intracellular diffusion of membrane-impermeant drugs through large ion channels (Figure 1E). The capsaicin TRPV1 and some P2X receptors open a large pore when activated, allowing permeation of large organic cations [56,57]. This biophysical property was ingeniously exploited to facilitate the entry of QX-314, a membrane-impermeant lidocaine derivative, into pain-sensing neurons [58]. QX-314 is normally inert on neurons because it has an intracellular site of action in Na_vs. However, it can selectively enter nociceptors by diffusing through open TRPV1 channels, which are abundant in these cells but virtually absent in other neurons. QX-314 remains trapped inside pain neurons for several hours, resulting in long-lasting local analgesia [58–60]. To gain rapidly reversible control over nociception, we designed a photoswitchable version of QX-314, named **QAQ** [61–63]. QAQ can rapidly and reversibly block blocks Na_vs in nociceptors, switching pain signaling on and off upon illumination with the appropriate wavelength of light.

Unlike all the methods presented in this review, this strategy does not necessarily require genetic manipulation. Rather, it exploits the sparse distribution of TRPV1 channels or P2X receptors to achieve targeted cell loading, and thus bears potential therapeutic interest. So far, QX-314 and QAQ have been coadministered with capsaicin to enable selective cell entry. Yet, recent studies suggest that capsaicin may not always be needed, since TRPV1 channels in central terminals are extensively hyperactive in neuropathic pain models [64]. Similarly, the retina is remodeled in animal models of retinal degeneration [65], with P2X receptors functionally upregulated in retinal ganglion cells [66]. This feature has been exploited to deliver photoswitchable blockers of potassium channels [61,67] specifically to OFF-ganglion cells, thereby restoring visual responses to blind retinas [65,66].

Concluding Remarks

Investigating the role of individual receptors and ion channels in particular brain regions requires methods for perturbing protein activity selectively, acutely, reversibly, and in a cell-specific fashion, ideally in the behaving animal. Diverse methods are being developed toward this goal. Yet, no method is universal, and virtually all have shortcomings, especially when considering their use *in vivo*. One important limitation lies in the limited therapeutic window for selective agonism/antagonism, which is classically in the range 10–100-fold (Table 1). Recent studies

demonstrate that with some optimization, potent agonists with exceptional selectivity (>10 000-fold) can be generated for PSAMs [11] and DREADDs [68], suggesting that such selectivity should be in principle attainable for other designer receptors. Full orthogonality can even be achieved, for instance using light-based methods (after ligand bioconjugation for PTLs and PORTLs). Yet, there is still a need for orthogonal labeling motifs that are efficient at lower doses (Box 1; see Outstanding Questions).

There is also a need for caution and appropriate controls when using chemogenetic approaches, even when reported to be fairly orthogonal. For instance, CNO was originally selected because of its excellent drug-like properties, but recent reports show that *in vivo* it is metabolically back-converted to clozapine, a molecule that not only activates DREADDs but also many other endogenous GPCRs [69]. Importantly, non-CNO analogs with improved selectivity have been developed, notably compound 21 [70] and perlapine [68], circumventing this potential issue.

Another important limitation to consider is invasiveness. DREADD activators, PSEMs, nicotine, and zolpidem have rapid central nervous system (CNS) penetration and distribution in mice and can therefore be applied systemically [7,11,17,18]. However, other approaches require local drug delivery in brain tissue through a cannula guide, either because of the instability of the compound in aqueous medium (e.g., maleimide-based PTLs) or because of poor blood brain penetration (e.g., DART), or both. Methods for improved systemic delivery are awaited. Similarly, the optical tools described in this review classically work with visible light (Table 1) and therefore require local light delivery with a chronically implanted optic fiber. Red-shifted chromophores that operate at more deeply penetrating wavelengths such as near-infrared light are currently under development [71] and should facilitate remote, transcranial control in the future.

Another important aspect to consider is receptor-type specificity. Techniques like DART or intracellular delivery methods target native receptors and therefore cannot differentiate between different receptor isoforms expressed on the same cell. Toxin-based methods provide increased selectivity but whether they can be used for acute and reversible control of receptors and ion channels *in vivo* is unclear. In contrast, methods that require genetic engineering of receptors, like PTL or PORTL, provide absolute receptor-type specificity and can help dissect the role of individual receptor subtypes in a circuit. However, molecular specificity comes at a cost: the requirement for ectopic expression of the target protein, which may affect expression level and/or patterns. Methods for overcoming this issue include the generation of transgenic knock-in animals [41] – ideally in a tissue-specific fashion – or the use of a subunit replacement strategy [34].

Finally, these tools bear strong potential not only for research purposes in animal models, but also for therapeutic applications in humans. Indeed, targeting drugs to particular neuronal populations may improve therapeutic efficacy, while decreasing the side effects associated with insufficient selectivity of conventional approaches. For instance, QX-314 or QAQ can selectively block the function of pain-sensing neurons in rodents, while leaving other sensory modalities unaffected [58,59,62], and do not require genetic modification, making them potential drug-like candidates for pain-selective local anesthesia in humans. Approaches requiring genetic manipulation are also being explored to treat CNS diseases in a titrated and cell-specific manner. This includes strategies for restoring the balance of excitation/inhibition selectively in epileptogenic zones, or for treating movement disorder in Parkinson's disease. For instance, DART technology has revealed that antagonizing AMPARs expressed on D2 neurons of the basal ganglia is more efficient at improving motor dysfunction than global antagonism through D1 and D2 neurons. Yet, it is not clear how this finding can be translated into human therapy. DREADDs and PSAMs are currently progressing into non-human primates [72,73]; an important step toward being used as

treatment to people. In addition, hM4Di, KORD, and new-generation PSAMs can be potently activated by low doses of olanzapine [74], salvinorin B [9], and varenecline [11], respectively, three drugs that are already clinically approved, thus facilitating translation to humans. Despite these important advances, considerable obstacles for implementing such approaches to the clinic remain, notably those associated with gene therapy and, to a lesser extent, drug delivery and selectivity.

Acknowledgments

We wish to thank Fabio Marti and Philippe Faure (Sorbonne Université) for their comments on the manuscript. This work was supported by grants from the Fondation pour la Recherche Médicale FRM (Equipe FRM DEQ2013326488), the Brain and Behavior Research Foundation (NARSAD Young Investigator Grant), the Agence Nationale de la Recherche (ANR-JCJC), the Institut National Du Cancer (TABAC-16-022), and the Fondation de France (Fondation Médisite). S.M. and R.D.C. were recipients of a fourth year PhD fellowship from FRM (FDT201904008060 and FDT20170437427, respectively).

References

1. Paoletti, P. *et al.* (2019) Optical control of neuronal ion channels and receptors. *Nat. Rev. Neurosci.* Published online July 9, 2019. https://doi.org/10.1038/s41583-019-0197-2
2. Hüll, K. *et al.* (2018) In vivo photopharmacology. *Chem. Rev.* 118, 10710–10747
3. Shields, B.C. *et al.* (2017) Deconstructing behavioral neuropharmacology with cellular specificity. *Science* 356. Published online April 7, 2017. https://doi.org/10.1126/science.aaj2161
4. Durand-de Cuttoli, R. *et al.* (2018) Manipulating midbrain dopamine neurons and reward-related behaviors with light-controllable nicotinic acetylcholine receptors. *eLife* 7, 15991
5. Bishop, A.C. *et al.* (2000) A chemical switch for inhibitor-sensitive alleles of any protein kinase. *Nature* 407, 395–401
6. Armbruster, B.N. *et al.* (2007) Evolving the lock to fit the key to create a family of G protein-coupled receptors potently activated by an inert ligand. *Proc. Natl. Acad. Sci.* 104, 5163–5168
7. Roth, B.L. (2016) DREADDs for Neuroscientists. *Neuron* 89, 683–694
8. Saloman, J.L. *et al.* (2016) Gi-DREADD expression in peripheral nerves produces ligand-dependent analgesia, as well as ligand-independent functional changes in sensory neurons. *J. Neurosci.* 36, 10769–10781
9. Vardy, E. *et al.* (2015) A new DREADD facilitates the multiplexed chemogenetic interrogation of behavior. *Neuron* 86, 936–946
10. Magnus, C.J. *et al.* (2011) Chemical and genetic engineering of selective ion channel-ligand interactions. *Science* 333, 1292–1296
11. Magnus, C.J. *et al.* (2019) Ultrapotent chemogenetics for research and potential clinical applications. *Science* 364, eaav5282
12. Atasoy, D. and Sternson, S.M. (2018) Chemogenetic tools for causal cellular and neuronal biology. *Physiol. Rev.* 98, 391–418
13. Kim, C.K. *et al.* (2017) Integration of optogenetics with complementary methodologies in systems neuroscience. *Nat. Rev. Neurosci.* 18, 222–235
14. Airan, R.D. *et al.* (2009) Temporally precise in vivo control of intracellular signalling. *Nature* 458, 1025–1029
15. Spangler, S.M. and Bruchas, M.R. (2017) Optogenetic approaches for dissecting neuromodulation and GPCR signaling in neural circuits. *Curr. Opin. Pharmacol.* 32, 56–70
16. Buhr, A. *et al.* (1997) Subtle changes in residue 77 of the gamma subunit of alpha1beta2gamma2 GABAA receptors drastically alter the affinity for ligands of the benzodiazepine binding site. *J. Biol. Chem.* 272, 11799–11804
17. Wulff, P. *et al.* (2007) From synapse to behavior: rapid modulation of defined neuronal types with engineered GABAA receptors. *Nat. Neurosci.* 10, 923–929
18. Drenan, R.M. and Lester, H.A. (2012) Insights into the neurobiology of the nicotinic cholinergic system and nicotine addiction from mice expressing nicotinic receptors harboring gain-of-function mutations. *Pharmacol. Rev.* 64, 869–879
19. Ngolab, J. *et al.* (2015) Functional upregulation of α4* nicotinic acetylcholine receptors in VTA GABAergic neurons increases sensitivity to nicotine reward. *J. Neurosci.* 35, 8570–8578
20. Pang, X. *et al.* (2016) Habenula cholinergic neurons regulate anxiety during nicotine withdrawal via nicotinic acetylcholine receptors. *Neuropharmacology* 107, 294–304
21. Leippe, P. *et al.* (2017) Specificity and speed: tethered photopharmacology. *Biochemistry* 56, 5214–5220
22. Fortin, J.-P. *et al.* (2009) Membrane-tethered ligands are effective probes for exploring class B1 G protein-coupled receptor function. *Proc. Natl. Acad. Sci.* 106, 8049–8054
23. Choi, C. and Nitabach, M.N. (2013) Membrane-tethered ligands: tools for cell-autonomous pharmacological manipulation of biological circuits. *Physiology* 28, 164–171
24. Auer, S. *et al.* (2010) Silencing neurotransmission with membrane-tethered toxins. *Nat. Methods* 7, 229–236
25. Ibañez-Tallon, I. and Nitabach, M.N. (2012) Tethering toxins and peptide ligands for modulation of neuronal function. *Curr. Opin. Neurobiol.* 22, 72–78
26. Ibañez-Tallon, I. *et al.* (2004) Tethering naturally occurring peptide toxins for cell-autonomous modulation of ion channels and receptors in vivo. *Neuron* 43, 7-7
27. Christoffel, D.J. *et al.* (2015) Excitatory transmission at thalamostriatal synapses mediates susceptibility to social stress. *Nat. Neurosci.* 18, 962–964
28. Stürzebecher, A.S. *et al.* (2010) An in vivo tethered toxin approach for the cell-autonomous inactivation of voltage-gated sodium channel currents in nociceptors. *J. Physiol.* 588, 1695–1707
29. Schmidt, D. *et al.* (2014) A fully genetically encoded protein architecture for optical control of peptide ligand concentration. *Nat. Commun.* 5, 1–8
30. Podewin, T. *et al.* (2018) Conditional and reversible activation of class A and B G protein-coupled receptors using tethered pharmacology. *ACS Cent. Sci.* 4, 166–179
31. Kubota, R. *et al.* (2018) Chemogenetic approach using Ni(II) complex-agonist conjugates allows selective activation of class A G-protein-coupled receptors. *ACS Cent. Sci.* 4, 1211–1221
32. Banghart, M.R. *et al.* (2004) Light-activated ion channels for remote control of neuronal firing. *Nat. Neurosci.* 7, 1381–1386
33. Fortin, D.L. *et al.* (2011) Optogenetic photochemical control of designer K+ channels in mammalian neurons. *J. Neurophysiol.* 106, 488–496
34. Sandoz, G. *et al.* (2012) Optical control of endogenous proteins with a photoswitchable conditional subunit reveals a role for TREK1 in GABAB signaling. *Neuron* 74, 1005–1014
35. Volgraf, M. *et al.* (2005) Allosteric control of an ionotropic glutamate receptor with an optical switch. *Nat. Chem. Biol.* 2, 47–52
36. Szobota, S. *et al.* (2007) Remote control of neuronal activity with a light-gated glutamate receptor. *Neuron* 54, 535–545
37. Berlin, S. *et al.* (2016) A family of photoswitchable NMDA receptors. *eLife* 5, e12040
38. Levitz, J. *et al.* (2013) Optical control of metabotropic glutamate receptors. *Nat. Neurosci.* 16, 507–516

39. Tochitsky, I. *et al.* (2012) Optochemical control of genetically engineered neuronal nicotinic acetylcholine receptors. *Nat. Chem.* 4, 105–111
40. Lin, W.-C. *et al.* (2014) Engineering a light-regulated GABAA receptor for optical control of neural inhibition. *ACS Chem. Biol.* 9, 1414–1419
41. Lin, W.-C. *et al.* (2015) A comprehensive optogenetic pharmacology toolkit for in vivo control of GABA(A) receptors and synaptic inhibition. *Neuron* 88, 879–891
42. Donthamsetti, P. *et al.* (2017) Optical control of dopamine receptors using a photoswitchable tethered inverse agonist. *J. Am. Chem. Soc.* 139, 18522–18535
43. Lemoine, D. *et al.* (2013) Optical control of an ion channel gate. *Proc. Natl. Acad. Sci.* 110, 20813–20818
44. Caporale, N. *et al.* (2009) LiGluR restores visual responses in rodent models of inherited blindness. *Mol. Ther.* 19, 1212–1219
45. Levitz, J. *et al.* (2016) A toolkit for orthogonal and in vivo optical manipulation of ionotropic glutamate receptors. *Front. Mol. Neurosci.* 9, 2
46. Broichhagen, J. *et al.* (2015) Orthogonal optical control of a G protein-coupled receptor with a SNAP-tethered photochromic ligand. *ACS Cent. Sci.* 1, 383–393
47. Levitz, J. *et al.* (2017) Dual optical control and mechanistic insights into photoswitchable group II and III metabotropic glutamate receptors. *Proc. Natl. Acad. Sci.* 114, E3546–E3554
48. Farrants, H. *et al.* (2018) SNAP-tagged nanobodies enable reversible optical control of a G protein-coupled receptor via a remotely tethered photoswitchable ligand. *ACS Chem. Biol.* 13, 2682–2688
49. Berry, M.H. *et al.* (2018) Restoration of patterned vision with an engineered photoactivatable G protein-coupled receptor. *Nat. Commun.* 2017, 1–12
50. Tsai, Y.-H. *et al.* (2015) Selective, rapid and optically switchable regulation of protein function in live mammalian cells. *Nat. Chem.* 7, 554–561
51. Kang, J.-Y. *et al.* (2013) In vivo expression of a light-activatable potassium channel using unnatural amino acids. *Neuron* 80, 358–370
52. Han, S. *et al.* (2017) Expanding the genetic code of *Mus musculus*. *Nat. Commun.* 8, 1–7
53. Tian, L. *et al.* (2012) Selective esterase-ester pair for targeting small molecules with cellular specificity. *Proc. Natl. Acad. Sci.* 109, 4756–4761
54. Gruber, T.D. *et al.* (2018) Cell-specific chemical delivery using a selective nitroreductase-nitroaryl pair. *ACS Chem. Biol.* 13, 2888–2896
55. Yang, Y. *et al.* (2015) Cell type-specific pharmacology of NMDA receptors using masked MK801. *eLife* 4, 9092
56. Chung, M.-K. *et al.* (2008) TRPV1 shows dynamic ionic selectivity during agonist stimulation. *Nat. Neurosci.* 11, 555–564
57. Khakh, B.S. *et al.* (1999) Neuronal P2X transmitter-gated cation channels change their ion selectivity in seconds. *Nat. Neurosci.* 2, 322–330
58. Binshtok, A.M. *et al.* (2007) Inhibition of nociceptors by TRPV1-mediated entry of impermeant sodium channel blockers. *Nature* 449, 607–610
59. Kim, H.Y. *et al.* (2010) Selectively targeting pain in the trigeminal system. *Pain* 150, 29–40
60. Roberson, D.P. *et al.* (2011) Targeting of sodium channel blockers into nociceptors to produce long-duration analgesia: a systematic study and review. *Br. J. Pharmacol.* 164, 48–58
61. Banghart, M.R. *et al.* (2009) Photochromic blockers of voltage-gated potassium channels. *Angew. Chem. Int. Ed. Engl.* 48, 9097–9101
62. Mourot, A. *et al.* (2012) Rapid optical control of nociception with an ion-channel photoswitch. *Nat. Methods* 9, 396–402
63. Mourot, A. *et al.* (2017) Understanding and improving photocontrol of ion channels in nociceptors with azobenzene photoswitches. *Br. J. Pharmacol.* 175, 2296–2311
64. Kim, Y.S. *et al.* (2014) Central terminal sensitization of TRPV1 by descending serotonergic facilitation modulates chronic pain. *Neuron* 81, 873–887
65. Tochitsky, I. *et al.* (2014) Restoring visual function to blind mice with a photoswitch that exploits electrophysiological remodeling of retinal ganglion cells. *Neuron* 81, 800–813
66. Tochitsky, I. *et al.* (2016) How azobenzene photoswitches restore visual responses to the blind retina. *Neuron* 92, 100–113
67. Mourot, A. *et al.* (2011) Tuning photochromic ion channel blockers. *ACS Chem. Neurosci.* 2, 536–543
68. Chen, X. *et al.* (2015) The first structure–activity relationship studies for designer receptors exclusively activated by designer drugs. *ACS Chem. Neurosci.* 6, 476–484
69. Gomez, J.L. *et al.* (2017) Chemogenetics revealed: DREADD occupancy and activation via converted clozapine. *Science* 357, 503–507
70. Thompson, K.J. *et al.* (2018) DREADD agonist 21 is an effective agonist for muscarinic-based DREADDs in vitro and in vivo. *ACS Pharmacol. Transl. Sci.* 1, 61–72
71. Dong, M. *et al.* (2017) Near-infrared photoswitching of azobenzenes under physiological conditions. *J. Am. Chem. Soc.* 139, 13483–13486
72. Eldridge, M.A.G. *et al.* (2015) Chemogenetic disconnection of monkey orbitofrontal and rhinal cortex reversibly disrupts reward value. *Nat. Neurosci.* 19, 37–39
73. Raper, J. *et al.* (2017) Metabolism and distribution of clozapine-N-oxide: implications for nonhuman primate chemogenetics. *ACS Chem. Neurosci.* 8, 1570–1576
74. Weston, M. *et al.* (2019) Olanzapine: a potent agonist at the hM4D(Gi) DREADD amenable to clinical translation of chemogenetics. *Sci. Adv.* 5, eaaw1567
75. Chen, X. and Wu, Y.-W. (2016) Selective chemical labeling of proteins. *Org. Biomol. Chem.* 14, 5417–5439

Résultats

6. Première publication scientifique

MANIPULATING MIDBRAIN DOPAMINE NEURONS AND REWARD-RELATED BEHAVIORS WITH LIGHT-CONTROLLABLE NICOTINIC ACETYLCHOLINE RECEPTORS

Durand-de Cuttoli R*, **MONDOLONI S***, Marti F, Lemoine D, Nguyen C, Naudé J, d'Izarny-Gargas T, Pons S, Maskos U, Trauner D, Kramer RH, Faure P**, Mourot A**

* co-first ** co-last

Les dynamiques d'activation des récepteurs nicotiniques de la VTA sont au cœur des processus qui engagent la mise en place de la dépendance à la nicotine. Les approches génétiques et pharmacologiques ont permis de faire une avancée considérable dans la compréhension de ces processus mais certaines questions restaient encore sans réponse. Il n'a par exemple pas été possible de bloquer spécifiquement les récepteurs β2 de la VTA par des approches génétiques ou pharmacologiques. Nous avons choisi d'implémenter la stratégie de pharmacologie optogénétique qui combine les avantages de la génétique, de la pharmacologie et de l'optique, utilisant des récepteurs nicotiniques photo-inhibables (LinAChRs ; Light-controlled nAChRs). L'avantage de cette stratégie est de pouvoir agir spécifiquement sur un nAChR avec une résolution spatiale et temporelle inégalable.

Lorsque nous avons commencé ce projet, la pharmacologie optogénétique avait été développée en système hétérologue et n'avait jamais été utilisée *in vivo* chez la souris éveillée (Paoletti et al., 2019). Les LinAChR avaient été développés par l'équipe de Richard Kramer (Berkeley) mais avaient uniquement été utilisés en oocyte de xénope (Tochitsky et al., 2012, **Fig6.1a**). Notre but était de déployer les β2 LinAChR chez la souris, afin de mettre en évidence le rôle des récepteurs nicotiniques β2 de la VTA dans l'activité des neurones DA et le renforcement à la nicotine. Deux défis principaux étaient à surmonter :

- Le premier consistait à s'assurer de la faisabilité de l'utilisation *in vivo* de l'outil chez la souris. En effet, le récepteur consiste en trois éléments qu'il faut amener chez la souris : le gène qui code le récepteur modifié, le ligand photochromique et la lumière. Nous avons pu montrer en système hétérologue et neuronal une photo-manipulation des courants nicotiniques. Cela a permis de démontrer que la sous-unité modifiée est capable de s'associer avec les sous-unités endogènes (possiblement α4) pour former un récepteur fonctionnel et photo-contrôlable.
- Le deuxième challenge consistait à implémenter cette stratégie dans une structure profonde telle que la VTA afin de photo-contrôler l'activité des récepteur β2* pendant des expériences électrophysiologiques ou comportementale *in vivo*. Deux étapes déterminantes ont permis de faire avancer le projet. La première était l'utilisation d'un système d'enregistrement Minimatrix de *Thomas recording* (TREC), chez l'animal anesthésié, qui permet d'amener une tétrode, une fibre optique et une canule d'injection au même endroit dans le cerveau (**Fig 6.1a-c**). La seconde a été le développement d'un guide canule qui permet d'injecter le photoswitch et d'introduire une fibre optique à travers le même guide canule (**Fig 6.1d**).

L'utilisation de cette stratégie nous a permis de faire le lien causal entre l'activité spontanée des neurones dopaminergiques, la modulation cholinergique du système et le renforcement à la nicotine. Les résultats obtenus ont confirmé que les récepteurs β2* de la VTA était impliqués dans l'activité régulière et en bouffée, mais surtout, ils ont révélé l'impact, en direct, du tonus cholinergique endogène sur l'activité des neurones DA. Nous avons pu mettre en évidence deux populations neuronales : la première population de neurones DA présente une activité spontanée plus élevé en présence d'ACh endogène (comme attendu), tandis que la deuxième population présente une activité plus faible en réponse à un tonus cholinergique. Nous avons aussi montré le rôle déterminant de l'activation des nAChR β2* dans les réponses à la nicotine et dans les processus qui sous-tendent la mise en place du renforcement à la nicotine.

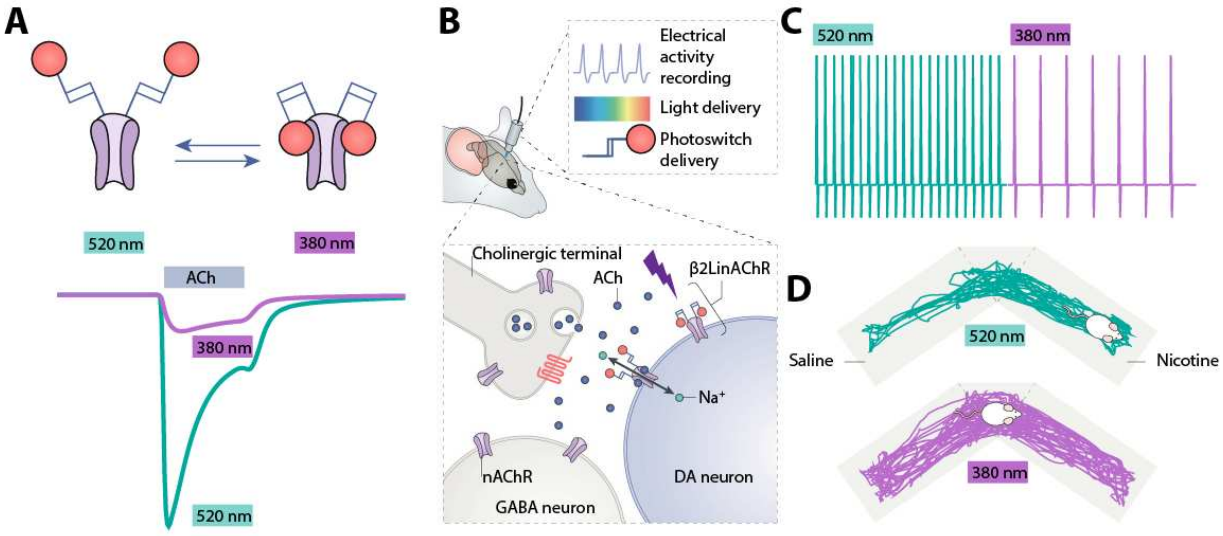

Figure 6.1 | Implantation des LinAChR in vivo. a. (Haut) Principe du LinAChR, activable par la nciotine ou l'ACh sous lumière verte (520 nm), et antagonisé par le photoswitch sous lumière violette (380 nm). (Bas) Photo-inhibition des courants nicotiniques en système hétérologue. **b.** Guide canule couplé à une électrode, permettant de délivrer localement la lumière et le ligand photoswitchable, et d'enregistrer l'activité électrique des neurones de la VTA. L'expression du β2 LinAChR peut être restreinte aux seuls neurones DA. **c.** Photo-contrôle de l'activité spontanée des neurones DA de la VTA, sous lumière verte et violette. **d.** Manipulation réversible de la préférence à la nicotine chez la souris.

eLIFE elifesciences.org

RESEARCH ARTICLE

Manipulating midbrain dopamine neurons and reward-related behaviors with light-controllable nicotinic acetylcholine receptors

Romain Durand-de Cuttoli[1†], Sarah Mondoloni[1†], Fabio Marti[1], Damien Lemoine[1], Claire Nguyen[1], Jérémie Naudé[1], Thibaut d'Izarny-Gargas[1], Stéphanie Pons[2], Uwe Maskos[2], Dirk Trauner[3], Richard H Kramer[4], Philippe Faure[1‡*], Alexandre Mourot[1‡*]

[1]Neuroscience Paris Seine – Institut de Biologie Paris Seine (NPS – IBPS), Sorbonne Université, INSERM, CNRS, Paris, France; [2]Unité de Neurobiologie Intégrative des Systèmes Cholinergiques, Department of Neuroscience, Institut Pasteur, Paris, France; [3]Department of Chemistry, New York University, New York, United States; [4]Department of Molecular and Cell Biology, University of California Berkeley, Berkeley, United States

Abstract Dopamine (DA) neurons of the ventral tegmental area (VTA) integrate cholinergic inputs to regulate key functions such as motivation and goal-directed behaviors. Yet the temporal dynamic range and mechanism of action of acetylcholine (ACh) on the modulation of VTA circuits and reward-related behaviors are not known. Here, we used a chemical-genetic approach for rapid and precise optical manipulation of nicotinic neurotransmission in VTA neurons in living mice. We provide direct evidence that the ACh tone fine-tunes the firing properties of VTA DA neurons through β2-containing (β2*) nicotinic ACh receptors (nAChRs). Furthermore, locally photo-antagonizing these receptors in the VTA was sufficient to reversibly switch nicotine reinforcement on and off. By enabling control of nicotinic transmission in targeted brain circuits, this technology will help unravel the various physiological functions of nAChRs and may assist in the design of novel therapies relevant to neuropsychiatric disorders.
DOI: https://doi.org/10.7554/eLife.37487.001

***For correspondence:** phfaure@gmail.com (PF); almourot@gmail.com (AM)

[†]These authors contributed equally to this work
[‡]These authors also contributed equally to this work

Competing interests: The authors declare that no competing interests exist.

Funding: See page 19

Received: 12 April 2018
Accepted: 03 August 2018
Published: 04 September 2018

Reviewing editor: Olivier Jacques Manzoni, Aix Marseille Univ, INSERM, INMED, France

Introduction

Cholinergic neurotransmission provides a widespread and diffuse signal in the brain (***Picciotto et al., 2012***; ***Sarter et al., 2009***). ACh alters neurotransmitter release from presynaptic terminals and affects neuronal integration and network activity, by acting through two classes of membrane receptors: metabotropic muscarinic receptors and ionotropic nicotinic ACh receptors (nAChRs). nAChRs consist of hetero- and homo-pentameric arrangements of α and β subunits (9 and 3 genes, respectively), yielding a high combinatorial diversity of channel composition, localization and function (***Zoli et al., 2015***). Nicotinic neuromodulation controls learning, memory and attention, and has been associated with the development of numerous neurological and psychiatric disorders, including epilepsy, schizophrenia, anxiety and nicotine addiction (***Taly et al., 2009***). Understanding how nAChRs mediate such diverse functions requires tools for controlling nicotinic neurotransmission in defined brain circuits.

ACh is a modulator of the VTA, a midbrain DAergic nucleus key in the processing of reward-related stimuli and in addiction (***Di Chiara and Imperato, 1988***; ***Pignatelli and Bonci, 2015***;

eLife digest Acetylcholine is one of the most abundant chemicals in the brain, with key roles in learning, memory and attention. Neurons throughout the brain use acetylcholine to exchange messages. Acetylcholine binds to two different classes of receptors on neurons: nicotinic and muscarinic. As the name suggests, nicotinic receptors also respond to nicotine, the main addictive substance in tobacco, while muscarinic receptors respond to muscarine, present in certain poisonous mushrooms.

Nicotinic and muscarinic receptors each consist of many different subtypes. But standard pharmacology techniques cannot discriminate between the effects of acetylcholine binding to these different subtypes. Likewise, they cannot distinguish between acetylcholine binding to the same receptor subtype on different neurons. Durand-de Cuttoli, Mondoloni et al. have now developed a new nanotechnology that uses light to target specific acetylcholine receptor subtypes in freely moving mice.

The technology was tested in a brain region called the VTA, which is part of the brain's reward system. Experiments showed that when acetylcholine binds to a specific subtype of nicotinic receptors on VTA neurons – called β2-containing receptors – it makes the neurons release the brain's reward signal, dopamine. Switching these receptors on and off changed how the mice responded to nicotine. With the receptors switched on, mice preferred locations associated with nicotine. Switching the receptors off removed this preference. Nicotine may thus be addictive in part because it triggers VTA neurons to release dopamine via its actions on β2-containing nicotinic receptors.

This new technology will help reveal the mechanisms of action of acetylcholine and nicotine. Blocking the effects of nicotine at a specific time and place in the mouse brain may uncover the receptors and brain regions that drive nicotine consumption. Smoking remains a major cause of preventable death worldwide. This new approach could help us develop strategies to prevent or treat addiction.

DOI: https://doi.org/10.7554/eLife.37487.002

Volkow and Morales, 2015). The pedunculopontine and laterodorsal tegmental nuclei (PPN and LDT) are the two major cholinergic inputs to the VTA (*Beier et al., 2015*). Optogenetic activation of PPN and LDT neurons modulates the firing patterns of VTA DA cells and reward-associated behaviors (*Lammel et al., 2012*; *Dautan et al., 2016*; *Xiao et al., 2016*), implicating ACh in these processes. Yet, whether ACh directly affects neuronal excitability at the post-synaptic level, or whether it potentiates the release of other neurotransmitters through pre-synaptic nicotinic and muscarinic receptors is not known.

Brain nAChRs are expressed in high densities in the VTA, and in strategic places such as somatic and dendritic sites on GABAergic, glutamatergic and DAergic VTA cells, as well as on pre-synaptic terminals from extra-VTA afferents and from intra-VTA GABAergic interneurons (*Changeux, 2010*; *Zoli et al., 2015*). They are also present on DAergic terminals in the Nucleus Accumbens (NAc) and the prefrontal cortex (*Grady et al., 2007*; *Changeux, 2010*). Genetic and pharmacological manipulations have implicated VTA nAChRs in tuning the activity of DA neurons and in mediating the addictive properties of nicotine (*Mameli-Engvall et al., 2006*; *Maskos et al., 2005*; *Morel et al., 2014*; *Naudé et al., 2016*; *Picciotto et al., 1998*; *Tapper et al., 2004*; *Tolu et al., 2013*). However, understanding the mechanism by which ACh and nicotine participate in these activities requires to comprehend the spatio-temporal dynamics of nAChRs activation. Genetic manipulations can eliminate specific nAChRs, but they cannot provide kinetic information about the time course of nAChR signals that could be crucial for actuating VTA circuits and goal-oriented behaviors. Moreover, gene knockout can have unintended consequences, which include compensatory changes in expression of other receptors or channels, homeostatic adaptations and developmental impairments (*King et al., 2003*). Pharmacological agents allow activation or inhibition of nAChRs, but they diffuse slowly in vivo, they have limited subtype specificity and they cannot be targeted to genetically-defined neuronal cell types.

To fill this gap between molecular and circuit knowledge, we have developed the optogenetic pharmacology for rapid and reversible photocontrol of genetically-targeted mammalian neurotransmitter receptors (**Kramer et al., 2013**). We previously demonstrated light-controllable nAChRs (LinAChRs) in Xenopus occcytes, a heterologous expression system (**Tochitsky et al., 2012**). Here, we deployed strategies for acutely and reversibly controlling nicotinic transmission in the VTA in the mammalian brain, in vivo. β2* receptors account for the great majority of VTA nAChRs and are crucial for the pathophysiology of nicotine addiction (**Maskos et al., 2005**; **Faure et al., 2014**). We demonstrate acute interruption of nicotinic signaling in the VTA and reveal that endogenous pontine ACh strongly impacts on the firing patterns of VTA DA neurons. Moreover, we reversibly prevented the induction of nicotine preference in behaving mice by locally photo-antagonizing the effect of nicotine on VTA β2* nAChRs. This approach to optically antagonize neurotransmitter receptors in vivo will help sense the different temporal dynamics of ACh concentrations, and unravel the contribution of specific nAChR isoforms to nicotinic neuromodulation of neural circuits and associated behaviors, including drug abuse.

Results

Design and characterization of β2LinAChR

The vast majority of nAChRs in the mouse VTA contains the β2 subunit (**Zoli et al., 2015**; **Faure et al., 2014**). Therefore, we engineered this subunit to enable installation of light sensitivity. We transposed the rat β2E61C mutation, used previously in nAChRs expressed in Xenopus oocytes (**Tochitsky et al., 2012**), to the mouse β2 subunit to generate a photosensitizable receptor that traffics and functions normally in the mouse brain. The single cysteine-substitution, which is used for the anchoring of the photoswitchable tethered ligand Maleimide-Azobenzene-Homocholine (MAHoCh), faces the agonist binding sites (**Figure 1A**). MAHoCh has a photo-isomerizable azobenzene group, flanked on one side with a thiol-reactive maleimide moiety for conjugation to the cysteine, and on the other with a homocholine ligand for competitive antagonism of nAChRs (**Figure 1B**). In darkness, the azobenzene group adopts the thermally stable, extended *trans* configuration. Illumination with near-UV (e.g. 380 nm) light isomerizes the azobenzene core to the twisted, *cis* configuration. The *cis* isomer reverses to *trans* either slowly in darkness or rapidly in green light (e.g. 500 nm). Receptor activation in response to ACh agonist remained unaltered in darkness after conjugation of MAHoCh to β2E61C. However, agonist activation is blocked in 380 nm light, when *cis* MAHoCh occupies the agonist binding pocket (**Figure 1C**). Photo-control is bi-directional, and antagonism is relieved under 500 nm light when MAHoCh is in its *trans* form.

To verify whether nAChR currents could be photo-controlled, the β2E61C mutant was co-expressed with the WT α4 subunit in Neuro-2a cells (**Figure 1D**). Cells were treated with MAHoCh and any remaining untethered photoswitch was washed away prior to electrophysiological recordings. As expected, currents evoked by both carbamylcholine (CCh) and nicotine were strongly inhibited under 380 nm light, when tethered *cis* MAHoCh competes with the agonist (**Figure 1E**). Currents rapidly (<500 ms) and fully returned to their initial amplitude upon 525 nm light illumination. Repeated light flashes reduced and increased current amplitude without decrement, consistent with photochemical studies showing that azobenzenes are very resistant to photobleaching (**Szymański et al., 2013**). Spectroscopic measurements show that *cis* MAHoCh reverts to *trans* in darkness, but very slowly, with a half-life of 74 min in solution (**Tochitsky et al., 2012**). Consistent with this, we found that nAChR responses remained suppressed in darkness for at least ten minutes after a single flash of 380 nm light, but quickly recovered upon illumination with 525 nm light (**Figure 1F**). Hence, LinAChR could be rapidly toggled between its functional and antagonized forms upon brief illumination with the proper wavelength of light, but could also remain suppressed several minutes in darkness, eliminating the need for constant illumination.

β2LinAChR enables inhibition of nicotinic currents in VTA DA neurons

We then tested whether nAChR currents could be photo-controlled in VTA DA neurons using β2LinAChR. To this aim, we virally targeted the cysteine-mutant β2 subunit together with eGFP under the control of the ubiquitous pGK promoter to the VTA of WT mice (**Figure 2A**). As expected, transgene expression was found at the injection site throughout the VTA both in TH^+ and TH^-

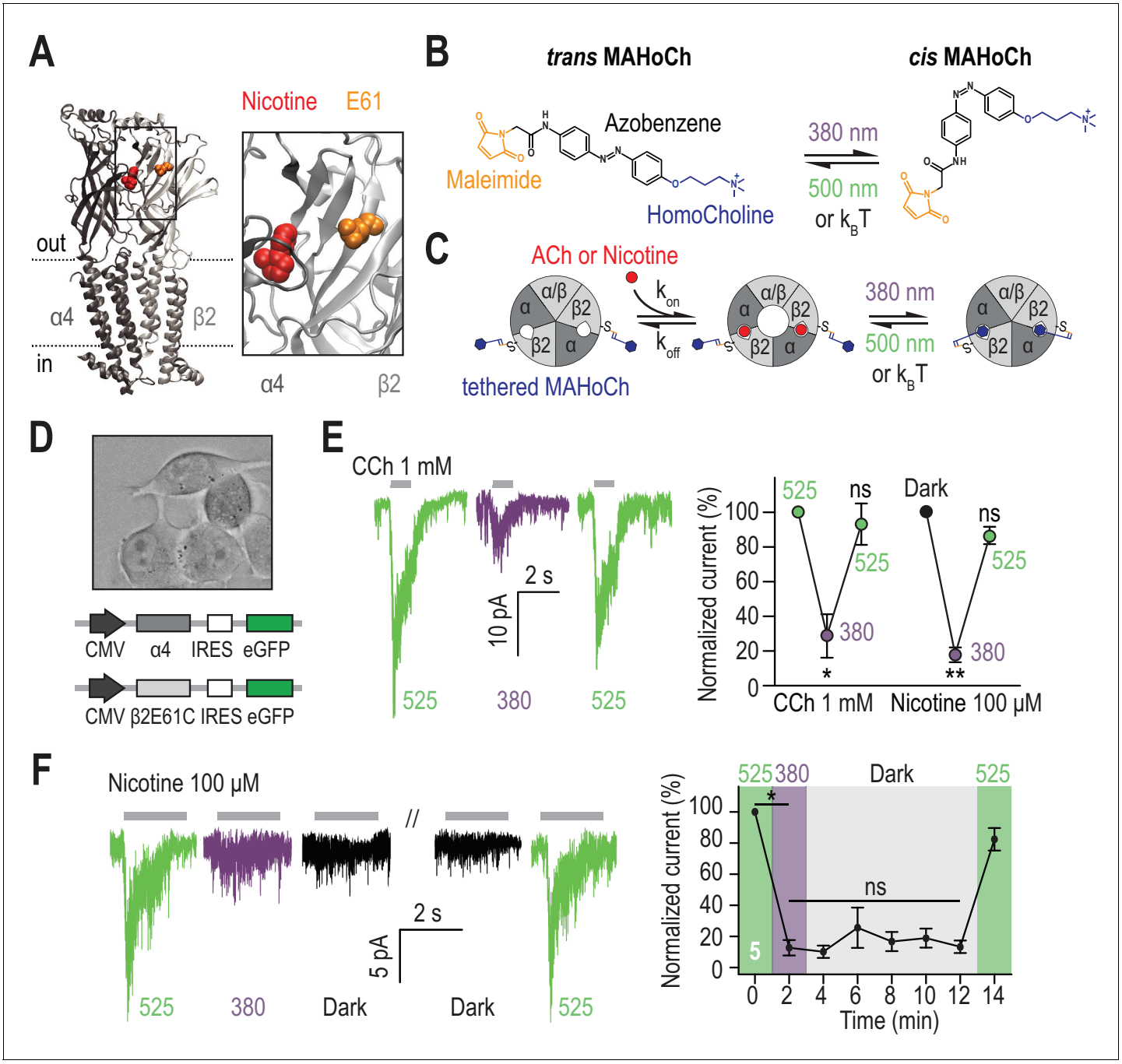

Figure 1. Design and characterization of β2LinAChR. (**A**) Crystal structure of the α4β2 nAChR (PDB ID 5KXI) (***Morales-Perez et al., 2016***) viewed parallel from the plasma membrane. The α4 subunit is in dark grey and the β2 subunit in light grey. The agonist binding sites are located in the extracellular binding domain, at the interface between the α and β subunits. Nicotine (red) and the amino acid E61 (orange) which has been mutated to cysteine in the β2LinAChR are represented as spheres. For clarity, only one αβ dimer is shown, and an extended view is shown on the right. (**B**) Chemical structure of *trans* and *cis* MAHoCh. The thiol-reactive group maleimide is shown in orange, the azobenzene photo-sensitive moiety in black, and the competitive antagonist homocholine in blue. In darkness, the azobenzene group adopts the thermally stable, extended *trans* configuration. Illumination with near-UV (380 nm) light photo-isomerizes the azobenzene core to the twisted, *cis* configuration. The *cis* isomer reverses to *trans* either slowly in dark conditions (k_BT) or rapidly under green light (500 nm). C*is-trans* photo-isomerization hence results in drastic changes in the geometry and end-to-end distance of MAHoCh. (**C**) Cartoon representation of β2LinAChR. MAHoCh is tethered to β2E61C, and the receptor still functions in the dark. Isomerizing the photoswitch back and forth between its *cis* and *trans* forms with two different wavelengths of light enables reversible photocontrol of the receptor: activatable under green light and antagonized under purple light. (**D**) Heterologous co-expression of α4 and β2E61C nAChR subunits in Neuro-2a cells. (**E**) Reversible photocontrol of α4β2LinAChR in Neuro-2a cells. Currents were recorded in whole-cell voltage-clamp mode at a potential

Figure 1 continued on next page

Figure 1 continued

of −60 mV and elicited by an application of CCh (1 mM, 1 s, n = 4) or nicotine (100 μM, 2 s, n = 5). Currents were strongly inhibited under 380 nm light (71.3 ± 12.5%, p=0.038 for CCh and 82.1 ± 4.2%, p=0.0082 for nicotine) and fully restored under 525 nm light (p=0.285 for CCh and 0.125 for nicotine). (**F**) Thermal stability of LinAChR photo-inhibition. After inhibition with 380 nm light, the amplitude of the current remained constant for at least 10 min in darkness (p=1 at t = 12 min), and was restored upon illumination with 525 nm light. All values represent mean ± SEM.

DOI: https://doi.org/10.7554/eLife.37487.003

The following source data is available for figure 1:

Source data 1. Source data for ***Figure 1E,F***.

DOI: https://doi.org/10.7554/eLife.37487.004

neurons (***Figure 2B***, ***Figure 2—figure supplement 1A***). In contrast, expression was absent in the PPN and LDT (***Figure 2—figure supplement 1B***), in agreement with the lack of retrograde transport for lentiviruses (***Mazarakis et al., 2001***). Four to six weeks after viral infection, transduced coronal slices were treated with MAHoCh, and nicotine-induced currents were recorded from GFP-positive DA neurons. VTA DA neurons were identified based on their anatomical localization and electrophysiological properties, (i.e. pacemaker activity and typical action potential waveform), which are robust indicators of the DAergic signature (***Figure 2—figure supplement 2A–B***). Currents evoked by a local puff of nicotine were strongly inhibited under 380 nm light, and fully restored under 525 nm light (***Figure 2C***). Photo-inhibition was robust at both low and high concentrations of nicotine, and was absent in non-transduced slices treated with MAHoCh (***Figure 2D***). The degree of photo-inhibition was smaller than that observed in heterologous expression system, suggesting that only a subset of β2* receptors incorporated the cysteine-mutated β2. Importantly, over-expression of β2E61C did not significantly affect the amplitude of nicotine-induced currents (***Figure 2E***), indicating that the total number of functional nAChRs at the cell surface was unchanged. Moreover, MAHoCh alone had no detectable off-target effect on other endogenous ion channels or on resting or active membrane properties of the cell (***Figure 2—figure supplement 2C,D***), indicating that the effect of light was specific for β2E61C* nAChRs. Overall, these experiments show that β2E61C associates with endogenous nAChR subunits in DA neurons, to produce receptors with normal neurophysiological roles, while allowing specific photo-control of nicotinic signaling.

β2*nAChRs control the firing patterns of VTA DA neurons

VTA DA neurons show two distinct patterns of electrical activity: tonic, regular-spiking in the low frequency range and transient sequences of high-frequency firing, referred to as bursts (***Paladini and Roeper, 2014***). Bursting activity, which is a crucial signal for behavioral conditioning (***Tsai et al., 2009***), is under the control of excitatory afferents from the PPN and LDT (***Lodge and Grace, 2006***; ***Paladini and Roeper, 2014***; ***Floresco et al., 2003***). We asked whether endogenous pontine ACh modulates the firing patterns of VTA DA neurons through β2*nAChRs. Testing this hypothesis required to deploy strategies for acutely manipulating nicotinic transmission in vivo, since DA neurons discharge only in pacemaker-like tonic activity in brain slices, due to cholinergic and glutamatergic afferents being severed (***Grace and Onn, 1989***). To this aim, we used a microdrive multielectrode manipulator (System mini matrix with five channels, ***Figure 3A***) directly mounted onto the head of an anaesthetized mouse. This system allowed us to stereotaxically deliver the photoswitch and record the spontaneous activity of putative DA (pDA) neurons, while delivering alternating flashes of 390 and 520 nm light in the VTA (***Figure 3A,B***). β2E61C was virally transduced in the VTA of WT mice and recordings were performed three to four weeks after infection. MAHoCh was infused in the VTA at least an hour before starting the electrophysiological recordings, to allow the excess of untethered photoswitch to be cleared. We first found that the spontaneous activity of pDA neurons from WT and transduced animals were not significantly different in darkness (***Figure 3—figure supplement 1A***), indicating that viral expression of β2E61C did not affect the native physiology of the cells. We then checked whether alternatively switching light between 390 and 520 nm (20 cycles) affected the spontaneous firing of pDA neurons, by calculating the absolute percent of photoswitching (defined as the absolute value of $((Freq_{520} - Freq_{390})/Freq_{390})$). Importantly, we found that switching wavelength impacted the spontaneous firing rate of MAHoCh-treated pDA

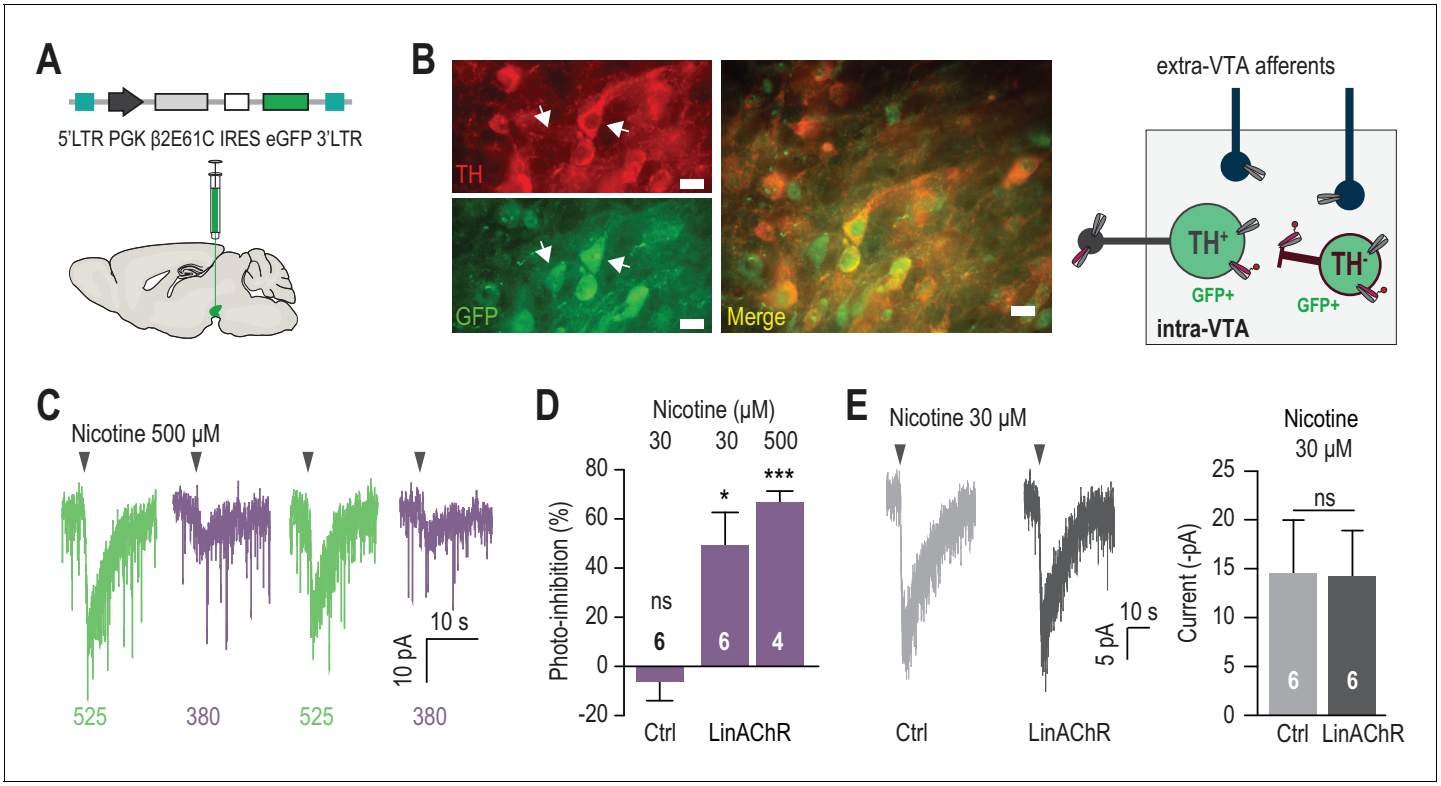

Figure 2. Reversible photo-inhibition of nAChR currents. (**A**) Viral transduction of the VTA using a lentivirus encoding pGK-β2E61C-IRES-eGFP. (**B**) Left, immunocytochemical identification of virally-transduced neurons (GFP-positive) 4 weeks after viral injection. DA neurons are labelled using anti-tyrosine hydroxylase (TH) antibodies. Note that the virus non-selectively transduces TH^+ and TH^- neurons (arrows). Scale bar 10 µm. Right, scheme illustrating LinAChR expression profile. The β2E61C subunit (red) is incorporated into nAChRs on the soma, dendrites and axon terminals of TH^+ and TH^- VTA neurons, but excluded from extra-VTA afferents. Local infusion of MAHoCh (red arm) into the VTA labels and photosensitizes solely intra-VTA receptors, and not receptors on DA terminals. (**C**) Representative photo-inhibition of nicotine-induced currents (500 µM, local puff 500 ms) recorded at −60 mV from a GFP-positive DA neuron labeled with MAHoCh (70 µM, 20 min) in an acute brain slice. (**D**) Average percent photo-inhibition of nicotinic currents ($1-(I_{380}/I_{525})$) evoked using a local puff (500 ms) of 30 µM (49.5 ± 13.2%, p=0.013, one sample t-test) or 500 µM nicotine (67.0 ± 4.3%, p=0.0006), recorded as in (**C**) from MAHoCh-treated GFP-positive DA neurons (n = 6 and 4 for nicotine 30 and 500 µM, respectively). Control neurons (MAHoCh alone, 30 µM nicotine, Ctrl) show no photo-inhibition (−6.3 ± 7.7%, p=0.453, n = 6). (**E**) Left: Representative currents induced by nicotine (30 µM) in a control neuron (Ctrl, grey) and a β2E61C-transduced neuron (LinAChR, black). Right: Control (n = 6) and transduced (n = 6) neurons display nicotine-induced currents of same amplitude (−14.5 ± 5.5 and −14.2 ± 4.7 pA, respectively, p=0.97). All values represent mean ± SEM.

DOI: https://doi.org/10.7554/eLife.37487.005

The following source data and figure supplements are available for figure 2:

Source data 1. Source data for ***Figure 2D,E***.

DOI: https://doi.org/10.7554/eLife.37487.008

Figure supplement 1. Selective transduction of β2E61C in the VTA of WT mice.

DOI: https://doi.org/10.7554/eLife.37487.006

Figure supplement 2. No adverse effect of MAHoCh on the basic electrophysiological properties of WT VTA DA neurons.

DOI: https://doi.org/10.7554/eLife.37487.007

neurons of transduced animals, but not of control WT animals (***Figure 3C,D***), further evidencing that the effect of light is specific to the anchoring of MAHoCh to the β2 cysteine mutant.

For transduced animals, only a fraction of pDA neurons responded to light. To separately evaluate responding from non-responding neurons, we set a threshold (15% absolute photoswitching) to exclude 95% of the control neurons (***Figure 3D***). Based on this threshold, about a third (33/93) of the pDA neurons of transduced animals responded to light, compared to 1/28 for control animals. Non-responding neurons probably were either not transduced, or received too little endogenous cholinergic drive. We then compared the activity of each responding pDA neuron under both wavelengths of light and observed that some neurons responded with increased firing and some with decreased firing. A majority of the neurons (Type 1, 24/33) showed decreased activity under 390 nm

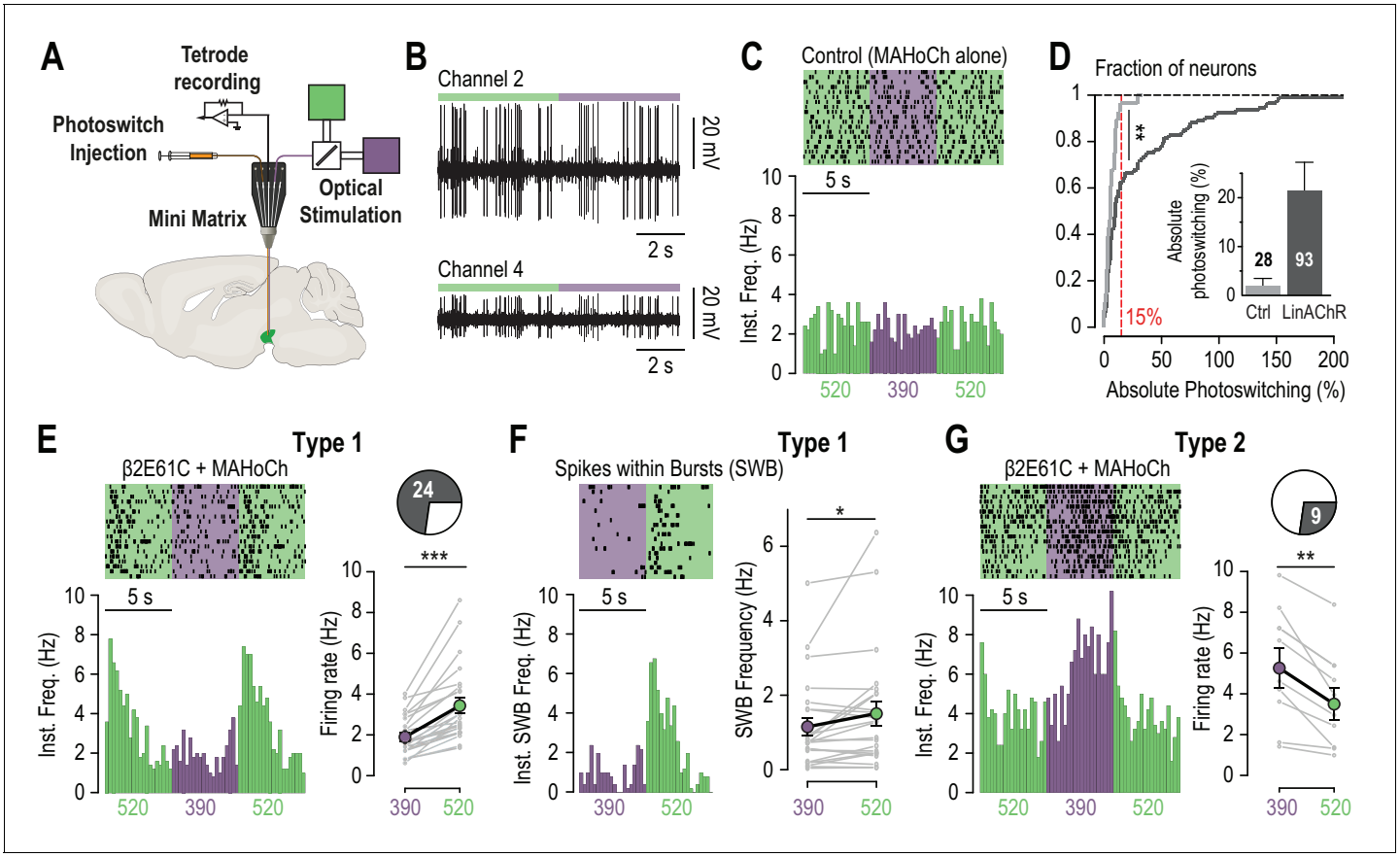

Figure 3. In vivo photo-control of endogenous cholinergic signaling. (**A**) Design of the experimental setup for concurrent recording and photocontrol of midbrain DA neurons in vivo. A micro-drive system (Mini Matrix) is mounted with a stereotaxic frame on the head of an anesthetized mouse, and enables to position in the VTA one cannula for photoswitch injection, up to three tetrodes for electrophysiological recordings, and one optic fiber connected to a beam combiner for optical stimulation. The photoswitch is injected at least an hour prior to the recordings. (**B**) Representative multi-unit recordings of transduced neurons on two channels of a tetrode while alternating illumination between 390 and 520 nm light. (**C**) Representative electrophysiological response of a MAHoCh-treated control neuron, while alternating illumination conditions between 390 (purple) and 520 nm light (green) every 5 s. Top, raster plot (n = 19 transitions) centered on the 390 nm light stimuli, and showing both the 390 to 520 and the 520 to 390 nm light transitions. Bottom, peri-stimulus time histogram (PSTH) of firing frequency using a 250 ms bin. (**D**) Change in firing frequency (expressed in absolute photoswitching) between 390 and 520 nm light for MAHoCh-treated control (Ctrl, light grey, n = 28) and β2E61C-transduced neurons (LinAChR, dark grey, n = 93). Photoswitching is calculated as $((Freq_{520} - Freq_{390})/Freq_{390})$ and represented in percent. Cumulative distribution indicates that virally transduced neurons significantly photoswitch compared to controls (p=0.0055, Kolmogorov-Smirnov test). Inset, absolute photoswitching for control neurons (1.87 ± 1.60%) is lower than that for transduced neurons (21.35 ± 5.90%). The threshold set at 15% absolute photoswitching (red) was used to determine the fraction of responding neurons in transduced animals (33/93, 35.5%). (**E**) Left, representative electrophysiological response of a virally transduced, MAHoCh-treated type 1 pDA neuron, represented as in (**C**). Right: Average firing rate of all type 1 pDA neurons (n = 24), under 520 (green) and 390 nm (purple) light. Firing frequency is significantly lower in 390 nm (1.85 Hz) compared to 520 nm light (3.41 Hz, $p=1.19e^{-07}$). (**F**) Top left, raster plot (n = 20 transitions) for the spikes contained within bursts (SWB) under 390 nm and 520 nm light, for the same neuron as in (**E**). Bottom left, PSTH of instantaneous SWB frequency using a 250 ms bin. Right, average SWB frequency of all type 1 pDA neurons (n = 24), under both wavelengths of light. SWB frequency is significantly lower in 390 compared to 520 nm light (p=0.043). (**G**) Left, representative electrophysiological response of a virally transduced, MAHoCh-treated type 2 pDA neuron, represented as in (**C**). Right: Average firing rate of all type 2 pDA neurons (n = 9), under 520 (green) and 390 nm (purple) light. Firing frequency is significantly higher in 390 nm (5.25 Hz) compared to 520 nm light (3.48 Hz, p=0.0039). All values represent mean ± SEM.

DOI: https://doi.org/10.7554/eLife.37487.009

The following source data and figure supplement are available for figure 3:

Source data 1. Source data for ***Figure 3C,G***.

DOI: https://doi.org/10.7554/eLife.37487.011

Figure supplement 1. Photocontrolling VTA β2LinAChRs in vivo.

DOI: https://doi.org/10.7554/eLife.37487.010

(*Figure 3E*), and a transient increase upon switching back to 520 nm, consistent with a direct nAChRs antagonism on VTA DA neurons by *cis* MAHoCh and relief from antagonism when MAHoCh is switched to its *trans* state. The increase in firing upon relief from antagonism suggests that ambient ACh is sufficient to drive nAChRs in an activated state. In addition, bursting activity was significantly reduced in 390 nm light in Type 1 neurons, when β2*nAChRs were antagonized (*Figure 3F*). Hence, these receptors play a causal role in determining the firing patterns of VTA DA neurons. A smaller fraction of pDA neurons (Type 2, 9/33) showed the opposite profile, i.e. increased activity under 390 nm light compared to 520 nm (*Figure 3G*). This observation suggests that extracellular ACh acts on β2*nAChRs to exert an inhibitory drive on a sub-population of VTA DA neurons, possibly through an indirect network mechanism or through β2LinAChRs expressed on GABAergic interneurons. In Type 2 pDA neurons, we observed no effect of light on AP bursts (*Figure 3—figure supplement 1B*). Altogether, these results indicate that spontaneously-released ACh acts through post-synaptic β2*nAChRs (i.e. receptors expressed on intra-VTA neurons, see *Figure 2B*) to bi-directionally modulate the tonic firing and increase the bursting activity of VTA DA neurons. This excitatory/inhibitory nicotinic drive is consistent with the duality of the responses observed upon optogenetic activation of pontine cholinergic axons (*Dautan et al., 2016*), yet it directly implicates nicotinic- and not muscarinic- ACh receptors. It is also consistent with the concurrent excitations and inhibitions observed in DA neurons upon nicotine systemic injections (*Eddine et al., 2015*).

Photo-controlling the effect of nicotine on VTA DA neurons

In WT mice, VTA DA neurons respond to nicotine with a rapid increase in firing frequency and in bursting activity, and these responses are totally absent in $\beta2^{-/-}$ mice (*Maskos et al., 2005*). Several pre- and post-synaptic mechanisms have been proposed to explain the effects of nicotine on DA cell firing (*Juarez and Han, 2016*; *Faure et al., 2014*). We tested whether blocking VTA β2LinAChRs resulted in a decrease response to nicotine in DA cells. To this aim, VTA DA neurons transduced with β2E61C were recorded in vivo using the juxta-cellular technique, which enables long, stable recordings and multiple drug injections (*Figure 4A,B*). Neurons that were successfully filled with neurobiotin (3 out of 7) were subsequently immuno-histologically identified as DAergic (*Figure 4—figure supplement 1A*). We found that the nicotine-induced variation in firing rate was much smaller under 390 nm light, when receptors were antagonized, and illumination with 520 nm light fully restored the initial response (*Figure 4C,D* and *Figure 4—figure supplement 1B*). Three of seven neurons tested showed spontaneous bursting, and all of these responded to nicotine by a variation in spikes within bursts (SWB) that appeared reduced under 390 nm light. Importantly, the response recorded from transduced animals was similar to that observed in WT animals (*Figure 4—figure supplement 1C,D*), further supporting the idea that the basic neurophysiological properties of DA neurons are unaffected by the viral transduction. Altogether, these experiments show that the effect of nicotine can be reversibly blocked with high spatial, temporal and pharmacological precision in defined brain structures, here the VTA.

Blocking VTA nAChRs is sufficient to disrupt preference to nicotine

The VTA is crucial for the motivational properties of many drugs of abuse, including nicotine (*Di Chiara and Imperato, 1988*; *Volkow and Morales, 2015*). In rodents, nicotine increases the activity of VTA DA neurons (*Mameli-Engvall et al., 2006*; *Maskos et al., 2005*) and boosts DA release in the NAc (*Di Chiara and Imperato, 1988*), signaling its reinforcing, rewarding effect. We tested whether optically blocking β2*nAChRs of the VTA was sufficient to prevent nicotine from producing its reinforcing properties. To this aim, we chronically implanted above the transduced VTA a guide cannula for local delivery of the chemical photoswitch and light (*Figure 5A*) and subjected mice to a conditioned-place preference (CPP) protocol (*Figure 5B*). Proper transduction and placement of the cannula guide were confirmed immunohistochemically (*Figure 5—figure supplement 1A*). Consistent with previous reports (*Walters et al., 2006*), WT animals showed a significant place preference for nicotine while $\beta2^{-/-}$ mice did not (*Figure 5C* and *Figure 5—figure supplement 1B*). To determine whether nicotine preference could be reversibly photo-controlled in individual animals, CPP tests were conducted with two groups of β2E61C-transduced animals. Pairings were performed first with nicotine and 390 nm light for group 1, and with nicotine and 520 nm light for group 2. Two months after the first CPP test, nicotine pairing was performed with the alternative light condition,

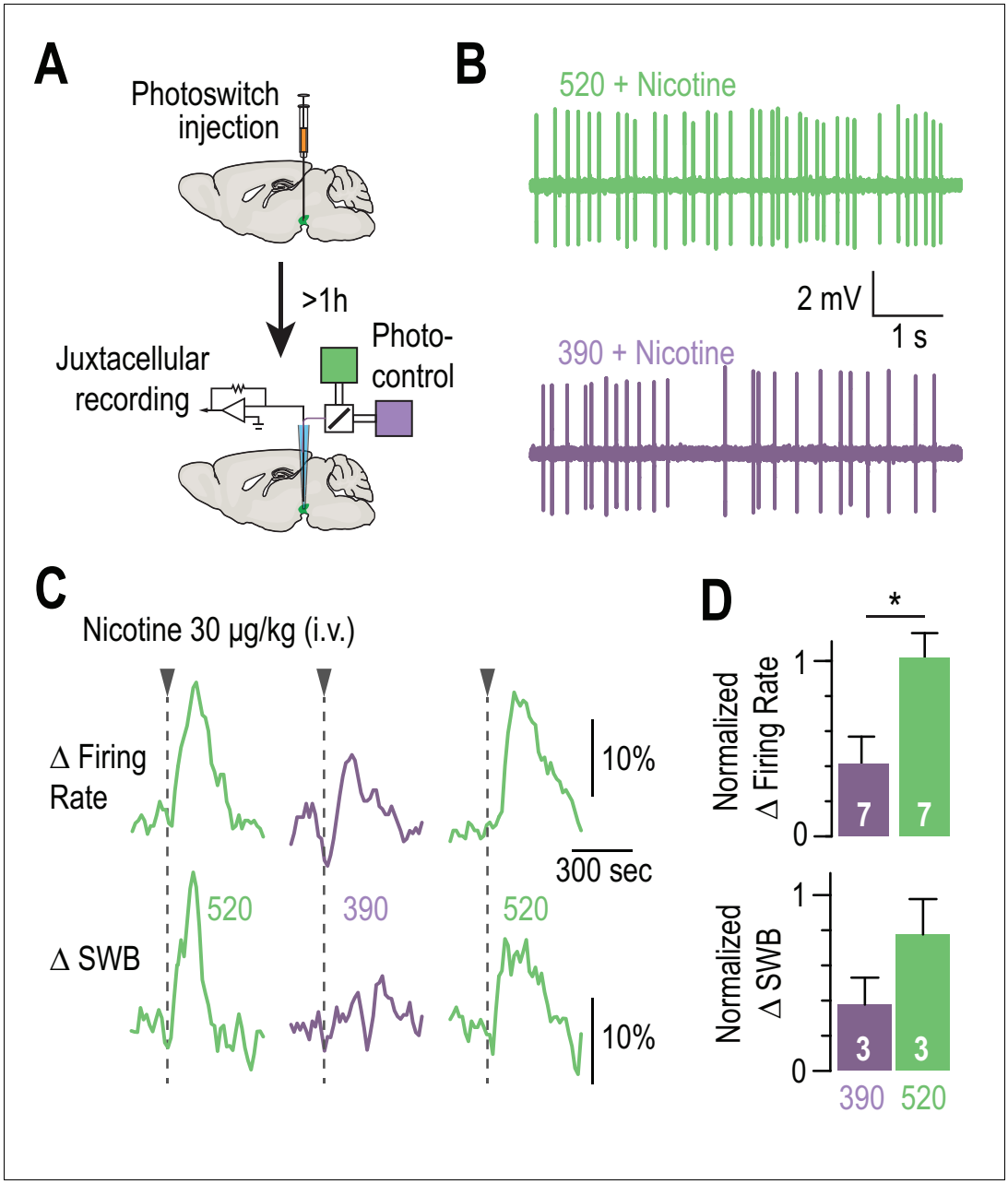

Figure 4. Blocking the effects of nicotine selectively in the VTA. (**A**) Experimental design for photoswitch injection and subsequent juxtacellular recording coupled to photocontrol. (**B**) Representative electrophysiological recording of one VTA DA neuron, during an i.v. injection of nicotine (30 µg/kg), under 520 (top, green) and 390 nm light (bottom, purple), showing greater electrical activity in green light. (**C**) Representative change in firing frequency (top) and in bursting activity (bottom) of a VTA DA neuron, elicited by an i.v. injection of nicotine (30 µg/kg), under 390 and 520 nm light, showing reversible photo-inhibition. (**D**) Top, average change in firing rate for VTA DA neurons (n = 7) upon nicotine injection under 390 (41.0 ± 15.7 %, purple) and 520 nm light (102.0 ± 14.0 %, green), normalized to the initial response in darkness. Change in firing frequency in 520 nm light is significantly different for 390 nm (p=0.015, Wilcoxon-Mann-Whitney test with Holm-Bonferroni correction) but not from darkness (p=0.81). Bottom, average change in SWB for bursting VTA DA neurons (n = 3) upon nicotine injection under 390 (37.7 ± 15.3 %, purple) and 520 nm light (77.5 ± 20.3 %, green), normalized to the initial response in darkness. All values represent mean ± SEM.

DOI: https://doi.org/10.7554/eLife.37487.012

The following source data and figure supplement are available for figure 4:

Source data 1. Source data for ***Figure 4D***.

Figure 4 continued on next page

Figure 4 continued

DOI: https://doi.org/10.7554/eLife.37487.014

Figure supplement 1. The response of VTA DA neurons to nicotine is similar in WT and in β2E61C-transduced animals.

DOI: https://doi.org/10.7554/eLife.37487.013

i.e. 520 nm light for group 1 and 390 nm light for group 2. For both groups, animals showed preference to nicotine under 520 but not under 390 nm light (***Figure 5D,E***). These results cannot be attributed to changes in general activity behavior, since locomotion was not affected by viral transduction or light (***Figure 5—figure supplement 1C***). Altogether, these experiments show that nicotine-CPP can be reversibly switched on and off in the same animal, by manipulating β2*nAChRs selectively located in the VTA.

Discussion

In this study, we used an optogenetic pharmacology strategy (***Kramer et al., 2013***) and demonstrated pharmacologically-specific, rapid local and reversible manipulation of brain nAChRs in behaving mice. Classical opsin-based optogenetics aims at turning specific neurons on or off for decoding neural circuits (***Kim et al., 2017***). Our strategy expands the optogenetic toolbox beyond excitation and inhibition by providing acute interruption of neurotransmission at the post-synaptic level, and provides mechanistic understanding of how specific transmitters and receptors contribute to modulation of circuits and behaviors.

Our method for photosensitizing receptors relies on the covalent attachment of a chemical photoswitch on a cysteine-modified receptor mutant. The photochemical properties of the azobenzene photoswitch make this strategy ideally suited for reversibly controlling neurotransmitter receptors

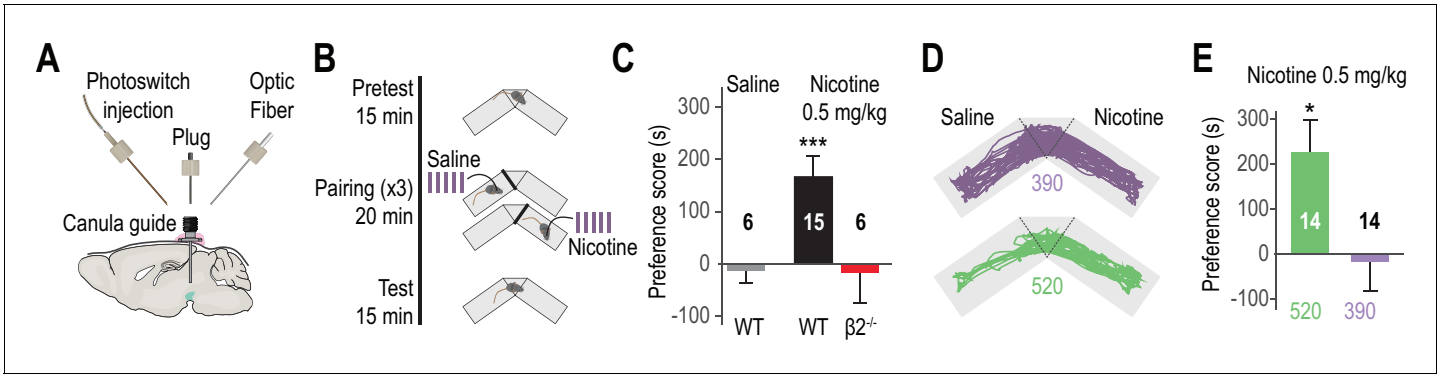

Figure 5. Reversibly disrupting nicotine preference. (**A**) Experimental design of the opto-fluidic device for opto-pharmacology experiments in freely-moving mice. The cannula guide is chronically implanted above the VTA and is used for both photoswitch and light delivery. (**B**) Nicotine-place preference protocol. Drug-free pretest (15 min) was followed by 3 consecutive days of pairing, which consisted in morning and evening saline and nicotine (0.5 mg/kg) conditioning sessions (20 min). For experiments using LinAChRs, mice were injected with the photoswitch in the morning and received light (390 or 520 nm, 2 s flashes at 0.1 Hz) in both pairing chambers. On day 5, mice were placed in the central chamber (no drug, no light) and were allowed to freely explore the environment. (**C**) Mean preference score (ps) for WT mice conditioned with saline (grey, n = 6, ps = −12.8 ± 24.0 s, p=0.69) and with nicotine (black, n = 15, ps = 165.9 ± 39.6 s, p=6.1e^{-04}), and for β2$^{-/-}$ mice conditioned with nicotine (red, n = 6, ps = −16.2 ± 58.7 s, p=0.44). (**D**) Representative trajectories of β2E61C-transduced and MAHoCh-treated mice conditioned with nicotine, under 390 (purple) and 520 nm light (green). (**E**) Mean preference for nicotine is abolished under 390 nm (purple, ps = −17.6 ± 63.8 s, p=0.80) and restored under 520 nm light (green, ps = 227.3 ± 72.1 s, p=0.015). Two groups of 7 mice were pooled. All values represent mean ± SEM.

DOI: https://doi.org/10.7554/eLife.37487.015

The following source data and figure supplement are available for figure 5:

Source data 1. Source data for ***Figure 5C,E***.

DOI: https://doi.org/10.7554/eLife.37487.017

Figure supplement 1. Nicotine-induced CPP.

DOI: https://doi.org/10.7554/eLife.37487.016

with high efficacy and at speeds that rival synaptic transmission (**Lemoine et al., 2013**; **Levitz et al., 2013**; **Lin et al., 2015**; **Szobota et al., 2007**). Comparatively, strategies for photosensitizing proteins based on the fusion of light-sensitive modules (**Rost et al., 2017**) or chromophore-assisted light-inactivation (**Lin et al., 2013**; **Takemoto et al., 2017**) are too slow or irreversible, respectively. Due to the constrains of bioconjugation, in vivo use of photoswitch-tethered receptors in mice has been restricted to the eye (**Gaub et al., 2014**) and to superficial layers of the cerebral cortex (**Levitz et al., 2016**; **Lin et al., 2015**). Here, we demonstrate rapid on and off control of neuronal nAChRs in deep brain structures and in freely behaving animals. Our data show that photoswitch delivery resulted in an absolute subtype-specificity control of β2*nAChRs, with no apparent off-target effect. Labeling was rapid (minutes) and, due to its covalent nature, persisted for many hours (we have detected strong photosensitization in vivo up to 9 hr after treatment). Importantly, due to the thermal stability of MAHoCh, receptor function was unperturbed in darkness, while brief flashes of light were sufficient to bistably toggle LinAChR between its resting and antagonized states.

The cysteine-modified subunit was transduced in the VTA of WT mice. This resulted in a local replacement of the native β2 subunit with the cysteine-mutated version, while leaving nicotinic signaling in other brain regions (notably cholinergic pontine afferents) unaffected. Even though the WT β2 subunit remained in transduced cells, photoswitch treatment resulted in robust photo-sensitization of cysteine-mutated β2*nAChRs, indicating incorporation into heteromeric receptors. The pool of receptors remained apparently unchanged, most likely because endogenous nAChR subunits (e.g. α4) limit the total number of heteropentamers at the cell surface. Replacing the WT subunit by its cysteine counterpart in a knock-in animal would guarantee complete gene replacement and untouched expression profile. Yet, viral transduction affords the advantage of allowing the engineered receptor to be targeted for expression in specific types of neurons and in defined neuronal circuits. We used this feature to optically control nAChRs at the level of VTA neurons (both DAergic and non-DAergic cells, see **Figure 2B**), while leaving pre-synaptic receptors from various afferents unaffected, which would be impossible with a transgenic animal. Collectively, our results show that β2E61C competes with native subunits to form functional receptors that, once labeled with MAHoCh, retain their natural functions in darkness, and are made photo-controllable.

Cholinergic neurons from PPN and LDT project extensively to the VTA and substantia nigra (**Beier et al., 2015**) and are thought to form connections with downstream DAergic and GABAergic neurons through non-synaptic volume transmission. Optogenetic activation of cholinergic pontine axons induces post-synaptic currents in VTA DA neurons that have both nicotinic and glutamatergic signatures (**Xiao et al., 2016**), suggesting that extracellular ACh potentiates glutamate release by activating nAChRs located on axon terminals. Contrasting with this view, we show here that activation of post-synaptic (i.e. from intra-site) β2 nAChRs by endogenous ACh is sufficient to fine tune both the tonic and burst firing modes of VTA DA neurons. Furthermore, our results add temporal and causal considerations to previous genetic studies (**Mameli-Engvall et al., 2006**; **Tolu et al., 2013**) by establishing a direct relationship between the activity of β2 nAChRs and the firing patterns of VTA DA neurons. The rebound activity that occurred within 500 ms after de-antagonizing LinAChRs indeed suggests that, even though cholinergic inputs to the VTA are considered sparse, the extracellular levels of ACh are sufficient to activate a large population of receptors and greatly modify the electrical activity of DA neurons. Moreover, we identified a sub-population of VTA DA neurons that is inhibited when β2 nAChRs are de-antagonized, which suggests multiple functional mechanisms by which the cholinergic brainstem neurons may influence the activity of midbrain DA neurons. These results are coherent with the growing body of evidence that show that VTA DA neurons are heterogeneous in their physiological properties (**Morales and Margolis, 2017**; **Yang et al., 2018**) and in their responses to drugs (**Juarez and Han, 2016**), including nicotine (**Eddine et al., 2015**).

The rewarding properties of nicotine, and especially reinforcement during the acquisition phase of addiction, implicate an elevation of DA in the NAc (**Di Chiara and Imperato, 1988**). Nicotine administration directly depolarizes and activates VTA DA neurons and, consequently, increases extracellular striatal DA (**Maskos et al., 2005**; **Tolu et al., 2013**). Nicotine can also increase DA neuron firing by acting on GABAergic and glutamatergic afferent terminals, from local interneurons and projection fibers (**Mansvelder et al., 2002**). Finally, nicotine also modulates DA release by desensitizing nAChRs expressed in the striatum at the level of DA terminals (**Rice and Cragg, 2004**). These different studies suggest alternative circuit mechanisms to explain the outcome of nicotine action on

VTA circuitry, for reviews see (**Juarez and Han, 2016**; **Faure et al., 2014**). We took advantage of the anatomical and cellular resolution of our approach, and locally blocked the effect of nicotine on VTA DA and non-DA neurons, while leaving pre-synaptic receptors of afferents from other brain areas and of striatal DA terminals unaffected. Our results show that β2*nAChRs of VTA neurons are a key player of both the response to nicotine at the cellular level, and the rewarding properties of this addictive substance at the behavioral level. Importantly, blocking the excitatory phasic input produced by nicotine was sufficient to completely prevent reinforcement learning. This is consistent with our results concerning the ability of β2 nAChRs to tune burst firing in DA neurons, and with the fact that activation of LDT-to-VTA cholinergic neurons causes positive reinforcement (**Dautan et al., 2016**; **Xiao et al., 2016**). All together, these results strongly suggest that these receptors have a central role in reward processing.

There is a considerable interest to target-specific nAChRs and specific circuits to treat psychiatric disorders such as addiction, depression or schizophrenia. Yet, we do not know which native receptor subtype mediates specific physiological or pathological function, hampering development of clinically effective drugs, notably for preventing or treating addiction. Optogenetic pharmacology offers the unique opportunity to locally and reversibly 'knock-out' the function of a specific receptor isoform in vivo, and to directly evaluate within the same animal the consequences at the cellular, circuit and behavioral levels. Our approach should be applicable to other photo-activatable and -inhibitable nAChR subtypes and other neuronal circuits, and may provide a platform for examining new translational strategies for treating neuropsychiatric disorders.

Materials and methods

Key resources table

Reagent type (species) or resource	Designation	Source or reference	Identifiers	Additional information
Antibody	Anti-tyrosine Hydroxylase produced in mouse	Sigma-Aldrich	T1299, RRID:AB_477560	
Antibody	Anti-Choline-Acetyltransferase produced in goat	Merck-Millipore	AB144, RRID:AB_90650	
Antibody	Anti-GFP produced in rabbit			
Antibody	Anti-GFP produced in chicken	Aves Lab	GFP-1020, RRID:AB_10000240	
Antibody	Anti-rabbit Cy2-conjugated produced in donkey	Jackson Immuno Research	711-225-152, RRID:AB_2340612	
Antibody	Anti-mouse Cy3-conjugated produced in donkey	Jackson Immuno Research	715-165-150, RRID:AB_2340813	
Antibody	Anti-chicken Alexa488-conjugated	Jackson Immuno Research	703-545-155, RRID:AB_2340375	
Antibody	anti-goat Alexa 555-conjugated produced in donkey	Life Technologies	A21432, RRID:AB_141788	
Antibody	AMCA-Streptavidin	Jackson ImmunoResearch	016-150-084, RRID:AB_2337243	
Strain, strain background (*mus musculus*, males)	C57Bl/6JRj	Janvier Laboratories, France	SC-C57J-M, RRID:MGI:5752053	

Continued on next page

Continued

Reagent type (species) or resource	Designation	Source or reference	Identifiers	Additional information
Strain, strain background (*mus musculus*, males)	ACNB2	https://doi.org/10.1038/374065a0		maintained on a C57BL6/J background
Strain, strain background (*lentivirus*)	Lenti-pGK-B2E61C-IRES-GFP	This paper		
Cell line (*mus musculus*)	Neuro 2a	Sigma-Aldrich	89121404-1VL, RRID:CVCL_0470	
Transfected construct (*mus musculus*)	pIRES-a4-IRES-GFP	https://doi.org/10.1038/nature03694		
Transfected construct (*mus musculus*)	pIRES-b2E61C-IRES-eGFP	this paper		
Chemical compound, drug	MAHoCh	https://doi.org/10.1038/nchem.1234		
Chemical compound, drug	NaCl	Sigma-Aldrich	S7653	
Chemical compound, drug	KCl	Sigma-Aldrich	P9333	
Chemical compound, drug	NaH2PO4	Sigma-Aldrich	S8282	
Chemical compound, drug	MgCl2	Sigma-Aldrich	M2670	
Chemical compound, drug	CaCl2	Sigma-Aldrich	233506	
Chemical compound, drug	NaHCO3	Sigma-Aldrich	S6297	
Chemical compound, drug	Sucrose	Sigma-Aldrich	S0389	
Chemical compound, drug	Glucose	Sigma-Aldrich	49159	
Chemical compound, drug	Kynurenic Acid	Sigma-Aldrich	K3375	
Chemical compound, drug	Albumin, from bovine serum	Sigma-Aldrich	A4503	
Chemical compound, drug	KGlu	Sigma-Aldrich	P1847	
Chemical compound, drug	HEPES	Sigma-Aldrich	H3375	
Chemical compound, drug	EGTA	Sigma-Aldrich	E3889	

Continued on next page

Continued

Reagent type (species) or resource	Designation	Source or reference	Identifiers	Additional information
Chemical compound, drug	ATP	Sigma-Aldrich	A9187	
Chemical compound, drug	GTP	Sigma-Aldrich	G8877	
Chemical compound, drug	Biocytin	Sigma-Aldrich	B4261	
Chemical compound, drug	Nicotine tartrate	Sigma-Aldrich	N5260	
Chemical compound, drug	Glucose	Sigma-Aldrich	G8270	
Chemical compound, drug	DMEM + Glutamax	Life Technologies	31966–021	
Chemical compound, drug	FBS	Life Technologies	10500–064	
Chemical compound, drug	Non-essential amino acids	Life Technologies	11140–035	
Chemical compound, drug	Pennicilin/ Streptomycin	Life Technologies	15140–122	
Chemical compound, drug	Trypsin	Life Technologies	15090–046	
Chemical compound, drug	Polylysine	Sigma-Aldrich	P6282	
Chemical compound, drug	DMSO	Sigma-Aldrich	D2650	
Chemical compound, drug	Carbamylcholine Chloride	Sigma-Aldrich	C4382	
Chemical compound, drug	DPBS 10x	Life Technologies	14200–067	
Chemical compound, drug	Neurobiotin Tracer	Vector laboratories	SP-1120	
Chemical compound, drug	Prolong Gold Antifade Reagent	Invitrogen	P36930	
Software, algorithm	MATLAB	MathWorks	RRID:SCR_001622	
Software, algorithm	R Project for Statistical Computing	http://www.r-project.org/	RRID:SCR_001905	
Software, algorithm	Fiji	http://fiji.sc	RRID:SCR_002285	

Continued on next page

Continued

Reagent type (species) or resource	Designation	Source or reference	Identifiers	Additional information
Software, algorithm	Adobe Illustrator CS6	Adobe	RRID:SCR_010279	
Software, algorithm	Clampfit (pClamp suite)	Molecular Devices	RRID:SCR_011323	

Animals

65 Wild-type male C57BL/6J mice were obtained from Janvier Laboratories (France) and 6 knockout SOPF-HO-ACNB2 ($\beta2^{-/-}$) male mice were obtained from Charles Rivers Laboratories (France). $\beta2^{-/-}$ mice were generated as described previously (***Picciotto et al., 1995***). Even though WT and $\beta2^{-/-}$ mice are not littermates the mutant line was generated more than 20 years ago, and has been back-crossed more than 20 generations with the WT C57BL/6J line and is more than 99.99% C57BL/6J. All experiments were performed on mice between 8 and 16 weeks of age. All experiments were performed in accordance with the recommendations for animal experiments issued by the European Commission directives 219/1990, 220/1990 and 2010/63, and approved by Sorbonne Université.

Chemical photoswitch

MAHoCh was synthesized as described previously (***Tochitsky et al., 2012***) and was stored as concentrated stock solutions (100 mM) in water-free DMSO at −80°C. For cell labeling, aqueous solutions of MAHoCh were prepared extemporaneously.

Light intensity measurements

Light intensities were measured with a power meter (1916 R, Newport) equipped with a UV-silicon wand detector (818-ST2-DB Newport).

Molecular biology and virus production

The cDNAs for the WT mouse β2 and α4 nAChR subunits were from previously-designed pIRES (CMV promoter) or pLenti (pGK promoter) vectors (***Maskos et al., 2005***). All the constructs are bicistronic, with an IRES-eGFP sequence designed to express eGFP and the nAChR subunit using the same promoter. The pLenti construct also contains the long terminal repeats, WPRE and virus elements for packaging into lentiviral vectors. The single cysteine mutation E61C was inserted into pIRES-CMV-β2-IRES-eGFP and pLenti-pGK-β2-IRES-eGFP by site-directed mutagenesis using the Quickchange II XL kit (Agilent). Mutations were verified by DNA sequencing. Lentiviruses were prepared as described previously (***Maskos et al., 2005***) with a titer of 150 ng of p24 protein in 2 µl.

Cell line

We used Neuro2A cells (Sigma Aldrich #89121404-1VL), a mouse neuroblastoma cell line classically used for nAChRs expression (***Xiao et al., 2011***). Cells were certified by Sigma-Aldrich. Mycoplasma contamination status were negative.

Cell culture, transfection and labeling

Briefly, Neuro2A cells were cultured in Dulbecco's Modified Eagle's Medium (DMEM), supplemented with 10% Foetal Bovine Serum (FBS), 1% non-essential amino-acids, 100 units/ml penicillin, 100 mg/ml streptomycin and 2 mM glutamax in a 5% CO_2 incubator at 37°C. Cells were transfected overnight with a 1:1 ratio of α4 and β2E61C subunits (pLenti-pGK-α4-IRES-eGFP and pLenti-pGK-β2E61C-IRES-eGFP), using calcium-phosphate transfection method (***Lemoine et al., 2016***). Cells were used 2–3 days after transfection for electrophysiology. Prior to recordings, cells were labeled with MAHoCh (20 µM in external solution) for 20 min.

Stereotaxic viral injections

WT mice (6–8 weeks) were anaesthetized with 1% isoflurane gas and placed in a stereotaxic frame (David Kopf). A small craniotomy was made above the location of the VTA. A lentivirus containing the construct pGK-β2E61C-IRES-eGFP was injected in the VTA (1 µl at the rate of 0.1 µl/min) with a

10 µl syringe (Hamilton) coupled with a polyethylene tubing to a 36 G cannula (Phymep), with the following coordinates [AP: −3.1 mm; ML:±0.4 mm; DV: −4.7 mm from bregma]. Mice were then housed during at least 4 weeks before electrophysiology or behavior experiments.

Midbrain slices preparation and labeling

4–8 weeks after viral infection, mice were deeply anesthetized with an i.p. injection of a mixture of ketamine (150 mg/kg, Imalgene 1000, Merial) and xylazine (60 mg/kg, Rompun 2%, Bayer). Coronal midbrain sections (250 µm) were sliced using a Compresstome (VF-200; Precisionary Instruments) after intra-cardiac perfusion of cold (0–4°C) sucrose-based artificial cerebrospinal fluid (SB-aCSF) containing (in mM): 125 NaCl, 2.5 KCl, 1.25 NaH_2PO_4, 5.9 $MgCl_2$, 26 $NaHCO_3$, 25 Sucrose, 2.5 Glucose, 1 Kynurenate. After 10 min at 35°C for recovery, slices were transferred into oxygenated (95% CO_2/5% O_2) aCSF containing (in mM): 125 NaCl, 2.5 KCl, 1.25 NaH_2PO_4, 2 $CaCl_2$, 1 $MgCl_2$, 26 $NaHCO_3$, 15 Sucrose, 10 Glucose at room temperature for the rest of the day. Slices were labeled individually with MAHoCh (70 µM) in oxygenated aCSF (1 ml) for 20 min, and transferred to a recording chamber continuously perfused at 2 ml/min with oxygenated aCSF.

Patch-clamp recordings

Patch pipettes (5–8 MΩ) were pulled from thin wall borosilicate glass (G150TF-3, Warner Instruments) using a micropipette puller (P-87, Sutter Instruments) and filled with a K-Gluconate based intra-pipette solution containing (in mM): 116 KGlu, 20 HEPES, 0.5 EGTA, 6 KCl, 2 NaCl, 4 ATP, 0.3 GTP and 2 mg/mL biocytin (pH adjusted to 7.2). Cells were visualized using an upright microscope with a Dodt contrast lens and illuminated with a white light source (Scientifica). A 460 nm LED (pE-2, Cooled) was used for visualizing eGFP positive cells (using a bandpass filter cube, AHF). Optical stimulation was applied through the microscope with two LEDs (380 and 525 nm, pE-2, CoolLED), with a light output of 6.5 and 15 mW, corresponding to 5 and 11.7 mW/mm^2 at the focal plane, respectively. Whole-cell recordings were performed using a patch-clamp amplifier (Axoclamp 200B, Molecular Devices) connected to a Digidata (1550 LowNoise acquisition system, Molecular Devices). Currents were recorded in voltage-clamp mode at −60 mV. Signals were low pass filtered (Bessel, 2 kHz) and collected at 10 kHz using the data acquisition software pClamp 10.5 (Molecular Devices). Electrophysiological recordings were extracted using Clampfit (Molecular Devices) and analyzed with R.

To record nicotinic currents from GFP-positive Neuro2A cells, we used the following external solution (containing in mM): 140 NaCl, 2.8 KCl, 2 $CaCl_2$, 2 $MgCl_2$, 10 HEPES, 12 glucose (pH 7.3 with NaOH). We used a computer-controlled, fast-perfusion stepper system (SF-77B, Harvard Apparatus) to apply nicotine-tartrate (100 µM, Sigma-Aldrich) or carbamylcholine chloride (CCh, 1 mM, Sigma-Aldrich), with an interval of 2 min, under different light conditions.

To record nicotinic currents from VTA DA neurons, local puffs (500 ms) of nicotine tartrate (30–500 µM in aCSF) were applied every minute, while alternating wavelengths, using a glass pipette (2–3 µm diameter) positioned 20 to 30 µm away from the soma and connected to a picospritzer (World Precision Instruments, adjusted to ~2 psi). DA neurons were characterized in current clamp mode as described in (***Lammel et al., 2008***), see ***Figure 2—figure supplement 2A***. In some instances, at the end of the recording, the pipette was retracted carefully to allow labeling of the neuron with biocytin (***Marx et al., 2012***).

In vivo juxtacellular recordings

4–8 weeks after viral infection, mice were deeply anaesthetized with chloral hydrate (8%, 400 mg/kg i.p.), supplemented as required to maintain optimal anesthesia throughout the experimental day. The scalp was opened and a hole was drilled in the skull above the location of the VTA. The saphenous vein was catheterized for intravenous administration of nicotine. Prior to recordings (at least 1 hr), 500 nl of a 400 µM solution of MAHoCh in aCSF were injected within the VTA at a rate of 50 nl/min. Extracellular recording electrodes were made from 1.5 mm O.D./1.17 mm I.D. borosilicate glass (Harvard Apparatus) using a vertical electrode puller (Narishige). Under a microscope, the tip was broken to obtain a diameter of 1–2 µm. The electrodes were filled with a 0.5% Na-Acetate solution containing 1.5% of neurobiotin tracer yielding impedances of 20–50 MΩ. Electrophysiological signals were amplified with a headstage (1x, Axon Instruments) coupled to a high-impedance amplifier

(Axoclamp-2A, Axon Instruments) and audio monitored (A.M. Systems Inc.). The signal was digitized (Micro-2, Cambridge Electronic Design), sampled at 12.5 kHz and recorded using Spike2 software (CED). DA neurons were sampled in the VTA with the following coordinates: [AP: −3 to −4 mm; ML: +0.3 to+0.6 mm; DV: −4 to −4.8 mm, from Bregma]. Spontaneously active pDA neurons were identified on the basis of previously established electrophysiological criteria: 1) regular firing rate; 2) firing frequency between 1 and 10 Hz; 3) half AP >1.1 ms. After a baseline recording of at least 5 min, a saline solution (0.9% sodium chloride) was injected into the saphenous vein, and after another 10 min, injections of nicotine- tartrate (30 µg/kg) were administered via the same route in a final volume of 10 µl and under different light conditions (Dark – 390 nm – 520 nm). Successive injections (up to 6) were performed after the neuron returned to its baseline, or when the firing activity returned stable for at least 3 min. Light was applied through an optical fiber (500 µm core, NA = 0.5, Prizmatix) inserted within the glass pipette electrode and coupled through a combiner to 390/520 nm ultra-high-power LEDs (Prizmatix), yielding an output intensity of 4–8 mW at the tip of the fiber for each wavelength. Light was TTL-controlled and applied 10 s before nicotine injection, for 30 s total. When possible, neurons were electroporated and neurobiotin was expulsed from the electrode using positive current pulses as already described (***Pinault, 1996***; ***Eddine et al., 2015***). Spikes Within Bursts (SWB) were identified as a sequence of spikes with the following features: (1) short intervals, (2) progressively decreasing spike amplitude, and (3) a progressively increasing inter-spike interval (ISI). When considering extracellular recordings, most studies use two criteria to automatically detect bursts: (1) their onset are defined by two consecutive spikes with an interval inferior to 80 ms, whenever (2) they are closed with an interval greater than 160 ms (***Grace and Bunney, 1984***). Firing rate and %SWB were measured on successive windows of 60 s, with a 45 s overlapping period. Responses to nicotine are presented as the mean percentage of firing frequency or %SWB variation from the baseline ±SEM. For photoswitching, maximum of firing variation induced by nicotine occurring 200 s after the injection in purple and green was normalized to the maximum of firing variation in darkness. Spikes were extracted with Spike2 (CED) and analyzed with R (https://www.r-project.org).

In vivo multi-unit extracellular recordings

4–8 weeks after viral infection, mice were deeply anaesthetized with chloral hydrate (8%, 400 mg/kg i.p.), supplemented as required to maintain optimal anesthesia throughout the experiment. The scalp was opened and a hole was drilled in the skull above the location of the VTA. We used a Mini-Matrix (***Figure 3A***, Thomas Recording) allowing us to lower within the VTA: up to 3 tetrodes (Tip shape A, Thomas Recording, Z = 1–2 MΩ), a stainless-steel cannula (OD 120 µm, Thomas Recording) for photoswitch injection and a tip-shaped quartz optical fiber (100 µm core, NA = 0.22, Thomas Recording) for photostimulation. The fiber was coupled to a 390/520 nm LED combiner (Prizmatix) with an output intensity of 200–500 µW at the tip of the fiber for both wavelengths. These five elements could be moved independently with micrometer precision. 500 nl of MAHoCh (400 µM in aCSF) were infused (rate: 1 nl/s) within the VTA, and tetrodes were subsequently lowered in the same zone to record neurons. Spontaneously active pDA neurons were recorded at least 30 min after MAHoCh infusion and were identified on the basis of the electrophysiological criteria used for juxtacellular recordings. The optical fiber was then lowered 100–200 µm above the tetrodes. Baseline activity was recorded for 200 s in darkness, prior to applying 5 s light flashes of alternative wavelengths (390 nm / 520 nm). Electrophysiological signals were acquired with a 20 channels preamplifier included in the Mini Matrix (Thomas Recording) connected to an amplifier (Digital Lynx SX 32 channels, Neuralynx) digitized and recorded using Cheetah software (Neuralynx). Spikes were detected using a custom-written Matlab routine and sorted using a classical principal component analysis associated with a cluster cutting method (SpikeSort3D Software, Neuralynx). Neurons were considered as responding when their change in firing rate (% Photoswitching) at the transition from violet to green light exceeded a threshold of 15%, defined as the maximal % photoswitching observed in controls. This threshold was used for all recorded neurons in every condition. To extract the spikes contained within bursting episodes (SWB) we used the same criteria described in the juxtacellular recordings section. They are represented as the frequency of SWB because of the short analysis window (5 s). All the data were analyzed with R (https://www.r-project.org) and Matlab (MathWorks).

Chronic guide cannula implantation

Following stereotaxic viral infection in the VTA (as described above), mice were implanted with a chronic opto-fluid guide cannula (Doric Lenses Inc, Canada, see ***Figure 5A***) using the same coordinates. This guide (length = 3 mm from skull surface, ID/OD = 320/430 µm) has interchangeable threaded connectors and is used either with a fluid injection needle (protruding to 4.8 mm from skull surface) for delivering MAHoCh, or with an optic fiber injector (240 µm core, NA = 0.63, protruding to 4.8 mm from skull surface) coupled to a ceramic ferrule (1.25 mm) for light delivery. In-between experiments, a plug is used to close the guide cannula and thus seal the implant. The implant is attached to the skull with a dental cement (SuperBond, Sun Medical).

Nicotine-induced place preference paradigm

The Conditioned Place Preference (CPP) box (Imetronic, France) consists of a Y-maze with one closed arm, and two other arms with manually operated doors. Two rectangular chambers (11 × 25 cm) with different cues (texture and color), are separated by a center triangular compartment (side of 11 cm). One pairing compartment has grey textured floor and walls and the other one has smooth black and white striped walls and floor. The first day (pretest) of the experiment, mice (n = 6–8 animals/group) explored the environment for 900 s (15 min) and the time spent in each compartment was recorded. Pretest data were used to segregate the animals with equal bias so each group has an initial preference score almost null, indicating no preference on average. On day 2, 3 and 4, animals received an i.p. injection of nicotine tartrate (0.5 mg/kg, in PBS) or an equivalent injection of saline (PBS), and immediately confined to one of the pairing chamber for 1200 s (20 min). The CPP test was performed using a single nicotine concentration (0.5 mg/kg) which is known to induce preference in mice (***Walters et al., 2006***). Groups were balanced so the animals do not always get nicotine in the same chamber. On the evening of the same day, mice received an injection of the alternate solution (nicotine or saline) and were placed in the opposite pairing chamber. The saline control animals received a saline injection in both pairing compartments. On day 5 (test), animals were allowed to explore the whole open-field for 900 s (15 min), and the time spent in each chamber was recorded. The preference score (ps) is expressed in seconds and is calculated by subtracting pretest from test data. Trajectories and time spent on each side are calculated based upon animal detection. Place preference and locomotor activity were recorded using a video camera, connected to a video-track system, out of sight of the experimenter. A home-made software (Labview 2014, National Instruments) tracked the animal, recorded its trajectory (20 frames per s) for 15 min and sent TTL pulses to the LED controller when appropriate (pairing sessions). For optogenetic pharmacology experiments, MAHoCh (400 µM in aCSF, 500 nl in 5 min) was injected early in the morning of pairing days (2, 3 and 4) under light gas anesthesia (Isoflurane 1%). 520/390 nm light was applied during pairing sessions (day 2, 3 and 4), on both sides, through a patch cord (500 µm core, NA = 0.5, Prizmatix, Israel) connected to the implanted ferrule with a sleeve and to the 390/520 nm combined UHP-LEDs (Prizmatix). Light was applied with the following pattern: 2 s pulses à 0.1 Hz with a measured output intensity of 10 mW at the tip of the patch cord. Light was not applied during pre-test and test. Behavioral data were collected and analyzed using home-made LabVIEW (National Instruments) and Matlab (MathWorks) routines.

Immunohistochemistry

After patch-clamp experiments, individual slices (250 µm) were transferred in 4% paraformaldehyde (PFA) for 12–24 hr and then to PBS, and kept at 4°C. At the end of in vivo experiments, transduced mice received, under deep anesthesia (Ketamine/Xylazine), an intra-cardiac perfusion of (1) PBS (50 ml) and (2) paraformaldehyde (4% PFA, 50 ml) and brains were rapidly removed and let in 4% PFA for 48–72 hr of fixation at 4°C. Serial 60 µm sections of the ROI were cut with a vibratome. Immunohistochemistry was performed as follows: Floating VTA brain sections were incubated 1 hr at 4°C in a solution of phosphate-buffered saline (PBS) containing 3% Bovine Serum Albumin (BSA, Sigma; A4503) and 0.2% Triton X-100 and then incubated overnight at 4°C with a mouse anti-Tyrosine Hydroxylase antibody (TH, Sigma, T1299) at 1:200 dilution and a rabbit anti-GFP antibody (Molecular Probes, A-6455) at 1:500 dilution in PBS containing 1.5% BSA and 0.2% Triton X-100. The following day, sections were rinsed with PBS and then incubated 3 hr at 22–25°C with Cy3-conjugated anti-mouse and Cy2-conjugated anti-rabbit secondary antibodies (Jackson ImmunoResearch, 715-165-

150 and 711-225-152) at 1:200 and 1:1000 dilution respectively in a solution of 1.5% BSA and 0.2% Triton X-100 in PBS. In the case of biocytin/neurobiotin labelling, TH identification of the neuron was performed using AMCA-conjugated Streptavidin (Jackson ImmunoResearch) at 1:200 dilution. Floating pons sections were incubated 1 hr at 4°C in a solution of phosphate-buffered saline containing 0.2% Gelatine from cold-water fish skin (Sigma; G7041) and 0.25% Triton X-100 (PBS-GT) and then incubated overnight at 4°C a goat anti-Choline Acetyl-Transferase antibody (ChAT, Merck-Millipore, AB144) at 1:200 dilution and a chicken anti-GFP antibody (Aves Lab, GFP-1020) at 1:500 dilution in PBS-GT. The following day, sections were rinsed with PBS and then incubated 3 hr at 22–25°C with a donkey anti-goat Alexa 555-conjugated (Invitrogen, A21432) and donkey anti-chicken Alexa 488-conjugated (Jackson ImmunoResearch, 703-545-155) at 1:200 and 1:1000 dilution respectively in a solution of PBS-GT. After three rinses in PBS (5 min), wet slices were mounted using Prolong Gold Antifade Reagent (Invitrogen, P36930). Microscopy was carried out either with a confocal microscope (Leica) or an epifluorescence microscope (Leica), and images captured using a camera and analyzed with ImageJ software.

Statistical analysis

No statistical methods were used to predetermine sample sizes. Data are plotted as mean ±SEM. Total number (n) of observations in each group and statistics used are indicated in figure and/or figure legend. Unless otherwise stated, comparisons between means were performed using parametric tests (two-sample t-test) when parameters followed a normal distribution (Shapiro test $p>0.05$), and non-parametric tests (here, Wilcoxon or Mann-Whitney (U-test)) when this was not the case. Homogeneity of variances was tested preliminarily and the t-tests were Welch-corrected if needed. Multiple comparisons were Holm-Bonferroni corrected. Comparison between the cumulative distributions of in vivo multi-unit recordings between controls and LinAChRs (***Figure 3D***) was performed using a Kolmogorov-Smirnov test. $p>0.05$ was considered to be not statistically significant.

Acknowledgments

Authors would like to thank Nadine Mouttajagane, Ambre Bonnet and Michael Martin for molecular biology work, and Justine Hadjerci, Steve Didienne and Samir Takillah for their help with electrophysiology and behavior experiments. This work was supported by the Agence Nationale de la Recherche (ANR-JCJC 2014 to A.M.), by a NARSAD Young Investigator Grant from the Brain and Behavior Research Foundation (to A.M.), by the Fondation pour la Recherche Médicale (Équipe FRM DEQ2013326488 to P.F.), by the French National Cancer Institute Grant TABAC-16–022 (to P.F.) by the Fédération de la Recherche pour le Cerveau (FRC Rotary Espoir en tête 2012 to P.F.) and by the Labex Bio-Psy. A.M. was recipient of a fundamental research prize from the Medisite Foundation for Neuroscience. R.D.C. was supported by a Ph.D. fellowship from the DIM Cerveau and Pensée program of the Région Ile-de-France, and by a fourth-year Ph.D. fellowship from FRM (FDT20170437427). D.L. was recipient of a Labex Biopsy post-doctoral fellowship. RHK was supported by grants from the NIH (U01-NS090527 and R01-NS100911). P.F. and A.M. laboratory is part of the École des Neurosciences de Paris Ile-de-France RTRA network. P.F. is member of LabEx Bio-Psy and of DHU Pepsy.

Additional information

Funding

Funder	Grant reference number	Author
DIM Cerveau Pensée	PhD fellowship	Romain Durand-de Cuttoli
Fondation pour la Recherche Médicale	PhD fellowship FDT20170437427	Romain Durand-de Cuttoli
Labex	Bio-Psy post-doctoral fellowship	Damien Lemoine
National Institutes of Health	U01-NS090527	Richard H Kramer

Fondation pour la Recherche Médicale	Equipe FRM DEQ2013326488	Philippe Faure
Institut National Du Cancer	TABAC-16-022	Philippe Faure
Fédération pour la Recherche sur le Cerveau	Rotary Espoir en tête 2012	Philippe Faure
Brain and Behavior Research Foundation	NARSAD Young Investigator Grant	Alexandre Mourot
Agence Nationale de la Recherche	ANR-JCJC	Alexandre Mourot
Fondation de France	Fondation Medisite fundamental research prize	Alexandre Mourot
National Institutes of Health	R01-NS100911	Richard H Kramer

The funders had no role in study design, data collection and interpretation, or the decision to submit the work for publication.

Author contributions

Romain Durand-de Cuttoli, Data curation, Formal analysis, Methodology, Writing—original draft, Writing—review and editing, Performed viral injections and cannula implantations, Slice patch-clamp experiments, In vivo electrophysiology, Behavioral studies and immunochemistry; Sarah Mondoloni, Data curation, Formal analysis, Methodology, Writing—original draft, Writing—review and editing, Performed cell culture and in vitro electrophysiology, Slice patch-clamp experiments and immunochemistry; Fabio Marti, Data curation, Formal analysis, Performed in vivo electrophysiology; Damien Lemoine, Data curation, Formal analysis, Performed cell culture and in vitro electrophysiology; Claire Nguyen, Data curation, Performed immunochemistry; Jérémie Naudé, Formal analysis; Thibaut d'Izarny-Gargas, Data curation, Performed slice patch-clamp experiments; Stéphanie Pons, Uwe Maskos, Dirk Trauner, Resources; Richard H Kramer, Resources, Funding acquisition, Writing—review and editing; Philippe Faure, Conceptualization, Supervision, Funding acquisition, Project administration, Writing—review and editing; Alexandre Mourot, Conceptualization, Data curation, Supervision, Funding acquisition, Methodology, Writing—original draft, Project administration, Writing—review and editing

Author ORCIDs

Romain Durand-de Cuttoli https://orcid.org/0000-0003-0240-7608
Jérémie Naudé https://orcid.org/0000-0001-5781-6498
Thibaut d'Izarny-Gargas https://orcid.org/0000-0002-6084-5836
Stéphanie Pons https://orcid.org/0000-0003-1027-0621
Philippe Faure https://orcid.org/0000-0003-3573-4971
Alexandre Mourot http://orcid.org/0000-0002-8839-7481

Ethics

Animal experimentation: All experiments were performed in accordance with the recommendations for animal experiments issued by the European Commission directives 219/1990, 220/1990 and 2010/63, and approved by Sorbonne Université.

Decision letter and Author response

Decision letter https://doi.org/10.7554/eLife.37487.020
Author response https://doi.org/10.7554/eLife.37487.021

Additional files

Supplementary files

- Transparent reporting form

DOI: https://doi.org/10.7554/eLife.37487.018

Data availability

All data generated or analyzed during this study are included in the manuscript and supporting files. Source data are provided for Figures 1 to 5.

References

Avale ME, Faure P, Pons S, Robledo P, Deltheil T, David DJ, Gardier AM, Maldonado R, Granon S, Changeux JP, Maskos U. 2008. Interplay of beta2* nicotinic receptors and dopamine pathways in the control of spontaneous locomotion. *Proceedings of the National Academy of Sciences* **105**:15991–15996. DOI: https://doi.org/10.1073/pnas.0807635105, PMID: 18832468

Beier KT, Steinberg EE, DeLoach KE, Xie S, Miyamichi K, Schwarz L, Gao XJ, Kremer EJ, Malenka RC, Luo L. 2015. Circuit architecture of VTA dopamine neurons revealed by systematic Input-Output mapping. *Cell* **162**: 622–634. DOI: https://doi.org/10.1016/j.cell.2015.07.015, PMID: 26232228

Changeux JP. 2010. Nicotine addiction and nicotinic receptors: lessons from genetically modified mice. *Nature Reviews Neuroscience* **11**:389–401. DOI: https://doi.org/10.1038/nrn2849, PMID: 20485364

Dautan D, Souza AS, Huerta-Ocampo I, Valencia M, Assous M, Witten IB, Deisseroth K, Tepper JM, Bolam JP, Gerdjikov TV, Mena-Segovia J. 2016. Segregated cholinergic transmission modulates dopamine neurons integrated in distinct functional circuits. *Nature Neuroscience* **19**:1025–1033. DOI: https://doi.org/10.1038/nn.4335, PMID: 27348215

Di Chiara G, Imperato A. 1988. Drugs abused by humans preferentially increase synaptic dopamine concentrations in the mesolimbic system of freely moving rats. *Proceedings of the National Academy of Sciences* **85**:5274–5278. DOI: https://doi.org/10.1073/pnas.85.14.5274, PMID: 2899326

Eddine R, Valverde S, Tolu S, Dautan D, Hay A, Morel C, Cui Y, Lambolez B, Venance L, Marti F, Faure P. 2015. A concurrent excitation and inhibition of dopaminergic subpopulations in response to nicotine. *Scientific Reports* **5**:8184. DOI: https://doi.org/10.1038/srep08184, PMID: 25640814

Faure P, Tolu S, Valverde S, Naudé J. 2014. Role of nicotinic acetylcholine receptors in regulating dopamine neuron activity. *Neuroscience* **282**:86–100. DOI: https://doi.org/10.1016/j.neuroscience.2014.05.040, PMID: 24881574

Floresco SB, West AR, Ash B, Moore H, Grace AA. 2003. Afferent modulation of dopamine neuron firing differentially regulates tonic and phasic dopamine transmission. *Nature Neuroscience* **6**:968–973. DOI: https://doi.org/10.1038/nn1103, PMID: 12897785

Gaub BM, Berry MH, Holt AE, Reiner A, Kienzler MA, Dolgova N, Nikonov S, Aguirre GD, Beltran WA, Flannery JG, Isacoff EY. 2014. Restoration of visual function by expression of a light-gated mammalian ion channel in retinal ganglion cells or ON-bipolar cells. *PNAS* **111**:E5574–E5583. DOI: https://doi.org/10.1073/pnas.1414162111, PMID: 25489083

Grace AA, Bunney BS. 1984. The control of firing pattern in nigral dopamine neurons: burst firing. *The Journal of Neuroscience* **4**:2877–2890. DOI: https://doi.org/10.1523/JNEUROSCI.04-11-02877.1984, PMID: 6150071

Grace AA, Onn SP. 1989. Morphology and electrophysiological properties of immunocytochemically identified rat dopamine neurons recorded in vitro. *The Journal of Neuroscience* **9**:3463–3481. DOI: https://doi.org/10.1523/JNEUROSCI.09-10-03463.1989, PMID: 2795134

Grady SR, Salminen O, Laverty DC, Whiteaker P, McIntosh JM, Collins AC, Marks MJ. 2007. The subtypes of nicotinic acetylcholine receptors on dopaminergic terminals of mouse striatum. *Biochemical Pharmacology* **74**: 1235–1246. DOI: https://doi.org/10.1016/j.bcp.2007.07.032, PMID: 17825262

Juarez B, Han MH. 2016. Diversity of dopaminergic neural circuits in response to drug exposure. *Neuropsychopharmacology* **41**:2424–2446. DOI: https://doi.org/10.1038/npp.2016.32, PMID: 26934955

Kim CK, Adhikari A, Deisseroth K. 2017. Integration of optogenetics with complementary methodologies in systems neuroscience. *Nature Reviews Neuroscience* **18**:222–235. DOI: https://doi.org/10.1038/nrn.2017.15, PMID: 28303019

King SL, Marks MJ, Grady SR, Caldarone BJ, Koren AO, Mukhin AG, Collins AC, Picciotto MR. 2003. Conditional expression in corticothalamic efferents reveals a developmental role for nicotinic acetylcholine receptors in modulation of passive avoidance behavior. *The Journal of Neuroscience* **23**:3837–3843. DOI: https://doi.org/10.1523/JNEUROSCI.23-09-03837.2003, PMID: 12736354

Kramer RH, Mourot A, Adesnik H. 2013. Optogenetic pharmacology for control of native neuronal signaling proteins. *Nature Neuroscience* **16**:816–823. DOI: https://doi.org/10.1038/nn.3424, PMID: 23799474

Lammel S, Hetzel A, Häckel O, Jones I, Liss B, Roeper J. 2008. Unique properties of mesoprefrontal neurons within a dual mesocorticolimbic dopamine system. *Neuron* **57**:760–773. DOI: https://doi.org/10.1016/j.neuron.2008.01.022, PMID: 18341995

Lammel S, Lim BK, Ran C, Huang KW, Betley MJ, Tye KM, Deisseroth K, Malenka RC. 2012. Input-specific control of reward and aversion in the ventral tegmental area. *Nature* **491**:212–217. DOI: https://doi.org/10.1038/nature11527, PMID: 23064228

Lemoine D, Durand-de Cuttoli R, Mourot A. 2016. Optogenetic control of mammalian ion channels with chemical photoswitches. *Methods in Molecular Biology* **1408**:177–193. DOI: https://doi.org/10.1007/978-1-4939-3512-3_12, PMID: 26965123

Lemoine D, Habermacher C, Martz A, Méry PF, Bouquier N, Diverchy F, Taly A, Rassendren F, Specht A, Grutter T. 2013. Optical control of an ion channel gate. *PNAS* **110**:20813–20818. DOI: https://doi.org/10.1073/pnas.1318715110, PMID: 24297890

Levitz J, Pantoja C, Gaub B, Janovjak H, Reiner A, Hoagland A, Schoppik D, Kane B, Stawski P, Schier AF, Trauner D, Isacoff EY. 2013. Optical control of metabotropic glutamate receptors. *Nature Neuroscience* **16**:507–516. DOI: https://doi.org/10.1038/nn.3346, PMID: 23455609

Levitz J, Popescu AT, Reiner A, Isacoff EY. 2016. A toolkit for orthogonal and in vivo optical manipulation of ionotropic glutamate receptors. *Frontiers in Molecular Neuroscience* **9**. DOI: https://doi.org/10.3389/fnmol.2016.00002, PMID: 26869877

Lin JY, Sann SB, Zhou K, Nabavi S, Proulx CD, Malinow R, Jin Y, Tsien RY. 2013. Optogenetic inhibition of synaptic release with chromophore-assisted light inactivation (CALI). *Neuron* **79**:241–253. DOI: https://doi.org/10.1016/j.neuron.2013.05.022, PMID: 23889931

Lin WC, Tsai MC, Davenport CM, Smith CM, Veit J, Wilson NM, Adesnik H, Kramer RH. 2015.In A comprehensive optogenetic pharmacology toolkit for in vivo control of GABA(A) Receptors and synaptic inhibition. *Neuron* **88**:879–891. DOI: https://doi.org/10.1016/j.neuron.2015.10.026, PMID: 26606997

Lodge DJ, Grace AA. 2006. The laterodorsal tegmentum is essential for burst firing of ventral tegmental area dopamine neurons. *PNAS* **103**:5167–5172. DOI: https://doi.org/10.1073/pnas.0510715103, PMID: 16549786

Mameli-Engvall M, Evrard A, Pons S, Maskos U, Svensson TH, Changeux JP, Faure P. 2006. Hierarchical control of dopamine neuron-firing patterns by nicotinic receptors. *Neuron* **50**:911–921. DOI: https://doi.org/10.1016/j.neuron.2006.05.007, PMID: 16772172

Mansvelder HD, Keath JR, McGehee DS. 2002. Synaptic mechanisms underlie nicotine-induced excitability of brain reward Areas. *Neuron* **33**:905–919. DOI: https://doi.org/10.1016/S0896-6273(02)00625-6, PMID: 11906697

Marx M, Günter RH, Hucko W, Radnikow G, Feldmeyer D. 2012. Improved biocytin labeling and neuronal 3D reconstruction. *Nature Protocols* **7**:394–407. DOI: https://doi.org/10.1038/nprot.2011.449, PMID: 22301777

Maskos U, Molles BE, Pons S, Besson M, Guiard BP, Guilloux JP, Evrard A, Cazala P, Cormier A, Mameli-Engvall M, Dufour N, Cloëz-Tayarani I, Bemelmans AP, Mallet J, Gardier AM, David V, Faure P, Granon S, Changeux JP. 2005. Nicotine reinforcement and cognition restored by targeted expression of nicotinic receptors. *Nature* **436**:103–107. DOI: https://doi.org/10.1038/nature03694, PMID: 16001069

Mazarakis ND, Azzouz M, Rohll JB, Ellard FM, Wilkes FJ, Olsen AL, Carter EE, Barber RD, Baban DF, Kingsman SM, Kingsman AJ, O'Malley K, Mitrophanous KA. 2001. Rabies virus glycoprotein pseudotyping of lentiviral vectors enables retrograde axonal transport and access to the nervous system after peripheral delivery. *Human Molecular Genetics* **10**:2109–2121. DOI: https://doi.org/10.1093/hmg/10.19.2109, PMID: 11590128

Morales M, Margolis EB. 2017. Ventral tegmental area: cellular heterogeneity, connectivity and behaviour. *Nature Reviews Neuroscience* **18**:73–85. DOI: https://doi.org/10.1038/nrn.2016.165, PMID: 28053327

Morales-Perez CL, Noviello CM, Hibbs RE. 2016. X-ray structure of the human α4β2 nicotinic receptor. *Nature* **538**:411–415. DOI: https://doi.org/10.1038/nature19785, PMID: 27698419

Morel C, Fattore L, Pons S, Hay YA, Marti F, Lambolez B, De Biasi M, Lathrop M, Fratta W, Maskos U, Faure P. 2014. Nicotine consumption is regulated by a human polymorphism in dopamine neurons. *Molecular Psychiatry* **19**:930–936. DOI: https://doi.org/10.1038/mp.2013.158, PMID: 24296975

Naudé J, Tolu S, Dongelmans M, Torquet N, Valverde S, Rodriguez G, Pons S, Maskos U, Mourot A, Marti F, Faure P. 2016. Nicotinic receptors in the ventral tegmental area promote uncertainty-seeking. *Nature Neuroscience* **19**:471–478. DOI: https://doi.org/10.1038/nn.4223, PMID: 26780509

Paladini CA, Roeper J. 2014. Generating bursts (and pauses) in the dopamine midbrain neurons. *Neuroscience* **282**:109–121. DOI: https://doi.org/10.1016/j.neuroscience.2014.07.032, PMID: 25073045

Picciotto MR, Higley MJ, Mineur YS. 2012. Acetylcholine as a neuromodulator: cholinergic signaling shapes nervous system function and behavior. *Neuron* **76**:116–129. DOI: https://doi.org/10.1016/j.neuron.2012.08.036, PMID: 23040810

Picciotto MR, Zoli M, Léna C, Bessis A, Lallemand Y, Le Novère N, Vincent P, Pich EM, Brûlet P, Changeux JP. 1995. Abnormal avoidance learning in mice lacking functional high-affinity nicotine receptor in the brain. *Nature* **374**:65–67. DOI: https://doi.org/10.1038/374065a0, PMID: 7870173

Picciotto MR, Zoli M, Rimondini R, Léna C, Marubio LM, Pich EM, Fuxe K, Changeux JP. 1998. Acetylcholine receptors containing the beta2 subunit are involved in the reinforcing properties of nicotine. *Nature* **391**:173–177. DOI: https://doi.org/10.1038/34413, PMID: 9428762

Pignatelli M, Bonci A. 2015. Role of dopamine neurons in reward and aversion: a synaptic plasticity perspective. *Neuron* **86**:1145–1157. DOI: https://doi.org/10.1016/j.neuron.2015.04.015, PMID: 26050034

Pinault D. 1996. A novel single-cell staining procedure performed in vivo under electrophysiological control: morpho-functional features of juxtacellularly labeled thalamic cells and other central neurons with biocytin or neurobiotin. *Journal of Neuroscience Methods* **65**:113–136. DOI: https://doi.org/10.1016/0165-0270(95)00144-1, PMID: 8740589

Rice ME, Cragg SJ. 2004. Nicotine amplifies reward-related dopamine signals in striatum. *Nature Neuroscience* **7**:583–584. DOI: https://doi.org/10.1038/nn1244, PMID: 15146188

Rost BR, Schneider-Warme F, Schmitz D, Hegemann P. 2017. Optogenetic tools for subcellular applications in neuroscience. *Neuron* **96**:572–603. DOI: https://doi.org/10.1016/j.neuron.2017.09.047, PMID: 29096074

Sarter M, Parikh V, Howe WM. 2009. Phasic acetylcholine release and the volume transmission hypothesis: time to move on. *Nature Reviews Neuroscience* **10**:383–390. DOI: https://doi.org/10.1038/nrn2635, PMID: 19377503

Szobota S, Gorostiza P, Del Bene F, Wyart C, Fortin DL, Kolstad KD, Tulyathan O, Volgraf M, Numano R, Aaron HL, Scott EK, Kramer RH, Flannery J, Baier H, Trauner D, Isacoff EY. 2007. Remote control of neuronal activity with a light-gated glutamate receptor. *Neuron* **54**:535–545. DOI: https://doi.org/10.1016/j.neuron.2007.05.010, PMID: 17521567

Szymański W, Beierle JM, Kistemaker HA, Velema WA, Feringa BL. 2013. Reversible photocontrol of biological systems by the incorporation of molecular photoswitches. *Chemical Reviews* **113**:6114–6178. DOI: https://doi.org/10.1021/cr300179f, PMID: 23614556

Takemoto K, Iwanari H, Tada H, Suyama K, Sano A, Nagai T, Hamakubo T, Takahashi T. 2017. Optical inactivation of synaptic AMPA receptors erases fear memory. *Nature Biotechnology* **35**:38–47. DOI: https://doi.org/10.1038/nbt.3710, PMID: 27918547

Taly A, Corringer PJ, Guedin D, Lestage P, Changeux JP. 2009. Nicotinic receptors: allosteric transitions and therapeutic targets in the nervous system. *Nature Reviews Drug Discovery* **8**:733–750. DOI: https://doi.org/10.1038/nrd2927, PMID: 19721446

Tapper AR, McKinney SL, Nashmi R, Schwarz J, Deshpande P, Labarca C, Whiteaker P, Marks MJ, Collins AC, Lester HA. 2004. Nicotine activation of alpha4* receptors: sufficient for reward, tolerance, and sensitization. *Science* **306**:1029–1032. DOI: https://doi.org/10.1126/science.1099420, PMID: 15528443

Tochitsky I, Banghart MR, Mourot A, Yao JZ, Gaub B, Kramer RH, Trauner D. 2012. Optochemical control of genetically engineered neuronal nicotinic acetylcholine receptors. *Nature Chemistry* **4**:105–111. DOI: https://doi.org/10.1038/nchem.1234, PMID: 22270644

Tolu S, Eddine R, Marti F, David V, Graupner M, Pons S, Baudonnat M, Husson M, Besson M, Reperant C, Zemdegs J, Pagès C, Hay YA, Lambolez B, Caboche J, Gutkin B, Gardier AM, Changeux JP, Faure P, Maskos U. 2013. Co-activation of VTA DA and GABA neurons mediates nicotine reinforcement. *Molecular Psychiatry* **18**:382–393. DOI: https://doi.org/10.1038/mp.2012.83, PMID: 22751493

Tsai HC, Zhang F, Adamantidis A, Stuber GD, Bonci A, de Lecea L, Deisseroth K. 2009. Phasic firing in dopaminergic neurons is sufficient for behavioral conditioning. *Science* **324**:1080–1084. DOI: https://doi.org/10.1126/science.1168878, PMID: 19389999

Volkow ND, Morales M. 2015. The brain on drugs: from reward to addiction. *Cell* **162**:712–725. DOI: https://doi.org/10.1016/j.cell.2015.07.046, PMID: 26276628

Walters CL, Brown S, Changeux JP, Martin B, Damaj MI. 2006. The beta2 but not alpha7 subunit of the nicotinic acetylcholine receptor is required for nicotine-conditioned place preference in mice. *Psychopharmacology* **184**:339–344. DOI: https://doi.org/10.1007/s00213-005-0295-x, PMID: 16416156

Xiao C, Cho JR, Zhou C, Treweek JB, Chan K, McKinney SL, Yang B, Gradinaru V. 2016. Cholinergic mesopontine signals govern locomotion and reward through dissociable midbrain pathways. *Neuron* **90**:333–347. DOI: https://doi.org/10.1016/j.neuron.2016.03.028, PMID: 27100197

Xiao C, Srinivasan R, Drenan RM, Mackey ED, McIntosh JM, Lester HA. 2011. Characterizing functional α6β2 nicotinic acetylcholine receptors in vitro: mutant β2 subunits improve membrane expression, and fluorescent proteins reveal responsive cells. *Biochemical Pharmacology* **82**:852–861. DOI: https://doi.org/10.1016/j.bcp.2011.05.005, PMID: 21609715

Yang H, de Jong JW, Tak Y, Peck J, Bateup HS, Lammel S. 2018. Nucleus accumbens subnuclei regulate motivated behavior via direct inhibition and disinhibition of VTA dopamine subpopulations. *Neuron* **97**:434–449. DOI: https://doi.org/10.1016/j.neuron.2017.12.022

Zoli M, Pistillo F, Gotti C. 2015. Diversity of native nicotinic receptor subtypes in mammalian brain. *Neuropharmacology* **96**:302–311. DOI: https://doi.org/10.1016/j.neuropharm.2014.11.003, PMID: 25460185

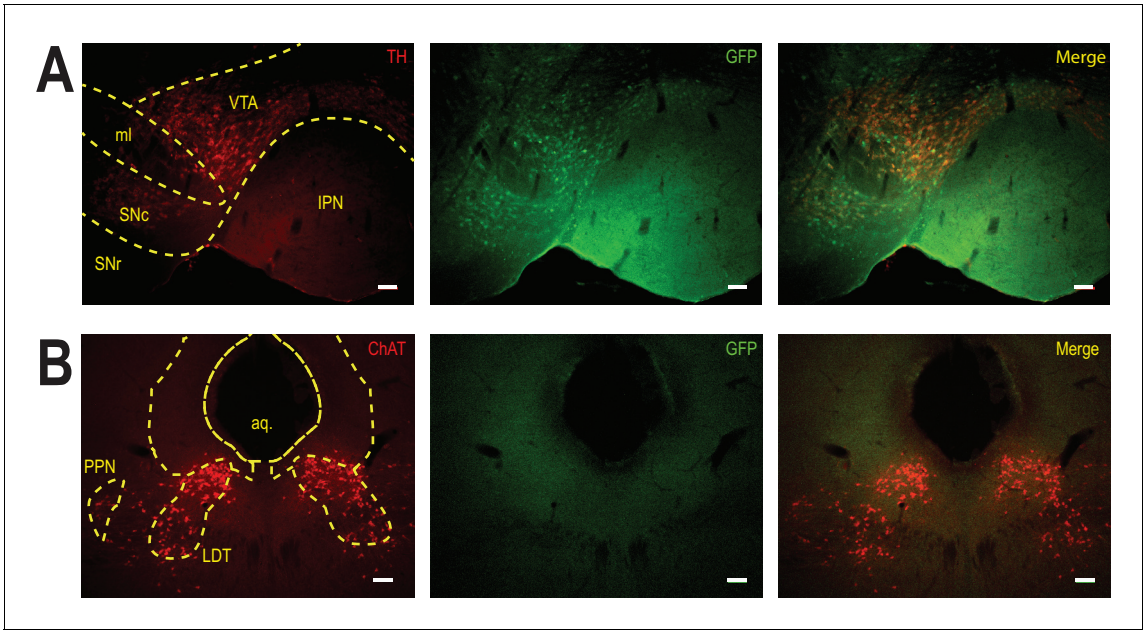

Figure 2—figure supplement 1. Selective transduction of β2E61C in the VTA of WT mice. (**A**) Viral transduction of the VTA using a lentivirus encoding pGK-β2E61C-IRES-eGFP. Immunocytochemical identification of virally-transduced neurons (GFP-positive, green). DA neurons are labelled using anti-tyrosine hydroxylase (TH) antibodies (red). Scale bar: 50 µm. IPN: interpeduncular nucleus, ml: medial lemniscus, SNc: substantia nigra pars compacta, SNR: substantia nigra pars reticulata, VTA: ventral tegmental area. (**B**) Immunocytochemical identification of pontine (i.e. PPN and LDT) cholinergic neurons with anti-ChAT antibodies (red). Note the absence of GFP signal is these afferents to the VTA. Scale bar: 100 µm. PPN: pedunculopontine nucleus; LDT: laterodorsal tegmental nucleus; aq.: aqueduct.

DOI: https://doi.org/10.7554/eLife.37487.006

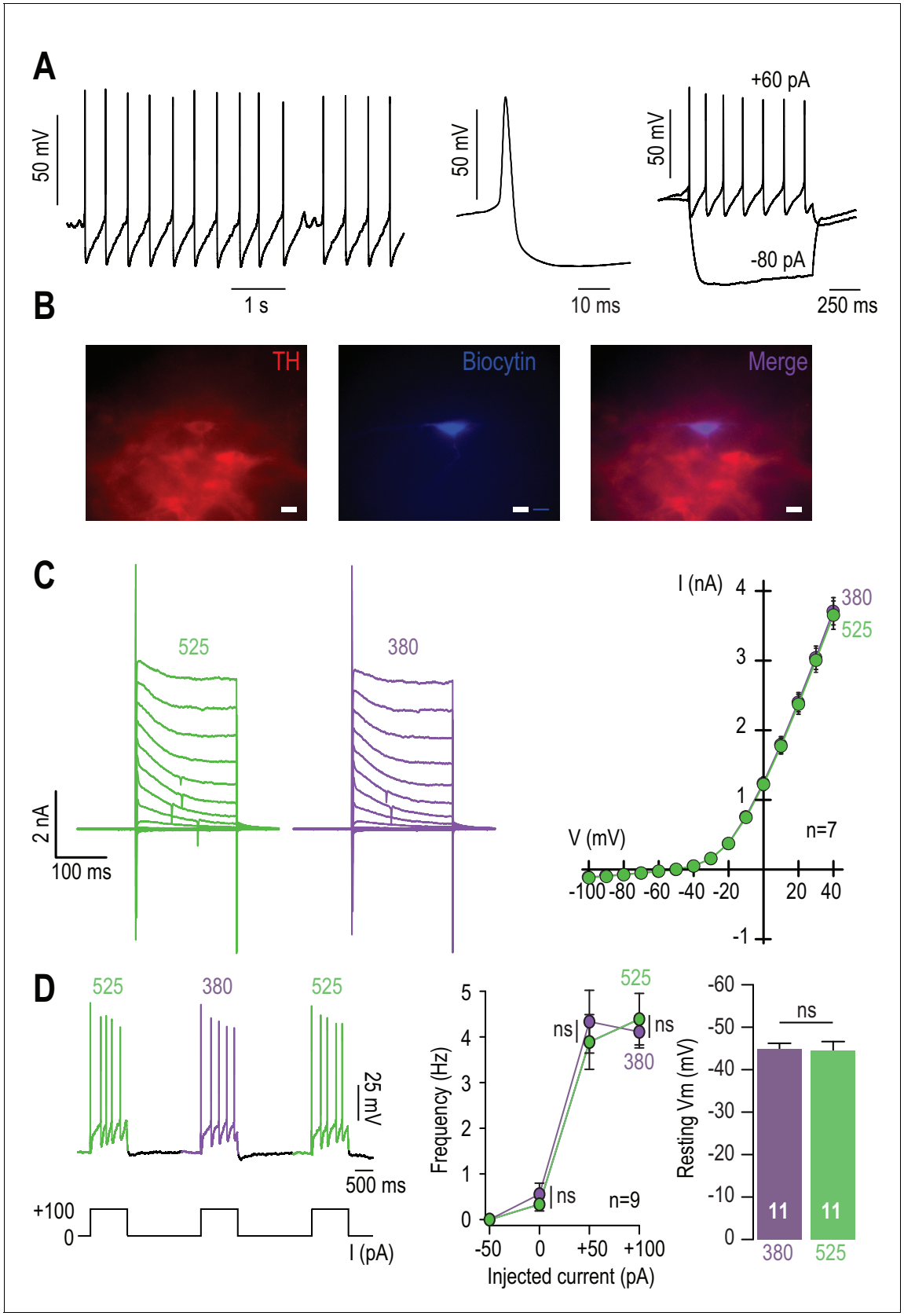

Figure 2—figure supplement 2. No adverse effect of MAHoCh on the basic electrophysiological properties of WT VTA DA neurons. (**A**) VTA DA neurons are characterized in patch-clamp configuration by their pacemaker activity and their pronounced after-hyperpolarization (left), and by their

Figure 2—figure supplement 2 continued on next page

Figure 2—figure supplement 2 continued

typical action potential waveform (middle). Right, they respond to depolarizing currents (+60 pA) by an increase in firing rate, and occasionally showed a sag component upon injection of hyperpolarizing current (−80 pA), in agreement with what has been described in (***Lammel et al., 2008***). (**B**) Immunocytochemical identification of VTA DA neurons using TH (red) and biocytin (blue) labeling. 19 VTA neurons were patched, of which 17 were considered DAergic based on their electrophysiological signatures (as in **A**). Out of these 17 putative DA neurons, 16 were found to be TH^+ (i.e. >94%). (**C**) Left, representative voltage-gated potassium currents recorded from a MAHoCH-treated WT VTA DA neuron in voltage-clamp mode, using 200 ms depolarization steps from −100 to +40 mV (holding potential −60 mV), under 380 (purple) and 525 nm light (green). Right, current versus voltage (I/V) curves for n = 7 MAHoCh-treated WT VTA DA neurons. The amplitudes of voltage-gated potassium currents are similar under both conditions. (**D**) Left, representative electrophysiological recording of a MAHoCh-treated, WT VTA DA neuron recorded in current clamp mode, upon injection of current (100 pA), and while alternating between 380 (purple) and 525 nm light (green). Middle, frequency versus current (F/I) curves for n = 9 MAHoCh-treated WT VTA DA neurons. The number of evoked spikes are similar under both conditions (p=0.75 for 100 pA step of current). Right, mean value of the resting membrane potential (Vm) of MAHoCh-treated VTA DA neurons (n = 11) is similar under both wavelengths of light (p=0.92). All values represent mean ± SEM.

DOI: https://doi.org/10.7554/eLife.37487.007

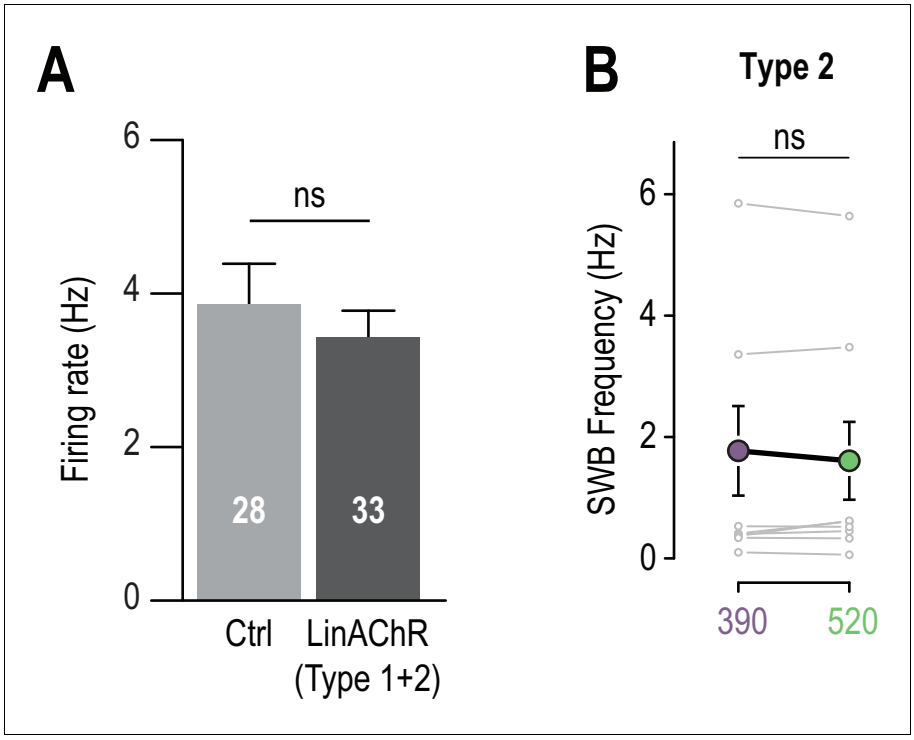

Figure 3—figure supplement 1. Photocontrolling VTA β2LinAChRs in vivo. (**A**) Mean firing rate of control neurons (MAHoCh alone n = 28) is not significantly different from mean firing rate of transduced neurons (Type 1 and 2 are pooled, n = 33, p=0.96). (B) Average SWB frequency of all type 2 pDA neurons (n = 9) is similar in 390 and 520 nm light. All values represent mean ± SEM.

DOI: https://doi.org/10.7554/eLife.37487.010

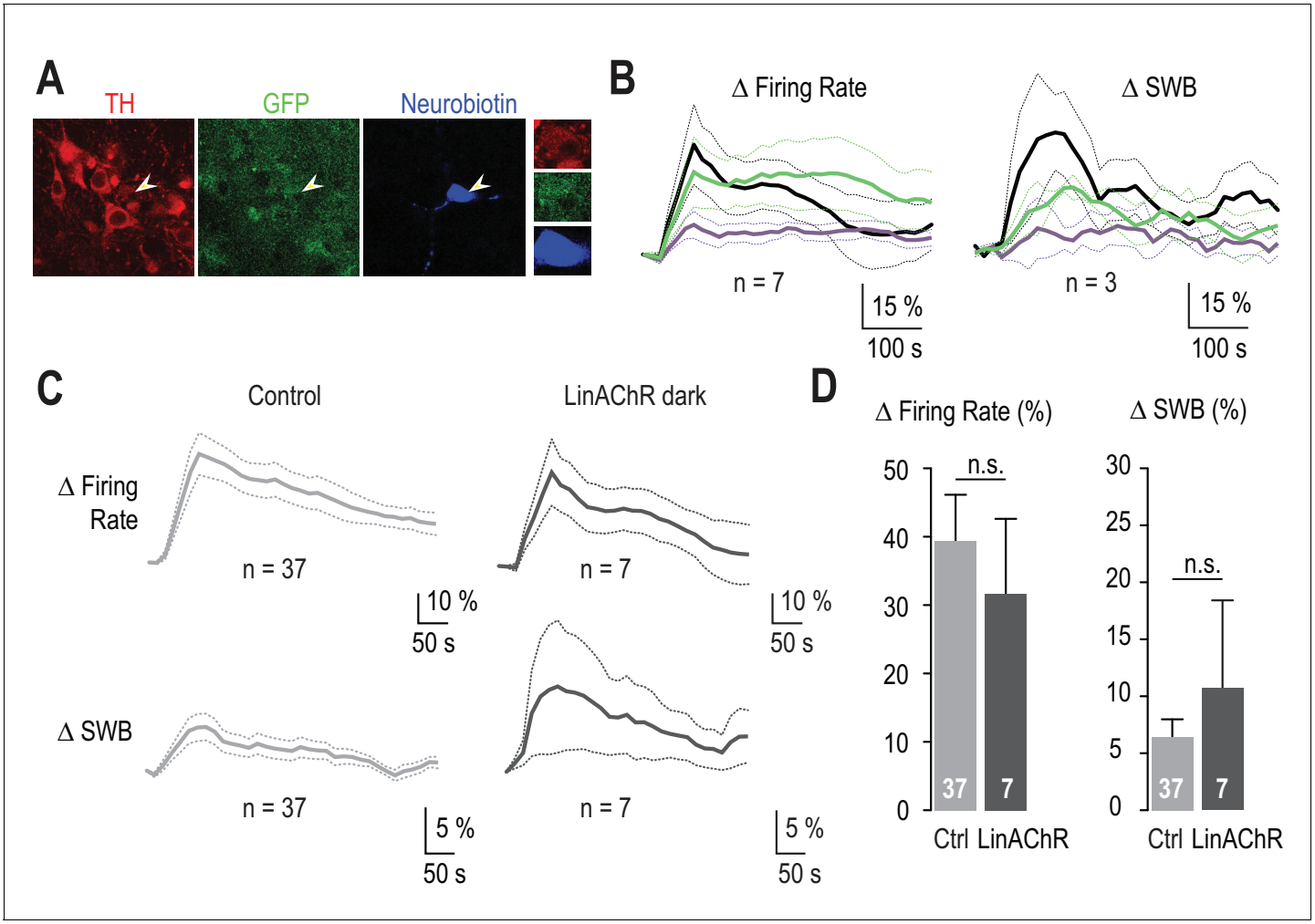

Figure 4—figure supplement 1. The response of VTA DA neurons to nicotine is similar in WT and in β2E61C-transduced animals. (**A**) Example of a recorded transduced DA neuron labeled with neurobiotin (blue) and identified with TH (red) and GFP (green) labeling. 3 out of 7 recorded neurons have been filled with neurobiotin, of which all were confirmed as DAergic by TH labeling. (**B**) Left, average change in firing rate for VTA DA neurons (n = 7) upon nicotine injection in darkness, and under 390 (purple) and 520 nm light (green). Right, average change in burst firing frequency upon nicotine injection in darkness, and under 390 (purple) and 520 nm light (green); only the busting VTA DA neurons were considered here (n = 3). (**C**) Average changes in firing rate (top) and in the percent of spikes within bursts (SWB, bottom) for VTA DA neurons from control (left, light grey, n = 37) and β2E61C-transduced animals (right, dark grey, n = 7), upon nicotine i.v. injection (30 µg/kg) in darkness. (**D**) Changes in firing frequency are not different between control ($\Delta_{\text{firing rate}}$ = 39.4 %, n = 37) and β2E61C-transduced animals ($\Delta_{\text{firing rate}}$ = 31.7 %, n = 7, p=0.53). Similarly, changes in the percent of SWB are not different between control and β2E61C-transduced animals ($\Delta\%_{\text{SWB}}$ = 6.44 % and 10.72%, respectively, p=0.68). All values represent mean ± SEM.

DOI: https://doi.org/10.7554/eLife.37487.013

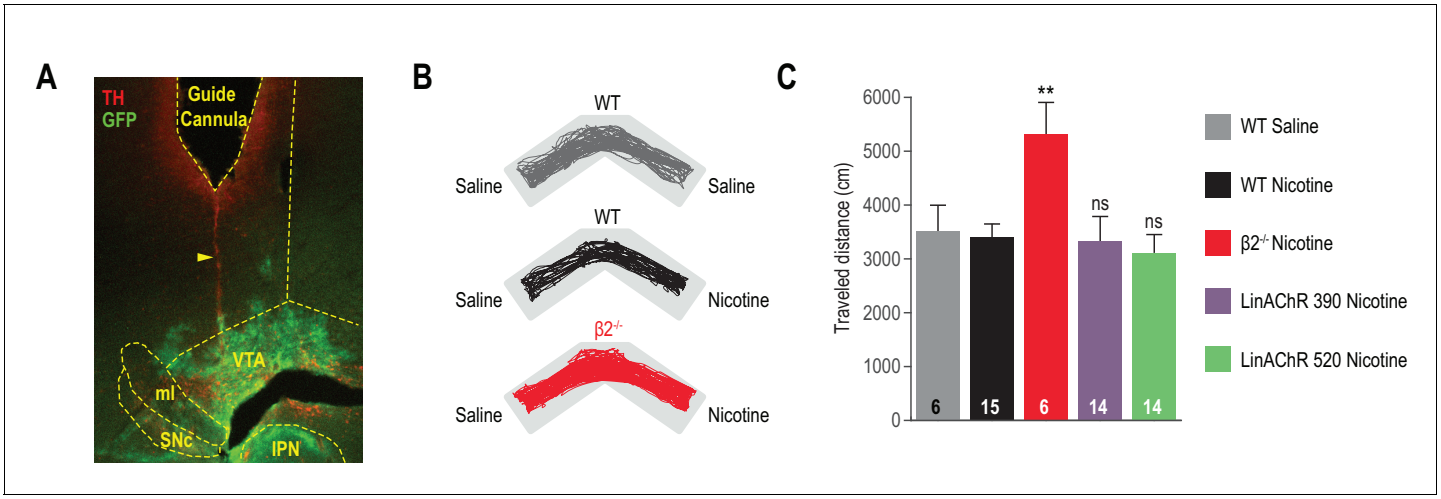

Figure 5—figure supplement 1. Nicotine-induced CPP. (**A**) Epi-fluorescence images of 60 µm coronal midbrain slices with immunostaining for dopamine neurons (tyrosine hydroxylase (TH), red) and transfected area (Green Fluorescent Protein (GFP), green) showing the track of an implanted guide cannula (yellow dashed outline). The yellow arrow-head points to the protruding optical fiber/cannula track. IPN: interpeduncular nucleus, ml: medial lemniscus, SNc: substantia nigra pars compacta, VTA: ventral tegmental area. (**B**) Representative trajectories for WT mice conditioned with saline (grey) or nicotine (black), and for $\beta2^{-/-}$ mice conditioned with nicotine (red). (**C**) Traveled distance in the CPP chamber on the test day, for WT mice conditioned with saline (grey) or nicotine (black), for $\beta2^{-/-}$ mice conditioned with nicotine (red), and for β2E61C-transduced mice conditioned with nicotine under 390 (purple) or 520 nm light (green). Locomotion for β2E61C-transduced mice is not different from WT animals (p=0.68 and p=0.45, respectively). In contrast, $\beta2^{-/-}$ mice showed greater travelled distance than WT animals (p=0.0062), as already reported (***Avale et al., 2008***). All values represent mean ± SEM.

DOI: https://doi.org/10.7554/eLife.37487.016

7. Deuxième publication scientifique

THE SENSITIVITY OF THE INTERPEDUNCULAR NUCLEUS DETERMINES THE THRESHOLD DOSE OF NICOTINE THAT TRIGGERS PERSISTENT AVERSION.

Sarah Mondoloni, Claire Nguyen, Romain Durand-de Cuttoli, Nicolas Torquet, Joachim Jehl, Stefania Tolu, Stéphanie Pons, Uwe Maskos, Fabio Marti[1], Philippe Faure* and Alexandre Mourot*

* co-last

La régulation de la consommation de nicotine reposerait sur la concomitance de différents processus neuronaux qui impliquent le renforcement, l'aversion et les symptômes de manque.

La consommation de nicotine est variable chez les individus, et tous ne deviennent pas dépendants. Dans cette étude, nous avons voulu mettre en évidence les différences interindividuelles qui existent dans les comportements de consommation de nicotine, et se servir de ces différences pour identifier les mécanismes régulant la consommation de nicotine. Pour ce faire, nous avons mis au point un test de préférence à deux bouteilles qui confère l'avantage de laisser les souris consommer volontairement de la nicotine. Nous pouvons ainsi corréler les stratégies de consommation de chaque individu en fonction de la concentration de nicotine dans le biberon. Pour cela, nous avons développé une analyse qui prend en compte le pourcentage de préférence de la souris pour le biberon qui contient de la nicotine et le degré d'indifférence de la souris face au choix.

Nous avons tout d'abord observé des différences interindividuelles importantes dans les stratégies de consommation. Ces différences ne relèvent pas d'une variation du niveau de consommation, mais bien d'une stratégie de consommation variable. Nous avons observé deux profils de prise de nicotine. Le premier groupe corresponds aux souris qui consomment de la nicotine tout au long de la tâche, et dont une partie titre leur consommation aux fortes doses de nicotine. Le second groupe est constitué de souris qui présentent une aversion à la nicotine, soit immédiate à de faibles doses, soit qui se développe au cours de la tâche de manière dose-dépendante. Ces souris averses présentent un comportement qui fait écho à l'apprentissage par renforcement de stimulus aversif, puisqu'elles ont appris à long terme, et indépendamment de la dose de nicotine, à éviter le biberon qui contient la drogue.

Ces résultats comportementaux mettent en évidences deux points importants. Premièrement, la nicotine n'est pas aversive seulement aux fortes doses, puisqu'une partie des souris évite la nicotine même à de faibles doses, et que le seuil de sensibilité aux effets aversifs est intrinsèque à chaque individu. Deuxièmement, la régulation de la consommation de nicotine par une stratégie de titration ne concerne qu'un très faible nombre de souris.

Puisque les comportements d'évitements spontanés des souris étaient un résultat inattendu et que l'activation de l'IPN joue un rôle déterminant dans l'aversion à la nicotine, nous avons évalué l'impact de la consommation de nicotine sur les courants nicotiniques de

l'IPN. Nous avons alors émis l'hypothèse que le niveau de sensibilité de l'IPN à la nicotine déterminerait le niveau d'aversion à la nicotine. En alliant traitement pharmacologique, approche génétique et réexpression locale, nous avons en effet montré que :

- La consommation de nicotine induit une réduction de la sensibilité à la nicotine des neurones de l'IPN, et diminue la proportion de souris qui développe de l'aversion à la nicotine.

- Les souris $\beta4^{-/-}$ ont une sensibilité réduite à la nicotine dans l'IPN, et ne présentent pas de comportement d'évitement. Ceci suggère que les récepteurs β4* jouent un rôle crucial dans la transmission neuronale qui sous-tend l'aversion à la nicotine.

- La réexpression de la sous-unité β4 dans l'IPN permet de rétablir les réponses à la nicotine et les comportements d'évitement.

L'aversion à la nicotine est une réponse comportementale qui permet de limiter la consommation de la nicotine a des doses nocives. La question est de savoir quelle est la part de cette réponse chez des individus qui sont dépendants à la nicotine. Ici, nous proposons que les mécanismes qui sous-tendent l'aversion à la nicotine sont progressivement atténués lors de prises chroniques de nicotine. Néanmoins, lorsque l'activation des récepteurs nicotiniques β4* de l'IPN est suffisante, cela permet d'enclencher des comportements d'évitement. Cette étude suggère que la régulation de la nicotine ne repose pas sur des processus de satiété, mais émerge d'une balance entre deux processus opposés.

The sensitivity of the interpeduncular nucleus determines the threshold dose of nicotine that triggers persistent aversion.

Sarah Mondoloni[1], Claire Nguyen[1], Romain Durand-de Cuttoli[1], Nicolas Torquet[1], Joachim Jehl[1], Stefania Tolu[1], Stéphanie Pons[2], Uwe Maskos[2], Fabio Marti[1], Philippe Faure[1*] and Alexandre Mourot[1*]

Affiliations :

1. Sorbonne Université, Inserm, CNRS, Neuroscience Paris Seine - Institut de biologie Paris Seine (NPS - IBPS), 75005 Paris, France.

2. Institut Pasteur, Unité Neurobiologie intégrative des systèmes cholinergiques, Département de neuroscience, 75724 Paris cedex, France.

* equal contributions

Correspondence to: almourot@gmail.com or phfaure@gmail.com

Keywords: nicotinic acetylcholine receptors, nicotine addiction, two-bottle choice paradigm, drug aversion

Abstract

Continued use of addictive drugs despite harmful consequences is a hallmark of addiction. Nicotine consumption is likely regulated through balancing the rewarding and aversive properties of the drug, yet the individual differences that determine the progression from initial experimentation to loss of control over the amount of drug intake remain poorly understood. Using a two-bottle choice nicotine-drinking paradigm, we observed that about half of the mice persisted in nicotine intake even at high concentrations, while the other half durably stopped consumption. We found that consumption was negatively correlated with the sensitivity of the interpeduncular nucleus (IPN) to nicotine, and that chronic nicotine, by weakening this sensitivity, increased the threshold dose triggering aversion, and hence boosted consumption. Lastly, using transgenic mice and viral transfer technologies, we causally identified β4-containing nicotinic acetylcholine receptors of the IPN as the molecular and cellular correlates of nicotine aversion. Collectively, our data provide a mechanistic explanation for the inter-individual variabilities in chronic nicotine consumption.

Introduction

Substance use disorder (SUD) is characterized by compulsive drug seeking and continued use despite punishment or harmful consequences (Association, 2013; Koob & Le Moal, 1997; Lüscher, Robbins, & Everitt, 2020). Perseverant drug-taking is observed in laboratory rodents, for instance when self-administration of cocaine is accompanied with mild footshock (Deroche-Gamonet, Belin, & Piazza, 2004), or when a bitter quinine solution is added to orally-consumed alcohol (Juarez et al., 2017; Siciliano et al., 2019). Aversion to the drug is classically elicited by a stimulus (electric shock, quinine…) that is external to the drug itself. However, some addictive substances, including nicotine, are inherently noxious and can therefore directly trigger aversive reactions in both humans and rodents (Fowler & Kenny, 2014; Wise, Yokel, & DeWit, 1976). Nicotine remains the most-widely used addictive substance in the world, and even though cigarette smoking is overall decreasing, the use of new products such as electronic cigarettes has risen dramatically in recent years (*WHO global report on trends in prevalence of tobacco use 2000-2025 third edition*, 2019). Therefore, understanding the neurobiological mechanisms of nicotine aversion is a fundamental step towards the development of efficient smoking-cessation therapies.

The dichotomous reinforcing/aversive nature of nicotine is believed to be key in the regulation of nicotine intake and in the maintenance of addiction (Fowler & Kenny, 2014; Verendeev & Riley, 2013). The physiological effects of nicotine are mediated through nicotinic acetylcholine receptors (nAChRs), pentameric ligand-gated ion channels encoded by a large multigene family. Nine α (α2-10) and three β

(β2-4) nAChR subunits are expressed in the brain, and assemble to form homo- and heteropentamers with various localizations and functions (Taly, Corringer, Guedin, Lestage, & Changeux, 2009; Zoli, Pistillo, & Gotti, 2015). The reinforcing properties of nicotine and establishment of consumption involve primarily α4β2 nAChRs of the mesolimbic dopamine reward circuit, located in the ventral tegmental area (VTA) (Durand-de Cuttoli et al., 2018; Maskos et al., 2005; Tapper et al., 2004; Tolu et al., 2013). In contrast, aversion to nicotine intake is believed to be mainly mediated by the medial habenulo-interpeduncular (MHb-IPN) axis (Fowler, Lu, Johnson, Marks, & Kenny, 2011; Frahm et al., 2011; Morton et al., 2018; Wolfman et al., 2018), a pathway deeply implicated in the regulation of aversive physiological states (Otsu et al., 2019; Yamaguchi, Danjo, Pastan, Hikida, & Nakanishi, 2013; Zhang et al., 2016). The Mhb-IPN pathway can also trigger both affective (anxiety) and somatic symptoms following nicotine withdrawal (Pang et al., 2016; Salas, Sturm, Boulter, & De Biasi, 2009; Zhao-Shea et al., 2015; Zhao-Shea, Liu, Pang, Gardner, & Tapper, 2013) and is involved in relapse to nicotine-seeking (Forget et al., 2018). Strikingly, the MHb-IPN axis expresses the highest density and diversity of neuronal nAChRs, notably the rare α5, α3 and β4 subunits (Zoli et al., 2015) that are encoded by the CHRNA5-A3-B4 gene cluster associated with a high risk of addiction in humans (Bierut et al., 2008; Lassi et al., 2016).

A distinct feature of addiction is that only some individuals lose control over their drug use, progressively shifting to compulsive drug intake (Deroche-Gamonet et al., 2004; George & Koob, 2017; Juarez et al., 2017; Pascoli et al., 2018; Siciliano et al., 2019). About a third to half of those who have tried smoking tobacco become regular users (Centers for Disease Control and Prevention (US), National Center for Chronic Disease Prevention and Health Promotion (US), Office on Smoking and Health (US), 2010). Individual differences in the respective sensitivities of the VTA and MHb-IPN systems likely contribute to the vulnerability to nicotine and to the severity of the addiction process (Antolin-Fontes et al., 2020; Harrington et al., 2016; Husson et al., 2020; Tuesta et al., 2017; Wolfman et al., 2018). Yet, the neural mechanism that make individuals more prone to maintain nicotine consumption versus durably stop are unclear. Here we used isogenic mice to study inter-individual differences in the sensitivity of the IPN to nicotine, and their role in the progression to regular use.

Results

Nicotine consumers and avoiders in WT mice.

We used a continuous access, two-bottle choice nicotine-drinking test to assess consumption profiles in wild-type C57Bl6 mice single-housed in their home cage (Fig. 1A). In this test, animals have continuous and concurrent access to two bottles that contain either a saccharine 2% solution (vehicle)

or nicotine plus saccharine. Saccharine was used in both bottles to mask the bitter taste of nicotine. After a 4-day habituation period with water in both bottles, nicotine concentration progressively increased in one bottle across 16 days, from 10 to 200 μg/ml (4 days at each concentration), while alternating nicotine-containing solution side every other day to control for side bias (Fig. 1B). Consumption from each bottle was measured every minute. We found that the daily nicotine dose consumed increased throughout the paradigm, to stabilize on average at about 10 mg/kg/day for the highest nicotine concentration tested (Fig. 1C, Fig. S1A). The progressive increase in nicotine consumption was associated with an overall decrease in preference for nicotine, especially for concentrations above 50 μg/ml (Fig. 1D). Altogether, at the population level, these results suggest that mice adjust their daily dose of nicotine by selecting the adapted bottle according to their own preference for the drug, resulting in nicotine titration, as previously reported (Fowler et al., 2011; Tuesta et al., 2017).

We then looked more precisely at individual nicotine consumption profiles, and found two major types of behaviors. Mice that displayed either a gradual increase or that reached a particular plateau in their consumption, and still had significant consumption for the highest dose tested, were termed “consumers” (Fig. 1E). Unexpectedly, we also found mice that actively avoided the nicotine-containing bottle, from the beginning or at some time point during the task, and which we named “avoiders”. Overall, only a small fraction of the mice readily titrated their nicotine intake (7/35), which contrasts with what can be observed at the population level in our and previous studies (Fowler et al., 2011; Tuesta et al., 2017). Avoiders and consumers showed on average similar nicotine intake for the low concentrations of nicotine (10 and 50 μg/ml, $p > 0.05$). But while nicotine intake increased throughout the task for consumers (16.933 ± 2.92 mg/kg/day for 200 μg/ml of nicotine) it dropped down to 2.57 ± 0.41 mg/kg/day for such high nicotine concentration in avoiders (Fig. 1F), and almost reached zero over the last three days (Fig. 1G). Preference ratio was fairly constant throughout the task for consumers (Fig. S1B). In contrast, preference for nicotine drastically decreased in a curvelinear fashion as nicotine increases for avoiders (Fig. S1B), with a pattern similar to what we observed in a two-bottle choice quinine-drinking test (Fig. S1C), suggesting that avoiders may have developed aversion towards nicotine.

Individual threshold doses for triggering nicotine aversion

The average consumption over four days is a good indicator of drug dose consumed and preference ratio. However, it does not take into account the choice patterns of the animals and their behavioral adaptations when bottles are swapped. Due to the oral nature of the test, it may be difficult for an animal to associate consumption in a particular bottle with the effects (whether positive or negative) of nicotine. We thus systematically analyzed individual preference ratios throughout the task. We found that some consumers actively tracked the side associated with nicotine when bottles were swapped, indicating

preference for the bottle containing nicotine, while others displayed a strong side preference and never alternated drinking side, and hence consumed nicotine in a more passive fashion (Fig. 2A). In contrast, all avoider mice readily displayed an active avoidance behavior for the nicotine-containing solution, whether they initially tracked the nicotine solution or not. To quantify the evolution of nicotine preference at the individual level throughout the task, and to better take into account the passive consumption behavior of some of the mice, we mapped each profile in a pseudo-ternary plot where two apices represent 0 (Sacc.) and 100 % nicotine (Nic.) preference, while the third apex represents 100 % side bias (Fig. 2B). Such ternary representation enabled us to represent the trajectory for each individual, from the water to the nicotine 200 μg/ml conditions, and to calculate the shortest distance from the point of interest to each apex, at each step of the task. We found that the behavior of consumers was on average fairly consistent throughout the task, while the behavior of avoiders was highly nicotine dose-dependent (Fig. 2B-C). Aversion to nicotine in avoider mice mainly occurred at the transition from 100 to 200 μg/ml, but some mice displayed a threshold as low as 10 μg/ml for avoidance-like behavior. In fact, the proportion of avoiders progressively developed as nicotine concentration increased in the bottle, to reach about 50 % at the end of the 20-day task (Fig. 2D). Altogether these results demonstrate that mice can discriminate nicotine from the control solution and that, at some specific threshold dose, some mice start actively avoiding the nicotine-containing bottle.

Do avoiders readily and durably learn to avoid the nicotine-containing solution, or do they just rapidly react to the dose to adjust their intake? To answer this question, we added a condition at the end of the two-bottle choice task, where a low concentration of nicotine (50 μg/ml) was proposed after the 200 μg/ml condition. We chose 50 μg/ml of nicotine because avoiders and consumers initially displayed comparable nicotine intake and preference at this dose (Fig. 1F, Fig. S1B). We hypothesized that if avoiders increased their preference at the 200-50 μg/ml transition, it would suggest a rapid adjustment to the concentration proposed. In contrast, if avoiders maintained a steady, low preference for nicotine, it would suggest a learning process whereby aversion towards nicotine is persistent. We found that indeed lowering nicotine concentration from 200 to 50 μg/ml did not increase nicotine preference ratio in avoiders (Fig. 2E), indicating that WT mice can develop learned aversion for nicotine during a self-administration task, resulting in durable change in behavior and nearly-complete cessation of consumption.

<u>The emergence of avoidance behavior correlated with the amplitude of nicotine-evoked currents in the IPN</u>

We then reasoned that the IPN, which is involved in nicotine aversion and in negative affective states (Fowler & Kenny, 2014; McLaughlin, Dani, & De Biasi, 2017; Molas, DeGroot, Zhao-Shea, & Tapper, 2017), may underlie the sensitivity to nicotine, and may thus be differently activated by nicotine in

avoiders and consumers. We used patch-clamp electrophysiology on brain slices to assess, at completion of the two-bottle choice task, the functional expression level of nAChRs in IPN neurons. We recorded neurons from the dorsal and rostral IPN (IPR/IPDL) because these neurons have high nAChR density and project to brain areas, such as pontine and raphe nuclei, that are implicated in psychiatric disorders (Hsu et al., 2013; Morton et al., 2018; Quina, Harris, Zeng, & Turner, 2017; Wolfman et al., 2018). To record nicotine-evoked currents, we used a local puff application of nicotine at a concentration (30 µM) close to the EC50 for heteromeric nAChRs (Fenster, Rains, Noerager, Quick, & Lester, 1997). We found that the amplitude of nicotine-induced currents was higher in IPN neurons of avoider mice compared to that of consumers (Fig. 2F). One hypothesis is that large nicotine-mediated currents in IPN neurons could underlie nicotine avoidance-like behavior. In line with this, we found a negative correlation between the average amplitude of nicotine-induced current in IPN neurons, and nicotine consumption behavior (measured over the last 24 h prior to patch-clamping, Fig. 2G). This correlation suggests that consumption level in mice is directly linked to the amplitude of the nicotine response in IPN neurons.

Chronic nicotine treatment alters both nicotinic transmission in the IPN and nicotine consumption in mice.

Whether chronic nicotine exposure progressively alters nicotine responses in the IPN (consumers being further exposed to high nicotine doses than avoiders) or whether an intrinsic difference pre-exists in consumer and avoiders, is unclear at this stage. To determine the effect of chronic nicotine exposure on nAChR current levels in IPN neurons, we passively and continuously exposed mice to nicotine using subcutaneously implanted osmotic minipumps. The concentration of nicotine in the minipump (10 mg/kg/d) was chosen to match the average voluntary intake of nicotine in the two-bottle choice task (Fig. 1C). After 4 weeks of nicotine delivery, we recorded nicotine-evoked currents from acute brain slices. We found that indeed, chronic nicotine reduced the amplitude of nicotine-evoked currents in the IPN of mice treated with nicotine compared to control mice treated with saline (Fig. 3A). These results are in agreement with what we observed in mice that underwent the two-bottle choice task, compared to naïve mice in their home cage (Fig S2A). Because IPN neurons are mostly silent in brain slices, and in order to preserve the entire circuitry intact, we decided to perform juxtacellular recordings of IPN neurons *in vivo*, and to characterize their response to an intravenous (i.v.) injection of nicotine (30 µg/kg). There is to our knowledge no description of *in vivo* recordings of IPN neurons, hence we solely considered neurons that were labelled in vivo with neurobiotin and confirmed to be within the IPN for the analysis. We found that nicotine i.v. injections induced an increase in the firing rate of IPN neurons compared to an injection of saline in naïve WT mice, and that this effect of nicotine was reduced after a passive exposition to nicotine (Fig.3B). Some of the IPN neurons responded to nicotine with a decrease in their firing rate, and this effect was lower in the nicotine group (Fig. S2B). Altogether, these *ex vivo* and *in vivo* recordings demonstrate that long-term exposure to nicotine potently reduces nicotine-evoked responses in mouse IPN neurons.

To verify the hypothesis that a modification in the nicotinic transmission of the IPN impacts nicotine aversion, we first evaluated the consequence of chronic nicotine exposure on nicotine consumption. Mice were implanted with an osmotic minipump to deliver nicotine and, after 20 days, were subjected to a modified two-bottle task that consisted in a rapid presentation to high doses (100 µg/ml) of nicotine (Fig. 3C). We chose this protocol to avoid the confounding effects of a gradual exposure to nicotine. We found that control mice treated with saline, but not those treated with nicotine, significantly decreased their preference for the nicotine-containing solution (Fig. 3C), gradually over the four days (Fig. S2C). This indicates that mice under chronic nicotine treatment developed tolerance for the aversive effects of nicotine. Overall, this resulted in greater nicotine intake for the group treated with nicotine than for the group treated with saline (Fig. 3C). When focusing on individuals, we observed that a single saline-treated mouse (1/23) increased its nicotine preference when nicotine was introduced in the task, while the great majority of the mice actively avoided nicotine. In contrast, a large fraction of the mice treated with nicotine (n=8/25) developed an increase in nicotine preference (Fig.3D). The two groups were identical in the water/water session. However, in the water/nicotine session, mice under nicotine presented a greater distance from the Saccharine apex, and a shorter distance from the Nicotine apex, compared to mice under saline (Fig. 3E). Altogether, these electrophysiological and behavioral data demonstrate that chronic exposure to nicotine decreases nicotine efficacy in the IPN, and also changes the threshold for triggering nicotine-aversion in individuals, resulting in increased consumption. Yet, whether the two are causally related remains to be demonstrated.

<u>β4*nAChRs mediate nicotine avoidance-like behavior.</u>

We turned to transgenic mice deleted for the β4 nAChR gene ($\beta4^{-/-}$ mice), because of the heavy expression of this subunit in the IPR region of the IPN (Grady et al., 2009; Harrington et al., 2016; Shih et al., 2014). We found that $\beta4^{-/-}$ mice displayed both greater nicotine preference and greater consumption than WT animals, with virtually no dose-dependent change in nicotine preference for $\beta4^{-/-}$ mice (Fig. 4A). When looking at individuals, we observed both active and passive nicotine-drinking profiles in $\beta4^{-/-}$ mice, as already observed in WT mice (13/35 passive mice for WT mice; 4/13 for $\beta4^{-/-}$ mice). Strikingly, none of the $\beta4^{-/-}$ mice showed aversion at high nicotine doses, which contrasts with the high proportion of avoiders in WT animals (Fig. 4B-C).

To verify whether responses to nicotine were affected in IPN neurons of $\beta4^{-/-}$ mice, we performed patch-clamp recordings. We found that the amplitude of nicotine-evoked currents in the IPN was three-fold lower in $\beta4^{-/-}$ than in WT mice (Fig. 4D), confirming that β4*nAChRs are the major receptor subtype in the IPN. Furthermore, chronic nicotine treatment had no significant effect on the amplitude of nAChR

currents in these knock-out mice (Fig. 4D), suggesting that the downregulation observed upon chronic nicotine treatment in the IPN of WT mice mainly affects β4*nAChRs. We then used *in vivo* juxtacellular recordings, and performed dose-responses (7.5 – 30 μg/kg) in order to assess the role of β4*nAChRs in the response to different dose of nicotine. In WT mice, nicotine i.v. injections resulted in a dose-dependent increase in IPN neuron activity (Fig. 4E). In $\beta4^{-/-}$ mice, nicotine responses were of smaller amplitude, especially for the highest nicotine dose tested (Fig. 4E), further demonstrating the important role of β4*nAChRs of the IPN in the response to nicotine. In both WT and $\beta4^{-/-}$ mice, we observed a population of neurons that decreased their firing rate in a dose-dependent manner, yet with no difference in the amplitude of the response between the two genotypes (Fig. S3A-C), suggesting that β4*nAChR are mainly involved in the increase- but not in the decrease- in neuronal activity in response to nicotine injection. Collectively, our results with $\beta4^{-/-}$ mice demonstrate the key role of this subunit in signaling aversion to nicotine, and its predominant role in sensing nicotine and activating the IPN.

<u>β4*nAChRs of the IPN are sufficient for nicotine avoidance-like behavior.</u>

To causally assess the role of β4*nAChRs of the IPN in nicotine aversion, and more generally in nicotine consumption, we targeted re-expression of β4 in the IPN specifically, using lentiviral vectors in $\beta4^{-/-}$ mice (KO-$\beta4^{IPN}$, Fig. 5A). A group of mice transduced with eGFP was used as a control (KO-GFP^{IPN}). Proper transduction in the IPN was verified using immunohistochemistry after completion of the two-bottle choice task (Fig. 5A) and mice with expression of GFP in the VTA were excluded from the analyzes. Transduction of β4, but not of GFP, in the IPN restored the amplitude of nicotine-evoked currents (U test, p-value=0.6, Fig. 5B). We then compared nicotine intake in both groups of mice in the two-bottle choice task. We found that re-expression of β4 in the IPN of $\beta4^{-/-}$ mice decreased nicotine consumption, especially for doses over 100 μg/ml, compared to the group transduced with eGFP in the IPN (Fig. 5C). Overall, consumption levels were similar in WT and in KO-$\beta4^{IPN}$ animals ($p>0.5$ for all doses), demonstrating the causal role of β4 nAChRs of the IPN in nicotine consumption behaviors. At the individual level, the proportion mice that avoided nicotine at 200 μg/kg was very low for KO-GFP^{IPN} (18.75 %) control mice, but greater for KO-$\beta4^{IPN}$ mice (33.33%, Fig. 5D-E). Mice with strong preference for nicotine were only found in the KO-GFP^{IPN} control group. Collectively, these data highlight the specific role of β4*nAChRs expressed at the level of IPN neurons in setting the threshold dose for nicotine aversion, and in the control of nicotine intake.

Discussion

We used a two-bottle choice paradigm to assess inter-individual differences in nicotine consumption in mice, and to evaluate how pre-exposure to nicotine modifies drug taking. Oral self-administration is a classical method for chronic nicotine administration as it provides rodents with ad libitum access to nicotine, likely mimicking administration in human smokers, while minimizing stress from handling (Pogun & C Collins, 2012). We observed that WT mice titrate their intake to achieve a consistent nicotine dose, in agreement with previous reports (Antolin-Fontes et al., 2020; Fowler et al., 2011; Tuesta et al., 2017), and discovered that mice knocked out for the β4 subunit did not, resulting in greater nicotine consumption, notably at high nicotine concentration. Our behavioral results are in agreement with the higher intracranial self-administration observed at high nicotine doses in $\beta4^{-/-}$ mice (Husson et al., 2020), and mirror those observed with transgenic TABAC mice overexpressing β4 at endogenous sites, which avoid nicotine and as a consequence consume very little nicotine (Frahm et al., 2011; Husson et al., 2020). Nevertheless, it should be noted that conflicting results have also been reported regarding the role of β4 nAChRs in nicotine consumption. Notably, intravenous self-administration was shown to be lower in $\beta4^{-/-}$ despite a higher sensitivity of the VTA to nicotine in these mice (Harrington et al., 2016), and self-administration was higher in TABAC mice despite reduced nicotine-induced activation of the VTA (Gallego et al., 2011). Interestingly, the increased consumption at high nicotine doses and absence of titration reported here for $\beta4^{-/-}$ mice resembles what was observed in mice deleted for the α5 subunit (Fowler et al., 2011), likely because these two nAChR subunits, which belong to the same gene cluster, co-assemble in brain tissue, notably the IPN, to produce functional nAChRs and participate in such behaviors.

One important limitation of population-level analyses is that they greatly limit the ability to examine inter-individual differences in drug taking behaviors. It is indeed increasingly acknowledged that in mice, as in humans, there is a substantial variability in the susceptibility for developing drug use disorders (Garcia-Rivas, Cannella, & Deroche-Gamonet, 2017; Juarez et al., 2017; Nesil, Kanit, Collins, & Pogun, 2011; Piazza, Deminière, Le Moal, & Simon, 1989; Siciliano et al., 2019). Yet why some individuals are more susceptible than others to become regular users remains largely unclear. Here we inspected drinking profiles in individual isogenic mice, and discovered wide inter-individual differences in nicotine vulnerability: about half of the WT mice, the avoiders, durably quit nicotine at a certain dose, while the other half, the consumers, continued consumption even at high doses of nicotine, classically described as aversive (Fowler & Kenny, 2014). Avoiders displayed variable threshold doses for aversion, and some of them even displayed aversion at the beginning of the task, when concentrations of nicotine were still low. This finding contrasts with the popular idea that aversion is only triggered by high doses of nicotine (Fowler et al., 2011; Fowler & Kenny, 2014; Frahm et al., 2011; Wolfman et al., 2018), but is in agreement with our observation that low concentrations of nicotine can potently engage the IPN circuitry in vivo. Consumers and $\beta4^{-/-}$ mice possibly have an aversion threshold too, but which exceeds the highest dose tested here. Importantly, very few of the mice showed what could be considered as “efficient titration”, emphasizing the needs to consider individual- as opposed to group- behavior in addiction research.

We further discovered that the functional level of expression of β4-containing nAChRs in the IPN are underlying these different sensitivities to the aversive properties of nicotine. Indeed, inter-individual variabilities for nicotine aversion were virtually eliminated in $\beta4^{-/-}$ mice, for which none of the animals quit drinking nicotine, and restored upon expression of β4 in the IPN. Strikingly, we observed a negative correlation between nicotine consumption and the sensitivity of the IPN to the drug: high nicotine drinking mice displayed low nicotine sensitivity in the IPN, whereas low nicotine drinking mice showed high nicotine sensitivity in the IPN. The state of the nicotinic neurotransmission in the IPN could thus be a predictive factor for nicotine intake. We believe that β4-containing nAChRs, by engaging the IPN circuitry, initiate a primary response to nicotine that, if above a certain threshold, will develop into aversion for the drug. In line with this, it was found that pharmacological or optogenetic stimulation of the MHb-IPN pathway could directly produce aversion (Morton et al., 2018; Tuesta et al., 2017; Wolfman et al., 2018). Our data further suggest that the aversion produced by nicotine is not just acute but also long-lasting, and hence may not just be involved in the satiety of drug intake through the balance between drug reward and aversion. Such sustained aversive reaction to nicotine was conditioned by nicotine itself, and required β4-containing nAChRs of the IPN for the onset, but most likely involves other molecular players and brain circuits for the long-term effects. Identifying these factors will be crucial in the context of tobacco dependence, as unpleasant initial responses to cigarettes is associated with a reduced likelihood of continued smoking (DiFranza et al., 2004).

One key question remains, as whether these differences between avoiders and consumers pre-exist, or whether they are experience-induced. The mice we used in this study were isogenic, yet epigenetic changes during development may affect the sensitivity of the IPN to nicotine. We did not observe major differences in the consumption levels of avoiders and consumers at the beginning of the task, for low concentrations of nicotine (<100 μg/ml), but cannot completely rule out pre-existing inter-individual differences. Alternatively, chronic nicotine could produce long-lasting molecular and cellular adaptations in the IPN circuitry, and these adaptations could affect nicotine aversion and consumption. In the VTA, chronic nicotine upregulates the number of functional β2-containing receptors at the cell surface (H. A. Lester et al., 2009; Sallette et al., 2005). We discovered that chronic nicotine had the opposite effect on β4-containing nAChRs of the IPN: it downregulated and/or desensitized these receptors, as evidenced by the decreased response to nicotine both ex and in vivo. This effect seems to be specific to β4-containing nAChRs, since chronic nicotine had virtually no consequence on the residual IPN nAChR current in $\beta4^{-/-}$ mice. These results contrast with the recent report of upregulated nAChR currents in IPN slices of nicotine-treated mice (Arvin et al., 2019). The reason for this discrepancy is unclear. Nevertheless, the behavioral results we obtained with nicotine-treated WT animals and with $\beta4^{-/-}$ mice completely match: both displayed reduced nAChR currents in IPN neurons, and increased nicotine consumption compared to naïve, WT animals. Our results suggest that long-term exposure to nicotine will increase the threshold for nicotine aversion, and thereby increase drug consumption. In other words,

nicotine history weakens the ability of nicotine to induce aversion in mice. In most nicotine replacement therapies such as gums or patches, nicotine is slowly administered over prolonged periods of time, to supposedly attenuate the negative emotional reactions elicited by nicotine withdrawal. However, our data show that animals under chronic nicotine administration will also develop tolerance to the aversive effects of nicotine, thus providing some possible explanation as to why such replacement strategies have very limited efficacy in the long term (Hartmann-Boyce, Chepkin, Ye, Bullen, & Lancaster, 2018), and highlighting the necessity to develop alternative medical approaches.

Material and Methods

Animals

Eight to sixteen-week old wild-type C57BL/6J (Janvier labs, France) and ACNB4 knock-out ($\beta4^{-/-}$) mice (Pasteur Institute, Paris) (Xu et al., 1999) were used for this study. $\beta4^{-/-}$ mice were backcrossed onto C57BL/6J background for more than 20 generations with C57BL/6J. Mice were maintained on a 12h light and dark cycle.

Two-bottle choice paradigm

Mice single-housed in a home cage were presented with two bottles of water (Volvic) for a habituation period of 4 days. After habituation, mice were presented with one bottle of saccharine solution (2%, Sigma Aldrich) and one bottle of nicotine (free base, Sigma Aldrich) plus saccharine (2%) solution diluted in water (adjusted to pH ~7.2 with NaOH). Unless otherwise noted, four different concentrations of nicotine were tested consecutively (10, 50, 100 to 200 µg/ml) with changes in concentration occurring every 4 days. For the two-bottle aversion task, a single nicotine concentration (100 µg/ml) was used after the habituation period. Bottles were swapped every other day to control for side preference. The drinking volume was measured every minute with an automated acquisition system (TSE system, Germany). Mice were weighed every other day to quantify the nicotine intake in mg/kg/day. Mice with a strong side bias (preference <20% or >80%) in the habituation period were not taken into account for the analyses.

Chronic nicotine treatment

Osmotic minipumps (2004, Alzet minipump) were implanted subcutaneously in 8-week-old mice anesthetized with isoflurane (1%). Minipumps continuously delivered nicotine (10 mg/kg/d) or saline (control) solution with a rate of 0.25 µl/h during 4 weeks.

Brain slice preparation

Mice were weighed and then anaesthetized with an intraperitoneal injection of a mixture of ketamine (150 mg/kg, Imalgene 1000, Merial, Lyon, France) and xylazine (60 mg/kg, Rompun 2%, Bayer France, Lyon, France). Blood was then fluidized by an injection of an anticoagulant (0.1mL, Heparin 1000 U/mL, Sigma) into the left ventricle, and an intra-cardiac perfusion of ice-cold (0-4°C), oxygenated (95% O_2/5% CO_2) sucrose-based artificial cerebrospinal fluid (SB-aCSF) was performed. The SB-aCSF solution contained (in mM): 125 NaCl, 2.5 KCl, 1.25 NaH_2PO_4, 5.9 $MgCl_2$, 26 $NaHCO_3$, 25 Sucrose, 2.5 Glucose, 1 Kynurenate (pH 7.2). After rapid brain sampling, slices (250 µm thick) were cut in SB-aCSF at 0-4°C using a Compresstome slicer (VF-200, Precisionary Instruments Inc.). Slices were then transferred to the same solution at 35°C for 10 min, then moved and stored in an oxygenated aCSF solution at room temperature. The aCSF solution contained in mM: 125 NaCl, 2.5 KCl, 1.25 NaH_2PO_4, 2 $CaCl_2$, 1 $MgCl_2$, 26 $NaHCO_3$, 15 sucrose, 10 glucose (pH 7.2). After a minimum 1h of rest, slices were placed individually in a recording chamber at room temperature and infused continuously with aCSF recording solution at a constant flow rate of about 2 ml/min.

Ex vivo patch-clamp recordings of IPN neurons

Patch pipettes (5-8 MΩ) were stretched from borosilicate glass capillaries (G150TF-3, Warner instruments) using a pipette puller (Sutter Instruments, P-87, Novato, CA) and were filled with a few microliters of an intracellular solution adjusted to a pH of 7.2, containing (in mM) : 116 K-gluconate, 20 HEPES, 0.5 EGTA, 6 KCl, 2 NaCl, 4 ATP, 0.3 GTP and 2 mg/mL biocytin. Biocytin was used to label recorded neurons. The slice of interest was placed in the recording chamber and viewed using a white light source and a straight microscope coupled to a Dodt contrast lens (Scientifica, Uckfield, UK). Whole-cell configuration recordings of IPN neurons were performed using an amplifier (Axoclamp 200B, Molecular Devices, Sunnyvale, CA) connected to a digitizer (Digidata 1550 LowNoise acquisition system, Molecular Devices, Sunnyvale, CA). Signal acquisition was performed at 10 kHz, filtered with a lowpass (Bessel, 2 kHz) and collected by the acquisition software pClamp 10.5 (Molecular Devices, Sunnyvale, CA). Nicotine tartrate (30 µM in aCSF) was locally and briefly applied (200 ms puffs) using a puff pipette (glass pipette ~3 µm diameter at the tip) positioned about 20-30 µm from the soma of the neuron. The pipette was connected to a Picospritzer (PV-800 PicoPump, World Precision Instruments) controlled with pClamp to generate transient pressure in the pipette (~2 psi). Nicotine-evoked currents were recorded in voltage-clamp mode at a membrane potential of -60 mV. All electrophysiology traces were extracted and pre-processed using Clampfit (Molecular Devices, Sunnyvale, CA) and analyzed with R.

In vivo electrophysiology

Mice were deeply anesthetized with chloral hydrate (8%, 400 mg/kg) and anesthesia was maintained throughout the experiment with supplements. Catheters were positioned in the saphenous veins of the mice to perform saline or nicotine intravenous injections. Nicotine hydrogen tartare salt (Sigma-Aldrich) was dissolved in 0.9% NaCl solution and pH was adjusted to 7.4. Nicotine solution was injected at a dose of 7.5, 15 and 30 µg/kg. Borosilicate glass tubings (1.5 mm O.D. / 1.17 mm I.D., Harvard Apparatus) were pulled using a vertical puller (Narishige). Glass pipettes were broken under a microscope to obtain a ~1 µm diameter at the tip. Electrodes were filled with a 0.5% NaCl solution containing 1.5% of neurobiotin tracer (AbCys) yielding impedances of 6-9 MΩ. Electrical signals were amplified by a high-impedance amplifier (Axon Instruments) and supervised through an audio monitor (A.M. Systems Inc.). The signal was digitized, sampled at 25 kHz and recorded on a computer using Spike2 (Cambridge Electronic Design) for later analysis. IPN neurons were recorded in an area corresponding to the following stereotaxic coordinates (4-5° angle): 3.3 - 3.6 mm posterior to bregma, 0.2 - 0.45 mm from medial to lateral and 4.3 - 5 mm below the brain surface. A 5 min-baseline was recorded prior to saline or nicotine i.v. injection. For the dose-response experiments, successive randomized injections of nicotine (or saline) were performed, interspaced with sufficient amount of time (> 10 min) to allow the neuron to return to its baseline.

Stereotaxic viral injections

8-week old mice were injected in the IPN with a lentivirus that co-expresses the WT β4 subunit together with eGFP (or only eGFP for control experiments) under the control of the pGK promoter. Lentiviruses were produced as previously described (Maskos et al., 2005). For viral transduction, mice were anaesthetized with a gas mixture containing 1-3% isoflurane (IsoVet®, Pyramal Healthcare Ltd., Nothumberland, UK) and placed in a stereotactic apparatus (David Kopf Instruments, Tujunga, CA). Unilateral injections (0.1µl/min) of 1µl of a viral solution (Lenti.pGK.β4.IRES.eGFP, titer 150 ng/µl of p24 protein; or Lenti.pGK.eGFP, titer 75 ng/µl of p24 protein) were performed using a cannula (diameter 36G, Phymep, Paris, France). The cannula was connected to a Hamilton syringe of 10 µL (Model 1701, Hamilton Robotics, Bonaduz, Switzerland) placed in a syringe pump (QSI, Stoelting Co, Chicago, IL, USA). Injections were performed in the IPN at the following coordinates (5° angle): from bregma ML - 0.4 mm, AP - 3.5 mm, and DV: - 4.7 mm (according to Paxinos & Franklin). Electrophysiological recordings were made at least 4 weeks after injection, the time required for the expression of the transgene, and proper expression was subsequently checked using immunohistochemistry.

Immunocytochemical identification

Immunostaining was performed as described in (Durand-de Cuttoli et al., 2018)*, with the following* primary antibodies: anti-tyrosine hydroxylase 1:500 (anti-TH, Sigma, T1299) and chicken anti-eYFP 1:500 (Life technologies Molecular Probes, A-6455). Briefly, serial 60 µm sections of the midbrain were cut with a vibratome. Slice were permeabilized for one hour in a solution of phosphate-buffered saline

(PBS) containing 3% Bovine Serum Albumin (BSA, Sigma; A4503). After incubated with primary antibodies overnight at 4℃ in a solution of 1.5% BSA and 0.2% Triton X-100, sections were washed with PBS and then incubated 1 hour with the secondary antibodies. The secondary antibodies were Cy3-conjugated anti-mouse 1:500 and alexa488-conjugated anti-chicken secondary 1:1000 (Jackson ImmunoResearch, 715-165-150 and 711-225-152). For the juxtacellular immunostaining, the recorded neurons were identified with the addition of 1:200 AMCA-conjugated streptavidin in the solution (Jackson ImmunoResearch). Slices were mounted using Prolong Gold Antifade Reagent (Invitrogen, P36930). Microscopy was carried out either with a confocal microscope (Leica) or an epifluorescence microscope (Leica), and images captured using a camera and analyzed with ImageJ.

Author contribution: SM and RDC performed patch-clamp recordings; SM, CN, ST and FM performed juxtacellular recordings; SM and CN performed stereotaxic injections; SM, CN and JJ performed behavioral tests; NT and SM developed analytical tools; SM and CN performed immunostainings, SP and UM provided viral tools and transgenic lines; SM, PF and AM designed the study; PF and AM acquired funding; SM, PF and AM wrote the article, with inputs from all the other authors.

Acknowledgments: authors would like to thank Ines Centeno-Lemaire for her help with behavioral tests. This work was supported by the Agence Nationale de la Recherche (ANR-JCJC 2014 to A.M.), by the Fondation pour la Recherche Médicale (Equipe FRM DEQ2013326488 to P.F.), by the French National Cancer Institute Grant TABAC-16–022 (to P.F.). A.M. was recipient of a fundamental research prize from the Medisite Foundation for Neuroscience. S.M. and R.D.C. were supported by a fourth-year fellowship from FRM (FDT201904008060 and FDT20170437427). P.F. and A.M. laboratory is part of the Ecole des Neurosciences de Paris Ile-de-France RTRA network.

References

Antolin-Fontes, B., Li, K., Ables, J. L., Riad, M. H., Görlich, A., Williams, M., et al. (2020). The habenular G-protein-coupled receptor 151 regulates synaptic plasticity and nicotine intake. *Proceedings of the National Academy of Sciences*, *117*(10), 5502–5509. http://doi.org/10.1073/pnas.1916132117

Arvin, M. C., Jin, X.-T., Yan, Y., Wang, Y., Ramsey, M. D., Kim, V. J., et al. (2019). Chronic nicotine exposure alters the neurophysiology of habenulo-interpeduncular circuitry. *Journal of Neuroscience*, 2816–18–52. http://doi.org/10.1523/JNEUROSCI.2816-18.2019

Association, A. P. (2013). Diagnostic and Statistical Manual of Mental Disorders (DSM-5®). *Annals of Intensive Care* (Vol. 8). American Psychiatric Pub. http://doi.org/10.1186/s13613-018-0377-7

Bierut, L. J., Stitzel, J. A., Wang, J. C., Hinrichs, A. L., Grucza, R. A., Xuei, X., et al. (2008). Variants in nicotinic receptors and risk for nicotine dependence. *The American Journal of Psychiatry*, *165*(9), 1163–1171. http://doi.org/10.1176/appi.ajp.2008.07111711

Centers for Disease Control and Prevention (US), National Center for Chronic Disease Prevention and Health Promotion (US), Office on Smoking and Health (US). (2010). How Tobacco Smoke Causes Disease: The Biology and Behavioral Basis for Smoking-Attributable Disease: A Report of the Surgeon General.

Deroche-Gamonet, V., Belin, D., & Piazza, P. V. (2004). Evidence for addiction-like behavior in the rat. *Science*, *305*(5686), 1014–1017. http://doi.org/10.1126/science.1099020

DiFranza, J. R., Savageau, J. A., Fletcher, K., Ockene, J. K., Rigotti, N. A., McNeill, A. D., et al. (2004). Recollections and repercussions of the first inhaled cigarette. *Addictive Behaviors*, *29*(2), 261–272. http://doi.org/10.1016/j.addbeh.2003.08.002

Durand-de Cuttoli, R., Mondoloni, S., Marti, F., Lemoine, D., Nguyen, C., Naudé, J., et al. (2018). Manipulating midbrain dopamine neurons and reward-related behaviors with light-controllable nicotinic acetylcholine receptors. *eLife*, *7*, 15991. http://doi.org/10.7554/eLife.37487

Fenster, C. P., Rains, M. F., Noerager, B., Quick, M. W., & Lester, R. A. (1997). Influence of subunit composition on desensitization of neuronal acetylcholine receptors at low concentrations of nicotine. *Journal of Neuroscience*, *17*(15), 5747–5759.

Forget, B., Scholze, P., Langa, F., Morel, C., Pons, S., Mondoloni, S., et al. (2018). A Human Polymorphism in CHRNA5 Is Linked to Relapse to Nicotine Seeking in Transgenic Rats. *Current Biology : CB*, *28*(20), 3244–3253.e7. http://doi.org/10.1016/j.cub.2018.08.044

Fowler, C. D., & Kenny, P. J. (2014). Nicotine aversion: Neurobiological mechanisms and relevance to tobacco dependence vulnerability. *Neuropharmacology*, *76 Pt B*, 533–544. http://doi.org/10.1016/j.neuropharm.2013.09.008

Fowler, C. D., Lu, Q., Johnson, P. M., Marks, M. J., & Kenny, P. J. (2011). Habenular α5 nicotinic receptor subunit signalling controls nicotine intake. *Nature*, 1–7. http://doi.org/10.1038/nature09797

Frahm, S., Ślimak, M. A., Ferrarese, L., Santos-Torres, J., Antolin-Fontes, B., Auer, S., et al. (2011). Aversion to Nicotine Is Regulated by the Balanced Activity of beta4 and alpha5 Nicotinic Receptor Subunits in the Medial Habenula. *Neuron*, *70*(3), 522–535. http://doi.org/10.1016/j.neuron.2011.04.013

Gallego, X., Molas, S., Amador-Arjona, A., Marks, M. J., Robles, N., Murtra, P., et al. (2011). Overexpression of the CHRNA5/A3/B4 genomic cluster in mice increases the sensitivity to nicotine and modifies its reinforcing effects. *Amino Acids*, *43*(2), 897–909. http://doi.org/10.1007/s00726-

011-1149-y

Garcia-Rivas, V., Cannella, N., & Deroche-Gamonet, V. (2017). Individual Variations in the Mechanisms of Nicotine Seeking: A Key for Research on Nicotine Dependence. *Neuropsychopharmacology*, *42*(3), 584–586. http://doi.org/10.1038/npp.2016.176

George, O., & Koob, G. F. (2017). Individual differences in the neuropsychopathology of addiction. *Dialogues in Clinical Neuroscience*, *19*(3), 217–229.

Grady, S. R., Moretti, M., Zoli, M. M., Marks, M. J. M., Zanardi, A. A., Pucci, L. L., et al. (2009). Rodent habenulo-interpeduncular pathway expresses a large variety of uncommon nAChR subtypes, but only the alpha3beta4* and alpha3beta3beta4* subtypes mediate acetylcholine release. *Journal of Neuroscience*, *29*(7), 2272–2282. http://doi.org/10.1523/JNEUROSCI.5121-08.2009

Harrington, L., Viñals, X., Herrera-Solís, A., Flores, A., Morel, C., Tolu, S., et al. (2016). Role of β4* Nicotinic Acetylcholine Receptors in the Habenulo-Interpeduncular Pathway in Nicotine Reinforcement in Mice. *Neuropsychopharmacology*, *41*(7), 1790–1802. http://doi.org/10.1038/npp.2015.346

Hartmann-Boyce, J., Chepkin, S. C., Ye, W., Bullen, C., & Lancaster, T. (2018). Nicotine replacement therapy versus control for smoking cessation. *Cochrane Database of Systematic Reviews*, *1*(8628), 7–196. http://doi.org/10.1002/14651858.CD000146.pub5

Hsu, Y.-W. A., Tempest, L., Quina, L. A., Wei, A. D., Zeng, H., & Turner, E. E. (2013). Medial habenula output circuit mediated by α5 nicotinic receptor-expressing GABAergic neurons in the interpeduncular nucleus. *Journal of Neuroscience*, *33*(46), 18022–18035. http://doi.org/10.1523/JNEUROSCI.2927-13.2013

Husson, M., Harrington, L., Tochon, L., Cho, Y., Ibañez-Tallon, I., Maskos, U., & David, V. (2020). β4-Nicotinic Receptors Are Critically Involved in Reward-Related Behaviors and Self-Regulation of Nicotine Reinforcement. *Journal of Neuroscience*, *40*(17), 3465–3477. http://doi.org/10.1523/JNEUROSCI.0356-19.2020

Juarez, B., Morel, C., Ku, S. M., Liu, Y., Zhang, H., Montgomery, S., et al. (2017). Midbrain circuit regulation of individual alcohol drinking behaviors in mice. *Nature Communications*, *8*(1), 2220. http://doi.org/10.1038/s41467-017-02365-8

Koob, G. F., & Le Moal, M. (1997). Drug abuse: hedonic homeostatic dysregulation. *Science*, *278*(5335), 52–58. http://doi.org/10.1126/science.278.5335.52

Lassi, G., Taylor, A. E., Timpson, N. J., Kenny, P. J., Mather, R. J., Eisen, T., & Munafò, M. R. (2016). The CHRNA5–A3–B4 GeneCluster and Smoking: FromDiscovery to Therapeutics. *Trends in Neurosciences*, *39*(12), 851–861. http://doi.org/10.1016/j.tins.2016.10.005

Lester, H. A., Xiao, C., Srinivasan, R., Son, C. D., Miwa, J., Pantoja, R., et al. (2009). Nicotine is a Selective Pharmacological Chaperone of Acetylcholine Receptor Number and Stoichiometry. Implications for Drug Discovery. *The AAPS Journal*, *11*(1), 167–177. http://doi.org/10.1208/s12248-009-9090-7

Lüscher, C., Robbins, T. W., & Everitt, B. J. (2020). The transition to compulsion in addiction. *Nature Reviews Neuroscience*, *21*(5), 1–17. http://doi.org/10.1038/s41583-020-0289-z

Maskos, U., Molles, B. E., Pons, S., Besson, M., Guiard, B. P., Guilloux, J. P., et al. (2005). Nicotine reinforcement and cognition restored by targeted expression of nicotinic receptors. *Nature*, *436*(7047), 103–107. http://doi.org/10.1038/nature03694

McLaughlin, I., Dani, J. A., & De Biasi, M. (2017). The medial habenula and interpeduncular nucleus circuitry is critical in addiction, anxiety, and mood regulation. *Journal of Neurochemistry*, *142*, 130–143. http://doi.org/10.1016/j.cpr.2005.05.001

Molas, S., DeGroot, S. R., Zhao-Shea, R., & Tapper, A. R. (2017). Anxiety and Nicotine Dependence: Emerging Role of the Habenulo-Interpeduncular Axis. *Trends in Pharmacological Sciences*, *38*(2), 169–180. http://doi.org/10.1016/j.tips.2016.11.001

Morton, G., Morton, G., Nasirova, N., Nasirova, N., Sparks, D. W., Sparks, D. W., et al. (2018). Chrna5-Expressing Neurons in the Interpeduncular Nucleus Mediate Aversion Primed by Prior Stimulation or Nicotine Exposure. *Journal of Neuroscience*, *38*(31), 6900–6920. http://doi.org/10.1523/JNEUROSCI.0023-18.2018

Nesil, T., Kanit, L., Collins, A. C., & Pogun, S. (2011). Individual differences in oral nicotine intake in rats. *Np*, *61*(1-2), 189–201. http://doi.org/10.1016/j.neuropharm.2011.03.027

Otsu, Y., Darcq, E., Pietrajtis, K., Mátyás, F., Schwartz, E., Bessaih, T., et al. (2019). Control of aversion by glycine-gated GluN1/GluN3A NMDA receptors in the adult medial habenula. *Science*, *366*(6462), 250–254. http://doi.org/10.1126/science.aax1522

Pang, X., Liu, L., Ngolab, J., Zhao-Shea, R., McIntosh, J. M., Gardner, P. D., & Tapper, A. R. (2016). Habenula cholinergic neurons regulate anxiety during nicotine withdrawal via nicotinic acetylcholine receptors. *Neuropharmacology*, *107*, 294–304. http://doi.org/10.1016/j.neuropharm.2016.03.039

Pascoli, V., Hiver, A., Zessen, R., Loureiro, M., Achargui, R., Harada, M., et al. (2018). Stochastic synaptic plasticity underlying compulsion in a model of addiction. *Nature*, *564*(7736), 1–22. http://doi.org/10.1038/s41586-018-0789-4

Piazza, P. V., Deminière, J. M., Le Moal, M., & Simon, H. (1989). Factors that predict individual vulnerability to amphetamine self-administration. *Science*, *245*(4925), 1511–1513. http://doi.org/10.1126/science.2781295

Pogun, S., & C Collins, A. (2012). Oral Nicotine Self-Administration in Rodents. *Journal of Addiction Research & Therapy*, *01*(S2), 1–19. http://doi.org/10.4172/2155-6105.S2-004

Quina, L. A., Harris, J., Zeng, H., & Turner, E. E. (2017). Specific connections of the interpeduncular subnuclei reveal distinct components of the habenulopeduncular pathway. *The Journal of Comparative Neurology*, *525*(12), 2632–2656. http://doi.org/10.1016/j.cub.2013.09.041

Salas, R., Sturm, R., Boulter, J., & De Biasi, M. (2009). Nicotinic Receptors in the Habenulo-Interpeduncular System Are Necessary for Nicotine Withdrawal in Mice. *Journal of Neuroscience*, *29*(10), 3014–3018. http://doi.org/10.1523/JNEUROSCI.4934-08.2009

Sallette, J., Pons, S., Devillers-Thiery, A., Soudant, M., Prado de Carvalho, L., Changeux, J.-P., & Corringer, P.-J. (2005). Nicotine Upregulates Its Own Receptors through Enhanced Intracellular Maturation. *Neuron*, *46*(4), 595–607. http://doi.org/10.1016/j.neuron.2005.03.029

Shih, P. Y., Engle, S. E., Oh, G., Deshpande, P., Puskar, N. L., Lester, H. A., & Drenan, R. M. (2014). Differential Expression and Function of Nicotinic Acetylcholine Receptors in Subdivisions of Medial Habenula. *Journal of Neuroscience*, *34*(29), 9789–9802. http://doi.org/10.1523/JNEUROSCI.0476-14.2014

Siciliano, C. A., Noamany, H., Chang, C.-J., Brown, A. R., Chen, X., Leible, D., et al. (2019). A cortical-brainstem circuit predicts and governs compulsive alcohol drinking. *Science*, *366*(6468), 1008–1012. http://doi.org/10.1126/science.aay1186

Taly, A., Corringer, P.-J., Guedin, D., Lestage, P., & Changeux, J.-P. (2009). Nicotinic receptors: allosteric transitions and therapeutic targets in the nervous system. *Nature Reviews Drug Discovery*, *8*(9), 733–750. http://doi.org/10.1038/nrd2927

Tapper, A. R., McKinney, S. L., Nashmi, R., Schwarz, J., Deshpande, P., Labarca, C., et al. (2004). Nicotine activation of alpha4* receptors: sufficient for reward, tolerance, and sensitization. *Science*, *306*(5698), 1029–1032. http://doi.org/10.1126/science.1099420

Tolu, S., Eddine, R., Marti, F., David, V., Graupner, M., Pons, S., et al. (2013). Co-activation of VTA DA and GABA neurons mediates nicotine reinforcement. *Molecular Psychiatry*, *18*(3), 382–393. http://doi.org/10.1038/mp.2012.83

Tuesta, L. M., Chen, Z., Duncan, A., Fowler, C. D., Ishikawa, M., Lee, B. R., et al. (2017). GLP-1 acts on habenular avoidance circuits to control nicotine intake. *Nature Neuroscience*, *20*(5), 708–716. http://doi.org/10.1038/nn.4540

Verendeev, A., & Riley, A. L. (2013). The role of the aversive effects of drugs in self-administration. *Behavioural Pharmacology*, *24*(5 and 6), 363–374. http://doi.org/10.1097/FBP.0b013e32836413d5

WHO global report on trends in prevalence of tobacco use 2000-2025 third edition. (2019). *WHO global report on trends in prevalence of tobacco use 2000-2025 third edition* (pp. 1–121).

Wise, R. A., Yokel, R. A., & DeWit, H. (1976). Both positive reinforcement and conditioned aversion from amphetamine and from apomorphine in rats. *Science*, *191*(4233), 1273–1275. http://doi.org/10.1126/science.1257748

Wolfman, S. L., Gill, D. F., Bogdanic, F., Long, K., Al-Hasani, R., McCall, J. G., et al. (2018). Nicotine aversion is mediated by GABAergic interpeduncular nucleus inputs to laterodorsal tegmentum. *Nature Communications*, *9*(1), 2710. http://doi.org/10.1038/s41467-018-04654-2

Xu, W., Orr-Urtreger, A., Nigro, F., Gelber, S., Sutcliffe, C. B., Armstrong, D., et al. (1999). Multiorgan autonomic dysfunction in mice lacking the beta2 and the beta4 subunits of neuronal nicotinic acetylcholine receptors. *Journal of Neuroscience*, *19*(21), 9298–9305.

Yamaguchi, T., Danjo, T., Pastan, I., Hikida, T., & Nakanishi, S. (2013). Distinct Roles of Segregated Transmissionof the Septo-Habenular Pathway in Anxiety and Fear. *Neuron*, *78*(3), 537–544. http://doi.org/10.1016/j.neuron.2013.02.035

Zhang, J., Tan, L., Ren, Y., Liang, J., Lin, R., Feng, Q., et al. (2016). Presynaptic Excitation via GABAB Receptors in Habenula Cholinergic Neurons Regulates Fear Memory Expression. *Cell*, *166*(3), 716–728. http://doi.org/10.1016/j.cell.2016.06.026

Zhao-Shea, R., DeGroot, S. R., Liu, L., Vallaster, M., Pang, X., Su, Q., et al. (2015). Increased CRF signalling in a ventral tegmentalarea-interpeduncular nucleus-medial habenulacircuit induces anxiety during nicotine withdrawal. *Nature Communications*, *6*, 1–13. http://doi.org/10.1038/ncomms7770

Zhao-Shea, R., Liu, L., Pang, X., Gardner, P. D., & Tapper, A. R. (2013). Activation of GABAergic Neuronsin the Interpeduncular Nucleus Triggers Physical Nicotine Withdrawal Symptoms. *Current Biology*, *23*(23), 2327–2335. http://doi.org/10.1016/j.cub.2013.09.041

Zoli, M., Pistillo, F., & Gotti, C. (2015). Diversity of native nicotinic receptor subtypes in mammalian brain. *Neuropharmacology*, *96*(Pt B), 302–311. http://doi.org/10.1016/j.neuropharm.2014.11.003

Figure Legends

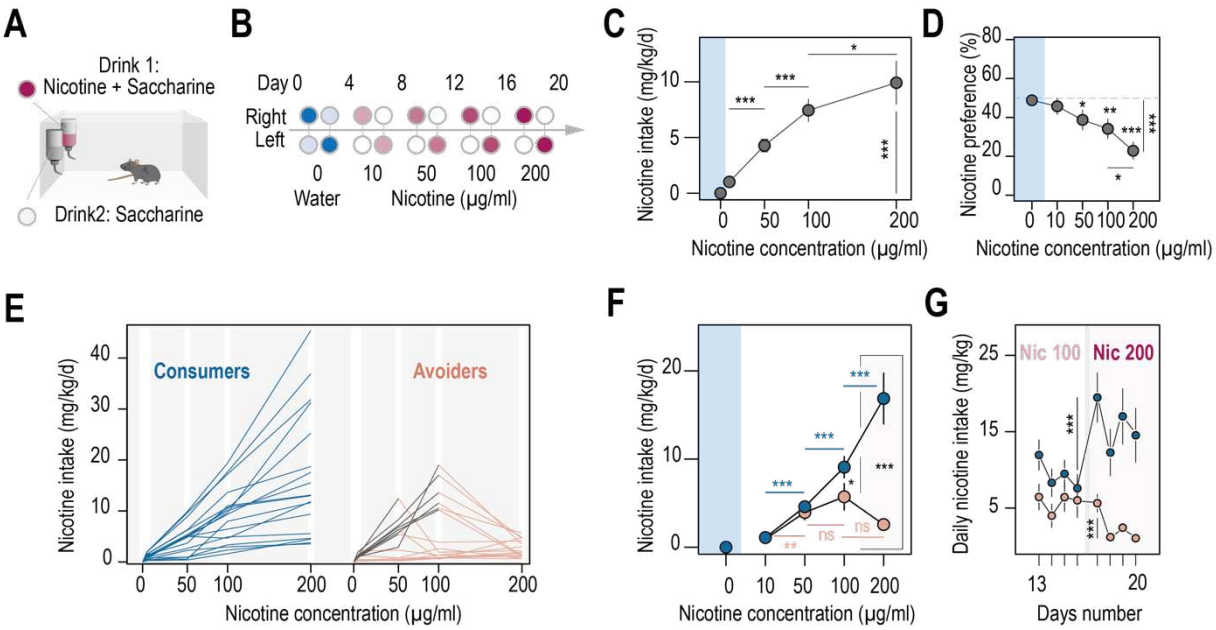

Figure 1: Two different profiles, consumers and avoiders, emerged in WT mice subjected to a two-bottle choice nicotine-drinking test. **A.** Continuous access, two-bottle choice setup. **B.** Two-bottle choice paradigm. Each dot represents a bottle and is color-coded according to whether it contains water (blue or light blue), nicotine plus 2% saccharine (red, gradient of color intensities according to the concentration), or 2% saccharine (white) solutions. Nicotine concentration in the bottle increased progressively from 10 to 50, 100 and 200 µg/ml. Each condition lasted 4 days, and the bottles were swapped every other day. **C.** Daily nicotine intake (mg/kg/d) averaged over four days, as a function of nicotine concentration in the bottle (Friedman test, n=35, df=3, $p<0.001$ and Mann-Whitney post-hoc test with Holm-Bonferroni correction). **D.** Nicotine preference (%) in WT mice for each dose of nicotine, averaged over four days (Friedman test, n=35, df=4, $p<0.001$ and Mann-Whitney post-hoc test with Holm-Bonferroni correction) **E.** Nicotine intake in individual consumers and avoiders. **F.** Nicotine consumption in consumers and avoiders for each nicotine dose, averaged over four days (Mann-Whitney comparison with a Bonferroni-Holm correction (non-Gaussian distribution)). **G.** Daily nicotine consumption in consumers and avoiders for the nicotine 100 and 200 µg/ml conditions. Note the change in consumption at day 2 of nicotine 200 µg/ml for avoiders. In all figure panels avoiders are depicted in pinkish-orange while consumers are in blue. *** $p<0.001$, ** $p<0.01$, * $p<0.05$.

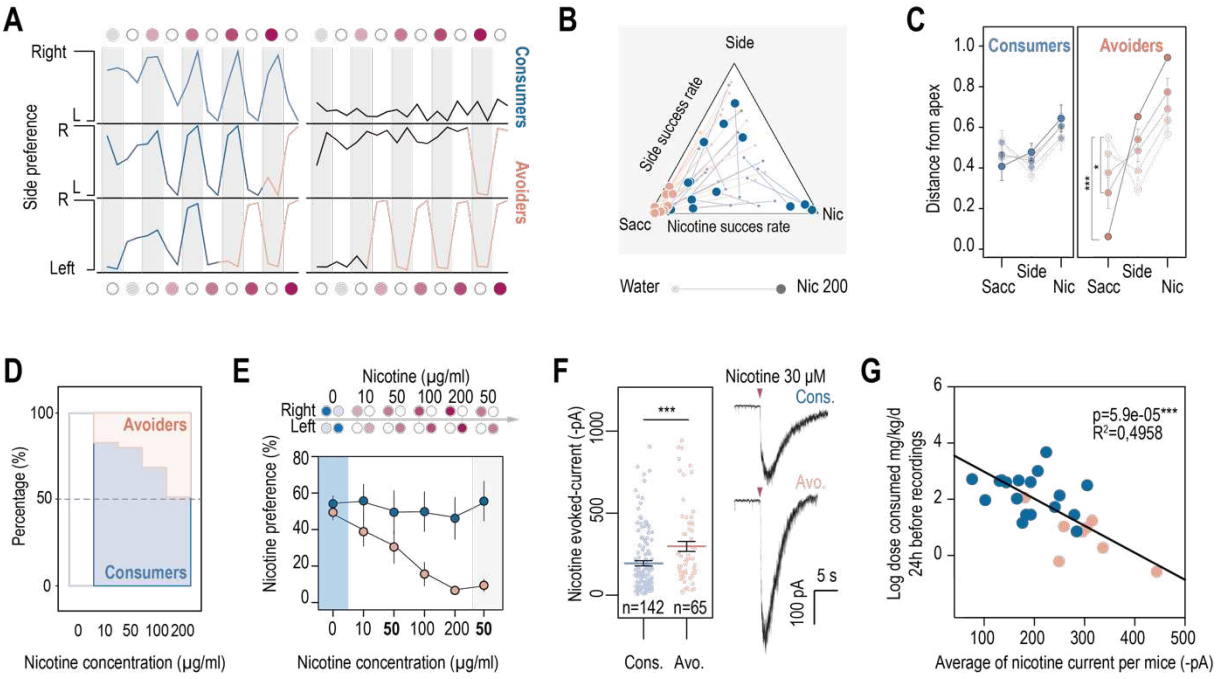

FIGURE 2

Figure 2: Nicotine consumption was negatively correlated with the amplitude of the nicotine response in IPN neurons. **A.** Representative examples of choice behaviors in WT mice when the right-hand side bottle contains either nicotine + saccharine (red dots, grey stripe) or saccharine only (white dots, white stripes). Consumers maintained their strategy throughout the 20-day long test, and either tracked the side associated with nicotine or had a strong side bias. Avoiders actively avoided the side associated with nicotine after a certain nicotine dose was reached in the bottle, whether they initially tracked nicotine or not. **B.** Pseudo-ternary diagram representing, for each individual, its side success rate over its nicotine success rate. Bottom left apex: 100% saccharine preference (Sacc); Bottom right apex: 100% nicotine preference (Nic); Top apex: 100% side preference (Side, absolute non-switchers). Small dots correspond to the habituation period (water vs. water) while bigger dots correspond to the condition with 200 µg/ml of nicotine in one bottle. Note how all avoider mice end up in the bottom left apex (0% nicotine preference) at the end of the task. **C.** Average distance from the three apices for each condition in the task (0, 10, 50, 100 and 200 µg/ml of nicotine, color-coded from light to dark), for consumers and avoiders. Only avoider mice significantly changed their drinking strategy as nicotine concentration increased (paired Mann-Whitney test with Holm-Bonferroni correction). **D.** Proportion of avoiders and consumers as nicotine concentration increases. **E.** Average nicotine preference (%) for avoider and consumer mice for each dose of nicotine in the two-bottle choice task. **F.** Representative and average currents recorded in voltage-clamp mode (-60 mV) from IPR/IPDL neurons of consumers (blue, n=142, -194.09 +/- 15.55 pA) and avoiders (red, n=65, -297.31+/- 30.33 pA) following a puff application of nicotine (30 µM, 200 ms). Avoiders presented greater nicotine-evoked currents than consumers (Mann-Whitney, p-value=1.375e-11). **G.** Correlation between the dose consumed (log scale, over the last 24h prior to the recording) and the averaged nicotine evoked-current per mouse (-pA). In all figure panels avoiders are depicted in pinkish-orange while consumers are in blue. *** p<0.001, ** p<0.01, * p<0.05.

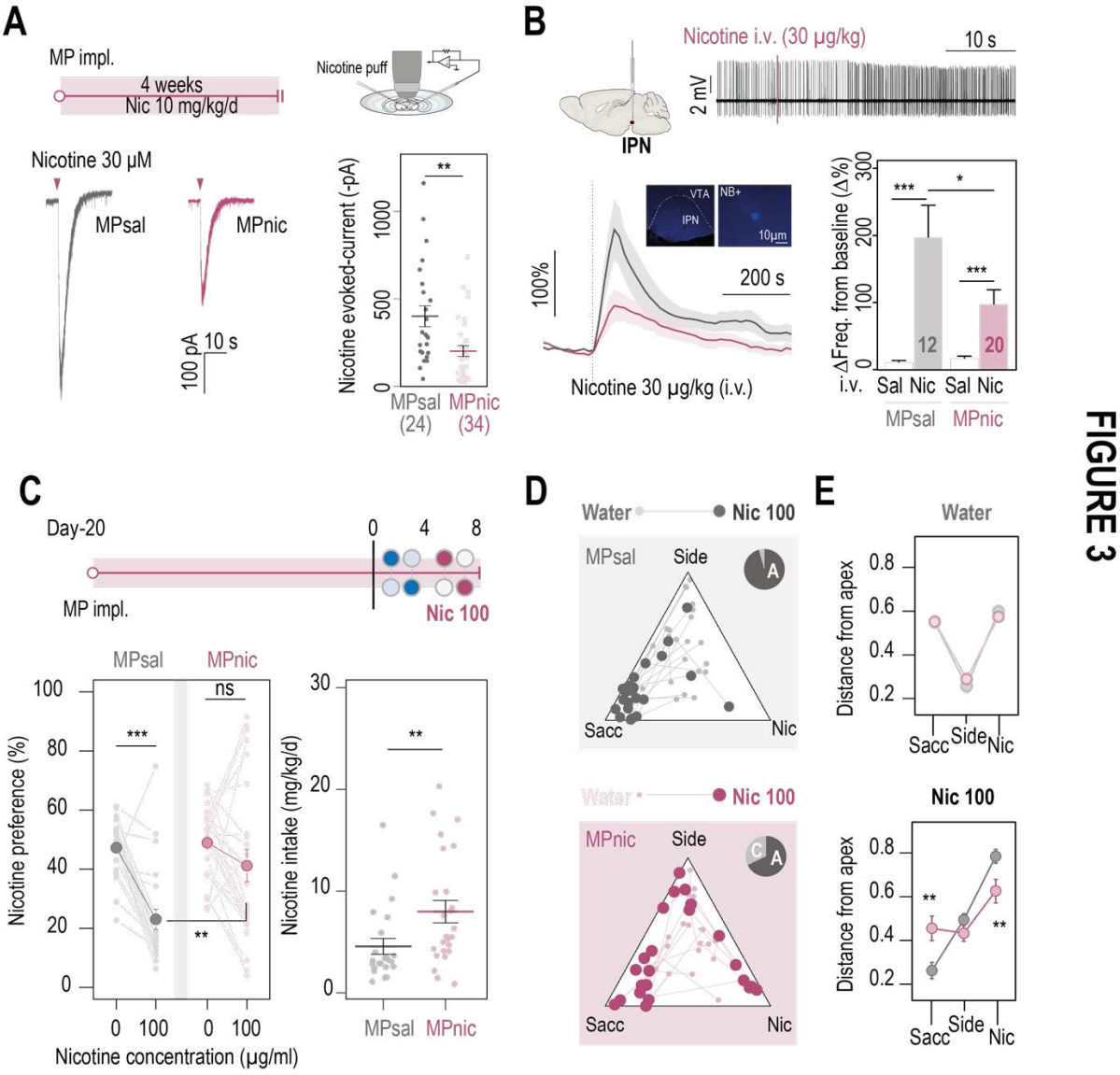

FIGURE 3

Figure 3: Chronic nicotine treatment alters both nAChR expression levels in the IPN and nicotine consumption in WT mice. **A.** Top, passive nicotine treatment protocol. Mice were implanted subcutaneously with an osmotic minipump (MP) that continuously delivered 10 mg/kg/d of nicotine. After 4 weeks of treatment, nicotine-evoked responses in IPR/IPDL neurons were recorded in whole-cell voltage-clamp mode (-60 mV) from IPN slices. Bottom, representative recordings and average current amplitudes following a puff application of nicotine (30 µM, 200 ms) in IPR/IPDL neurons of mice treated either with saline (n=24, -400.96 +/- 59.24 pA) or nicotine (n=34, -201.75 +/- 36.87 pA). Nicotine treatment reduced the amplitude of nicotine-evoked currents in IPR/IPDL neurons (Mann-Whitney, p-value=0.001466). **B.** *In vivo* juxtacellular recordings of nicotine-evoked responses in IPN neurons of saline- and nicotine-treated animals. Top, representative electrophysiological recording of an IPN neuron, during an i.v. injection of nicotine (30 µg/kg). Bottom, average time course and average amplitude of the change in firing frequency from baseline after an i.v. injection of saline and nicotine (30µg/kg), for IPN neurons from saline- and nicotine-treated mice. Responses were decreased by the chronic exposure to nicotine (p = 0.035, Mann-Whitney). All neurons were confirmed to be within the IPN using juxtacellular labeling with neurobiotin (NB). **C.** Top, modified two-bottle choice protocol used

to evaluate the impact of a long-term exposure to nicotine on nicotine intake. Mice were implanted subcutaneously with a minipump that delivered 10 mg/kg/d of nicotine continuously 20 days before performing the modified two-bottle choice task. After 4 days of water vs. water habituation, mice were directly exposed to a high concentration of nicotine (100 µg/ml). Bottom, nicotine preference and consumption at 0 and 100 µg/ml of nicotine, for mice under a chronic treatment of nicotine or saline. The saline group displayed a higher avoidance-like behavior (n=23, from 47,27+/-2.01% to 23.05+/-3.43%, p-value=1.669e-05, Mann-Whitney paired test) than the nicotine group (n=25, from 48.94+/-2.45 to 41.21+/-5.46%, p-value=0.16, Mann-Whitney paired test), leading to lower nicotine consumption (p-value=0.004309 and 0.003485, Mann-Whitney in nicotine condition for nicotine intake and nicotine preference). **D.** Pseudo-ternary diagrams representing each saline- and nicotine-treated mouse for its side success rate over its nicotine success rate. Small dots correspond to the habituation period (water vs. water) while bigger dots correspond to the condition with 100 µg/ml of nicotine in one bottle. Inserts: pie charts illustrating the proportion of avoiders (light grey) and consumers (dark grey) for each condition. **E.** Average distance from each apex in the water vs. water (top) and water vs. nicotine 100 µg/ml conditions (bottom). Saline-treated mice developed a strategy to avoid nicotine, but not nicotine-treated mice ($p\text{-value}_{Sacc}$=0.012927, $p\text{-value}_{Side}$=0.267800 $p\text{-value}_{Nic}$=0.012927, Mann-Whitney test with Holm-Bonferroni correction). In all figure panels nicotine-treated animals are displayed in red and saline-treated (control) animals in grey.

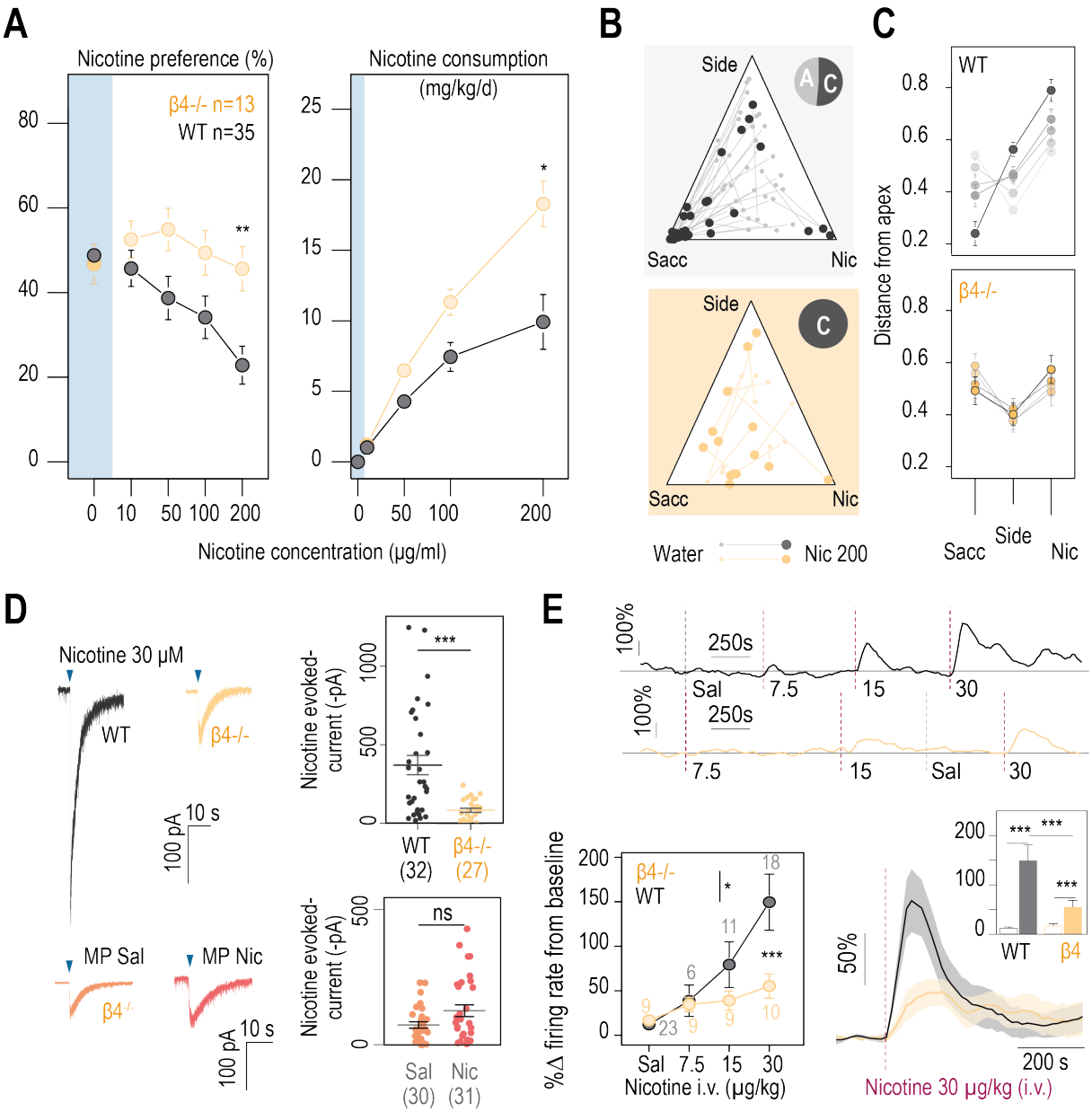

FIGURE 4

Figure 4: β4-containing nicotinic receptors are essential for triggering nicotine avoidance-like behavior in mice. **A.** Left, average nicotine preference (%) in WT and β4-/- mice for each dose of nicotine in the two-bottle choice task. WT mice decreased their nicotine preference (Friedman test, n=35, df=4, p<0.001 and Mann-Whitney post-hoc test with Holm-Bonferroni correction) while $\beta4^{-/-}$ mice displayed a stable preference throughout the task (Friedman test, n=13, df=4, p-value=0.1141). WT mice avoided the nicotine-containing bottle more than $\beta4^{-/-}$ mice (Mann-Whitney test with Holm-Bonferroni correction). Right, average nicotine consumption (mg/kg/d) in $\beta4^{-/-}$ and WT mice as a function of the concentration of nicotine in the bottle (Friedman test, n=35, df=3, p<0.001 and Mann-Whitney post-hoc test with Holm-Bonferroni correction). $\beta4^{-/-}$ mice consumed more nicotine than WT mice (Mann-Whitney test). **B.** Ternary diagram representing each WT and $\beta4^{-/-}$ individual for its side success rate over its nicotine success rate. Small dots correspond to the habituation period (water vs. water) while bigger dots

correspond to the condition with 200 µg/ml of nicotine in one bottle. Inserts: pie charts illustrating the proportion of avoiders (light grey) and consumers (dark grey) for each genotype at the end of the task. Note the absence of avoiders in β4$^{-/-}$ mice. **C.** Average distance from each apex during the two-bottle choice task (0, 10, 50, 100 and 200 µg/ml of nicotine). **D.** Left, representative currents following a puff application of nicotine (30 µM, 200 ms) on IPR/IPDL neurons from naïve WT and β4$^{-/-}$ mice, or from saline-treated (orange) and nicotine-treated (dark orange) β4$^{-/-}$ mice. Right, average nicotine-evoked currents recorded in IPR/IPDL neurons from naïve WT (n=32, -370.59+/-61.21 pA) and β4$^{-/-}$ (n=27, -83.34 +/- 13.12 pA) mice, and from β4$^{-/-}$ chronically treated with either saline (Sal, n=30, -71.89 +/- 11.54 pA) or nicotine (Nic, n=31, -122.96 +/- 21.25 pA). β4$^{-/-}$ mice presented a large decrease in nicotine-evoked currents (Mann-Whitney, p-value=4.113e-05). Nicotine treatment did not alter nicotine-evoked currents in IPR/IPDL neurons of β4$^{-/-}$ mice (Mann-Whitney, p-value=0.1521). **E.** Juxtacellular recordings nicotine-evoked responses in IPN neurons in naïve WT and β4$^{-/-}$ mice. Top, representative example of the variation in firing frequency of an IPN neuron, following repeated i.v. injections of nicotine at 7.5, 15 and 30 µg/kg, in WT and β4$^{-/-}$ mice. Bottom left, dose-dependent change in firing rate from baseline following i.v. injections of nicotine ($p < 0.05$). All recorded neurons were neurobiotin-labelled to confirm their localization within the IPN. Bottom right, average nicotine-evoked responses at 30 µg/kg of nicotine in IPN neurons from WT and β4$^{-/-}$ mice. Insert, average amplitude of the change in firing frequency from baseline after an i.v. injection of saline and nicotine (30µg/kg), for IPN neurons from WT and β4$^{-/-}$ mice. Responses were lower in β4$^{-/-}$ than in WT mice ($p < 0.001$, Mann Whitney). In all figure panels WT animals are depicted in grey and β4$^{-/-}$ mice in yellow. *** $p<0.001$, ** $p<0.01$, * $p<0.05$.

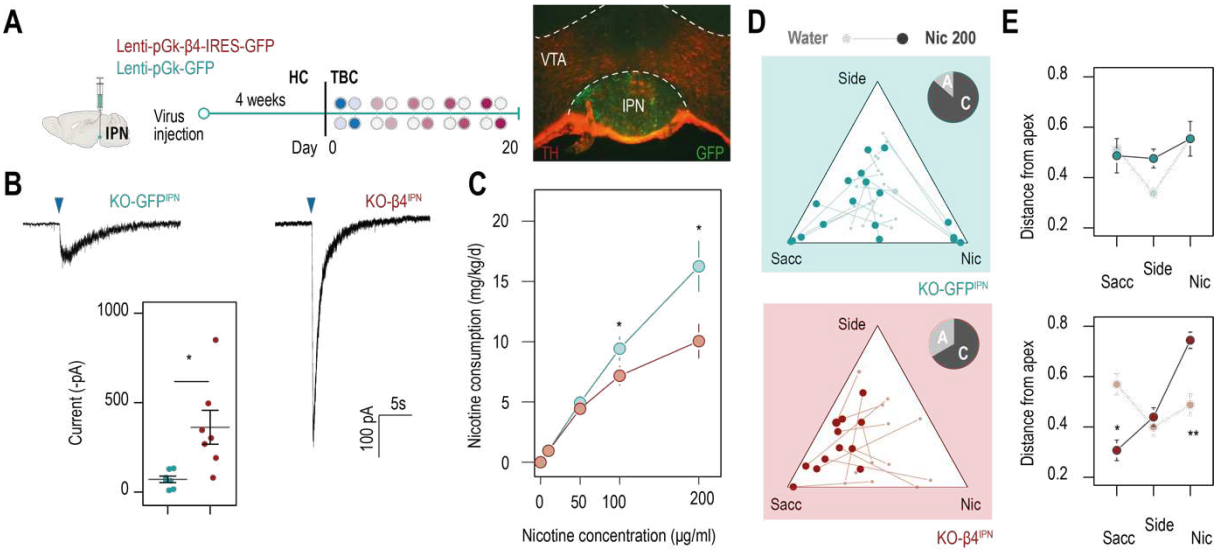

FIGURE 5

Figure 5: β4-containing nAChRs of the IPN are involved in the control of nicotine consumption and in spontaneous nicotine avoidance-like behavior in mice. **A.** Protocol: stereotaxic transduction of the β4 subunit together with GFP (or GFP alone in control mice) in the IPN of β4$^{-/-}$ mice, and subsequent two-bottle choice task. Right: coronal section highlighting proper viral transduction of lenti-pGK-β4-IRES-GFP in the IPN. **B.** Validation of the re-expression using patch-clamp electrophysiology recordings. Representative currents and average responses following a puff application of nicotine (30 µM, 200 ms)

on IPR/IPDL neurons from $\beta4^{-/-}$ mice transduced in the IPN with either lenti-pGK-β4-IRES-GFP (KO-$\beta4^{IPN}$, n=7, -361.97 +/- 94.85 pA) or pGK-GFP (KO-GFP^{IPN}, n=7, -70.65+/-18.30 pA; Mann-Whitney, p-value=0.004079). **C.** Average nicotine consumption was lower in KO-$\beta4^{IPN}$ than in KO-GFP^{IPN} (Mann-Whitney test and Bonferroni-Holm correction). **D.** Ternary diagram representing each $\beta4^{-/-}$ mouse, transduced with either β4 or GFP, and illustrating their side success rate over their nicotine success rate. Small dots correspond to the habituation period (water vs. water) while bigger dots correspond to the condition with 200 µg/ml of nicotine in one bottle. Inserts: pie charts illustrating the proportion of avoiders (light grey) and consumers (dark grey) for each condition at the end of the task. **E.** Average distance from each apex during the two-bottle choice task (0, 10, 50, 100 and 200 µg/ml of nicotine). for KO-$\beta4^{IPN}$ and KO-GFP^{IPN} mice. In all figure panels KO-$\beta4^{IPN}$ mice are depicted in red and KO-GFP^{IPN} (control) mice in green. *** $p<0.001$, ** $p<0.01$, * $p<0.05$.

Supplementary Material

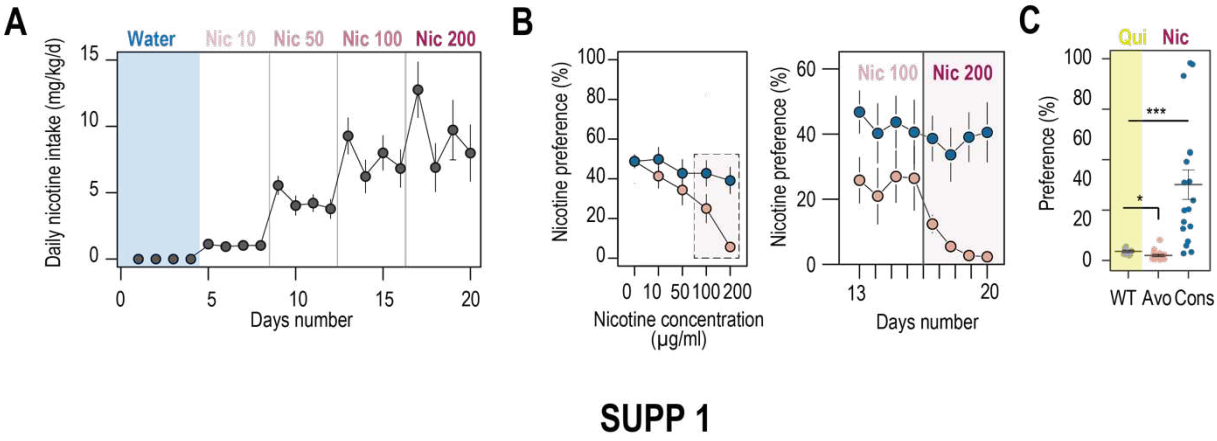

Figure S1: A. Nicotine intake measure every day (mg/kg/d) for WT mice in the two-bottle choice task (n=35). **B.** Average nicotine preference (%) for avoider and consumer mice for each dose of nicotine throughout the task (left) and for the last 8 days (right). **C.** Quinine preference in WT animals, compared to nicotine preference in avoider and consumer mice. *** p<0.001, ** p<0.01, * p<0.05.

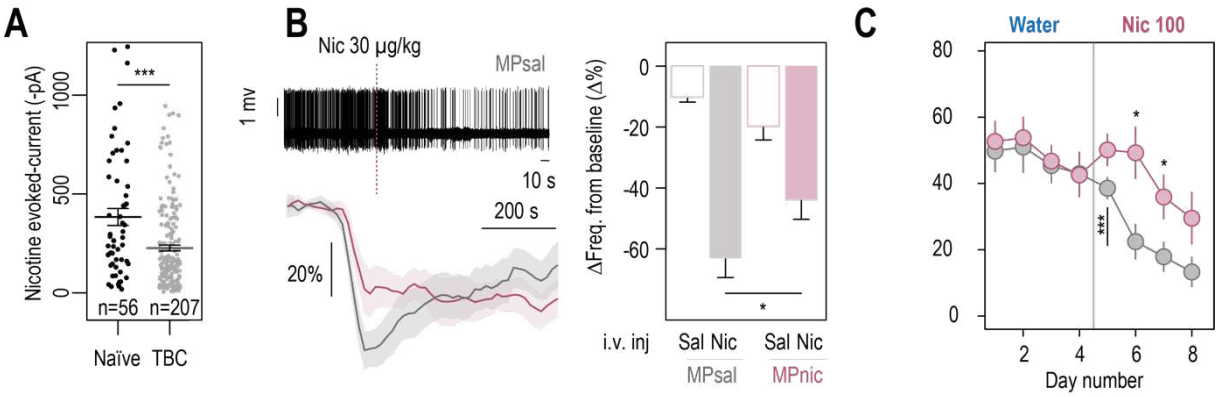

SUPP 2

Figure S2: A. Currents recorded in voltage-clamp mode (-60 mV) from IPR/IPDL neurons of naïve mice kept in their home-cage (black, n=64, -383.60 +/- 42.89 pA) and of mice that underwent the two-bottle choice task (TBC, grey, n=207, -226.98 +/- 14.64 pA) following a puff application of nicotine (30 µM, 200 ms). Nicotinic currents in TBC mice were of smaller amplitude than those from naïve mice (Mann-Whitney, p-value=0.0002367). **B.** In vivo juxtacellular recordings of nicotine-evoked responses in nicotine-inhibited IPN neurons of saline- and nicotine-treated animals. Top left, representative electrophysiological recording of an IPN neuron, during an i.v. injection of nicotine (30 µg/kg). Bottom left, average time course and amplitude of the change in firing frequency from baseline after an i.v. injection of saline and nicotine (30µg/kg), for IPN neurons of saline- and nicotine-treated mice. Right, responses were on average lower after chronic exposure to nicotine ($p<0.05$). **C.** Daily nicotine preference (%) for saline- and nicotine-treated mice, for each day in the two-bottle choice task. In saline-treated mice, avoidance to nicotine appears from the second nicotine exposition day. *** $p<0.001$, ** $p<0.01$, * $p<0.05$.

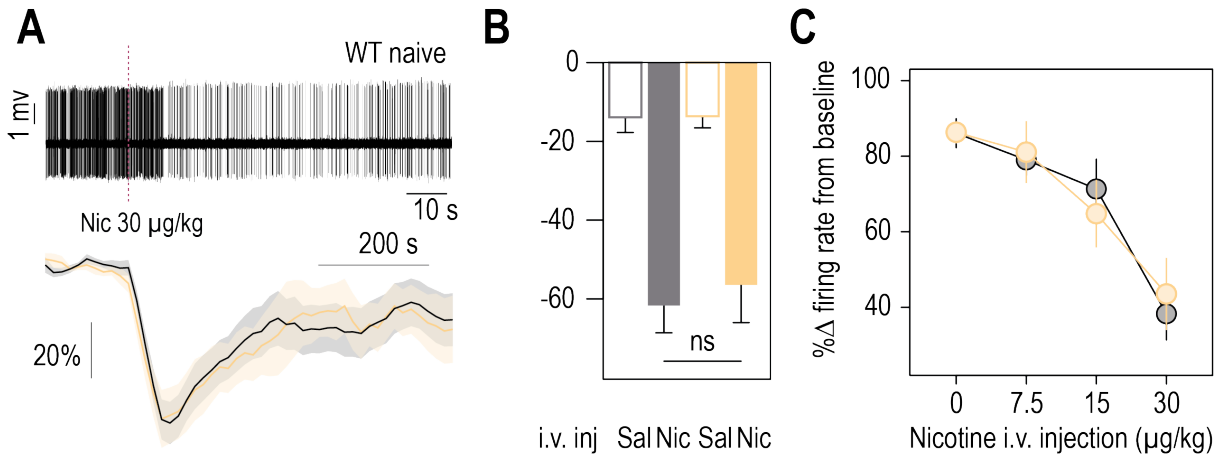

SUPP 3

Figure S3: In vivo juxtacellular recordings of nicotine-evoked responses in nicotine-inhibited IPN neurons of WT and $\beta4^{-/-}$ animals. **A.** Top, representative electrophysiological recording of an IPN neuron, during an i.v. injection of nicotine (30 µg/kg). Bottom, average time course and amplitude of the change in firing frequency from baseline after an i.v. injection of saline and nicotine (30µg/kg), for WT (black) and $\beta4^{-/-}$ animals (yellow). **B.** Average amplitude of the change in firing frequency from baseline after an i.v. injection of saline and nicotine (30µg/kg). **C.** Dose-dependent change in firing rate from baseline following i.v. injections of nicotine at 7.5, 15 and 30 mg/kg. *** p<0.001, ** p<0.01, * p<0.05.

Discussion

8. Discussion générale

L'addiction à la nicotine est une maladie psychiatrique qui résulte du détournement par la nicotine de divers circuits neuronaux. L'utilisation uniquement récréative de produits tabagiques est rare et la majorité des individus qui consomment occasionnellement de la nicotine vont tomber dans le cercle vicieux de l'addiction. La prise répétée de nicotine va modifier les niveaux d'expression des nAChR et les poids synaptiques au sein de divers circuits. Sachant qu'il existe une grande variété de nAChRs avec des cinétiques d'activation et de désensibilisation différentes, ainsi que des distributions tissulaires distinctives, une des questions qui m'a intéressée pendant ma thèse était de savoir quels sous-types de nAChR et quels circuits spécifiques participent aux différentes étapes menant à une consommation régulière et pathologique.

Trois éléments déterminants contribueraient à la transition d'une consommation occasionnelle à une consommation régulière, voire compulsive, de nicotine. Premièrement, les effets du renforcement positif dès l'administration de nicotine sont considérés comme étant d'une importance capitale non seulement dans l'initiation mais aussi dans le maintien du tabagisme. Deuxièmement, le manque causé par un sevrage tabagique serait un facteur motivationnel contribuant à la persistance de la consommation et à la rechute. Enfin, l'effet aversif immédiat induit par l'action directe de la nicotine est considéré comme déterminant pour éviter le contact avec la drogue, mais sa contribution dans le contrôle de la consommation est moins claire. Ce qui m'a intéressée au cours de cette thèse était de comprendre la contribution des effets positifs et négatifs dans l'initiation et le maintien de la dépendance à la nicotine, mais aussi de caractériser l'implication de récepteurs et de circuits spécifiques dans ces mécanismes.

8.1 Le rôle des récepteurs nicotiniques β2* de la VTA

Les modèles génétiques et les agents pharmacologiques ont permis de décrire en détails les processus neuronaux qui sous-tendent le renforcement à la nicotine. Mais ces outils présentent également des limites, soit de résolution temporelle et de compensation développementale pour la génétique, soit d'un manque de spécificité moléculaire et cellulaire pour les composés pharmacologiques.

L'utilisation de la souris $\beta2^{-/-}$ a permis de mettre en évidence le rôle crucial des nAChR β2* de la VTA dans la réponse à la nicotine des neurones DA et dans le renforcement à cette drogue (Mameli-Engvall et al., 2006; Maskos et al., 2005; Tolu et al., 2013). Notamment, il a été montré que la réponse en *burst* des neurones DA nécessite la présence simultanée des récepteurs nicotiniques β2* dans les neurones DA et GABAergiques de la VTA (Tolu et al., 2013). De plus, cette réponse en bouffée de potentiels d'actions est nécessaire pour le renforcement à la nicotine.

Nous avons utilisé la stratégie de pharmacologie optogénétique qui permet de contrôler, de manière aiguë et avec la lumière, l'activité du récepteur nicotinique β2*, mimant ainsi un « *knock-out* » local et réversible. Afin d'utiliser les β2LinAChR dans la VTA, nous

avons réalisé des injections stéréotaxiques d'un lentivirus qui permet d'exprimer la sous-unité β2 mutée (β2E61C) chez des souris de type sauvage sous le contrôle d'un promoteur fort et ubiquitaire. Nous avons montré que β2E61C est capable de s'associer avec les sous-unités nicotiniques endogènes (e.g. α4) pour former un récepteur fonctionnel et photocontrôlable. De manière importante, les réponses à la nicotine observées *ex-* et *in-vivo* chez les souris qui surexpriment β2E61C sont identiques (dans le noir) aux réponses chez des souris contrôle, ce qui suggère que l'expression des nAChR est soumise à une régulation importante, probablement limitée par les niveaux d'expression endogène de la sous-unité α4. Deux aspects importants du contrôle de l'activité des neurones dopaminergiques ont émergé de ces expériences : la modulation endogène et la réponse à la nicotine.

La modulation cholinergique endogène :

L'optopharmacologie permet un blocage réversible et rapide des récepteurs nicotiniques. L'utilisation de cette technique a donc permis de poser la question du tonus cholinergique et de son action sur les neurones DA. Nous avons enregistré *in vivo* chez l'animal anesthésié l'activité basale des neurones DA, tout en interrompant brièvement la neurotransmission nicotinique, en antagonisant les nAChR β2 de la VTA avec la lumière (e.g alternance de lumières verte et violette toutes les 5 secondes). Considérant que les nAChR sont des récepteurs cationiques excitateurs (Changeux, 2010a), nous avons observé de manière attendue une réduction de l'activité régulière et en *burst* chez une majorité de neurones DA, lorsque les récepteurs sont photo-antagonisés (**Fig 8.1**). Ces résultats ont permis de mettre en évidence, chez l'animal anesthésié, un tonus cholinergique au sein de la VTA qui participe à l'activité régulière et en bouffée des neurones DA.

De manière inattendue, nous avons observé que les changements d'activité électrique les plus intenses ont lieu lors de la transition de la lumière verte à violette, c'est à dire lors de la dissociation de l'antagoniste. Le fait d'inhiber les récepteurs en positionnant l'antagoniste dans le site ACh (sous lumière verte) n'a en fait que très peu d'effet sur l'activité spontanée (**Fig 8.1**). Une de nos hypothèses serait que, en condition normale, le tonus cholinergique induirait une désensibilisation partielle des nAChR, et que sous lumière violette le photoswitch protégerait les récepteurs de cette désensibilisation, en se liant aux sites ACh et en maintenant les récepteurs sous l'état de repos (**Fig 8.1**). Lors du passage de violet à vert, l'isomérisation du photoswitch permettrait alors de libérer de manière synchrone les sites ACh, ce qui conduirait à l'activation d'un fort *pool* de nAChRs par l'ACh endogène. Ceci se traduirait donc par un rebond d'activité électrique. Pour confirmer cette hypothèse, il faudrait dans un premier temps vérifier, en système hétérologue, que le photoswitch sous forme *cis*, en antagonisant les récepteurs de manière compétitive, est en effet capable de maintenir les récepteurs dans un état de repos et de les protéger de la désensibilisation. Les expériences que nous avons réalisées dans ce sens n'ont malheureusement pas abouti, notamment car l'expression des nAChR en cellules Neuro2A est délicate (données non publiées). Il serait néanmoins intéressant de continuer dans cette voie, afin d'apporter une démonstration fonctionnelle de la désensibilisation des nAChRs par l'ACh *in vivo*.

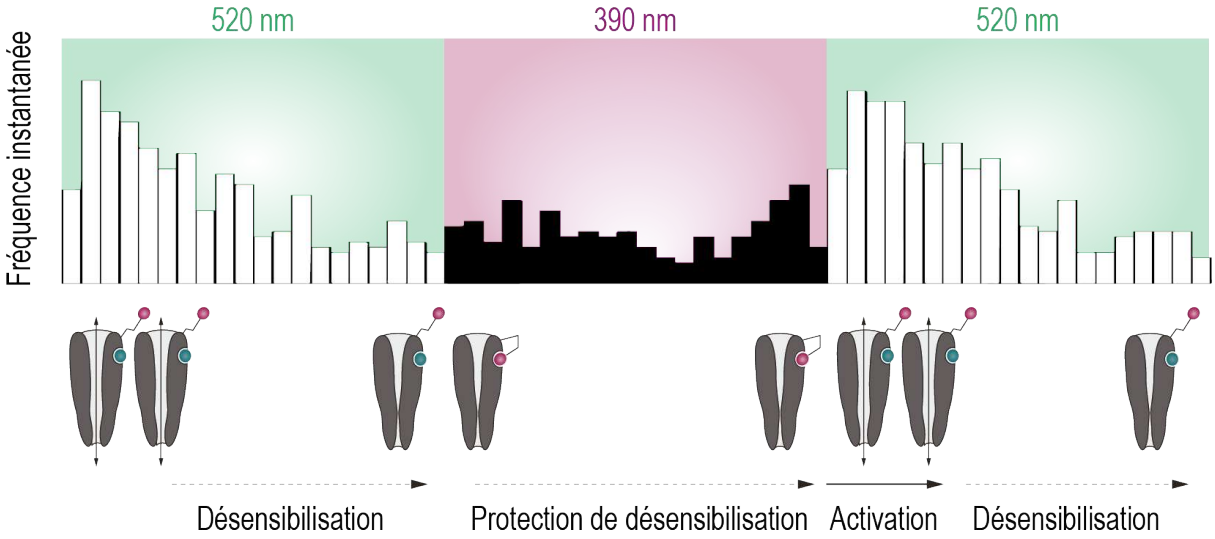

Figure 8.1 | Protection de la désensibilisation : Représentation de l'activité d'un neurone DA enregistré lors de la photorégulation des LinAChR (Haut). La photoinhibition des LinAChR permettraient de protéger les récepteurs de la désensibilisation (bas). La désinhibition rapide de toutes les LinAChR seraient à l'origine d'une synchronisation de l'activation des récepteurs laissant place à un pic d'activité des neurones DA.

Nous avons également observé une seconde population de neurones, minoritaire, qui répond par une augmentation de fréquence instantanée lors de la photo-antagonisation des récepteurs nicotiniques. Ces résultats corroborent une étude précédente qui a montré que lors de l'activation optogénétique des neurones cholinergiques des noyaux du pont, certains neurones DA répondent par une diminution de leur taux de décharge (Dautan et al., 2016). De plus, il a été montré au laboratoire que la nicotine excite et inhibe deux populations de neurones DA distinctes (Eddine et al., 2015), qui projettent respectivement vers le NAcc et vers l'amygdale (Nguyen et al., 2020, **Annexes**). Plusieurs questions persistent : (1) Cette population de neurones excités sous lumière violette correspond-elle aux neurones DA qui sont inhibés par la nicotine ? (2) Quels sont les mécanismes moléculaires ou les connexions neuronales qui sous-tendent une augmentation de l'activité des neurones DA lors de la photo-inhibition des nAChR β2 de la VTA ? Il faut rappeler que, dans cette étude, nous avons exprimé les β2LinAChR de manière ubiquitaire dans la VTA, sur tous les types neuronaux. Il est donc possible que cette réponse observée résulte d'une inhibition locale induite par un antagonisme des β2LinAChR exprimés sur les interneurones GABAergiques. Afin de tester cette hypothèse, nous avons restreint l'expression du β2LinAChR dans les neurones DA grâce à l'utilisation de souris DAT-cre et d'un virus floxé. Les mêmes types de réponses ont été observées chez ces souris (**Fig 8.2**), ce qui suggère que cette inhibition n'a pas besoin des interneurones GABA. Si les mécanismes qui sous-tendent l'inhibition par l'ACh sont les mêmes que ceux qui induisent une inhibition par la nicotine, il se pourrait qu'ils reposent sur l'activation des auto-récepteurs D2. En effet, le laboratoire a montré (Eddine et al., 2015) que le blocage des récepteurs D2 par l'éticlopride abolit la réponse inhibés des neurones DA suite à une injection de nicotine. Par conséquent, l'inhibition pourrait résulter soit de l'activation des autorécepteurs D2 *via* une libération de DA somatodentritique locale, soit d'un effet réseau.

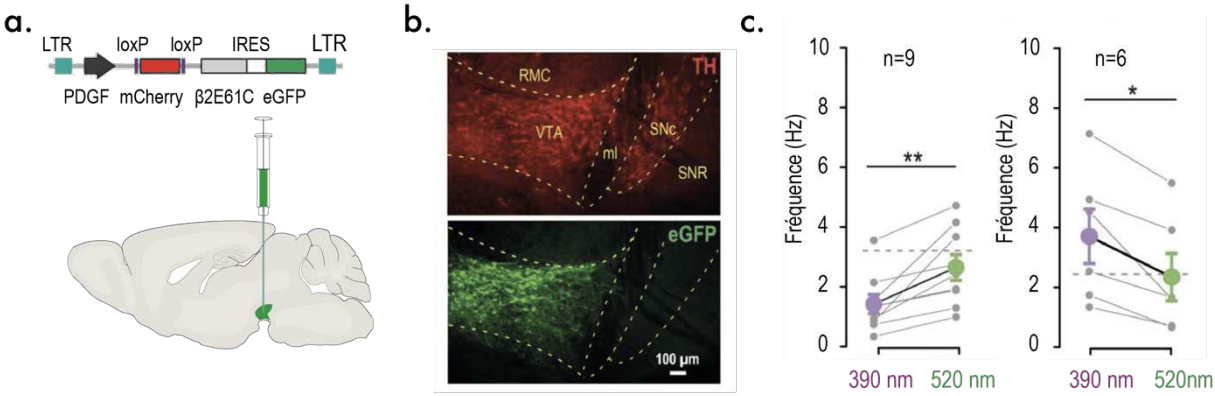

Figure 8.2 | Expression conditionnelle de β2E61C dans les neurones DA de la VTA : a. Construction permettant l'expression conditionnelle du mutant cystéine dans les neurones exprimant la cre-recombinase. La transfection lentivirale de cette construction chez les souris DATiCRE permet de restreindre l'expression aux neurones DA. **b.** Immunohistochimie de la TH (rouge) et de la eGFP (vert). **c.** Une population de neurones DA de la VTA voit son activité diminuer lors de la photo-inhibition des β2*LinAChR sous lumière violette (panel de gauche, n=9) alors qu'une autre population voit son activité augmenter (panel de droite, n=6).

L'action de la nicotine sur les neurones DA :

Grâce à des enregistrements électrophysiologiques *ex vivo* et *in vivo*, nous avons montré une diminution de 50-60 % des réponses à la nicotine en antagonisant les β2nAChR de la VTA avec la lumière. Cette diminution peut sembler faible, cependant notre approche a été réalisée chez des souris de type sauvage qui expriment de manière endogène la sous-unité β2 non mutée. L'incorporation de β2E61C dans les pentamères est probablement partielle avec une présence de récepteurs endogènes insensibles à la photo-régulation. Nous ne savons pas si l'occupation d'un seul site agoniste par le photoswitch (ou par un antagoniste de manière générale) est suffisante pour bloquer l'activation du récepteur. Il est néanmoins possible que ce soit le cas, étant donné que le récepteur a besoin de deux agonistes pour s'ouvrir de manière efficace (Auerbach, 2012). Ces éléments posent une limite à notre capacité à bloquer les récepteurs.

Malgré ce blocage incomplet, dans cette étude nous avons pu abolir le comportement de préférence de place à la nicotine en photo-antagonisant les nAChR β2* contenus dans la VTA, sans toucher aux récepteurs axonaux des neurones DA. Par rapport aux expériences de réexpression, les effets du blocage uniquement au niveau somatodendritique, permet de conclure (1) que les récepteurs β2* somatodendritiques de la VTA sont nécessaires pour la mise en place d'un renforcement à la nicotine, et (2) que l'action directe de la nicotine sur les terminaisons axonales de la VTA n'est pas suffisante pour pallier au blocage des récepteurs somatodendritiques et induire une préférence de place. De plus, dans ce paradigme, la photo-inhibition des récepteurs β2* est réalisée au cours du *pairing,* qui est l'étape au cours de laquelle on associe un contexte à l'effet appétitif de la nicotine, mais pas lors du jour du *test*, qui évalue la préférence de place. Cette approche nous permet de tester le rôle des nAChR à un instant spécifique des processus d'apprentissage par renforcement. Notamment, nous avons montré ici que c'est l'activation des nAChR β2* de la VTA au cours de l'apprentissage, et pas nécessairement lors du *recall,* qui est primordiale pour induire du renforcement à la nicotine.

Les nAChR sont exprimés sur différents types neuronaux et présentent une localisation cellulaire variable car ils peuvent être somato-dentritiques ou présynaptiques. La transduction virale permet de conférer une spécificité cellulaire au photo-contrôle, car elle permet de cibler un noyau neuronal (la VTA par exemple), voire de cibler un type de neurones (par exemple les neurones DA spécifiquement, chez les souris DAT-Cre). Le caractère optique de cette méthode permet également de manipuler les récepteurs des terminaisons axonales, sans impacter les récepteurs somatodendritiques, ou inversement. Néanmoins, cette technologie de pharmacologie optogénétique est contraignante, car elle nécessite d'apporter trois éléments au même endroit dans le cerveau : le gène, le photoswitch, et la lumière. Ces contraintes expliquent en partie pourquoi cette technologie n'a pas été largement adoptée par la communauté des neurosciences (Paoletti et al., 2019). Récemment, nous avons développé des souris *knock-in* β2E61C et β4E61C, où les gènes natifs sont remplacés par les mutants ponctuels. Chez ces souris, le remplacement de la sous-unité est total, ce qui devrait permettre d'éviter tout risque de surexpression, ou d'expression ectopique. De plus, ces souris devraient permettre de faciliter le photocontrôle, en s'affranchissant de l'étape de transduction virale par stéréotaxie. Cependant, ces souris ne permettront pas de restreindre l'expression du récepteur mutant dans une population de neurones donnés. L'expérimentateur devra donc juger, suivant le type d'expérience, quelle stratégie d'expression reste la plus judicieuse.

De l'effet aigu à l'addiction :

Les théories computationnelles du renforcement aux drogues d'abus reposent en partie sur le détournement de l'encodage de l'erreur de prédiction de récompense (RPE) (Keiflin and Janak, 2015; Redish, 2004, Fig 8.3a). Au fur et à mesure d'un apprentissage, l'activation phasique des neurones DA est normalement transférée du moment de l'obtention de la récompense au moment du prédicteur. L'activité au moment de la récompense, qui signe une évaluation instantanée de l'erreur de prédiction de récompense est normalement ramenée à zéro en fin d'apprentissage. Cette absence d'activité dopaminergique signifie que la valeur de la récompense attendue est correctement estimée. Dans le contexte de la prise de drogue, l'hypothèse serait que le pic phasique se décale effectivement au prédicteur, mais que l'obtention de la récompense (drogue) continue à déclencher une réponse dopaminergique positive (Fig 8.3a) qui reflèterait une sous-évaluation de la valeur attendue. En ajoutant donc une augmentation non compensable de la dopamine induite par la drogue à un modèle d'apprentissage, on construit un système qui sur-sélectionne les actions menant à la prise de drogue (Redish, 2004). Cette action directe, pharmacologique et non compensable des drogues sur le système dopaminergique permettrait donc de court-circuiter l'encodage normal de la valeur (Keiflin and Janak, 2015; Redish, 2004, Fig 8.3b).

L'enregistrement des neurones DA pendant une tâche d'auto-administration de nicotine n'a, à ma connaissance, pas été réalisé. Il serait néanmoins intéressant de comprendre quelle est la contribution des nAChR β2* dans le pic phasique prédictif de la récompense ou au moment son obtention. D'un point de vue de l'apprentissage par renforcement aux drogues d'abus, l'utilisation de β2 LinAChR permettrait de bloquer rapidement et de manière réversible les récepteurs au début de l'apprentissage ou après la

consolidation de celle-ci, ou encore à un moment précis de la tâche, par exemple pendant la prédiction ou à l'obtention de la récompense.

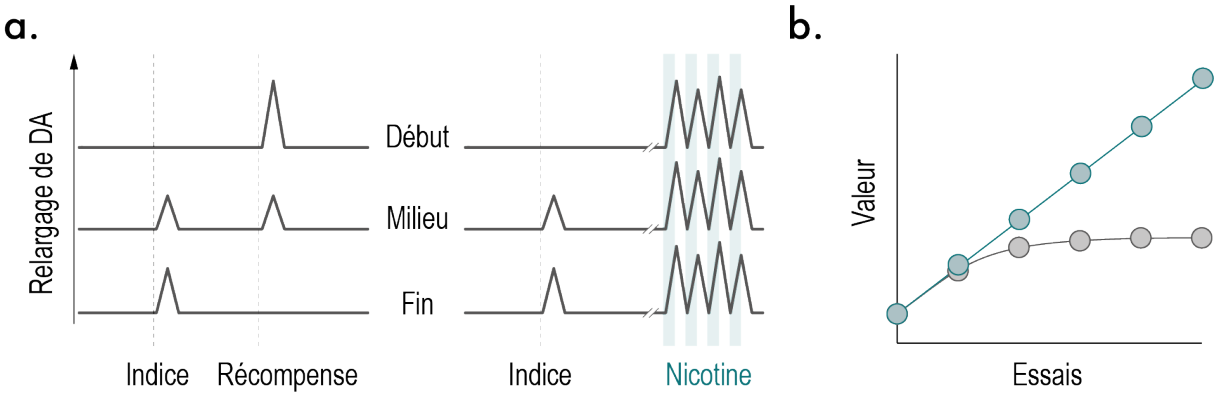

Figure 8.3 | Erreur de prédiction de récompense et nicotine : a. Représentation de la libération de dopamine dans le NAcc au cours d'un apprentissage conditionné, lors de l'obtention d'une récompense naturelle (gauche) et de nicotine (droite). **b.** Prédiction de l'évaluation de la valeur des récompenses aux cours des essais. *Figure adaptée de Keiflin and Janak, 2015*

Cette hypothèse n'est étayée que par peu de données, ne tient pas compte des effets des drogues sur les récepteurs qui désensibilisent rapidement, et ne considère pas les altérations à long terme des circuits. L'exposition à long terme de nicotine, qu'elle soit passive ou active lors de tâches d'auto-administration, induit une augmentation de l'activité spontanée des neurones DA de la VTA (Caille et al., 2009; Morel et al., 2018; Tolu et al., 2017). Nous avons montré au laboratoire que cet effet à long terme de la nicotine sur l'activité basale des neurones DA se traduit par une altération des prises de décision chez la souris (Dongelmans et al., en préparation). Notamment, les animaux sous nicotine chronique visitent plus souvent les points d'une arène associés à des fortes probabilités de récompense que ceux associés à de faibles probabilités de récompenses, c'est-à-dire qu'ils vont principalement exploiter les récompenses plutôt que d'explorer les endroits faiblement récompensés. De plus, la réponse à la nicotine des neurones DA de la VTA est diminuée suite à un traitement à long terme de nicotine (Morel et al., 2018; Nashmi et al., 2007). Ces effets peuvent s'expliquer par la désensibilisation des récepteurs α4β2* (Brody et al., 2006) et l'*upregulation* des nAChR α4* dans les interneurones GABAergiques de la VTA (Nashmi et al., 2007). Il est suggéré que cette diminution de réponse des neurones est à l'origine de l'apparition d'une tolérance, puisque pour activer de la même manière le système dopaminergique, il faudrait augmenter la prise de nicotine, notion indispensable à intégrer dans les hypothèses du court-circuitage de la RPE.

Sachant que l'activité basale des neurones DA est plus élevée lors d'une exposition à long terme de nicotine et qu'il y a la mise en place d'une tolérance, il est important de comprendre si ces altérations du système de récompense peuvent altérer la prise de décision des animaux lors de la consommation de drogue d'abus.

8.2 Aversion et régulation de la consommation de nicotine

La régulation de la consommation de nicotine repose sur la synergie de processus complexes qui incitent ou limitent la prise de nicotine. Pour étudier ces mécanismes, nous

avons utilisé une tâche de choix à deux biberons dont un seul contient de la nicotine. Cette tâche est idéale pour étudier les stratégies de consommation des animaux, puisqu'ils ont le choix de consommer activement ou d'éviter la drogue. Un autre avantage, par rapport à des tâches plus classiques d'auto-administration, est qu'elle est continue. Elle permet donc aux animaux de consommer à leur rythme, dans des conditions plus proches des rythmes de consommation d'un humain. La prise de nicotine sur une échelle de temps plus longue permet également d'étudier l'effet de la nicotine à long terme sur la régulation de l'expression des récepteurs nicotiniques.

Régulation de la consommation de nicotine :

La titration est souvent considérée comme un des moyens principaux de régulation de la consommation de nicotine. C'est-à-dire que les animaux développent des stratégies qui leur permettent de consommer une quantité quotidienne de nicotine constante, malgré un apport en nicotine par prise qui peut être variable (i.e. changement de concentrations). Lorsque nous analysons nos expériences de consommation sur la population de souris, nous arrivons à la même conclusion que la majorité des articles scientifiques, où en moyenne la consommation de nicotine repose sur une régulation titrée. Cependant, nous avons observé de larges différences interindividuelles, où peu d'animaux développent une véritable stratégie de titration. Environ la moitié des animaux développe une aversion à la nicotine, soit dès l'introduction de nicotine dans la tâche, soit au cours de la tâche, tandis que les autres animaux vont principalement augmenter de manière linéaire leur consommation de nicotine avec la dose.

Prendre en compte la variabilité interindividuelle est à notre sens un élément important dans l'analyse comportementale (Garcia-Rivas et al., 2017). Une telle variabilité de consommation de drogue d'abus a aussi été observée pour l'alcool (Juarez et al., 2017; Siciliano et al., 2019), la cocaïne (Pascoli et al., 2015) ou les amphétamines (Piazza et al., 1989). Dans ces études, les auteurs distinguent les groupes d'animaux soit en fonction de leur type de consommation (e.g. plus ou moins forte) (Juarez et al., 2017), soit à leur capacité à prendre compulsivement de la drogue malgré la distribution de punitions telles qu'un choc électrique (Pascoli et al., 2015; Siciliano et al., 2019). Dans notre étude, nous nous sommes intéressés à ce phénotype assez surprenant des souris qui développent une aversion à une certaine dose de nicotine dans le biberon, faible ou forte suivant les individus. Ces résultats montrent que : (1) la nicotine n'est pas aversive seulement aux fortes doses, (2) il existe un seuil de déclenchement de l'aversion qui est intrinsèque à chaque individus – et qui possiblement n'a pas été atteint chez les souris qui continuent de consommer – et (3) l'aversion est persistante dans le temps.

Ces résultats soulèvent une question primordiale : comment les animaux peuvent-ils arrêter spontanément de consommer de la nicotine, sachant la consommation devrait persister grâce au renforcement à la nicotine et à l'état de manque ? Dans cette tâche à deux biberons, il est possible que le renforcement à la nicotine soit faible ou peu efficace. Cependant, une partie des animaux présente une attraction forte pour le biberon à la nicotine, ce qui démontre que ces animaux sont capables de mettre en place un renforcement et un comportement orienté vers la nicotine. De plus, on observe aussi que certains animaux

semblent être indifférents et consomment passivement de la nicotine. Concernant l'état de manque, les symptômes se mettent en place en réponse à une altération de la neurotransmission de circuits neuronaux, et l'intensité de ces symptômes dépend de la durée de la dépendance à la nicotine (Hughes, 1992; Hughes et al., 1984; Kenny and Markou, 2001). Pour les animaux qui ont arrêté de consommer de la nicotine au début du paradigme, c'est-à-dire plutôt aux faibles doses de nicotine, l'exposition à la nicotine n'est certainement pas suffisante pour induire une altération des circuits neuronaux impliqués dans l'état de manque. Pour les animaux qui ont arrêté de consommer de la nicotine à la plus forte dose, ils ont été exposés pendant 12 jours à la nicotine. Chez les rongeurs, deux semaines de traitement à la nicotine devraient être suffisantes pour induire des symptômes de manque (Damaj et al., 2003; Hilario et al., 2012; Matta et al., 2007; Salas, 2004; Skjei and Markou, 2003). Il est donc possible que dans notre paradigme les symptômes de manque ne permettent pas de contrebalancer les effets aversifs de la nicotine.

Nous avons observé que les effets précédemment décrits dépendent des récepteurs nicotiniques β4*. En effet, aucune des souris $\beta4^{-/-}$ ne développe d'évitement actif à la nicotine, et les réponses à la nicotine sont drastiquement réduites dans l'IPN de ces souris. Le phénotype des souris $\beta4^{-/-}$ est proche de celui des souris qui consomment de manière abusive de la nicotine. La réexpression dans l'IPN de la sous-unité β4 est suffisante pour rétablir les déficits de réponse à la nicotine et comportementaux. Ces résultats mettent en évidence le rôle de des β4*nAChR de l'IPN dans le déclenchement de l'aversion.

Réponse aiguë de l'IPN à la nicotine :

Ces résultats nous ont amenés à étudier la transmission nicotinique de l'IPN car (1) la voie habénulo-interpédonculaire semble être au cœur de l'aversion à la nicotine, et (2) le noyau interpédonculaire est la porte de sortie de cette voie.

Que cela soit en électrophysiologie *ex vivo* ou *in vivo,* les neurones de l'IPN présentent des réponses à la nicotine très variables. Ces résultats sont cohérents avec le fait que les neurones de l'IPN sont hétérogènes dans leurs propriétés physiologiques (DeGroot et al., 2020; Zhao-Shea et al., 2015), leurs réponses à la nicotine (Arvin et al., 2019; Hsu et al., 2013; Shih et al., 2014), et ont des afférences et efférences variées (Antolin-Fontes et al., 2015). Dans notre étude, nous avons enregistré les neurones de l'IPN sans les distinguer en fonction de leur type neuronale (GABA, SST, PV…) ou leur site de projection. Il serait donc intéressant de connaître l'identité de ces neurones, pour mieux comprendre l'impact fonctionnel de l'activation de ces différents types cellulaires. Une étude récente, grâce à l'utilisation de souris rapportrices, a permis de montrer que les neurones SST, PV et glutamatergiques ont des courants nicotiniques faibles, tandis les neurones GAD2+ présentent toujours une variabilité dans la réponse à la nicotine (Arvin et al., 2019). J'ai aussi réalisé cette caractérisation sur les neurones SST+ en utilisant une souris SST-cre et j'ai observé les mêmes résultats. Plus récemment, nous avons commencé à m'intéresser aux neurones de l'IPN en fonction de leur projection. Nous avons réalisé des injections de marqueurs rétrogrades (rétrobilles de latex) dans les structures cibles telles que le raphé et le LDTg. Les résultats préliminaires obtenus ne permettent malheureusement pas de conclure

quant à l'identité des neurones à forte densité de nAChR β4*, ni à l'implication d'un circuit spécifique.

Il est communément admis dans la littérature que de faibles doses de nicotine ne permettraient pas d'activer la voie habénulo-interpédonculaire (Fowler et al., 2011), de par son expression en récepteurs de basse affinité pour la nicotine (i.e. nAChR β4*, associé ou non à α5) (Beiranvand et al., 2014; Shih et al., 2014). Cependant, à notre connaissance aucune étude n'avait caractérisé la réponse à la nicotine de ces neurones chez la souris *in vivo*. Nous avons pu montrer grâce à nos enregistrements en juxtacelullaire que les neurones de l'IPN répondent de manière significative à des doses faibles de nicotine (7,5 µg/kg), qui sont par ailleurs insuffisantes pour induire une activation des neurones dopaminergiques (Eddine et al., 2015). Cela pourrait expliquer pourquoi la première expérience de consommation de cigarettes peut être négative (DiFranza et al., 2004; Pomerleau et al., 1993; Riedel et al., 2003; Sartor et al., 2010).

Enfin, les enregistrements en juxtacellulaire montrent qu'il existe une population de neurones activés et une population de neurones inhibés à la nicotine. De manière intéressante, nous avons observé que l'absence de nAChR β4* impacte principalement la population des neurones activés, celle-ci répondant par une augmentation d'amplitude beaucoup plus faible chez les $\beta4^{-/-}$ que chez les WT. La réponse des neurones inhibés n'est pas changée. Ceci suggère que les nAChR β4* jouent un rôle spécifique dans l'activation des neurones de l'IPN, et donc que les neurones activés de l'IPN pourraient être les neurones qui contribuent à l'émergence d'une aversion à la nicotine.

Tolérance à l'aversion, circuits neuronaux et homéostasie :

Nous avons observé que les souris qui développent de l'aversion à la nicotine présentent des courants nicotiniques plus forts dans l'IPN que celles qui consomment régulièrement. Nous ne savons pas si ces différences au niveau de l'IPN préexistent chez les animaux, ou si elles sont induites par la consommation de nicotine. Cependant, nous avons constaté qu'un traitement à long terme de nicotine induit une diminution de ces courants, et en retour une diminution de l'évitement du biberon qui contient de la nicotine. Nous proposons donc que la consommation de nicotine diminue progressivement la sensibilité à la nicotine dans l'IPN, et permet d'élever le seuil de déclenchement d'une aversion. Cette hypothèse va dans le sens du développement d'une tolérance, et permet d'expliquer pourquoi certains individus continuent de consommer de la nicotine même à forte dose. L'aversion se déclencherait lorsqu'une dose seuil serait franchie et correspondrait à une activation suffisante des neurones de l'IPN. Une fois cette dose seuil franchie, l'aversion déclenchée semble persistante. Des expériences complémentaires sont néanmoins nécessaires pour étudier la stabilité dans le temps de cet effet. J'ai notamment réalisé des enregistrements des courants nicotiniques suite à un sevrage de 24h, et observé que l'amplitude des courants nicotiniques était restaurée à un niveau comparable aux souris naïves (**Fig8.4**). Le retour à un niveau normal de la transmission nicotinique permettrait donc de re-sensibiliser l'IPN et rétablir une réponse aversive efficace. L'apprentissage du stimulus aversif devrait néanmoins reposer sur des changements de poids synaptiques au sein de circuits spécifiques de l'IPN ou d'autres circuits.

Au laboratoire, nous avons montré que la nicotine produit simultanément une activation les neurones DA qui projettent vers le NAcc (Nguyen et al., 2020, **Annexe**) pour induire le renforcement à la nicotine (Tolu et al., 2013), et une inhibition des neurones DA qui projettent vers l'amygdale pour augmenter le niveau d'anxiété des souris (Nguyen et al., 2020, **Annexe**). Sachant que les circuits de l'amygdale jouent un rôle primordial dans la mémoire émotionnelle (Tovote et al., 2015), il est possible que l'activation conjointe des voies habénulo-interpédonculaire et VTA-Amygdale jouent un rôle à la fois dans l'initiation des effets aversifs, et dans la consolidation de cette mémoire aversive.

Nous avons observé qu'un traitement chronique à la nicotine réduisait drastiquement l'amplitude des courants nicotiniques dans l'IPN. Une telle *downregulation* ressemble à une régulation homéostatique de l'expression des nAChR, puisque la plasticité homéostatique permet de limiter une neurotransmission lorsque celle-ci est trop sollicitée. Deux questions persistent : la *dowregulation* touche-t-elle tous les nAChR, et quels sont les mécanismes qui permettent de limiter le nombre de nAChR fonctionnels dans l'IPN ?

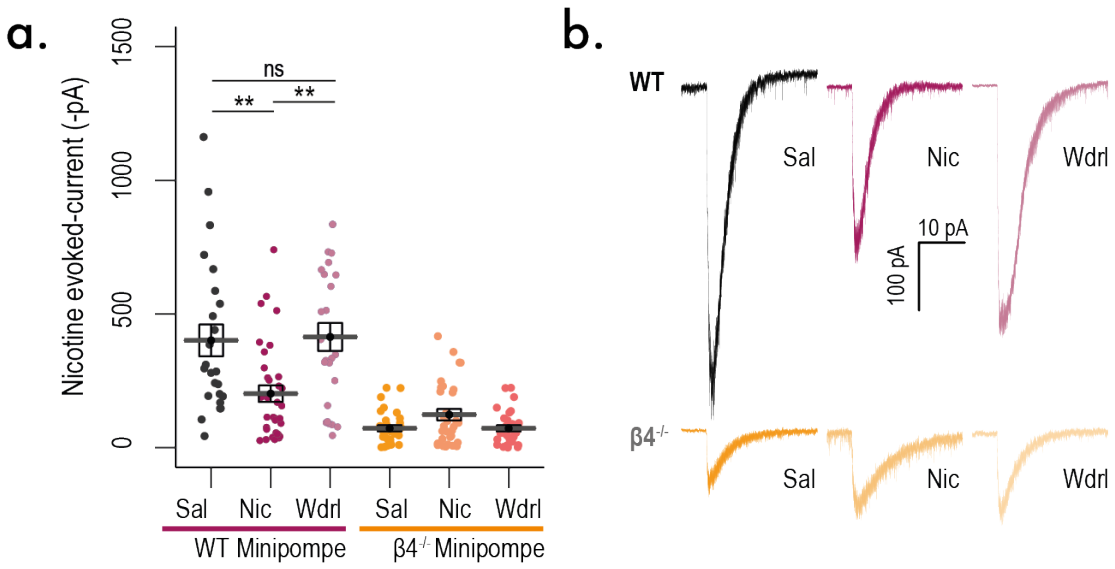

Figure 8.4 | Effet d'une exposition à long terme de nicotine et du sevrage sur les courants nicotiniques de l'IPN : a. Moyenne des courants évoqués par la nicotine (200 ms puff, 30 µM) chez des souris de type sauvage (WT) ou invalidées pour la sous-unité β4. Les enregistrements sont réalisés chez des souris qui ont reçu un traitement à la nicotine (10 mg/kg/j, minipompe osmotique) ou de saline pendant 4 semaines, ou 24h après un sevrage (Wdrl). **b.** Courants nicotiniques représentatifs enregistrés dans chaque condition.

Nous avons observé chez les souris $\beta4^{-/-}$ que ni l'exposition chronique à la nicotine, ni le sevrage n'altèrent les courants nicotiniques de l'IPN. Ces résultats suggèrent que le traitement à long terme de nicotine dans l'IPN n'altère pas l'expression des autres nAChR de l'IPN (principalement β2*), mais diminue le nombre de β4*nAChR fonctionnels de l'IPN pendant l'exposition à long terme de nicotine, et le ré-augmente après un sevrage (**Fig 8.4**). Il existe trois mécanismes possibles qui permettraient d'expliquer cette *downregulation* : une désensibilisation induite par une exposition à long terme de nicotine (Lester et al., 2009), une internalisation avec une réduction du *turnover,* ou une diminution de la synthèse/expression

des β4*nAChR. Afin d'évaluer ces différentes possibilités, quelques expériences s'offrent à nous. Notamment, nous pourrions réaliser une étude quantitative du nombre de transcrits (ARNm) couplée à des marquages radioligands. Si, la quantité de β4*nAChR est inchangée, il faudrait réaliser une étude complémentaire pour savoir si l'exposition à long terme induit une désensibilisation ou une internalisation des nAChR.

Afin de sonder les variations de densité de nAChR β4 fonctionnels à la surface des neurones, avons imaginé une approche innovante, qui repose sur l'utilisation de souris *knock-in* β4 E61C que nous avons récemment développées. La stratégie, que nous avons nommée CRAP, pour *current recovery after photoswitching*, pourrait permettre d'évaluer les dynamiques de turnover des récepteurs (**Fig 8.5**). Son nom est inspiré du FRAP (*fluorescence recovery after photobleaching*) qui permet d'évaluer les cinétiques de diffusion moléculaire après photoblanchiment du fluorophore. Le principe serait d'injecter le photoswitch localement dans l'IPN chez la souris *in vivo*, et de préparer des tranches de cerveau à différents temps après l'injection. Le pourcentage de photo-régulation nous servira de mesure directe du nombre de récepteurs β4 exprimés à la membrane. Par conséquent, si les β4* nAChR sont bel et bien désensibilisés par la nicotine chronique, le photoswitch pourra se fixer sur le récepteur mutant β4E61C. Si en revanche les nAChR sont internalisés, le ligand ne pourra pas se fixer sur les β4*nAChR, car le marquage maléimide-thiol marche uniquement en surface des cellules (Paoletti et al., 2019). Ainsi, une photo-régulation des courants nicotiniques supérieure à la souris contrôle (sans sevrage) indiquerait que les récepteurs sont présents à la membrane et probablement désensibilisés. Au contraire, en cas d'un pourcentage de photorégulation plus faible que la condition contrôle, cela suggèrerait que le ligand photochromique attachable ne s'est pas lié covalemment aux récepteurs, laissant place à un mécanisme d'internalisation.

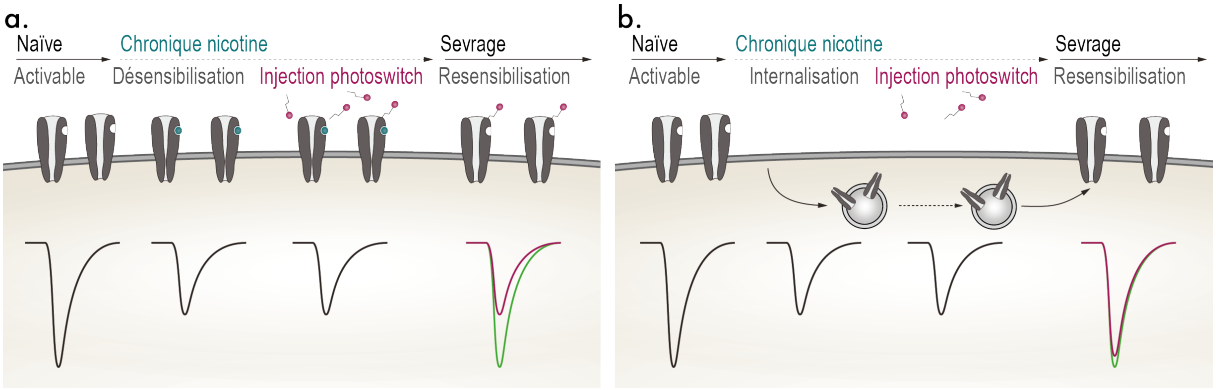

Figure 8.5 | CRAP – Current recovery after photoswitching : a. Condition attendue dans le cas où les récepteurs nicotiniques sont désensibilisés suivant un traitement à long terme de nicotine. La fixation covalente du *photoswitch* permettra d'évaluer le pourcentage de récepteurs désensibilisés. **b.** Condition attendue dans le cas où les récepteurs nicotiniques sont internalisés suite un traitement à long terme de nicotine. Une absence de photoswitching est attendue, puisque le photoswitch ne pourra pas se lier covalemment aux récepteurs internalisés.

8.3 Conclusion générale

Les effets subjectifs perçus chez les individus lors de la première expérience d'inhalation de nicotine peuvent être positifs ou négatifs (DiFranza et al., 2004; Pomerleau et al., 1993; Riedel et al., 2003; Sartor et al., 2010). Par ailleurs, cette sensibilité à la nicotine semble prédire la gravité de la dépendance : les personnes qui font l'expérience d'effets négatifs forts ne vont généralement pas répéter cette action, tandis que les individus qui ressentent des effets récompensants ont un risque plus élevé de devenir dépendants (DiFranza et al., 2004; Pomerleau et al., 1993; Riedel et al., 2003; Sartor et al., 2010). Néanmoins, pour les fumeurs réguliers qui ont reporté une expérience initiale désagréable, il est fortement supposé que les effets aversifs se sont effacés suite à la mise en place d'une tolérance (Pomerleau et al., 1993).

Les individus ne présentent pas tous la même vulnérabilité face aux addictions, et les récepteurs nicotiniques eux-mêmes participent à cette variabilité interindividuelle. Des polymorphismes nucléotidiques humains sur le cluster de gènes qui codent les sous-unités α5, β4 et α3 sont associés à une consommation excessive de nicotine (Bierut et al., 2008). Ces sous-unités ont un rôle dans la modulation des réponses de la voie dopaminergique (Harrington et al., 2016; Morel et al., 2014) et de la voie habénulo-interpédonculaire (Fowler et al., 2011; Frahm et al., 2011; Husson et al., 2020).

Au cours de cette thèse je me suis intéressée aux effets de la nicotine sur ces deux circuits, afin de comprendre le rôle des récepteurs et de leur état dans la mise en place de l'addiction. J'ai pris conscience pendant cette thèse de la difficulté à classer de manière stéréotypée les réponses neuronales ou comportementales. Cette variabilité est une composante importante de nos études, et elle demande à être prise en compte. Au niveau des populations de neurones, la variabilité des réponses est souvent ramenée à des différences anatomiques et fonctionnelles. La question est par exemple de savoir si les neurones de l'IPN qui sont excités ou inhibés par la nicotine font partie de réseaux distincts. Ce sont des questions qui ont également motivé notre travail sur les neurones DA de la VTA inhibés par la nicotine (Annexe). Au niveau comportemental, le raisonnement que nous faisons me parait différent. Il semble exister plusieurs stratégies de consommation : les individus peuvent titrer leur consommation, éviter le biberon de nicotine à une dose donnée, ou encore être motivés par la récompense associée à la nicotine et traquer le biberon correspondant. Toutes ces stratégies reposent sur des principes « primaires » d'approches et d'évitements, avec des effets à court terme et à long terme de la nicotine sur ces comportements. Ces stratégies ne sont certainement pas exclusives, c'est-à-dire qu'un individu peut adapter sa stratégie, ou en intégrer de nouvelles face à un environnement changeant.

Mettre en évidence ces différences, et quantifier le poids de chacun de ces effets me semble être une étape essentielle pour (1) mieux prédire la transition vers des comportements aberrants de consommation et (2) ouvrir sur une recherche des différences interindividuelles qui pourraient sous-tendre des vulnérabilités aux drogues.

Bibliographie

Bibliographie

Ables, J.L., Görlich, A., Antolin-Fontes, B., Wang, C., Lipford, S.M., Riad, M.H., Ren, J., Hu, F., Luo, M., Kenny, P.J., et al. (2017). Retrograde inhibition by a specific subset of interpeduncular α5 nicotinic neurons regulates nicotine preference. Proceedings of the National Academy of Sciences *114*, 13012–13017.

Agetsuma, M., Aizawa, H., Aoki, T., Nakayama, R., Takahoko, M., Goto, M., Sassa, T., Amo, R., Shiraki, T., Kawakami, K., et al. (2010). The habenula is crucial for experience-dependent modification of fear responses in zebrafish. Nature Neuroscience *13*, 1354–1356.

Aizawa, H., Amo, R., and Okamoto, H. (2011). Phylogeny and Ontogeny of the Habenular Structure. Frontiers in Neuroscience *5*.

Aizawa, H., Kobayashi, M., Tanaka, S., Fukai, T., and Okamoto, H. (2012). Molecular characterization of the subnuclei in rat habenula. The Journal of Comparative Neurology *520*, 4051–4066.

Alkondon, M., Pereira, E.F.R., Cartes, W.S., Maelicke, A., and Albuquerque, E.X. (1997). Choline is a Selective Agonist of α7 Nicotinic Acetylcholine Receptors in the Rat Brain Neurons. European Journal of Neuroscience *9*, 2734–2742.

Andres, K.H., D□ring, M.V., and Veh, R.W. (1999). Subnuclear organization of the rat habenular complexes. The Journal of Comparative Neurology *407*, 130–150.

Andrianarivelo, A., Saint-Jour, E., Walle, R., Trifilieff, P., and Vanhoutte, P. (2019). Modulation and functions of dopamine receptor heteromers in drugs of abuse-induced adaptations. Neuropharmacology *152*, 42–50.

Antolin-Fontes, B., Ables, J.L., Görlich, A., and Ibañez-Tallon, I. (2015). The habenulo-interpeduncular pathway in nicotine aversion and withdrawal. Neuropharmacology *96*, 213–222.

Antolin-Fontes, B., Li, K., Ables, J.L., Riad, M.H., Görlich, A., Williams, M., Wang, C., Lipford, S.M., Dao, M., Liu, J., et al. (2020). The habenular G-protein–coupled receptor 151 regulates synaptic plasticity and nicotine intake. Proceedings of the National Academy of Sciences *117*, 5502–5509.

Arias, H.R. (1997). Topology of ligand binding sites on the nicotinic acetylcholine receptor. Brain Research Reviews *25*, 133–191.

Arvin, M.C., Jin, X.-T., Yan, Y., Wang, Y., Ramsey, M.D., Kim, V.J., Beckley, N.A., Henry, B.A., and Drenan, R.M. (2019). Chronic Nicotine Exposure Alters the Neurophysiology of Habenulo-Interpeduncular Circuitry. The Journal of Neuroscience *39*, 4268–4281.

Ashton, H., Marsh, V., Millman, J., Rawlins, M., Telford, R., and Thompson, J. (1980). Biphasic dose-related responses of the CNV (contingent negative variation) to I.V. nicotine in man. British Journal of Clinical Pharmacology *10*, 579–589.

Auerbach, A. (2012). Thinking in cycles: MWC is a good model for acetylcholine receptor-channels: MWC as a model for acetylcholine receptor-channels. The Journal of Physiology *590*, 93–98.

Avale, M.E., Faure, P., Pons, S., Robledo, P., Deltheil, T., David, D.J., Gardier, A.M., Maldonado, R., Granon, S., Changeux, J.-P., et al. (2008). Interplay of 2* nicotinic receptors and dopamine pathways in the control of spontaneous locomotion. Proceedings of the National Academy of Sciences *105*, 15991–15996.

Baddick, C.G., and Marks, M.J. (2011). An autoradiographic survey of mouse brain nicotinic acetylcholine receptors defined by null mutants. Biochemical Pharmacology *82*, 828–841.

Balcita-Pedicino, J.J., Omelchenko, N., Bell, R., and Sesack, S.R. (2011). The inhibitory influence of the lateral

habenula on midbrain dopamine cells: Ultrastructural evidence for indirect mediation via the rostromedial mesopontine tegmental nucleus. The Journal of Comparative Neurology *519*, 1143–1164.

Beier, K.T., Steinberg, E.E., DeLoach, K.E., Xie, S., Miyamichi, K., Schwarz, L., Gao, X.J., Kremer, E.J., Malenka, R.C., and Luo, L. (2015). Circuit Architecture of VTA Dopamine Neurons Revealed by Systematic Input-Output Mapping. Cell *162*, 622–634.

Beiranvand, F., Zlabinger, C., Orr-Urtreger, A., Ristl, R., Huck, S., and Scholze, P. (2014). Nicotinic acetylcholine receptors control acetylcholine and noradrenaline release in the rodent habenulo-interpeduncular complex: Nicotinic receptors in the habenula-IPN complex. British Journal of Pharmacology *171*, 5209–5224.

Benowitz, N.L., Kuyt, F., and Jacob, P. (1984). Influence of nicotine on cardiovascular and hormonal effects of cigarette smoking. Clinical Pharmacology and Therapeutics *36*, 74–81.

Benowitz, N.L., Hukkanen, J., and Jacob, P. (2009). Nicotine Chemistry, Metabolism, Kinetics and Biomarkers. In Nicotine Psychopharmacology, J.E. Henningfield, E.D. London, and S. Pogun, eds. (Berlin, Heidelberg: Springer Berlin Heidelberg), pp. 29–60.

Benwell, M.E.M., Balfour, D.J.K., and Anderson, J.M. (1988). Evidence that Tobacco Smoking Increases the Density of (?)-[^{3} H]Nicotine Binding Sites in Human Brain. Journal of Neurochemistry *50*, 1243–1247.

Bierut, L.J., Stitzel, J.A., Wang, J.C., Hinrichs, A.L., Grucza, R.A., Xuei, X., Saccone, N.L., Saccone, S.F., Bertelsen, S., Fox, L., et al. (2008). Variants in Nicotinic Receptors and Risk for Nicotine Dependence. American Journal of Psychiatry *165*, 1163–1171.

Blaha, C., Allen, L., Das, S., Inglis, W., Latimer, M., Vincent, S., and Winn, P. (1996). Modulation of dopamine efflux in the nucleus accumbens after cholinergic stimulation of the ventral tegmental area in intact, pedunculopontine tegmental nucleus-lesioned, and laterodorsal tegmental nucleus-lesioned rats. The Journal of Neuroscience *16*, 714–722.

Boyden, E.S., Zhang, F., Bamberg, E., Nagel, G., and Deisseroth, K. (2005). Millisecond-timescale, genetically targeted optical control of neural activity. Nature Neuroscience *8*, 1263–1268.

Brejc, K., van Dijk, W.J., Klaassen, R.V., Schuurmans, M., van der Oost, J., Smit, A.B., and Sixma, T.K. (2001). Crystal structure of an ACh-binding protein reveals the ligand-binding domain of nicotinic receptors. Nature *411*, 269–276.

Brody, A.L., Mandelkern, M.A., London, E.D., Olmstead, R.E., Farahi, J., Scheibal, D., Jou, J., Allen, V., Tiongson, E., Chefer, S.I., et al. (2006). Cigarette Smoking Saturates Brain ±4^{2}2 Nicotinic Acetylcholine Receptors. ARCH GEN PSYCHIATRY *63*, 9.

Bromberg-Martin, E.S., Matsumoto, M., and Hikosaka, O. (2010). Dopamine in Motivational Control: Rewarding, Aversive, and Alerting. Neuron *68*, 815–834.

Brown, M.T.C., Tan, K.R., O'Connor, E.C., Nikonenko, I., Muller, D., and Lüscher, C. (2012). Ventral tegmental area GABA projections pause accumbal cholinergic interneurons to enhance associative learning. Nature *492*, 452–456.

Caille, S., Guillem, K., Cador, M., Manzoni, O., and Georges, F. (2009). Voluntary Nicotine Consumption Triggers In Vivo Potentiation of Cortical Excitatory Drives to Midbrain Dopaminergic Neurons. Journal of Neuroscience *29*, 10410–10415.

Centers for Disease Control and Prevention (US), National Center for Chronic Disease Prevention and Health Promotion (US), and Office on Smoking and Health (US) (2010). How Tobacco Smoke Causes Disease: The Biology and Behavioral Basis for Smoking-Attributable Disease: A Report of the Surgeon General (Atlanta (GA): Centers for Disease Control and Prevention (US)).

Chang, C.Y., Esber, G.R., Marrero-Garcia, Y., Yau, H.-J., Bonci, A., and Schoenbaum, G. (2016). Brief optogenetic inhibition of dopamine neurons mimics endogenous negative reward prediction errors. Nature Neuroscience *19*, 111–116.

Chang, C.Y., Gardner, M.P.H., Conroy, J.C., Whitaker, L.R., and Schoenbaum, G. (2018). Brief, But Not Prolonged, Pauses in the Firing of Midbrain Dopamine Neurons Are Sufficient to Produce a Conditioned Inhibitor. The Journal of Neuroscience *38*, 8822–8830.

Changeux, J.-P. (2010a). Nicotine addiction and nicotinic receptors: lessons from genetically modified mice. Nature Reviews Neuroscience *11*, 389–401.

Changeux, J.-P. (2010b). Allosteric Receptors: From Electric Organ to Cognition. Annual Review of Pharmacology and Toxicology *50*, 1–38.

Changeux, J.-P. (2018). The nicotinic acetylcholine receptor: a typical 'allosteric machine.' Phil. Trans. R. Soc. B *373*, 20170174.

Chevalier, G., and Deniau, J.M. (1990). Disinhibition as a basic process in the expression of striatal functions. Trends in Neurosciences *13*, 277–280.

Choi, K., Lee, Y., Lee, C., Hong, S., Lee, S., Kang, S.J., and Shin, K.S. (2016). Optogenetic activation of septal GABAergic afferents entrains neuronal firing in the medial habenula. Scientific Reports *6*, 34800.

Chudasama, Y., and Robbins, T.W. (2004). Dopaminergic Modulation of Visual Attention and Working Memory in the Rodent Prefrontal Cortex. Neuropsychopharmacology *29*, 1628–1636.

Coddington, L.T., and Dudman, J.T. (2018). The timing of action determines reward prediction signals in identified midbrain dopamine neurons. Nature Neuroscience *21*, 1563–1573.

Colombo, S.F., Mazzo, F., Pistillo, F., and Gotti, C. (2013). Biogenesis, trafficking and up-regulation of nicotinic ACh receptors. Biochemical Pharmacology *86*, 1063–1073.

Corbett, D., and Wise, R.A. (1980). Intracranial self-stimulation in relation to the ascending dopaminergic systems of the midbrain: A moveable electrode mapping study. Brain Research *185*, 1–15.

Corrigall, W.A., and Coen, K.M. (1989). Nicotine maintains robust self-administration in rats on a limited-access schedule. Psychopharmacology *99*, 473–478.

Corrigall, W., Coen, K., Zhang, J., and Adamson, L. (2002). Pharmacological manipulations of the pedunculopontine tegmental nucleus in the rat reduce self-administration of both nicotine and cocaine. Psychopharmacology *160*, 198–205.

Corrigall, W.A., Coen, K.M., and Adamson, K.L. (1994). Self-administered nicotine activates the mesolimbic dopamine system through the ventral tegmental area. Brain Research *653*, 278–284.

Corringer, P.-J., Sallette, J., and Changeux, J.-P. (2006). Nicotine enhances intracellular nicotinic receptor maturation: A novel mechanism of neural plasticity? Journal of Physiology-Paris *99*, 162–171.

Cox, J., and Witten, I.B. (2019). Striatal circuits for reward learning and decision-making. Nature Reviews Neuroscience *20*, 482–494.

Creese, I., Burt, D.R., and Snyder, S.H. (1976). Dopamine Receptor Binding Predicts Clinical and Pharmacological Potencies of Antischizophrenic Drugs. Science, New Series *192*, 481–483.

Dale, H.H. (1914). The action of certain esters of choline, and their relation to muscarine. J Pharmacol Exp Ther *6*, 147-190.

Damaj, M.I., Kao, W., and Martin, B.R. (2003). Characterization of Spontaneous and Precipitated Nicotine Withdrawal in the Mouse. Journal of Pharmacology and Experimental Therapeutics *307*, 526–534.

Dani, J.A. (2003). Roles of dopamine signaling in nicotine addiction. Molecular Psychiatry *8*, 255–256.

Dani, J.A., and Bertrand, D. (2007). Nicotinic Acetylcholine Receptors and Nicotinic Cholinergic Mechanisms of the Central Nervous System. Annual Review of Pharmacology and Toxicology *47*, 699–729.

Dani, J.A., and De Biasi, M. (2013). Mesolimbic Dopamine and Habenulo-Interpeduncular Pathways in Nicotine Withdrawal. Cold Spring Harbor Perspectives in Medicine *3*, a012138–a012138.

Dani, J.A., and Heinemann, S. (1996). Molecular and cellular aspects of nicotine abuse. Neuron *16*, 905–908.

Datta, S., and Siwek, D.F. (2002). Single cell activity patterns of pedunculopontine tegmentum neurons across the sleep-wake cycle in the freely moving rats. Journal of Neuroscience Research *70*, 611–621.

Dautan, D., Souza, A.S., Huerta-Ocampo, I., Valencia, M., Assous, M., Witten, I.B., Deisseroth, K., Tepper, J.M., Bolam, J.P., Gerdjikov, T.V., et al. (2016). Segregated cholinergic transmission modulates dopamine neurons integrated in distinct functional circuits. Nat Neurosci *19*, 1025–1033.

Dayan, P., and Balleine, B.W. (2002). Reward, Motivation, and Reinforcement Learning. Neuron *36*, 285–298.

De Biasi, M., and Dani, J.A. (2011). Reward, Addiction, Withdrawal to Nicotine. Annual Review of Neuroscience *34*, 105–130.

Degos, B., Deniau, J.-M., Chavez, M., and Maurice, N. (2013). Subthalamic Nucleus High-Frequency Stimulation Restores Altered Electrophysiological Properties of Cortical Neurons in Parkinsonian Rat. PLoS ONE *8*, e83608.

DeGroot, S.R., Zhao-Shea, R., Chung, L., Klenowski, P.M., Sun, F., Molas, S., Gardner, P.D., Li, Y., and Tapper, A.R. (2020). Midbrain Dopamine Controls Anxiety-like Behavior by Engaging Unique Interpeduncular Nucleus Microcircuitry. Biological Psychiatry.

Deisseroth, K. (2015). Optogenetics: 10 years of microbial opsins in neuroscience. Nature Neuroscience *18*, 1213–1225.

Deniau, J.-M., Degos, B., Bosch, C., and Maurice, N. (2010). Deep brain stimulation mechanisms: beyond the concept of local functional inhibition: Deep brain stimulation mechanisms. European Journal of Neuroscience *32*, 1080–1091.

Di Chiara, G., and Imperato, A. (1988). Drugs abused by humans preferentially increase synaptic dopamine concentrations in the mesolimbic system of freely moving rats. Proceedings of the National Academy of Sciences *85*, 5274–5278.

DiFranza, J.R., Savageau, J.A., Fletcher, K., Ockene, J.K., Rigotti, N.A., McNeill, A.D., Coleman, M., and Wood, C. (2004). Recollections and repercussions of the first inhaled cigarette. Addictive Behaviors *29*, 261–272.

Drenan, R.M., Grady, S.R., Whiteaker, P., McClure-Begley, T., McKinney, S., Miwa, J.M., Bupp, S., Heintz, N., McIntosh, J.M., Bencherif, M., et al. (2008). In Vivo Activation of Midbrain Dopamine Neurons via Sensitized, High-Affinity α6∗ Nicotinic Acetylcholine Receptors. Neuron *60*, 123–136.

Duncan, A., Heyer, M.P., Ishikawa, M., Caligiuri, S.P.B., Liu, X., Chen, Z., Vittoria Micioni Di Bonaventura, M., Elayouby, K.S., Ables, J.L., Howe, W.M., et al. (2019). Habenular TCF7L2 links nicotine addiction to diabetes. Nature *574*, 372–377.

Durand-de Cuttoli, R., Mondoloni, S., and Mourot, A. (2017). Dissection optique du rôle des récepteurs nicotiniques neuronaux à l'aide de récepteurs photo-contrôlables. Biologie Aujourd'hui *211*, 173–188.

Durand-de Cuttoli, R., Mondoloni, S., Marti, F., Lemoine, D., Nguyen, C., Naudé, J., d'Izarny-Gargas, T., Pons, S., Maskos, U., Trauner, D., et al. (2018). Manipulating midbrain dopamine neurons and reward-related behaviors with light-controllable nicotinic acetylcholine receptors. ELife *7*, e37487.

Eddine, R., Valverde, S., Tolu, S., Dautan, D., Hay, A., Morel, C., Cui, Y., Lambolez, B., Venance, L., Marti, F., et al. (2015). A concurrent excitation and inhibition of dopaminergic subpopulations in response to nicotine. Scientific Reports *5*.

Everitt, B.J. (2014). Neural and psychological mechanisms underlying compulsive drug seeking habits and drug memories - indications for novel treatments of addiction. European Journal of Neuroscience *40*, 2163–2182.

Exley, R., Maubourguet, N., David, V., Eddine, R., Evrard, A., Pons, S., Marti, F., Threlfell, S., Cazala, P., McIntosh, J.M., et al. (2011). Distinct contributions of nicotinic acetylcholine receptor subunit 4 and subunit 6 to the reinforcing effects of nicotine. Proceedings of the National Academy of Sciences *108*, 7577–7582.

Exley, R., McIntosh, J.M., Marks, M.J., Maskos, U., and Cragg, S.J. (2012). Striatal 5 Nicotinic Receptor Subunit Regulates Dopamine Transmission in Dorsal Striatum. Journal of Neuroscience *32*, 2352–2356.

Exley, R., Clements, M.A., Hartung, H., McIntosh, J.M., Franklin, M., Bermudez, I., and Cragg, S.J. (2013). Striatal dopamine transmission is reduced after chronic nicotine with a decrease in α6-nicotinic receptor control in nucleus accumbens. European Journal of Neuroscience n/a-n/a.

Faure, P., Tolu, S., Valverde, S., and Naudé, J. (2014). Role of nicotinic acetylcholine receptors in regulating dopamine neuron activity. Neuroscience *282*, 86–100.

Fenster, C.P., Rains, M.F., Noerager, B., Quick, M.W., and Lester, R.A.J. (1997). Influence of Subunit Composition on Desensitization of Neuronal Acetylcholine Receptors at Low Concentrations of Nicotine. The Journal of Neuroscience *17*, 5747–5759.

Fenster, C.P., Whitworth, T.L., Sheffield, E.B., Quick, M.W., and Lester, R.A.J. (1999). Upregulation of Surface α4β2 Nicotinic Receptors Is Initiated by Receptor Desensitization after Chronic Exposure to Nicotine. The Journal of Neuroscience *19*, 4804–4814.

Fields, H.L., Hjelmstad, G.O., Margolis, E.B., and Nicola, S.M. (2007). Ventral Tegmental Area Neurons in Learned Appetitive Behavior and Positive Reinforcement. Annual Review of Neuroscience *30*, 289–316.

Fiorillo, C.D., Tobler, P., and Schultz, W. (2003). Discrete Coding of Reward Probability and Uncertainty by Dopamine Neurons. Science *299*, 1898–1902.

Flanigan, M.E., Aleyasin, H., Li, L., Burnett, C.J., Chan, K.L., LeClair, K.B., Lucas, E.K., Matikainen-Ankney, B., Durand-de Cuttoli, R., Takahashi, A., et al. (2020). Orexin signaling in GABAergic lateral habenula neurons modulates aggressive behavior in male mice. Nature Neuroscience *23*, 638–650.

Floresco, S.B. (2013). Prefrontal dopamine and behavioral flexibility: shifting from an "inverted-U" toward a family of functions. Frontiers in Neuroscience *7*.

Forget, B., Scholze, P., Langa, F., Morel, C., Pons, S., Mondoloni, S., Besson, M., Durand-de Cuttoli, R., Hay, A., Tricoire, L., et al. (2018). A Human Polymorphism in CHRNA5 Is Linked to Relapse to Nicotine Seeking in Transgenic Rats. Current Biology *28*, 3244-3253.e7.

Foulds, J. (2003). Effect of smokeless tobacco (snus) on smoking and public health in Sweden. Tobacco Control *12*, 349–359.

Fowler, C.D., and Kenny, P.J. (2014). Nicotine aversion: Neurobiological mechanisms and relevance to tobacco dependence vulnerability. Neuropharmacology *76*, 533–544.

Fowler, C.D., Lu, Q., Johnson, P.M., Marks, M.J., and Kenny, P.J. (2011). Habenular α5 nicotinic receptor subunit signalling controls nicotine intake. Nature *471*, 597–601.

Frahm, S., Ślimak, M.A., Ferrarese, L., Santos-Torres, J., Antolin-Fontes, B., Auer, S., Filkin, S., Pons, S., Fontaine, J.-F., Tsetlin, V., et al. (2011). Aversion to Nicotine Is Regulated by the Balanced Activity of β4 and α5 Nicotinic Receptor Subunits in the Medial Habenula. Neuron *70*, 522–535.

Gallego, X., Molas, S., Amador-Arjona, A., Marks, M.J., Robles, N., Murtra, P., Armengol, L., Fernández-Montes, R.D., Gratacòs, M., Pumarola, M., et al. (2012). Overexpression of the CHRNA5/A3/B4 genomic cluster in mice increases the sensitivity to nicotine and modifies its reinforcing effects. Amino Acids *43*, 897–909.

Garcia-Rill, E. (1991). THE PEDUNCULOPONTINE NUCLEUS. 27.

Garcia-Rivas, V., Cannella, N., and Deroche-Gamonet, V. (2017). Individual Variations in the Mechanisms of Nicotine Seeking: A Key for Research on Nicotine Dependence. Neuropsychopharmacology *42*, 584–586.

Gasbarri, A., Sulli, A., and Packard, M.G. (1997). The dopaminergic mesencephalic projections to the hippocampal formation in the rat. Progress in Neuro-Psychopharmacology and Biological Psychiatry *21*, 1–22.

George, A.A., Lucero, L.M., Damaj, M.I., Lukas, R.J., Chen, X., and Whiteaker, P. (2012). Function of Human 3 4 5 Nicotinic Acetylcholine Receptors Is Reduced by the 5(D398N) Variant. Journal of Biological Chemistry *287*, 25151–25162.

Girault, J.-A., and Greengard, P. (2004). The Neurobiology of Dopamine Signaling. ARCH NEUROL *61*, 5.

Goldberg, S.R., Spealman, R.D., and Goldberg, D.M. (1981). Persistent Behavior at High Rates Maintained by Intravenous Self-Administration of Nicotine. Science, New Series *214*, 573–575.

Gonon, F.G. (1988). Nonlinear relationship between impulse flow and dopamine released by rat midbrain dopaminergic neurons as studied by in vivo electrochemistry. Neuroscience *24*, 19–28.

Grace, A.A. (1995). The tonic/phasic model of dopamine system regulation: its relevance for understanding how stimulant abuse can alter basal ganglia function. Drug and Alcohol Dependence *37*, 111–129.

Grace, A.A., and Bunney, B.S. (1983). Intracellular and extracellular electrophysiology of nigral dopaminergic neurons--1. Identification and characterization. *10*, 301–315.

Grace, A.A., and Bunney, B.S. (1984a). The control of firing pattern in nigral dopamine neurons: burst firing. *4*, 2877–2890.

Grace, A.A., and Bunney, B.S. (1984b). The control of firing pattern in nigral dopamine neurons: single spike firing. *4*, 2866–2886.

Grace, A.A., and Onn, S.-P. (1989). Morphology and Electrophysiological Properties of lmmunocytochemically Identified Rat Dopamine Neurons Recorded in wifro. 19.

Grace, A.A., Floresco, S.B., Goto, Y., and Lodge, D.J. (2007). Regulation of firing of dopaminergic neurons and control of goal-directed behaviors. Trends in Neurosciences *30*, 220–227.

Grady, S.R., Moretti, M., Zoli, M., Marks, M.J., Zanardi, A., Pucci, L., Clementi, F., and Gotti, C. (2009). Rodent Habenulo-Interpeduncular Pathway Expresses a Large Variety of Uncommon nAChR Subtypes, But Only the 3 4 and 3 3 4 Subtypes Mediate Acetylcholine Release. Journal of Neuroscience *29*, 2272–2282.

Grieder, T.E., Sellings, L.H., Vargas-Perez, H., Ting-A-Kee, R., Siu, E.C., Tyndale, R.F., and van der Kooy, D. (2010). Dopaminergic Signaling Mediates the Motivational Response Underlying the Opponent Process to Chronic but Not Acute Nicotine. Neuropsychopharmacology *35*, 943–954.

Gruber, C., Kahl, A., Lebenheim, L., Kowski, A., Dittgen, A., and Veh, R.W. (2007). Dopaminergic projections from the VTA substantially contribute to the mesohabenular pathway in the rat. Neuroscience Letters *427*, 165–170.

Gutkin, B.S., Dehaene, S., and Changeux, J.-P. (2006). A neurocomputational hypothesis for nicotine addiction. Proceedings of the National Academy of Sciences *103*, 1106–1111.

Haber, S.N., Fudge, J.L., and McFarland, N.R. (2000). Striatonigrostriatal Pathways in Primates Form an Ascending Spiral from the Shell to the Dorsolateral Striatum. The Journal of Neuroscience *20*, 2369–2382.

Hall, F.S., Der-Avakian, A., Gould, T.J., Markou, A., Shoaib, M., and Young, J.W. (2015). Negative affective states and cognitive impairments in nicotine dependence. Neuroscience & Biobehavioral Reviews *58*, 168–185.

Harrington, L., Viñals, X., Herrera-Solís, A., Flores, A., Morel, C., Tolu, S., Faure, P., Maldonado, R., Maskos, U., and Robledo, P. (2016). Role of β4* Nicotinic Acetylcholine Receptors in the Habenulo–Interpeduncular Pathway in Nicotine Reinforcement in Mice. Neuropsychopharmacology *41*, 1790–1802.

Hay, Y.A., Lambolez, B., and Tricoire, L. (2016). Nicotinic Transmission onto Layer 6 Cortical Neurons Relies on Synaptic Activation of Non-α7 Receptors. Cerebral Cortex *26*, 2549–2562.

Hemmendinger, L.M., and Moore, R.Y. (1984). Interpeduncular nucleus organization in the rat: Cytoarchitecture and histochemical analysis. Brain Research Bulletin *13*, 163–179.

Henderson, B.J., and Lester, H.A. (2015). Inside-out neuropharmacology of nicotinic drugs. Neuropharmacology *96*, 178–193.

Henningfield, J.E., Miyasato, K., and Jasinski, D.R. (1983). Cigarette smokers self-administer intravenous nicotine. Pharmacology Biochemistry and Behavior *19*, 887–890.

Herkenham, M., and Nauta, W.J.H. (1979). Efferent connections of the habenular nuclei in the rat. The Journal of Comparative Neurology *187*, 19–47.

Herzog, E., Gilchrist, J., Gras, C., Muzerelle, A., Ravassard, P., Giros, B., Gaspar, P., and El Mestikawy, S. (2004). Localization of VGLUT3, the vesicular glutamate transporter type 3, in the rat brain. Neuroscience *123*, 983–1002.

Hikosaka, O. (2010). The habenula: from stress evasion to value-based decision-making. Nature Reviews Neuroscience *11*, 503–513.

Hilario, M.R.F., Turner, J.R., and Blendy, J.A. (2012). Reward Sensitization: Effects of Repeated Nicotine Exposure and Withdrawal in Mice. Neuropsychopharmacology *37*, 2661–2670.

Hille, B. (2001). Ion Channels of Excitable Membranes.

Hnasko, T.S., Hjelmstad, G.O., Fields, H.L., and Edwards, R.H. (2012). Ventral Tegmental Area Glutamate Neurons: Electrophysiological Properties and Projections. Journal of Neuroscience *32*, 15076–15085.

Hsu, Y.-W.A., Tempest, L., Quina, L.A., Wei, A.D., Zeng, H., and Turner, E.E. (2013). Medial Habenula Output Circuit Mediated by 5 Nicotinic Receptor-Expressing GABAergic Neurons in the Interpeduncular Nucleus. Journal of Neuroscience *33*, 18022–18035.

Hsu, Y.-W.A., Morton, G., Guy, E.G., Wang, S.D., and Turner, E.E. (2016). Dorsal Medial Habenula Regulation of Mood-Related Behaviors and Primary Reinforcement by Tachykinin-Expressing Habenula Neurons. ENeuro *3*.

Hu, H., Cui, Y., and Yang, Y. (2020). Circuits and functions of the lateral habenula in health and in disease. Nature Reviews Neuroscience *21*, 277–295.

Hughes, J.R. (1992). Tobacco Withdrawal in Self-Quitters. 9.

Hughes, J.R., Hatsukami, D.K., Pickens, R.W., Krahn, D., Malin, S., and Luknic, A. (1984). Effect of nicotine on the tobacco withdrawal syndrome. Psychopharmacology *83*, 82–87.

Husson, M., Harrington, L., Tochon, L., Cho, Y., Ibañez-Tallon, I., Maskos, U., and David, V. (2020). β4-Nicotinic Receptors Are Critically Involved in Reward-Related Behaviors and Self-Regulation of Nicotine Reinforcement. The Journal of Neuroscience *40*, 3465–3477.

Hyland, B.I., Reynolds, J.N.J., Hay, J., Perk, C.G., and Miller, R. (2002). Firing modes of midbrain dopamine cells in the freely moving rat. Neuroscience *114*, 475–492.

Ikemoto, S. (2007). Dopamine reward circuitry: Two projection systems from the ventral midbrain to the nucleus accumbens–olfactory tubercle complex. Brain Research Reviews *56*, 27–78.

Isaac, P.F., and Rand, M.J. (1972). Cigarette smoking and plasma levels of nicotine. Nature *236*, 308–310.

Jackson, M.B. (1986). Kinetics of unliganded acetylcholine receptor channel gating. Biophysical Journal *49*, 663–672.

Jhou, T.C., Fields, H.L., Baxter, M.G., Saper, C.B., and Holland, P.C. (2009). The Rostromedial Tegmental Nucleus (RMTg), a GABAergic Afferent to Midbrain Dopamine Neurons, Encodes Aversive Stimuli and Inhibits Motor Responses. Neuron *61*, 786–800.

Jhou, T.C., Good, C.H., Rowley, C.S., Xu, S. -p., Wang, H., Burnham, N.W., Hoffman, A.F., Lupica, C.R., and Ikemoto, S. (2013). Cocaine Drives Aversive Conditioning via Delayed Activation of Dopamine-Responsive Habenular and Midbrain Pathways. Journal of Neuroscience *33*, 7501–7512.

de Jong, J.W., Afjei, S.A., Pollak Dorocic, I., Peck, J.R., Liu, C., Kim, C.K., Tian, L., Deisseroth, K., and Lammel, S. (2019). A Neural Circuit Mechanism for Encoding Aversive Stimuli in the Mesolimbic Dopamine System. Neuron *101*, 133-151.e7.

Juarez, B., Morel, C., Ku, S.M., Liu, Y., Zhang, H., Montgomery, S., Gregoire, H., Ribeiro, E., Crumiller, M., Roman-Ortiz, C., et al. (2017). Midbrain circuit regulation of individual alcohol drinking behaviors in mice. Nat Commun *8*, 2220.

Karpen, J.W., and Ruiz, M. (2002). Ion channels: does each subunit do something on its own? 8.

Katz, B., and Thesleff, S. (1957). A study of the 'desensitization' produced by acetylcholine at the motor end-plate. The Journal of Physiology *138*, 63–80.

Kawaja, M., Flumerfelt, B., and Hrycyshyn, A.W. (1990). A comparison of the subnuclear and ultrastructural distribution of acetylcholinesterase and choline acetyltransferase in the rat interpeduncular nucleus. Bruin Research Bulletin *24*, 517–523.

Kebabian, J.W., and Greengard, P. (1971). Dopamine-Sensitive Adenyl Cyclase: Possible Role in Synaptic Transmission. Science *174*, 1346–1349.

Keiflin, R., and Janak, P.H. (2015). Dopamine Prediction Errors in Reward Learning and Addiction: From Theory to Neural Circuitry. Neuron *88*, 247–263.

Kenny, P.J., and Markou, A. (2001). Neurobiology of the nicotine withdrawal syndrome. Pharmacology Biochemistry and Behavior *70*, 531–549.

Keskitalo, K., Broms, U., Heliovaara, M., Ripatti, S., Surakka, I., Perola, M., Pitkaniemi, J., Peltonen, L., Aromaa, A., and Kaprio, J. (2009). Association of serum cotinine level with a cluster of three nicotinic acetylcholine receptor genes (CHRNA3/CHRNA5/CHRNB4) on chromosome 15. Human Molecular Genetics *18*, 4007–4012.

Kim, U., and Chung, L. (2007). Dual GABAergic Synaptic Response of Fast Excitation and Slow Inhibition in the Medial Habenula of Rat Epithalamus. Journal of Neurophysiology *98*, 1323–1332.

Kim, K.M., Baratta, M.V., Yang, A., Lee, D., Boyden, E.S., and Fiorillo, C.D. (2012). Optogenetic Mimicry of the Transient Activation of Dopamine Neurons by Natural Reward Is Sufficient for Operant Reinforcement. PLoS ONE *7*, e33612.

Kitai, S.T., Shepard, P.D., Callaway, J.C., and Scroggs, R. (1999). Afferent modulation of dopamine neuron firing patterns. Current Opinion in Neurobiology *9*, 690–697.

Klaus, A., Alves da Silva, J., and Costa, R.M. (2019). What, If, and When to Move: Basal Ganglia Circuits and Self-Paced Action Initiation. Annual Review of Neuroscience *42*, 459–483.

Klein, M.O., Battagello, D.S., Cardoso, A.R., Hauser, D.N., Bittencourt, J.C., and Correa, R.G. (2019). Dopamine: Functions, Signaling, and Association with Neurological Diseases. Cellular and Molecular Neurobiology *39*, 31–59.

Klink, R., de Kerchove d'Exaerde, A., Zoli, M., and Changeux, J.-P. (2001). Molecular and physiological diversity of nicotinic acetylcholine receptors in the midbrain dopaminergic nuclei. The Journal of Neuroscience *21*, 1452–1463.

Kobayashi, Y., Sano, Y., Vannoni, E., Goto, H., Suzuki, H., Oba, A., Kawasaki, H., Kanba, S., Lipp, H.-P., Murphy, N.P., et al. (2013). Genetic dissection of medial habenula–interpeduncular nucleus pathway function in mice. Frontiers in Behavioral Neuroscience *7*.

Koob, G.F., and Le Moal, M. (1997). Drug Abuse: Hedonic Homeostatic Dysregulation. Science *278*, 52–58.

Koob, G.F., and Le Moal, M. (2006). Neurobiology of addiction.

Koob, G.F., and Le Moal, M. (2008). Addiction and the Brain Antireward System. Annual Review of Psychology *59*, 29–53.

Koob, G.F., and Volkow, N.D. (2010). Neurocircuitry of Addiction. Neuropsychopharmacology *35*, 217–238.

Kotzyba-Hibert, F., Kessler, P., Zerbib, V., Grutter, T., Bogen, C., Takeda, K., Hammadi, A., Knerr, L., and Goeldner, M. (1997). Nicotinic Acetylcholine Receptor Labeled with a Tritiated, Photoactivatable Agonist: A New Tool for Investigating the Functional, Activated State. Bioconjugate Chem *8*, 472–480.

Kozlowski, L.T., and Herman, C.P. (1984). The Interaction of Psychosocial and Biological Determinants of Tobacco Use: More on the Boundary Model1. Journal of Applied Social Psychology *14*, 244–256.

Krashia, P., Moroni, M., Broadbent, S., Hofmann, G., Kracun, S., Beato, M., Groot-Kormelink, P.J., and Sivilotti, L.G. (2010). Human α3β4 Neuronal Nicotinic Receptors Show Different Stoichiometry if They Are Expressed in Xenopus Oocytes or Mammalian HEK293 Cells. PLoS ONE *5*, e13611.

Kroeger, D., Ferrari, L.L., Petit, G., Mahoney, C.E., Fuller, P.M., Arrigoni, E., and Scammell, T.E. (2017). Cholinergic, Glutamatergic, and GABAergic Neurons of the Pedunculopontine Tegmental Nucleus Have Distinct Effects on Sleep/Wake Behavior in Mice. The Journal of Neuroscience *37*, 1352–1366.

Kruse, A.C., Kobilka, B.K., Gautam, D., Sexton, P.M., Christopoulos, A., and Wess, J. (2014). Muscarinic acetylcholine receptors: novel opportunities for drug development. Nature Reviews Drug Discovery *13*, 549–560.

Kuo, Y.-P., Xu, L., Eaton, J.B., Zhao, L., Wu, J., and Lukas, R.J. (2005). Roles for Nicotinic Acetylcholine Receptor Subunit Large Cytoplasmic Loop Sequences in Receptor Expression and Function. J Pharmacol Exp Ther *314*, 455–466.

Kuryatov, A., Berrettini, W., and Lindstrom, J. (2011). Acetylcholine Receptor (AChR) 5 Subunit Variant

Associated with Risk for Nicotine Dependence and Lung Cancer Reduces (4 2)2 5 AChR Function. Molecular Pharmacology *79*, 119–125.

Kutlu, M.G., and Gould, T.J. (2015). Nicotine modulation of fear memories and anxiety: Implications for learning and anxiety disorders. Biochemical Pharmacology *97*, 498–511.

Lak, A., Stauffer, W.R., and Schultz, W. (2014). Dopamine prediction error responses integrate subjective value from different reward dimensions. Proceedings of the National Academy of Sciences *111*, 2343–2348.

Lammel, S., Hetzel, A., Häckel, O., Jones, I., Liss, B., and Roeper, J. (2008). Unique Properties of Mesoprefrontal Neurons within a Dual Mesocorticolimbic Dopamine System. Neuron *57*, 760–773.

Lammel, S., Ion, D.I., Roeper, J., and Malenka, R.C. (2011). Projection-Specific Modulation of Dopamine Neuron Synapses by Aversive and Rewarding Stimuli. Neuron *70*, 855–862.

Lammel, S., Lim, B.K., Ran, C., Huang, K.W., Betley, M.J., Tye, K.M., Deisseroth, K., and Malenka, R.C. (2012). Input-specific control of reward and aversion in the ventral tegmental area. Nature *491*, 212–217.

Lammel, S., Steinberg, E.E., Földy, C., Wall, N.R., Beier, K., Luo, L., and Malenka, R.C. (2015). Diversity of Transgenic Mouse Models for Selective Targeting of Midbrain Dopamine Neurons. Neuron *85*, 429–438.

Laviolette, S.R., and van der Kooy, D. (2004). The neurobiology of nicotine addiction: bridging the gap from molecules to behaviour. Nature Reviews Neuroscience *5*, 55–65.

Lecca, S., Melis, M., Luchicchi, A., Ennas, M.G., Castelli, M.P., Muntoni, A.L., and Pistis, M. (2011). Effects of Drugs of Abuse on Putative Rostromedial Tegmental Neurons, Inhibitory Afferents to Midbrain Dopamine Cells. Neuropsychopharmacology *36*, 589–602.

Lecca, S., Meye, F.J., and Mameli, M. (2014). The lateral habenula in addiction and depression: an anatomical, synaptic and behavioral overview. European Journal of Neuroscience *39*, 1170–1178.

Lecca, S., Meye, F.J., Trusel, M., Tchenio, A., Harris, J., Schwarz, M.K., Burdakov, D., Georges, F., and Mameli, M. (2017). Aversive stimuli drive hypothalamus-to-habenula excitation to promote escape behavior. ELife *6*.

Lee, A., Mathuru, A.S., Teh, C., Kibat, C., Korzh, V., Penney, T.B., and Jesuthasan, S. (2010). The Habenula Prevents Helpless Behavior in Larval Zebrafish. Current Biology *20*, 2211–2216.

Lemoine, D., Jiang, R., Taly, A., Chataigneau, T., Specht, A., and Grutter, T. (2012). Ligand-Gated Ion Channels: New Insights into Neurological Disorders and Ligand Recognition. Chemical Reviews *112*, 6285–6318.

Léna, C., Changeux, J.-P., and Mulle, C. (1993). Evidence for "preterminal" nicotinic receptors on GABAergic axons in the rat interpeduncular nucleus. Journal of Neuroscience *13*, 2680–2688.

Lester, H.A., Xiao, C., Srinivasan, R., Son, C.D., Miwa, J., Pantoja, R., Banghart, M.R., Dougherty, D.A., Goate, A.M., and Wang, J.C. (2009). Nicotine is a Selective Pharmacological Chaperone of Acetylcholine Receptor Number and Stoichiometry. Implications for Drug Discovery. The AAPS Journal *11*, 167–177.

Lewis, A.S., and Picciotto, M.R. (2020). Regulation of aggressive behaviors by nicotinic acetylcholine receptors: Animal models, human genetics, and clinical studies. Neuropharmacology *167*, 107929.

Lima, L.B., Bueno, D., Leite, F., Souza, S., Gonçalves, L., Furigo, I.C., Donato, J., and Metzger, M. (2017). Afferent and efferent connections of the interpeduncular nucleus with special reference to circuits involving the habenula and raphe nuclei: **L IMA ET AL** . Journal of Comparative Neurology *525*, 2411–2442.

Liu, Q., Kuo, Y.-P., Shen, J., Lukas, R.J., and Wu, J. (2015). Roles of nicotinic acetylcholine receptor β subunit cytoplasmic loops in acute desensitization and single-channel features. Neuroscience *289*, 315–323.

Lodge, D.J., and Grace, A.A. (2006). The laterodorsal tegmentum is essential for burst firing of ventral tegmental area dopamine neurons. Proceedings of the National Academy of Sciences *103*, 5167–5172.

Loewi, O. (1922). Über humorale Übertragbarkeit der Herznervenwirkung. 201–213.

Luscher, C. (2013). Drug-Evoked Synaptic Plasticity Causing Addictive Behavior. Journal of Neuroscience *33*, 17641–17646.

Lynagh, T., and Pless, S.A. (2014). Principles of agonist recognition in Cys-loop receptors. Front. Physiol. *5*.

Mameli, M., Halbout, B., Creton, C., Engblom, D., Parkitna, J.R., Spanagel, R., and Lüscher, C. (2009). Cocaine-evoked synaptic plasticity: persistence in the VTA triggers adaptations in the NAc. Nature Neuroscience *12*, 1036–1041.

Mameli-Engvall, M., Evrard, A., Pons, S., Maskos, U., Svensson, T.H., Changeux, J.-P., and Faure, P. (2006). Hierarchical Control of Dopamine Neuron-Firing Patterns by Nicotinic Receptors. Neuron *50*, 911–921.

Mansvelder, H.D., and McGehee, D.S. (2000). Long-Term Potentiation of Excitatory Inputs to Brain Reward Areas by Nicotine. Neuron *27*, 349–357.

Mansvelder, H.D., Keath, J.R., and McGehee, D.S. (2002). Synaptic Mechanisms Underlie Nicotine-Induced Excitability of Brain Reward Areas. Neuron *33*, 905–919.

Mansvelder, H.D., De Rover, M., McGehee, D.S., and Brussaard, A.B. (2003). Cholinergic modulation of dopaminergic reward areas: upstream and downstream targets of nicotine addiction. European Journal of Pharmacology *480*, 117–123.

Mansvelder, H.D., Mertz, M., and Role, L.W. (2009). Nicotinic modulation of synaptic transmission and plasticity in cortico-limbic circuits. Seminars in Cell & Developmental Biology *20*, 432–440.

Margolis, E.B., Lock, H., Hjelmstad, G.O., and Fields, H.L. (2006). The ventral tegmental area revisited: is there an electrophysiological marker for dopaminergic neurons?: Electrophysiological properties of VTA neurons. The Journal of Physiology *577*, 907–924.

Maron, D.J., and Fortmann, S.P. (1987). Nicotine yield and measures of cigarette smoke exposure in a large population: are lower-yield cigarettes safer? American Journal of Public Health *77*, 546–549.

Maroteaux, M., and Mameli, M. (2012). Cocaine Evokes Projection-Specific Synaptic Plasticity of Lateral Habenula Neurons. Journal of Neuroscience *32*, 12641–12646.

Marti, F., Arib, O., Morel, C., Dufresne, V., Maskos, U., Corringer, P.-J., de Beaurepaire, R., and Faure, P. (2011). Smoke Extracts and Nicotine, but not Tobacco Extracts, Potentiate Firing and Burst Activity of Ventral Tegmental Area Dopaminergic Neurons in Mice. Neuropsychopharmacology *36*, 2244–2257.

Maskos, U. (2009). The cholinergic mesopontine tegmentum is a relatively neglected nicotinic master modulator of the dopaminergic system: relevance to drugs of abuse and pathology: Nicotinic master modulation. British Journal of Pharmacology *153*, S438–S445.

Maskos, U., Molles, B.E., Pons, S., Besson, M., Guiard, B.P., Guilloux, J.-P., Evrard, A., Cazala, P., Cormier, A., Mameli-Engvall, M., et al. (2005). Nicotine reinforcement and cognition restored by targeted expression of nicotinic receptors. Nature *436*, 103–107.

Mathis, V., and Kenny, P.J. (2019). From controlled to compulsive drug-taking: The role of the habenula in addiction. Neuroscience & Biobehavioral Reviews *106*, 102–111.

Mathuru, A.S., and Jesuthasan, S. (2013). The medial habenula as a regulator of anxiety in adult zebrafish. Frontiers in Neural Circuits *7*.

Matsumoto, M., and Hikosaka, O. (2007). Lateral habenula as a source of negative reward signals in dopamine neurons. Nature *447*, 1111–1115.

Matta, S.G., Balfour, D.J., Benowitz, N.L., Boyd, R.T., Buccafusco, J.J., Caggiula, A.R., Craig, C.R., Collins, A.C., Damaj, M.I., Donny, E.C., et al. (2007). Guidelines on nicotine dose selection for in vivo research. Psychopharmacology *190*, 269–319.

Mazzo, F., Pistillo, F., Grazioso, G., Clementi, F., Borgese, N., Gotti, C., and Colombo, S.F. (2013). Nicotine-Modulated Subunit Stoichiometry Affects Stability and Trafficking of 3 4 Nicotinic Receptor. Journal of Neuroscience *33*, 12316–12328.

McBride, W.J., Murphy, J.M., and Ikemoto, S. (1999). Localization of brain reinforcement mechanisms: intracranial self-administration and intracranial place-conditioning studies. Behavioural Brain Research *101*, 129–152.

McLaughlin, I., Dani, J.A., and De Biasi, M. (2017). The medial habenula and interpeduncular nucleus circuitry is critical in addiction, anxiety, and mood regulation. Journal of Neurochemistry *142*, 130–143.

Melis, M., Spiga, S., and Diana, M. (2005). The Dopamine Hypothesis of Drug Addiction: Hypodopaminergic State. In International Review of Neurobiology, (Elsevier), pp. 101–154.

Meye, F.J., Trusel, M., Soiza-Reilly, M., and Mameli, M. (2017). Neural circuit adaptations during drug withdrawal — Spotlight on the lateral habenula. Pharmacology Biochemistry and Behavior *162*, 87–93.

Miller, A.D., and Blaha, C.D. (2005). Midbrain muscarinic receptor mechanisms underlying regulation of mesoaccumbens and nigrostriatal dopaminergic transmission in the rat. European Journal of Neuroscience *21*, 1837–1846.

Mirenowicz, J., and Schultz, W. (1996). Preferential activation of midbrain dopamine neurons by appetitive rather than aversive stimuli. Nature *379*, 449–451.

Miyazawa, A., Fujiyoshi, Y., and Unwin, N. (2003). Structure and gating mechanism of the acetylcholine receptor pore. Nature *423*, 949–955.

Molas, S., DeGroot, S.R., Zhao-Shea, R., and Tapper, A.R. (2017a). Anxiety and Nicotine Dependence: Emerging Role of the Habenulo-Interpeduncular Axis. Trends in Pharmacological Sciences *38*, 169–180.

Molas, S., Zhao-Shea, R., Liu, L., DeGroot, S.R., Gardner, P.D., and Tapper, A.R. (2017b). A circuit-based mechanism underlying familiarity signaling and the preference for novelty. Nature Neuroscience.

Moore, R.Y., and Bloom, F.E. (1978). Central Catecholamine Neuron Systems: Anatomy and Physiology of the Dopamine Systems. Annual Review of Neuroscience *1*, 129–169.

Morales, M., and Margolis, E.B. (2017). Ventral tegmental area: cellular heterogeneity, connectivity and behaviour. Nature Reviews Neuroscience *18*, 73–85.

Morales-Perez, C.L., Noviello, C.M., and Hibbs, R.E. (2016). X-ray structure of the human α4β2 nicotinic receptor. Nature *538*, 411–415.

Morel, C., Fattore, L., Pons, S., Hay, Y.A., Marti, F., Lambolez, B., De Biasi, M., Lathrop, M., Fratta, W., Maskos, U., et al. (2014). Nicotine consumption is regulated by a human polymorphism in dopamine neurons. Molecular Psychiatry *19*, 930–936.

Morel, C., Fernandez, S.P., Pantouli, F., Meye, F.J., Marti, F., Tolu, S., Parnaudeau, S., Marie, H., Tronche, F., Maskos, U., et al. (2018). Nicotinic receptors mediate stress-nicotine detrimental interplay via dopamine cells' activity. Molecular Psychiatry *23*, 1597–1605.

Morton, G., Nasirova, N., Sparks, D.W., Brodsky, M., Sivakumaran, S., Lambe, E.K., and Turner, E.E. (2018). Chrna5-Expressing Neurons in the Interpeduncular Nucleus Mediate Aversion Primed by Prior Stimulation or Nicotine Exposure. The Journal of Neuroscience *38*, 6900–6920.

Murphy, C.A., DiCamillo, A.M., Haun, F., and Murray, M. (1996). Lesion of the habenular efferent pathway produces anxiety and locomotor hyperactivity in rats: a comparison of the effects of neonatal and adult lesions. Behavioural Brain Research *81*, 43–52.

Nagel, G., Szellas, T., Huhn, W., Kateriya, S., Adeishvili, N., Berthold, P., Ollig, D., Hegemann, P., and Bamberg, E. (2003). Channelrhodopsin-2, a directly light-gated cation-selective membrane channel. Proceedings of the National Academy of Sciences *100*, 13940–13945.

Nair-Roberts, R.G., Chatelain-Badie, S.D., Benson, E., White-Cooper, H., Bolam, J.P., and Ungless, M.A. (2008). Stereological estimates of dopaminergic, GABAergic and glutamatergic neurons in the ventral tegmental area, substantia nigra and retrorubral field in the rat. Neuroscience *152*, 1024–1031.

Nashmi, R., Xiao, C., Deshpande, P., McKinney, S., Grady, S.R., Whiteaker, P., Huang, Q., McClure-Begley, T., Lindstrom, J.M., Labarca, C., et al. (2007). Chronic Nicotine Cell Specifically Upregulates Functional 4* Nicotinic Receptors: Basis for Both Tolerance in Midbrain and Enhanced Long-Term Potentiation in Perforant Path. Journal of Neuroscience *27*, 8202–8218.

Naudé, J., Tolu, S., Dongelmans, M., Torquet, N., Valverde, S., Rodriguez, G., Pons, S., Maskos, U., Mourot, A., Marti, F., et al. (2016). Nicotinic receptors in the ventral tegmental area promote uncertainty-seeking. Nature Neuroscience *19*, 471–478.

Naudé, J., Didienne, S., Takillah, S., Prévost-Solié, C., Maskos, U., and Faurej, P. (2018). Acetylcholine-dependent phasic dopamine activity signals exploratory locomotion and choices (Neuroscience).

Nelson, M.E., Kuryatov, A., Choi, C.H., Zhou, Y., and Lindstrom, J. (2003). Alternate stoichiometries of α4β2 nicotinic acetylcholine receptors. Molecular Pharmacology *63*, 332–341.

Neubig, R.R., Boyd, N.D., and Cohen, J.B. (1982). Conformations of Torpedo acetylcholine receptor associated with ion transport and desensitization. Biochemistry *21*, 3460–3467.

Nguyen, C., Mondoloni, S., Centeno, I., Durand-de Cuttoli, R., Tolu, S., Valverde, S., Le Borgne, T., Hannesse, B., Pons, S., Maskos, U., et al. (2020). Distinct dopamine circuits transmit the reinforcing and anxiogenic effects of nicotine (Neuroscience).

Norton, A.B.W., Jo, Y.S., Clark, E.W., Taylor, C.A., and Mizumori, S.J.Y. (2011). Independent neural coding of reward and movement by pedunculopontine tegmental nucleus neurons in freely navigating rats: Reward and movement codes of PPTg neurons. European Journal of Neuroscience *33*, 1885–1896.

Nuno-Perez, A., Tchenio, A., Mameli, M., and Lecca, S. (2018). Lateral Habenula Gone Awry in Depression: Bridging Cellular Adaptations With Therapeutics. Front. Neurosci. *12*, 485.

Nutt, D., King, L.A., Saulsbury, W., and Blakemore, C. (2007). Development of a rational scale to assess the harm of drugs of potential misuse. The Lancet *369*, 1047–1053.

Olds, J., and Milner, P. (1954). Positive reinforcement produced by electrical stimulation of septal area and other regions of rat brain. Journal of Comparative and Physiological Psychology *47*, 419–427.

Otsu, Y., Lecca, S., Pietrajtis, K., Rousseau, C.V., Marcaggi, P., Dugué, G.P., Mailhes-Hamon, C., Mameli, M., and Diana, M.A. (2018). Functional Principles of Posterior Septal Inputs to the Medial Habenula. Cell Reports *22*, 693–705.

Otsu, Y., Darcq, E., Pietrajtis, K., Mátyás, F., Schwartz, E., Bessaih, T., Abi Gerges, S., Rousseau, C.V., Grand,

T., Dieudonné, S., et al. (2019). Control of aversion by glycine-gated GluN1/GluN3A NMDA receptors in the adult medial habenula. Science *366*, 250–254.

Ouagazzal, A.-M., Kenny, P.J., and File, S.E. (1999). Modulation of behaviour on trials 1 and 2 in the elevated plus-maze test of anxiety after systemic and hippocampal administration of nicotine. Psychopharmacology *144*, 54–60.

Paladini, C.A., and Roeper, J. (2014). Generating bursts (and pauses) in the dopamine midbrain neurons. Neuroscience *282*, 109–121.

Pang, X., Liu, L., Ngolab, J., Zhao-Shea, R., McIntosh, J.M., Gardner, P.D., and Tapper, A.R. (2016). Habenula cholinergic neurons regulate anxiety during nicotine withdrawal via nicotinic acetylcholine receptors. Neuropharmacology *107*, 294–304.

Paoletti, P., Ellis-Davies, G.C.R., and Mourot, A. (2019). Optical control of neuronal ion channels and receptors. Nature Reviews Neuroscience.

Pascoli, V., Terrier, J., Hiver, A., and Lüscher, C. (2015). Sufficiency of Mesolimbic Dopamine Neuron Stimulation for the Progression to Addiction. Neuron *88*, 1054–1066.

Pascoli, V., Hiver, A., Van Zessen, R., Loureiro, M., Achargui, R., Harada, M., Flakowski, J., and Lüscher, C. (2018). Stochastic synaptic plasticity underlying compulsion in a model of addiction. Nature *564*, 366–371.

Perez, E., Quijano-Cardé, N., and De Biasi, M. (2015). Nicotinic mechanisms modulate ethanol withdrawal and modify time course and symptoms severity of simultaneous withdrawal from alcohol and nicotine. Neuropsychopharmacology *40*, 2327–2336.

Piazza, P., Deminiere, J., Le Moal, M., and Simon, H. (1989). Factors that predict individual vulnerability to amphetamine self-administration. Science *245*, 1511–1513.

Picciotto, M.R. (2003). Nicotine as a modulator of behavior: beyond the inverted U. Trends in Pharmacological Sciences *24*, 493–499.

Picciotto, M.R., Zoli, M., Rimondini, R., Léna, C., Marubio, L.M., Merlo Pich, E., Fuxe, K., and Changeux, J.-P. (1998). Acetylcholine receptors containing the b2 subunit are involved in the reinforcing properties of nicotine. Nature *391*, 173–177.

Picciotto, M.R., Higley, M.J., and Mineur, Y.S. (2012). Acetylcholine as a Neuromodulator: Cholinergic Signaling Shapes Nervous System Function and Behavior. Neuron *76*, 116–129.

Pidoplichko, V.I., DeBiasi, M., Williams, J.T., and Dani, J.A. (1997). Nicotine activates and desensitizes midbrain dopamine neurons. Nature *390*, 401–404.

Pomerleau, O.F., Collins, A.C., Shiftman, S., and Pomerleau, C.S. (1993). Why Some People Smoke and Others Do Not: New Perspectives. 9.

Pons, S., Fattore, L., Cossu, G., Tolu, S., Porcu, E., McIntosh, J.M., Changeux, J.P., Maskos, U., and Fratta, W. (2008). Crucial Role of 4 and 6 Nicotinic Acetylcholine Receptor Subunits from Ventral Tegmental Area in Systemic Nicotine Self-Administration. Journal of Neuroscience *28*, 12318–12327.

Qi, J., Zhang, S., Wang, H.-L., Barker, D.J., Miranda-Barrientos, J., and Morales, M. (2016). VTA glutamatergic inputs to nucleus accumbens drive aversion by acting on GABAergic interneurons. Nature Neuroscience *19*, 725–733.

Quina, L.A., Harris, J., Zeng, H., and Turner, E.E. (2017). Specific connections of the interpeduncular subnuclei reveal distinct components of the habenulopeduncular pathway: QUINA et al. Journal of Comparative Neurology

525, 2632–2656.

Redish, A.D. (2004). Addiction as a computational process gone awry. Science *306*, 1944–1947.

Ren, J., Qin, C., Hu, F., Tan, J., Qiu, L., Zhao, S., Feng, G., and Luo, M. (2011). Habenula "Cholinergic" Neurons Corelease Glutamate and Acetylcholine and Activate Postsynaptic Neurons via Distinct Transmission Modes. Neuron *69*, 445–452.

Reynaud, M. (2016). Traité d'addictologie.

Reynolds, J.N.J., Hyland, B.I., and Wickens, J.R. (2001). A cellular mechanism of reward-related learning. Nature *413*, 67–70.

Rice, M.E., and Cragg, S.J. (2004). Nicotine amplifies reward-related dopamine signals in striatum. Nature Neuroscience *7*, 583–584.

Riedel, B., Blitstein, J., Robinson, L., Murray, D., and Klesges, R. (2003). The reliability and predictive value of adolescents' reports of initial reactions to smoking. Nicotine & Tobacco Research *5*, 553–559.

Riley, A.L. (2011). The paradox of drug taking: The role of the aversive effects of drugs. Physiology & Behavior *103*, 69–78.

Robbins, T.W., and Everitt, B.J. (1999). Drug addiction: bad habits add up. Nature *398*, 567–570.

Robertson, S.J., and Edwards, F.A. (1998). ATP and glutamate are released from separate neurones in the rat medial habenula nucleus: frequency dependence and adenosine-mediated inhibition of release. The Journal of Physiology *508*, 691–701.

Roeper, J. (2013). Dissecting the diversity of midbrain dopamine neurons. Trends in Neurosciences *36*, 336–342.

Roesch, M.R. (2004). Neuronal Activity Related to Reward Value and Motivation in Primate Frontal Cortex. Science *304*, 307–310.

Root, D.H., Mejias-Aponte, C.A., Zhang, S., Wang, H.-L., Hoffman, A.F., Lupica, C.R., and Morales, M. (2014). Single rodent mesohabenular axons release glutamate and GABA. Nature Neuroscience *17*, 1543–1551.

Russell, M.A., Jarvis, M., Iyer, R., and Feyerabend, C. (1980). Relation of nicotine yield of cigarettes to blood nicotine concentrations in smokers. BMJ *280*, 972–976.

Russo, S.J., and Nestler, E.J. (2013). The brain reward circuitry in mood disorders. Nature Reviews Neuroscience *14*, 609–625.

Salamone, J.D., and Correa, M. (2002). Motivational views of reinforcement: implications for understanding the behavioral functions of nucleus accumbens dopamine. Behavioural Brain Research *137*, 3–25.

Salas, R. (2004). Decreased Signs of Nicotine Withdrawal in Mice Null for the 4 Nicotinic Acetylcholine Receptor Subunit. Journal of Neuroscience *24*, 10035–10039.

Salas, R., Sturm, R., Boulter, J., and De Biasi, M. (2009). Nicotinic Receptors in the Habenulo-Interpeduncular System Are Necessary for Nicotine Withdrawal in Mice. Journal of Neuroscience *29*, 3014–3018.

Sallette, J., Pons, S., Devillers-Thiery, A., Soudant, M., Prado de Carvalho, L., Changeux, J.-P., and Corringer, P.J. (2005). Nicotine Upregulates Its Own Receptors through Enhanced Intracellular Maturation. Neuron *46*, 595–607.

Sarter, M., Parikh, V., and Howe, W.M. (2009). Phasic acetylcholine release and the volume transmission hypothesis: time to move on. Nature Reviews Neuroscience *10*, 383–390.

Sartor, C.E., Lessov-Schlaggar, C.N., Scherrer, J.F., Bucholz, K.K., Madden, P.A.F., Pergadia, M.L., Grant, J.D., Jacob, T., and Xian, H. (2010). Initial response to cigarettes predicts rate of progression to regular smoking: Findings from an offspring-of-twins design. Addictive Behaviors *35*, 771–778.

Scarr, E. (2012). Muscarinic Receptors: Their Roles in Disorders of the Central Nervous System and Potential as Therapeutic Targets. CNS Neuroscience & Therapeutics *18*, 369–379.

Schachter, S., Silverstein, B., Kozlowski, L.T., Perlick, D., Herman, C.P., and Liebling, B. (1977). Studies of the interaction of psychological and pharmacological determinants of smoking. Journal of Experimental Psychology: General *106*, 3–4.

Schilström, B., Rawal, N., Mameli-Engvall, M., Nomikos, G.G., and Svensson, T.H. (2003). Dual effects of nicotine on dopamine neurons mediated by different nicotinic receptor subtypes. The International Journal of Neuropsychopharmacology *6*, 1–11.

Schultz, W. (1986). Responses of midbrain dopamine neurons to behavioral trigger stimuli in the monkey. Journal of Neurophysiology *56*, 1439–1461.

Schultz, W. (1997). Dopamine neurons and their role in reward mechanisms. Current Opinion in Neurobiology *7*, 191–197.

Schultz, W. (2000). Multiple reward signals in the brain. Nature Reviews Neuroscience *1*, 199–207.

Schultz, W. (2007). Multiple Dopamine Functions at Different Time Courses. Annual Review of Neuroscience *30*, 259–288.

Schultz, W. (2017). Reward prediction error. Current Biology *27*, R369–R371.

Schultz, W., and Dickinson, A. (2000). Neuronal Coding of Prediction Errors. Annual Review of Neuroscience *23*, 473–500.

Schultz, W., Apicella, P., and Ljungberg, T. (1993). Responses of monkey dopamine neurons to reward and conditioned stimuli during successive steps of learning a delayed response task. The Journal of Neuroscience *13*, 900–913.

Schultz, W., Dayan, P., and Montague, P.R. (1997). A Neural Substrate of Prediction and Reward. Science *275*, 1593–1599.

Sekiguchi, H., Pavey, G., and Dean, B. (2019). Altered levels of dopamine transporter in the frontal pole and dorsal striatum in schizophrenia. Npj Schizophrenia *5*.

Shepard, P.D., and Bunney, B.S. (1988). Effects of apamin on the discharge properties of putative dopamine-containing neurons in vitro. Brain Research *463*, 380–384.

Shi, W.-X. (2009). Electrophysiological Characteristics of Dopamine Neurons: A 35-Year Update. In Birth, Life and Death of Dopaminergic Neurons in the Substantia Nigra, G. Giovanni, V. Di Matteo, and E. Esposito, eds. (Vienna: Springer Vienna), pp. 103–119.

Shih, P.-Y., Engle, S.E., Oh, G., Deshpande, P., Puskar, N.L., Lester, H.A., and Drenan, R.M. (2014). Differential Expression and Function of Nicotinic Acetylcholine Receptors in Subdivisions of Medial Habenula. Journal of Neuroscience *34*, 9789–9802.

Shih, P.-Y., McIntosh, J.M., and Drenan, R.M. (2015). Nicotine Dependence Reveals Distinct Responses from Neurons and Their Resident Nicotinic Receptors in Medial Habenula. Molecular Pharmacology *88*, 1035–1044.

Siciliano, C.A., Noamany, H., Chang, C.-J., Brown, A.R., Chen, X., Leible, D., Lee, J.J., Wang, J., Vernon, A.N., Vander Weele, C.M., et al. (2019). A cortical-brainstem circuit predicts and governs compulsive alcohol drinking.

Science *366*, 1008–1012.

Skjei, K.L., and Markou, A. (2003). Effects of repeated withdrawal episodes, nicotine dose, and duration of nicotine exposure on the severity and duration of nicotine withdrawal in rats. Psychopharmacology *168*, 280–292.

Ślimak, M.A., Ables, J.L., Frahm, S., Antolin-Fontes, B., Santos-Torres, J., Moretti, M., Gotti, C., and Ibañez-Tallon, I. (2014). Habenular expression of rare missense variants of the β4 nicotinic receptor subunit alters nicotine consumption. Frontiers in Human Neuroscience *8*.

Smit, A.B., Brejc, K., Syed, N., and Sixma, T.K. (2003). Structure and Function of AChBP, Homologue of the Ligand-Binding Domain of the Nicotinic Acetylcholine Receptor. Annals of the New York Academy of Sciences *998*, 81–92.

Soria-Gómez, E., Busquets-Garcia, A., Hu, F., Mehidi, A., Cannich, A., Roux, L., Louit, I., Alonso, L., Wiesner, T., Georges, F., et al. (2015). Habenular CB1 Receptors Control the Expression of Aversive Memories. Neuron *88*, 306–313.

Sparling, B.A., and DiMauro, E.F. (2017). Progress in the discovery of small molecule modulators of the Cys-loop superfamily receptors. Bioorganic & Medicinal Chemistry Letters *27*, 3207–3218.

Srinivasan, R., Pantoja, R., Moss, F.J., Mackey, E.D.W., Son, C.D., Miwa, J., and Lester, H.A. (2011). Nicotine up-regulates α4β2 nicotinic receptors and ER exit sites via stoichiometry-dependent chaperoning. The Journal of General Physiology *137*, 59–79.

Staley, J.K. (2006). Human Tobacco Smokers in Early Abstinence Have Higher Levels of beta2* Nicotinic Acetylcholine Receptors than Nonsmokers. Journal of Neuroscience *26*, 8707–8714.

Stamatakis, A.M., Sparta, D.R., Jennings, J.H., McElligott, Z.A., Decot, H., and Stuber, G.D. (2014). Amygdala and bed nucleus of the stria terminalis circuitry: Implications for addiction-related behaviors. Neuropharmacology *76*, 320–328.

Steinberg, E.E., Keiflin, R., Boivin, J.R., Witten, I.B., Deisseroth, K., and Janak, P.H. (2013). A causal link between prediction errors, dopamine neurons and learning. Nature Neuroscience *16*, 966–973.

Stokes, C., Treinin, M., and Papke, R.L. (2015). Looking below the surface of nicotinic acetylcholine receptors. Trends in Pharmacological Sciences *36*, 514–523.

Stuber, G.D., Hnasko, T.S., Britt, J.P., Edwards, R.H., and Bonci, A. (2010). Dopaminergic Terminals in the Nucleus Accumbens But Not the Dorsal Striatum Corelease Glutamate. Journal of Neuroscience *30*, 8229–8233.

Sutherland, R.J., and Nakajima, S. (1981). Self-stimulation of the habenular complex in the rat. Journal of Comparative and Physiological Psychology *95*, 781–791.

Swanson', L.W. (1982). The Projections of the Ventral Tegmental Area and Adjacent Regions: A Combined Fluorescent Retrograde Tracer and Immunofluorescence Study in the Rat. 33.

Taly, A., Corringer, P.-J., Guedin, D., Lestage, P., and Changeux, J.-P. (2009). Nicotinic receptors: allosteric transitions and therapeutic targets in the nervous system. Nature Reviews Drug Discovery *8*, 733–750.

Tammimäki, A., Herder, P., Li, P., Esch, C., Laughlin, J.R., Akk, G., and Stitzel, J.A. (2012). Impact of human D398N single nucleotide polymorphism on intracellular calcium response mediated by α3β4α5 nicotinic acetylcholine receptors. Neuropharmacology *63*, 1002–1011.

Tan, K.R., Yvon, C., Turiault, M., Mirzabekov, J.J., Doehner, J., Labouèbe, G., Deisseroth, K., Tye, K.M., and Lüscher, C. (2012). GABA Neurons of the VTA Drive Conditioned Place Aversion. Neuron *73*, 1173–1183.

Tang, W., Kochubey, O., Kintscher, M., and Schneggenburger, R. (2020). A VTA to Basal Amygdala Dopamine

Projection Contributes to Signal Salient Somatosensory Events during Fear Learning. The Journal of Neuroscience *40*, 3969–3980.

Tapia, L., Kuryatov, A., and Lindstrom, J. (2006). Ca2+ Permeability of the (4)3(beta2)2 Stoichiometry Greatly Exceeds That of (4)2(beta2)3 Human Acetylcholine Receptors. Molecular Pharmacology *71*, 769–776.

Tapper, A.R. (2004). Nicotine Activation of 4* Receptors: Sufficient for Reward, Tolerance, and Sensitization. Science *306*, 1029–1032.

Tecuapetla, F., Patel, J.C., Xenias, H., English, D., Tadros, I., Shah, F., Berlin, J., Deisseroth, K., Rice, M.E., Tepper, J.M., et al. (2010). Glutamatergic Signaling by Mesolimbic Dopamine Neurons in the Nucleus Accumbens. Journal of Neuroscience *30*, 7105–7110.

Thompson, A.J., Lester, H.A., and Lummis, S.C.R. (2010). The structural basis of function in Cys-loop receptors. Quarterly Reviews of Biophysics *43*, 449–499.

Threlfell, S., Lalic, T., Platt, N.J., Jennings, K.A., Deisseroth, K., and Cragg, S.J. (2012). Striatal Dopamine Release Is Triggered by Synchronized Activity in Cholinergic Interneurons. Neuron *75*, 58–64.

Tochitsky, I., Banghart, M.R., Mourot, A., Yao, J.Z., Gaub, B., Kramer, R.H., and Trauner, D. (2012). Optochemical control of genetically engineered neuronal nicotinic acetylcholine receptors. Nature Chemistry *4*, 105–111.

Tolu, S., Eddine, R., Marti, F., David, V., Graupner, M., Pons, S., Baudonnat, M., Husson, M., Besson, M., and Reperant, C. (2013). Co-activation of VTA DA and GABA neurons mediates nicotine reinforcement. Molecular Psychiatry *18*, 382.

Tolu, S., Marti, F., Morel, C., Perrier, C., Torquet, N., Pons, S., de Beaurepaire, R., and Faure, P. (2017). Nicotine enhances alcohol intake and dopaminergic responses through β2* and β4* nicotinic acetylcholine receptors. Scientific Reports *7*, 45116.

Tong, Z.-Y., Overton, P.G., and Clark, D. (1996). Stimulation of the prefrontal cortex in the rat induces patterns of activity in midbrain dopaminergic neurons which resemble natural burst events. Synapse *22*, 195–208.

Tovote, P., Fadok, J.P., and Lüthi, A. (2015). Neuronal circuits for fear and anxiety. Nature Reviews Neuroscience *16*, 317–331.

Tritsch, N.X., and Sabatini, B.L. (2012). Dopaminergic Modulation of Synaptic Transmission in Cortex and Striatum. Neuron *76*, 33–50.

Tsai, H.-C., Zhang, F., Adamantidis, A., Stuber, G.D., Bonci, A., de Lecea, L., and Deisseroth, K. (2009). Phasic Firing in Dopaminergic Neurons Is Sufficient for Behavioral Conditioning. Science *324*, 1080–1084.

Tuesta, L.M., Chen, Z., Duncan, A., Fowler, C.D., Ishikawa, M., Lee, B.R., Liu, X.-A., Lu, Q., Cameron, M., Hayes, M.R., et al. (2017). GLP-1 acts on habenular avoidance circuits to control nicotine intake. Nature Neuroscience *20*, 708–716.

Unwin, N. (1992). Nicotinic Acetylcholine receptor at 9A resolution_ Unwin 2003. J. Mol. Biol 1101:1124.

Unwin, N. (2005). Refined Structure of the Nicotinic Acetylcholine Receptor at 4Å Resolution. Journal of Molecular Biology *346*, 967–989.

Vale-Martínez, A., Martí-Nicolovius, M., Guillazo-Blanch, G., Coll-Andreu, M., and Morgado-Bernal, I. (1997). Effects of Habenular Lesions upon Two-Way Active Avoidance Conditioning in Rats. Neurobiology of Learning and Memory *68*, 68–74.

Valjent, E., Pages, C., Herve, D., Girault, J.-A., and Caboche, J. (2004). Addictive and non-addictive drugs induce

distinct and specific patterns of ERK activation in mouse brain. European Journal of Neuroscience *19*, 1826–1836.

Van Dort, C.J., Zachs, D.P., Kenny, J.D., Zheng, S., Goldblum, R.R., Gelwan, N.A., Ramos, D.M., Nolan, M.A., Wang, K., Weng, F.-J., et al. (2015). Optogenetic activation of cholinergic neurons in the PPT or LDT induces REM sleep. Proceedings of the National Academy of Sciences *112*, 584–589.

Varani, A.P., and Balerio, G.N. (2012). GABAB receptors involvement in the effects induced by nicotine on anxiety-related behaviour in mice. Pharmacological Research *65*, 507–513.

Wagner, F., Stroh, T., and Veh, R.W. (2014). Correlating habenular subnuclei in rat and mouse by using topographic, morphological, and cytochemical criteria: Subnuclear organization of the mouse habenula. Journal of Comparative Neurology *522*, 2650–2662.

Walters, C.L., Brown, S., Changeux, J.-P., Martin, B., and Damaj, M.I. (2006). The β2 but not α7 subunit of the nicotinic acetylcholine receptor is required for nicotine-conditioned place preference in mice. Psychopharmacology *184*, 339–344.

Wang, J.C., Cruchaga, C., Saccone, N.L., Bertelsen, S., Liu, P., Budde, J.P., Duan, W., Fox, L., Grucza, R.A., Kern, J., et al. (2009). Risk for nicotine dependence and lung cancer is conferred by mRNA expression levels and amino acid change in CHRNA5. Human Molecular Genetics *18*, 3125–3135.

Watabe-Uchida, M., Zhu, L., Ogawa, S.K., Vamanrao, A., and Uchida, N. (2012). Whole-Brain Mapping of Direct Inputs to Midbrain Dopamine Neurons. Neuron *74*, 858–873.

Weber, M., David-Pfeuty, T., and Changeux, J.P. (1975). Regulation of binding properties of the nicotinic receptor protein by cholinergic ligands in membrane fragments from Torpedo marmorata. Proceedings of the National Academy of Sciences *72*, 3443–3447.

Webster, J.F., Vroman, R., Balueva, K., Wulff, P., Sakata, S., and Wozny, C. (2020). Disentangling neuronal inhibition and inhibitory pathways in the lateral habenula. Scientific Reports *10*.

Weiss, F., Maldonado-Vlaar, C.S., Parsons, L.H., Kerr, T.M., Smith, D.L., and Ben-Shahar, O. (2000). Control of cocaine-seeking behavior by drug-associated stimuli in rats: Effects on recovery of extinguished operant-responding and extracellular dopamine levels in amygdala and nucleus accumbens. Proceedings of the National Academy of Sciences *97*, 4321–4326.

Westbrook, A., and Braver, T.S. (2016). Dopamine Does Double Duty in Motivating Cognitive Effort. Neuron *89*, 695–710.

Williams, B.M., Temburni, M.K., Levey, M.S., Bertrand, S., Bertrand, D., and Jacob, M.H. (1998). The long internal loop of the α3 subunit targets nAChRs to subdomains within individual synapses on neurons in vivo. Nat Neurosci *1*, 557–562.

Wirtshafter, D. (1980). The Role of Interpeduncular Connections with the Tegmentum in Avoidance Learning I. 5.

Wise, R.A. (1998). Drug-activation of brain reward pathways. Drug and Alcohol Dependence *51*, 13–22.

Wise, R.A., and Koob, G.F. (2014). The Development and Maintenance of Drug Addiction. Neuropsychopharmacology *39*, 254–262.

Wolfman, S.L., Gill, D.F., Bogdanic, F., Long, K., Al-Hasani, R., McCall, J.G., Bruchas, M.R., and McGehee, D.S. (2018). Nicotine aversion is mediated by GABAergic interpeduncular nucleus inputs to laterodorsal tegmentum. Nature Communications *9*.

Wooltorton, J.R.A., Pidoplichko, V.I., Broide, R.S., and Dani, J.A. (2003). Differential Desensitization and

Distribution of Nicotinic Acetylcholine Receptor Subtypes in Midbrain Dopamine Areas. The Journal of Neuroscience *23*, 3176–3185.

Xiao, C., Cho, J.R., Zhou, C., Treweek, J.B., Chan, K., McKinney, S.L., Yang, B., and Gradinaru, V. (2016). Cholinergic Mesopontine Signals Govern Locomotion and Reward through Dissociable Midbrain Pathways. Neuron *90*, 333–347.

Yamaguchi, T., Wang, H.-L., Li, X., Ng, T.H., and Morales, M. (2011). Mesocorticolimbic Glutamatergic Pathway. Journal of Neuroscience *31*, 8476–8490.

Yamaguchi, T., Danjo, T., Pastan, I., Hikida, T., and Nakanishi, S. (2013). Distinct Roles of Segregated Transmission of the Septo-Habenular Pathway in Anxiety and Fear. Neuron *78*, 537–544.

Yang, H., de Jong, J.W., Tak, Y., Peck, J., Bateup, H.S., and Lammel, S. (2018). Nucleus Accumbens Subnuclei Regulate Motivated Behavior via Direct Inhibition and Disinhibition of VTA Dopamine Subpopulations. Neuron *97*, 434-449.e4.

Yoo, J.H., Zell, V., Gutierrez-Reed, N., Wu, J., Ressler, R., Shenasa, M.A., Johnson, A.B., Fife, K.H., Faget, L., and Hnasko, T.S. (2016). Ventral tegmental area glutamate neurons co-release GABA and promote positive reinforcement. Nature Communications *7*.

Zhang, F., Wang, L.-P., Brauner, M., Liewald, J.F., Kay, K., Watzke, N., Wood, P.G., Bamberg, E., Nagel, G., Gottschalk, A., et al. (2007). Multimodal fast optical interrogation of neural circuitry. Nature *446*, 633–639.

Zhang, J., Tan, L., Ren, Y., Liang, J., Lin, R., Feng, Q., Zhou, J., Hu, F., Ren, J., Wei, C., et al. (2016). Presynaptic Excitation via GABA B Receptors in Habenula Cholinergic Neurons Regulates Fear Memory Expression. Cell *166*, 716–728.

Zhang, S., Qi, J., Li, X., Wang, H.-L., Britt, J.P., Hoffman, A.F., Bonci, A., Lupica, C.R., and Morales, M. (2015). Dopaminergic and glutamatergic microdomains in a subset of rodent mesoaccumbens axons. Nature Neuroscience *18*, 386–392.

Zhao-Shea, R., Liu, L., Soll, L.G., Improgo, M.R., Meyers, E.E., McIntosh, J.M., Grady, S.R., Marks, M.J., Gardner, P.D., and Tapper, A.R. (2011). Nicotine-Mediated Activation of Dopaminergic Neurons in Distinct Regions of the Ventral Tegmental Area. Neuropsychopharmacology *36*, 1021–1032.

Zhao-Shea, R., Liu, L., Pang, X., Gardner, P.D., and Tapper, A.R. (2013). Activation of GABAergic Neurons in the Interpeduncular Nucleus Triggers Physical Nicotine Withdrawal Symptoms. Current Biology *23*, 2327–2335.

Zhao-Shea, R., DeGroot, S.R., Liu, L., Vallaster, M., Pang, X., Su, Q., Gao, G., Rando, O.J., Martin, G.E., George, O., et al. (2015). Increased CRF signalling in a ventral tegmental area-interpeduncular nucleus-medial habenula circuit induces anxiety during nicotine withdrawal. Nature Communications *6*, 6770.

Zhong, W., Gallivan, J.P., Zhang, Y., Li, L., Lester, H.A., and Dougherty, D.A. (1998). From ab initio quantum mechanics to molecular neurobiology: A cation- binding site in the nicotinic receptor. Proceedings of the National Academy of Sciences *95*, 12088–12093.

Zoli, M. (1998). Identification of Four Classes of Brain Nicotinic Receptors Using. 12.

Zoli, M., Pistillo, F., and Gotti, C. (2015). Diversity of native nicotinic receptor subtypes in mammalian brain. Neuropharmacology *96*, 302–311.

(2013). Diagnostic and statistical manual of mental disorders: DSM-5 (Washington, DC: American Psychiatric Publishing).

Annexes

Article

Current Biology

A Human Polymorphism in CHRNA5 Is Linked to Relapse to Nicotine Seeking in Transgenic Rats

Highlights

- The nicotinic α5 subunit is necessary for the acquisition of nicotine-SA in rats
- α5SNP rats (rs16969968 polymorphism) self-administer more nicotine at high doses
- α5SNP rats exhibit higher nicotine-induced reinstatement of nicotine seeking
- Activation of interpeduncular nucleus neurons by nicotine is reduced in α5SNP rats

Authors

Benoit Forget, Petra Scholze, Francina Langa, ..., Alexandre Mourot, Philippe Faure, Uwe Maskos

Correspondence

benforget@hotmail.fr (B.F.), umaskos@pasteur.fr (U.M.)

In Brief

Forget et al. show that transgenic rats expressing a human nicotinic receptor polymorphism self-administer more nicotine at high doses and exhibit higher nicotine-induced reinstatement of nicotine seeking than wild-types. This relapse is associated with reduced neuronal activity in the interpeduncular nucleus.

Forget et al., 2018, Current Biology *28*, 3244–3253
October 22, 2018
https://doi.org/10.1016/j.cub.2018.08.044

CellPress

CellPress

Current Biology
Article

A Human Polymorphism in CHRNA5 Is Linked to Relapse to Nicotine Seeking in Transgenic Rats

Benoit Forget,[1,5,*] Petra Scholze,[2] Francina Langa,[3] Carole Morel,[4] Stephanie Pons,[1] Sarah Mondoloni,[4] Morgane Besson,[1] Romain Durand-de Cuttoli,[4] Audrey Hay,[4] Ludovic Tricoire,[4] Bertrand Lambolez,[4] Alexandre Mourot,[4] Philippe Faure,[4] and Uwe Maskos[1,*]

[1]Unité de Neurobiologie Intégrative des Systèmes Cholinergiques, Department of Neuroscience, CNRS UMR 3571, Institut Pasteur, Paris, France

[2]Department of Pathobiology of the Nervous System, Center for Brain Research, Medical University of Vienna, Spitalgasse 4, Vienna 1090, Austria

[3]Mouse Genetics Engineering Center, CNRS URA 2578, Institut Pasteur, Paris, France

[4]Sorbonne Universités, UPMC Univ Paris 06, INSERM, CNRS, Neuroscience Paris Seine - Institut de Biologie Paris Seine (NPS - IBPS), 75005 Paris, France

[5]Lead Contact

*Correspondence: benforget@hotmail.fr (B.F.), umaskos@pasteur.fr (U.M.)

https://doi.org/10.1016/j.cub.2018.08.044

SUMMARY

Tobacco addiction is a chronic and relapsing disorder with an important genetic component that represents a major public health issue. Meta-analysis of large-scale human genome-wide association studies (GWASs) identified a frequent non-synonymous SNP in the gene coding for the α5 subunit of nicotinic acetylcholine receptors (α5SNP), which significantly increases the risk for tobacco dependence and delays smoking cessation. To dissect the neuronal mechanisms underlying the vulnerability to nicotine addiction in carriers of the α5SNP, we created rats expressing this polymorphism using zinc finger nuclease technology and evaluated their behavior under the intravenous nicotine-self-administration paradigm. The electrophysiological responses of their neurons to nicotine were also evaluated. α5SNP rats self-administered more nicotine at high doses and exhibited higher nicotine-induced reinstatement of nicotine seeking than wild-type rats. Higher reinstatement was associated with altered neuronal activity in several discrete areas that are interconnected, including in the interpeduncular nucleus (IPN), a GABAergic structure that strongly expresses α5-containing nicotinic receptors. The altered reactivity of IPN neurons of α5SNP rats to nicotine was confirmed electrophysiologically. In conclusion, the α5SNP polymorphism is a major risk factor for nicotine intake at high doses and for relapse to nicotine seeking in rats, a dual effect that reflects the human condition. Our results also suggest an important role for the IPN in the higher relapse to nicotine seeking observed in α5SNP rats.

INTRODUCTION

Tobacco addiction, a chronic and relapsing disorder, is expected to contribute to 100 million deaths worldwide this century [1]. Nicotine, the principal psychoactive substance of tobacco smoke that leads to addiction, is a potent agonist for nicotinic acetylcholine receptors (nAChRs) [2]. These pentameric, ligand-gated ion channels are abundant throughout the brain, where different subunits (α2–α6, α7, and β2–β4) co-assemble in varying combinations with diverse functional properties [3]. The elucidation of the biological action of nicotine on addiction-like processes in general, and on relapse in particular, addresses an urgent public health issue. It is well established that genetic and environmental factors influence tobacco dependence [4]. Recently, several independent large-scale human genome-wide association studies (GWASs) identified variants in a region on human chromosome 15 encoding the α3, α5, and β4 nAChR subunits that increase the risk for nicotine dependence [5–7]. One of these variants, the non-synonymous SNP rs16969968 found in exon 5 of the α5 gene (α5SNP), causes an amino acid change D398N. This SNP is very frequent in the general population, in approximately 35% of Europeans and 50% of Middle Eastern populations, and has been associated with an increased risk for nicotine dependence, lower ratings of aversive effect, cognitive enhancement following nicotine administration, and delayed smoking cessation [6, 8–10].

The α5 nAChR subunit is expressed in discrete regions of the mammalian CNS, including the cerebral cortex, cerebellum, thalamus, striatum, hippocampus, substantia nigra, interpeduncular nucleus (IPN), ventral tegmental area (VTA), and medial habenula (mHb) [11, 12].

The role of the α5 subunit and the consequences of the presence of the minor variant rs16969968 (α5SNP) have to some extent been investigated *in vitro* and in animal models of nicotine addiction. *In vitro* data suggest that the α5SNP confers a partial loss of function to the nAChRs in which it is expressed [6, 13, 14], including in human induced pluripotent stem (iPS)-derived neurons [15]. *In vivo* studies showed that mice lacking the α5 subunit, or rats with downregulation of the α5 subunit in the mHb,

increase their nicotine self-administration at high doses [16, 17]. In addition, data from our laboratory demonstrated that mice lacking the α5 subunit and expressing the α5SNP subunit specifically in dopaminergic (DA) neurons of the VTA exhibit an increase in self-administration of high nicotine doses and a reduction in responsiveness of DA neurons to nicotine injections [17]. However, these studies did not investigate the involvement of the α5 subunit in features linked to extended nicotine intake, such as relapse to nicotine seeking after extinction, a critical facet of the addiction process. Furthermore, these studies did not assess the consequences of the constitutive presence of the α5SNP, which is the only valid model of the human condition.

Considering that intravenous nicotine self-administration can be maintained for longer periods in rats than in mice with nicotine plasma level more similar to what is observed in human smokers [18], we created knockout rats for the α5 subunit (α5KO rats) and knockin rats constitutively expressing the α5SNP (α5SNP rats). Until recently, the toolbox of rat genetics lacked the ability to easily introduce site-directed, heritable mutations into the genome to create knockout or knockin rats. This is now possible with the development of programmable nuclease technology [19], such as the zinc finger nuclease (ZFN) technology that induces sequence-specific double-strandbreaks when injected into the pronucleus of single-cell embryos [20], and is accompanied by negligible off-target activity compared to CRISPR/Cas9 technology [21, 22].

The α5KO and α5SNP rats generated with ZFN technology were then used to investigate the impact of the α5SNP and of the gene deletion on multiple behaviors related to nicotine addiction and, in particular, on several procedures of reinstatement of nicotine seeking after extinction, a valid model of relapse [23]. Behavioral experiments were combined with c-Fos immunostaining to correlate neuronal responses to nicotine with relapse to nicotine seeking and completed with *in vivo* and *ex vivo* electrophysiological studies.

RESULTS

Creation and Validation of α5KO and α5SNP Rats

To create α5KO rats, the ZFN pair was designed to target the beginning of exon 5 of the nAChR α5 subunit gene, which codes for most of the transmembrane domains of the subunit [24]. The ZFN pair was injected into the pronucleus of rat single-cell embryo. Screening 40 founder rats yielded 13 (32.5%) that harbored genetic modifications at the locus of interest, and sequencing revealed mostly deletions, from 10 to 184 bp. For the α5SNP rat line, the ZFN pair was designed to target the end of exon 5, 50 base pairs away from the rs16969968 polymorphism location. The ZFN pair was injected into the pronucleus of rat single-cell embryos with a template DNA of 1,603 bp homology and containing the α5SNP at its center. Screening 26 founder rats yielded 3 (11.5%) that harbored the insertion of the α5SNP at the locus of interest. Multiple conditions were tested, and the results are summarized in Figure S1.

The primers used for genotyping and the characteristics of the ZFNs are indicated in Figure S2.

Two founders were chosen to generate the α5KO and α5SNP lines, respectively, because of the presence of a large 184-bp deletion or of the presence of the α5SNP, with no additional modifications (Figures 1A and 1B) and no off-target alterations (Figures S3A and S4A).

We then investigated by immunoprecipitation (IP) with subunit-specific antibodies the levels of α5 subunits and of total heteromeric nAChRs in multiple brain areas. The majority of α5 subunit proteins were detected in the IPN (Figure 1C). We did not observe any significant differences between the levels of α5-containing nAChRs (α5*nAChRs) in α5SNP and wild-type (WT) rats, in every brain area tested. In contrast, the α5 subunit protein was not detectable in α5KO rats, confirming gene deletion. There was overall no modification in the total number of hetero-oligomeric receptors in any of the brain areas analyzed of α5KO or α5SNP rats (Figure 1D).

Nicotine Self-Administration of α5SNP, α5KO, and WT Rats

α5SNP, α5KO, and WT rats were then submitted to chronic intravenous nicotine self-administration (nicotine-SA), the gold standard model for investigating the reinforcing effects of nicotine [25] (see STAR Methods). We analyzed the acquisition of the behavior by progressively increasing the number of active lever presses necessary for the rats to obtain an injection of nicotine (0.03 mg/kg/infusion) from 1 to 5 over 15 sessions (Figure 2A). Although α5SNP and WT rats acquired nicotine-SA similarly, α5KO rats failed to do so, especially when the ratio to obtain a nicotine injection increased to 5 (Figure 2A). Thus, in our conditions, α5KO rats were unable to acquire nicotine-SA at this dose. This effect seems specific to nicotine because the three groups acquired food-SA similarly (Figure 2B).

α5SNP and WT rats were then allowed to self-administer multiple doses of nicotine according to a Latin square design (0–0.09 mg/kg/injection) to establish a dose-response curve. α5SNP and WT rats self-administered the same amount of nicotine at 0.01 and 0.03 mg/kg, but α5SNP rats consumed significantly more nicotine at higher doses (0.06 and 0.09 mg/kg; Figure 2C). When saline was substituted for nicotine during consecutive sessions, rats of both groups displayed similar extinction of their active lever-pressing behavior (Figure 2D), indicating that nicotine expectation drives the lever-pressing behavior and that the α5SNP has no effect on extinction. We then shifted the schedule of reinforcement to a progressive ratio, as previously described [26], allowing the measurement of the incentive motivational and rewarding properties of nicotine [27]. We found no significant difference between genotypes with this schedule of reinforcement for 0.03 mg/kg of nicotine, i.e., on their breaking point measured as the number of reinforcements received during the test (Figure 2E). However, α5SNP rats reached a significantly higher breaking point than WT rats for the dose of 0.06 mg/kg (Figure 2E). This result suggests that the higher nicotine intake at 0.06 mg/kg by α5SNP rats is most likely due to greater motivation or lesser aversion for this dose of nicotine.

In and *Ex Vivo* Electrophysiology of VTA DA Neurons in α5SNP, α5KO, and WT Rats

Considering the importance of VTA DA neurons in the acquisition of SA of psychostimulants in general and of nicotine in particular [28, 29], we recorded *in vivo* the electrophysiological properties

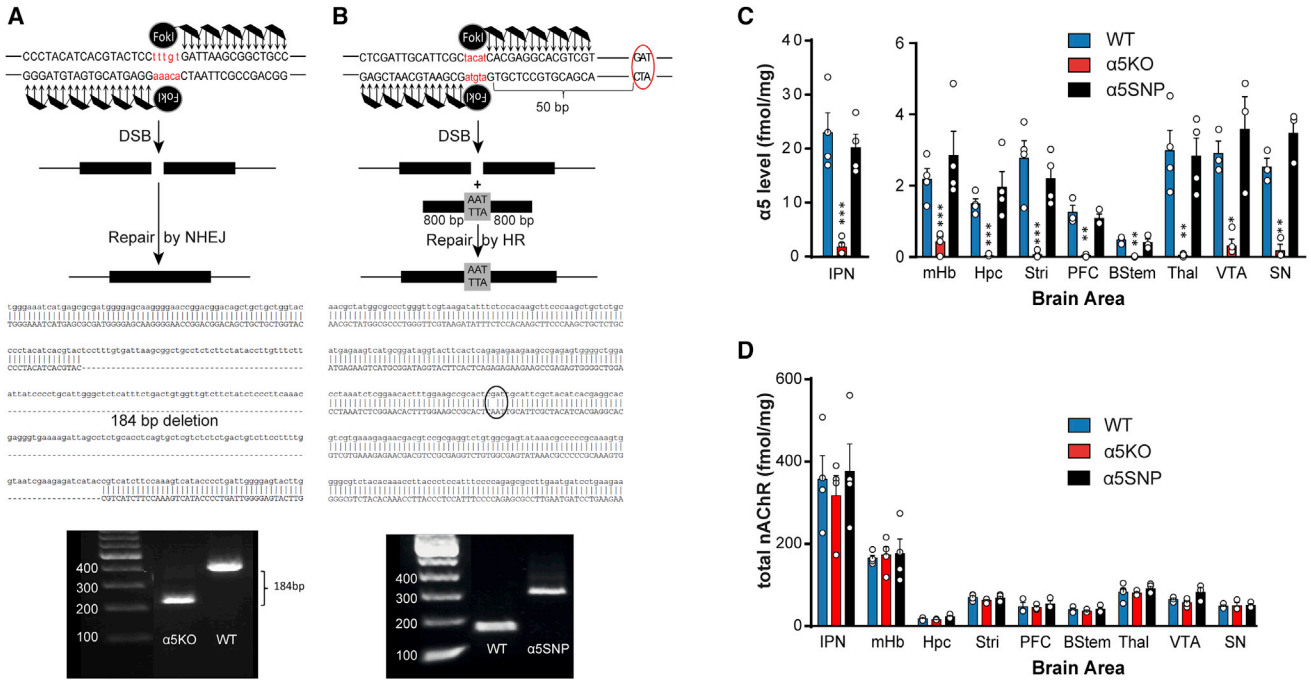

Figure 1. Creation and Validation of α5KO and α5SNP Rats

(A) Creation of α5KO rats. ZFNs containing 5 or 6 fingers were designed to target coding sequences of interest at the beginning of the exon 5 of *CHRNA5* gene for site-specific double-strand break (DSB) in the DNA. ZFNs were injected into the pronucleus of rat one-cell embryos (mRNA, 2 ng/μL). This induced a 184-bp deletion in the gene after non-homologous end joining (NHEJ), verified by sequencing and alignment with WT sequence (lower case) and by PCR followed by migration on a 2% agarose gel.

(B) Creation of α5SNP rats. ZFNs containing 5 fingers were designed to target coding sequences of interest (gray lines) at the end of the exon 5 of *CHRNA5*, 50 bp away from the potential site of the α5SNP (codons circled in red) for site-specific DSB in the DNA. ZFNs were injected into the pronucleus of rat one-cell embryos (mRNA, 2 ng/μL) with a plasmid containing the α5SNP in the middle of a 1,600-bp DNA sequence homologous to the WT sequence. This induced the insertion of the α5SNP after homologous recombination (HR), verified by sequencing and alignment with WT sequence (lowercase) and by PCR followed by Taq 1 restriction enzyme digestion and migration on a 2% agarose gel.

(C and D) Levels of expression of the α5*nAChR (C) and of total heteromeric nicotinic receptors (D) in homozygous α5KO, α5SNP, and WT rats. Experiments were performed with immunoprecipitation with subunit-specific antibodies (in fmol/mg of tissue) in the interpeduncular nucleus (IPN), medial habenula (mHb), hippocampus (Hpc), striatum (Stri), prefrontal cortex (PFC), brain stem (BStem), thalamus (Thal), ventral tegmental area (VTA), and substantia nigra (SN). The overall number of nAChRs was determined by combined immunoprecipitation with anti-β2 plus anti-β4 antibodies. *$p < 0.05$; **$p < 0.01$; ***$p < 0.001$ versus WT (Dunnett's multiple comparison test for each brain area after one-way ANOVA). α5SNP versus WT: non-significant in every brain area. Mean and SEM are represented.

See also Figures S1, S2, S3, and S4 and STAR Methods.

of these neurons under baseline conditions and their response to intravenous injection of nicotine in α5KO, α5SNP, and WT rats (see STAR Methods). We did not observe any differences between genotypes in the spontaneous activity of these neurons, neither in terms of firing frequency nor in terms of bursting activity (Figure 3A). However, whereas DA neurons of WT and α5SNP rats increased their firing frequency in response to 0.03 mg/kg of nicotine, DA neurons of α5KO rats did not respond to this dose and increased their frequency only in response to the highest dose of nicotine (0.09 mg/kg; Figure 3B; the VTA DA neurons response of WT and α5SNP rats to the 0.09 mg/kg nicotine dose is not available). This is in agreement with VTA DA neurons of α5KO rats exhibiting much weaker responses to saturating concentration of the nicotinic agonist dimethylphenylpiperazinium (DMPP) in brain slices, compared to WT and α5SNP rats (Figure 3C). These electrophysiological results highlight the importance of the α5 subunit of nAChRs in the activity of DA neurons of the VTA in response to nicotine and may explain why α5KO rats failed to acquire the nicotine-SA at 0.03 mg/kg. It thus provides a neurobiological correlate of our behavioral results.

Reinstatement of Nicotine Seeking after Extinction in α5SNP and WT Rats

An extinction phase was then conducted by withholding nicotine and its associated visual cue, inducing a progressive and similar decrease of the responding of α5SNP and WT rats on the active lever until stabilization (Figure 4A). After stable extinction, rats were tested for reinstatement of nicotine seeking induced by cue, cue + nicotine (0.1 mg/kg, subcutaneous [s.c.]), or nicotine priming alone (0.1 mg/kg, s.c.) in comparison with extinction sessions with saline priming injections (see STAR Methods). WT and α5SNP rats exhibited a similar cue-induced reinstatement of nicotine seeking. In contrast, α5SNP rats had a significantly higher level of reinstatement after exposure to either cue + nicotine or nicotine alone, compared to WT rats (Figure 4B),

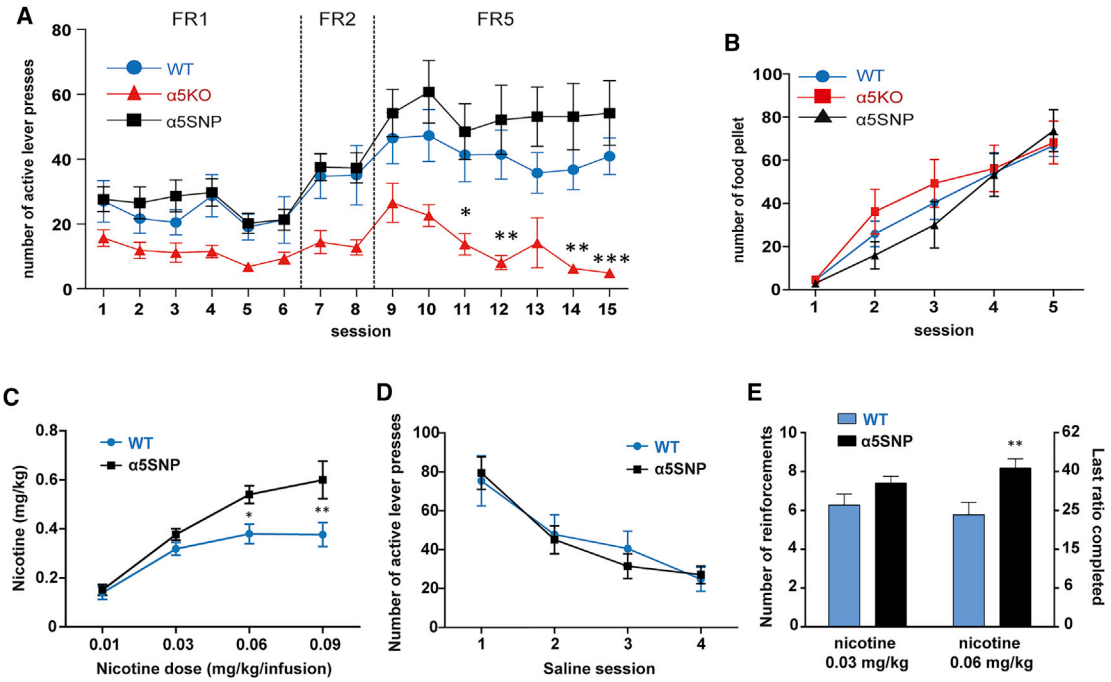

Figure 2. WT and α5SNP, but Not α5KO Rats, Acquired Nicotine Self-Administration, and α5SNP Rats Self-Administered More Nicotine at High Doses

(A) Number of active lever pressing during the acquisition of the nicotine-SA (0.03 mg/kg/infusion) in WT, α5SNP, and α5KO rats. WT (n = 15), α5SNP (n = 14), and α5KO (n = 15) are shown. The two-way ANOVA performed on the number of active lever presses during these 15 sessions indicated a significant effect of session ($F_{14,574}$ = 17.16; p < 0.0001), genotype ($F_{2,41}$ = 9.05; p = 0.0006), and interaction ($F_{28,574}$ = 3.751; p < 0.0001). Post hoc analysis (Bonferroni's multiple comparison test): WT versus α5KO: *p < 0.05 on session 11; **p < 0.01 on sessions 12 and 14; ***p < 0.001 on session 15. The two-way ANOVA performed on the number of inactive lever presses during these 15 sessions revealed no significant effect of genotype ($F_{2,41}$ = 2.02; NS). The two-way ANOVA performed on the number of nicotine infusions during these 15 sessions indicated a significant effect of session ($F_{14,574}$ = 22.9; p < 0.0001) and genotype ($F_{2,41}$ = 23.2; p < 0.0001). Post hoc analysis (Bonferroni's multiple comparison test): WT versus α5KO: *p < 0.05 on sessions 8 and 11; **p < 0.01 on sessions 2–5 and ***p < 0.001 on sessions 7 and 12–15. Mean and SEM are represented.

(B) Number of food pellets earned during the food self-administration training (continuous reinforcement, no associated cues) from self-administration experiment 1 in WT, α5SNP, and α5KO rats. WT (n = 17), α5SNP (n = 16), and α5KO (n = 15) are shown. The two-way ANOVA performed on the number of food pellets self-administered revealed no significant effect of genotype ($F_{2,45}$ = 0.35; p = 0.7; NS) but a significant effect of session ($F_{4,180}$ = 65.38; p < 0.0001) and no interaction ($F_{8,180}$ = 1.13; p = 0.34; NS). Mean and SEM are represented.

(C) Amount of nicotine (mg/kg) consumed during nicotine (0.01–0.09 mg/kg/infusion)-SA under FR5 schedule of reinforcement in WT and α5SNP rats (N = 9 per group). The two-way ANOVA indicated a significant effect of nicotine concentration ($F_{3,48}$ = 17.16; p < 0.0001), genotype ($F_{1,16}$ = 7.62; p = 0.014), and interaction ($F_{3,48}$ = 4.08; p = 0.01). Post hoc analysis (Bonferroni's multiple comparison test): WT versus α5SNP: *p < 0.05 for 0.06 mg/kg/infusion; **p < 0.01 for 0.09 mg/kg/infusion. Mean and SEM are represented.

(D) Saline substitution. Number of active lever presses in WT (n = 8) and α5SNP rats (n = 9) during four consecutive sessions with saline substituted to nicotine and nicotine-associated cues still present (from the first self-administration experiment) is shown. The two-way ANOVA indicated a significant effect of session ($F_{3,45}$ = 31.53; p < 0.0001), but not of genotype ($F_{1,15}$ = 0.02; p = 0.89; NS) or interaction ($F_{3,45}$ = 0.52; p = 0.65; NS). Mean and SEM are represented.

(E) Number of reinforcements and last ratio completed in WT and α5SNP rats under a progressive ratio of reinforcement schedule at the nicotine doses of 0.03 and 0.06 mg/kg/injection. The two-way ANOVA indicated a significant effect of genotype ($F_{1,18}$ = 7.47; p = 0.013), a non-significant effect of nicotine concentration ($F_{1,18}$ = 0.206; NS), and a significant interaction ($F_{1,18}$ = 4.48; p = 0.048). Post hoc analysis (Bonferroni's multiple comparison test): WT versus α5SNP: p = 0.09 (NS) for 0.03 mg/kg/infusion and p = 0.0068 for 0.06 mg/kg/infusion (**). WT rats: n = 9; α5SNP rats: n = 11. Mean and SEM are represented.

See also STAR Methods.

suggesting that the presence of the rs16969968 polymorphism leads to higher level of relapse after re-exposure to nicotine, but not to nicotine-associated cues alone.

To confirm and extend these behavioral data, we performed a second nicotine-SA experiment on new groups of α5SNP and WT rats. The acquisition of SA behavior was carried out as before, and we confirmed (1) that both groups acquired the task equally, (2) the absence of difference between genotypes in the pattern of extinction, and (3) the increased level of relapse of α5SNP versus WT rats induced by cue + nicotine or nicotine alone (Figure 4C), with no difference in inactive lever presses (Figure S5). This highlights the robustness, reproducibility, and specificity of the nicotine-induced high-relapsing phenotype observed in α5SNP rats.

Neuronal Activation during Nicotine-Induced Reinstatement of Nicotine Seeking

In order to dissect the effect of the rs16969968 polymorphism on relapse, we investigated the expression of the c-Fos immediate early gene product, considered as a marker of neuronal

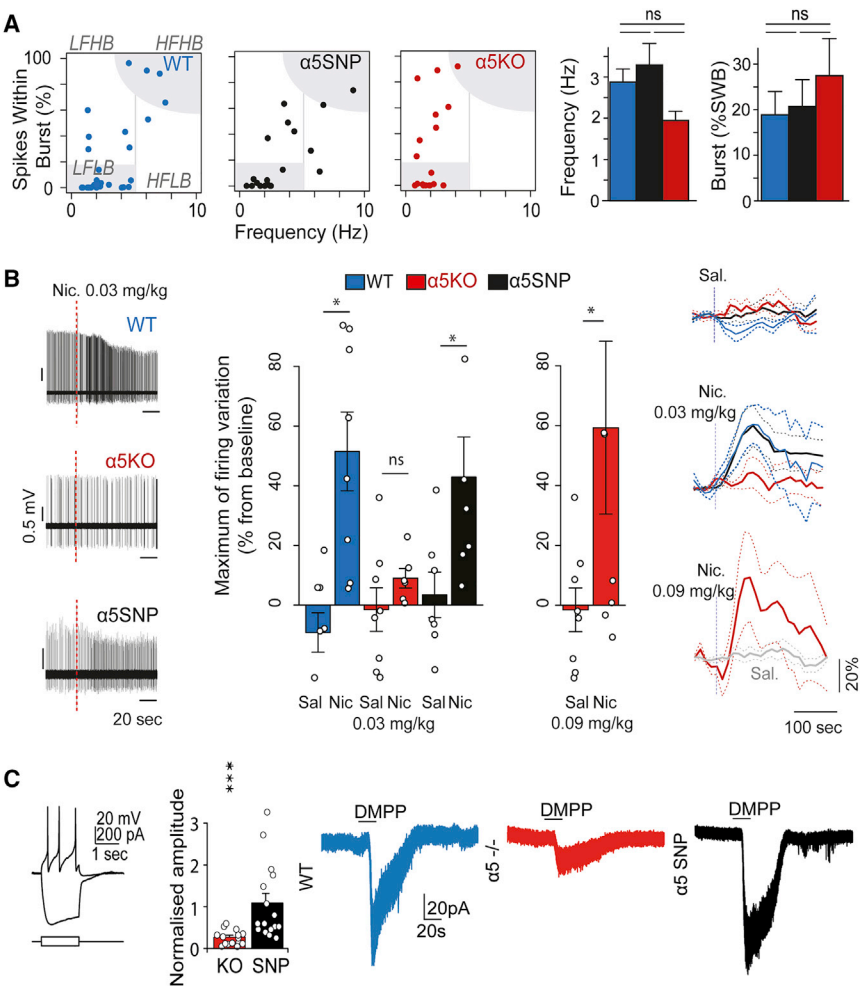

Figure 3. WT and α5SNP, but Not α5KO Rats, Have Dopamine Neurons that Respond to Low Nicotine

(A) Spontaneous VTA DA neuron frequency and bursting activity recorded *in vivo* in WT, α5SNP, and α5KO rats. Plot of mean firing frequency (Hz) against percentage of spikes within a burst (% SWB) for n = 34 individual cells in WT (blue), n = 19 in α5SNP (black), and n = 18 in α5KO (red) rats is shown; ns ($p > 0.05$; Wilcoxon test with corrections). Four main functional sub-populations are delineated by gray masks. These sub-populations are indicative of four different relationships between firing rate and %SWB (low firing low burst; low firing high burst; low firing high burst; high firing high burst).

(B) VTA DA neurons of WT and α5SNP rats respond to low dose of nicotine, and α5KO rats VTA DA neurons require higher nicotine. Left: typical electrophysiological recording depicting the changes in firing pattern elicited by 0.03 mg/kg intravenous (i.v.) nicotine injection (dashed line) in wild-type (WT), α5KO, and α5SNP rats is shown. Middle: DA cell firing activity at 0.03 mg/kg/injection for n = 34 individual cells in WT (blue), n = 19 in α5SNP (black), and n = 18 in α5KO (red) rats and at 0.09 mg/kg/injection for α5KO rats, compared to baseline is shown. Post hoc Wilcoxon test: $^*p < 0.05$. Right: mean ± SEM of increased response from baseline in firing activity of WT (blue), α5SNP (black), and α5KO (red) rats for indicated nicotine concentrations (time of injection indicated by vertical dashed blue lines) is shown. Mean and SEM are represented.

(C) VTA DA neurons of α5KO rats exhibit a lower response to a saturating dose of DMPP (100 μM) than WT and α5SNP rats. The left panel illustrates typical voltage responses of neurons to depolarizing and hyperpolarizing current pulses in acute slices. Middle: histogram of current responses normalized to the response in WT rat is shown. WT (n = 10) versus α5KO (n = 15): z = 141, $^{***}p = 0.00083$; α5KO versus α5SNP: z = 90.5, p = 0.00017; WT versus α5SNP (n = 16): z = 24.5, p = 0.59; NS; Mann-Whitney test. Right: local application of DMPP induces an inward current in voltage clamp recording of neurons from WT, α5KO, and α5SNP rats. Mean and SEM are represented.

See also STAR Methods.

activation [30], during nicotine-induced reinstatement of nicotine-seeking sessions in multiple brain areas (see STAR Methods). Nicotine-induced reinstatement of nicotine seeking was associated with an increase of c-Fos expression in several brain areas in both WT and α5SNP rats compared to saline condition (Figure 5A). Interestingly, a significantly higher expression was observed in the medial part of the lateral habenula (LHbm) and the lateral hypothalamus (LH) of α5SNP rats compared to WT rats (Figure 5B), two structures that have been previously associated with relapse to drug seeking [31, 32]. Conversely, a lower c-Fos expression was observed in the IPN of α5SNP compared to WT rats (Figures 5A and 5B), and the number of c-Fos-positive cells in the IPN was negatively correlated with the level of reinstatement of nicotine seeking (Figure 5C). Considering the high expression of the α5 nAChR subunit in the IPN (Figure 1C), these results suggest a major role of this structure in the participation of the rs16969968 polymorphism on nicotine-induced reinstatement of nicotine seeking. In order to investigate whether the lower activation of IPN neurons of α5SNP rats is related to the density of nicotinic currents in this structure, we recorded *ex vivo* the electrophysiological response to nicotine of IPN neurons of naive WT, α5SNP, and α5KO rats. We observed that nicotine-evoked currents were strongly reduced in both α5SNP and α5KO rats compared to WT rats, without a significant difference between α5SNP and α5KO rats (Figure 5D). This result indicates that the deficit in IPN neuron reactivity to nicotine in α5SNP rats is already present before chronic nicotine self-administration and may represent a constitutive predisposition factor for relapse to nicotine seeking.

DISCUSSION

Creation of the α5SNP and α5KO Rats

In humans, the α5SNP (rs16969968), which is frequent in the general population, has been robustly associated with an increased risk for nicotine dependence and lung cancer [6, 8, 9]. However, the type of behavior related to nicotine addiction affected by this polymorphism, such as acquisition, motivation for the drug or

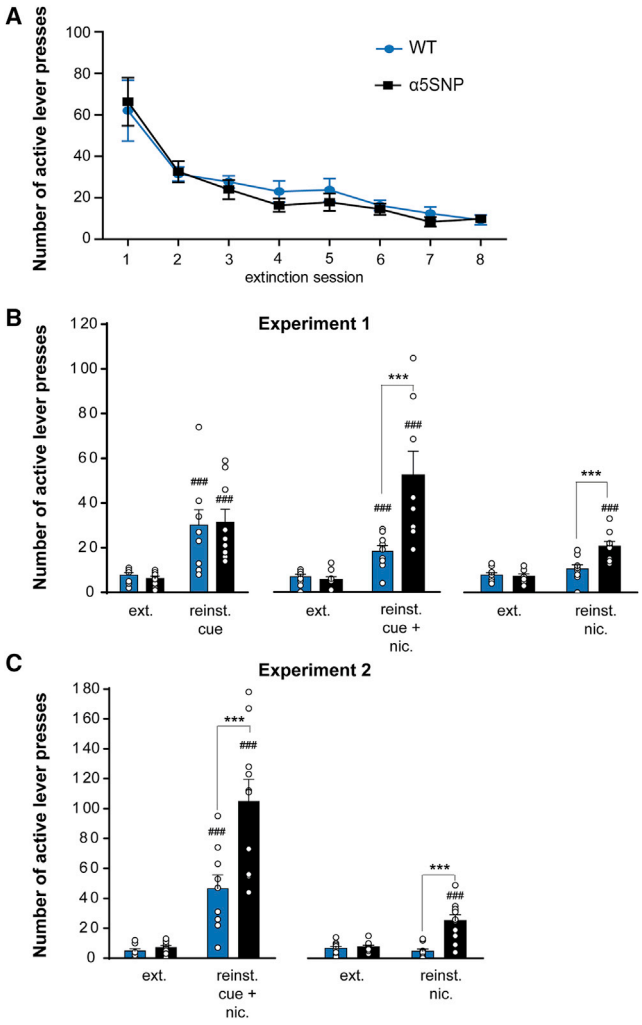

Figure 4. α5SNP Rats Exhibit Higher Nicotine-Induced Reinstatement of Nicotine Seeking Than WT Rats

(A) Extinction behavior of WT and α5SNP rats when nicotine and nicotine-associated cues where withheld (experiment 1; n = 9 per group). Two-way ANOVA, genotype effect: NS. Mean and SEM are represented.

(B) Reinstatement of nicotine seeking (active lever presses) after extinction (with saline-priming injections) induced by visual cue, cue + nicotine (0.1 mg/kg), and nicotine alone (0.1 mg/kg) in WT and α5SNP rats from experiment 1. The two-way ANOVA performed on cue-induced reinstatement (n = 9 per group) indicated a significant effect of reinstatement ($F_{1,16}$ = 32.9; p < 0.0001), but not of genotype ($F_{1,16}$ = 0.001; p = 0.97; NS) nor interaction ($F_{1,16}$ = 0.011; p = 0.74). ###p < 0.0001 on extinction versus reinstatement for both genotypes (Bonferroni's multiple comparison test). The two-way ANOVA performed on cue + nicotine-induced reinstatement (WT rats: n = 9; α5SNP rats: n = 8) indicated a significant effect of reinstatement ($F_{1,15}$ = 31.63; p < 0.0001), genotype ($F_{1,15}$ = 7.9; p = 0.0132), and interaction ($F_{1,15}$ = 11.66; p = 0.0038). Post hoc analysis (Bonferroni's multiple comparison test) WT versus α5SNP: p < 0.001 (***) on reinstatement (NS on extinction). ###p < 0.0001 on extinction versus reinstatement for both genotypes. The two-way ANOVA performed on nicotine-induced reinstatement (n = 9 per group) indicated a significant effect of reinstatement ($F_{1,16}$ = 27.6; p < 0.0001), genotype ($F_{1,16}$ = 8.2; p = 0.011), and interaction ($F_{1,16}$ = 11.95; p = 0.0033). Post hoc analysis (Bonferroni's multiple comparison test) WT versus α5SNP: p < 0.001 (***) on reinstatement (NS on extinction). ###p < 0.0001 on extinction versus reinstatement for α5SNP, but not WT rats (NS). Mean and SEM are represented.

(C) Reinstatement of nicotine seeking (active lever presses) after extinction (with saline-priming injections) induced by cue + nicotine (0.1 mg/kg) and nicotine alone (0.1 mg/kg) in WT and α5SNP rats from experiment 2. The two-way ANOVA performed on cue + nicotine-induced reinstatement (WT rats: n = 9; α5SNP rats: n = 10) indicated a significant effect of reinstatement ($F_{1,17}$ = 68.03; p < 0.0001), genotype ($F_{1,17}$ = 9.92; p = 0.0058), and interaction ($F_{1,17}$ = 11; p = 0.0041). Post hoc analysis (Bonferroni's multiple comparison test) WT versus α5SNP: p < 0.001 (***) on reinstatement (NS on extinction). ###p < 0.0001 on extinction versus reinstatement for both genotypes. The two-way ANOVA performed on nicotine-induced reinstatement (WT rats: n = 9; α5SNP rats: n = 10) indicated a significant effect of reinstatement ($F_{1,17}$ = 13.46; p = 0.0019), genotype ($F_{1,17}$ = 13.9; p = 0.0017), and interaction ($F_{1,17}$ = 21.42; p = 0.0002). Post hoc analysis (Bonferroni's multiple comparison test) WT versus α5SNP: p < 0.001 (***) on reinstatement (NS on extinction). ###p < 0.0001 on extinction versus reinstatement for α5SNP, but not WT rats (NS). Mean and SEM are represented.

See also Figure S5 and STAR Methods.

relapse, and the neuronal mechanism involved, are not perfectly understood.

Only transgenic mice have been used so far to study the role of distinct nicotinic receptor subtypes in behavioral and neurophysiological functions over the past decades, mostly because of the lack of tools to efficiently manipulate the rat genome. These studies showed that the lack of α5, constitutively or locally in the mHb, confers an increase of nicotine-SA at high doses [16, 17] and an increase in anxiety [33]. Interestingly, the expression of the α5SNP in the VTA or the hippocampus (Hpc) of α5KO mice did not fully restore the phenotypes, contrary to the re-expression of the WT α5 subunit [17, 33]. This can be explained by the partial loss of function of α5*nAChRs induced by the α5SNP as shown *in vitro* [6, 13–15]. Such studies have provided important information, but they did not model the human situation where the presence of the α5SNP is constitutive or investigate the impact of the α5SNP on relapse to nicotine seeking, a hallmark of nicotine addiction. Several technologies have been recently developed for targeted gene disruption in zygotes, including engineered nonspecific nucleases that are fused to sequence-specific DNA binding domains, such as ZFNs and transcription activator-like effector nucleases (TALENs), and CRISPR-associated Cas9 nucleases [22].

In the present study, we generated transgenic knockouts for the α5 nicotinic receptor subunit and knockin rats constitutively expressing the α5SNP using ZFN technology. At the optimal concentration and form (2 ng/μL, mRNA), the ZFN pair used for α5KO rats induced genetic modifications (mostly deletions from 10 to 184 bp) in 55% of the cases and the ZFN pair used for α5SNP rats co-administered with a homologous DNA template containing the α5SNP led to the creation of α5SNP rats with a rate of 11.5%. These rates are high and comparable to what has been obtained with the most recent CRISPR/Cas9 technique but without the frequent off-target effect usually associated with this technique [21, 22].

These results underscore the usefulness of using the genome-editing tools recently developed, and in particular the ZFN technology, to create better animal models of human conditions with good specificity in a short time frame.

These novel rat models allowed us to study the involvement of the α5 nAChR subunit and the rs16969968 polymorphism in

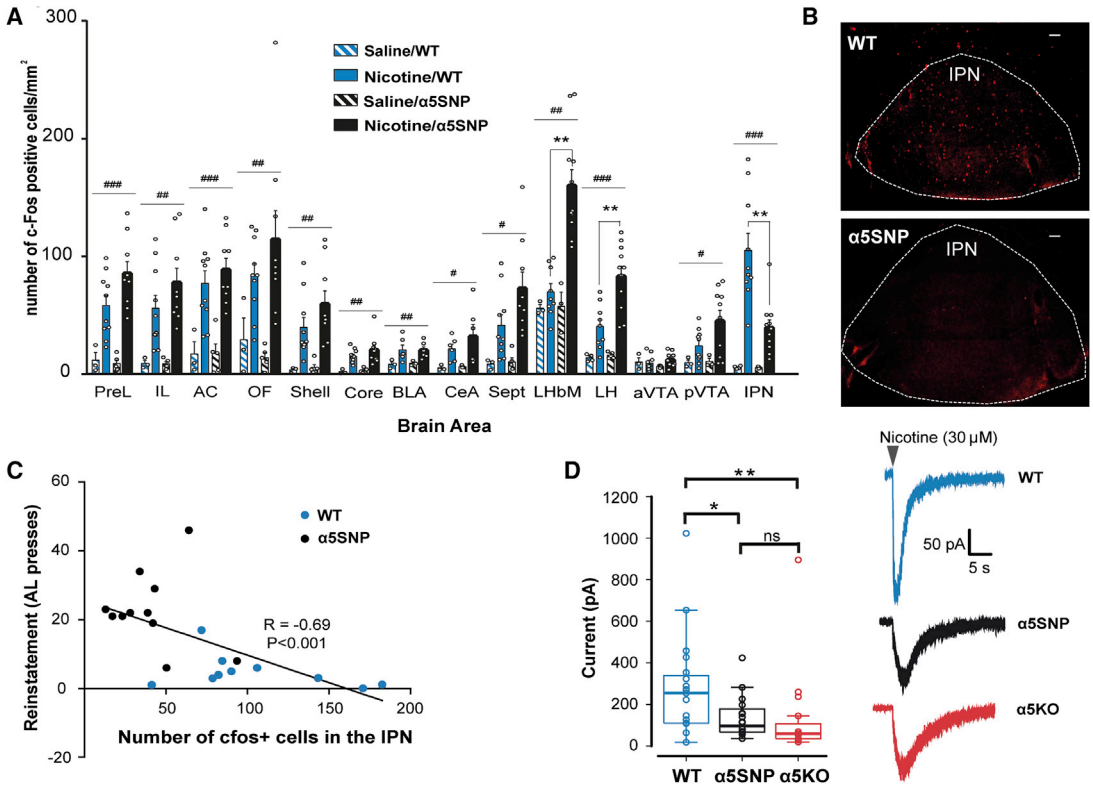

Figure 5. c-Fos Expression during Reinstatement of Nicotine Seeking in WT and α5SNP Rats and Nicotine-Induced Activity in the IPN of WT, α5KO, and α5SNP Rats

(A) Quantification of expression of the c-Fos protein (number of c-Fos-positive cells/mm^2) during nicotine-induced reinstatement of nicotine seeking or extinction with saline injection in WT and α5SNP rats. The two-way ANOVAs performed on the number of c-Fos-positive cells/mm^2 indicated a significant effect of treatment in the prelimbic cortex (PreL) ($F_{1,23}$ = 33.01; p < 0.0001), infralimbic cortex (IL) ($F_{1,23}$ = 19.46; p = 0.0002), anterior cingulate cortex (AC) ($F_{1,23}$ = 27.19; p < 0.0001), orbitofrontal cortex (OF) ($F_{1,23}$ = 13.54; p = 0.0012), shell and core of the nucleus accumbens (shell, $F_{1,23}$ = 16.19; p = 0.0005 and core, $F_{1,23}$ = 18.82; p = 0.0002), basolateral and central amygdala (BLA, $F_{1,14}$ = 9.85; p = 0.0073 and CeA $F_{1,14}$ = 6.76; p = 0.021), septum (Sept) ($F_{1,23}$ = 13.23; p = 0.014), medial part of the lateral habenula (LHbm) ($F_{1,22}$ = 14.6; p = 0.0009), lateral hypothalamus (LH) ($F_{1,24}$ = 28.09; p < 0.0001), posterior ventral tegmental area (pVTA) ($F_{1,22}$ = 6.7; p = 0.017), and interpeduncular nucleus (IPN) ($F_{1,24}$ = 23.2; p < 0.0001). The genotype and interaction (genotype X treatment) effects were only significant in the IPN ($F_{1,24}$ = 5.69, p = 0.025 and $F_{1,24}$ = 5.636, p = 0.026, respectively), the LHbm ($F_{1,22}$ = 9.181, p = 0.0061 and $F_{1,22}$ = 57.45, p = 0.0122, respectively), and the LH ($F_{1,24}$ = 6.41, p = 0.0183 and $F_{1,24}$ = 5.152, p = 0.0325, respectively). Post hoc analysis (Bonferroni's multiple comparison test) WT versus α5SNP: **p < 0.01 on reinstatement (NS on extinction with saline condition). Saline versus nicotine: ###p < 0.0001; ##p < 0.01; #p < 0.05. Mean and SEM are represented.

(B) Representative c-Fos immunofluorescence in the IPN (red) performed on brain slices of WT and α5SNP rats after nicotine-induced reinstatement of nicotine seeking test. The horizontal white bar represents 50 µm. This c-Fos expression has been observed in two independent experiments.

(C) Correlation between the number of c-Fos-positive cells in the IPN and the level of reinstatement during the nicotine-induced reinstatement of nicotine seeking test. WT rats (blue, n = 10) and α5SNP rats (black, n = 11) are shown. Two-tailed Spearman R = −0.69; p = 0.0005.

(D) *Ex vivo* nicotine-evoked current in IPN neurons of WT, α5SNP, and α5KO rats. Current amplitudes following a puff application of nicotine (30 µM, 200 ms) on IPN neurons were larger in WT rats (n = 19) than α5SNP (Holm-Bonferroni corrected U-test; n = 20; *p = 0.0486) and α5KO rats (n = 15; **p = 0.0092). The Kruskal-Wallis testing (one-way ANOVA; H-test) for the 3 group comparison shows a robust genotypic effect (p = 0.00387; chi-square = 11.1088 and df = 2).

See also STAR Methods.

behaviors more difficult to attain in mice models, such as long-term self-administration and reinstatement of nicotine seeking.

Phenotypes of α5SNP and α5KO Rats in Nicotine Self-Administration and Relapse

We showed that α5*nAChRs are necessary for the establishment of nicotine-SA and nicotine-induced activity of DA neurons in the VTA at 0.03 mg/kg. This is consistent with a previous report showing that α5KO mice are self-administering nicotine only at high doses and not when the dose is around 0.03 mg/kg/injection [17], but not with another study indicating that these mice acquire nicotine (0.03 mg/kg/injection) SA as well as WT mice [16], although it is difficult to extrapolate the efficiency of specific nicotine doses between mice and rats due to differences in nicotine metabolism [34]. Yet this observation supports the idea that α5*nAChRs strongly contribute to the sensitivity to nicotine as previously shown for several functions in mice [17, 33, 35].

In addition, α5SNP rats were able to acquire the nicotine-SA at 0.03 mg/kg as well as WT rats but self-administered significantly more nicotine at high doses in fixed and progressive ratio procedures. This result is in line with a previous study from our lab showing that the expression of the α5SNP in VTA's dopaminergic neurons of α5KO mice induced nicotine-SA at higher doses than with the re-expression of the WT subunit [17].

Thus, the increase in nicotine-SA at high doses might be due to the presence of the α5SNP in dopaminergic neurons of the VTA, but we cannot dismiss a potential role of the mHb in this effect, because it has been described as a key structure in the control of nicotine intake and aversion in mice [16, 36].

We also discovered that, although the α5SNP does not contribute to extinction behavior after chronic nicotine-SA or to cue-induced reinstatement of nicotine seeking, it reproducibly increases nicotine-induced reinstatement of nicotine seeking. This constitutes an important finding, considering the high frequency of relapse in nicotine addiction.

Taken together, our data demonstrate that the rs16969968 polymorphism is a major factor for nicotine intake at high doses and for relapse to nicotine seeking in rats, a dual effect that may explain the increased risk for nicotine dependence and delayed smoking cessation observed in humans [6, 8, 9].

Neuronal Activation during Nicotine-Induced Relapse: Implication of the IPN

Finally, we found that the α5SNP increased the neuronal activity in the LH and the medial division of the LHb during nicotine-induced reinstatement of nicotine seeking but decreased the neuronal activity in the IPN. The neuronal activity in the IPN was negatively correlated to the level of nicotine-induced reinstatement of nicotine seeking, suggesting an important role of this structure in the increase in relapse induced by nicotine in α5SNP rats. We also showed on brain slices that the rs16969968 polymorphism confers a profound deficit in the reactivity of IPN neurons to nicotine, comparable to the absence of the α5 subunit. This is in line with the decrease in the function of nAChRs in response to nicotine induced by the polymorphism, as previously reported in a study showing that the lack of α5 prevents nicotine-evoked elevations of intracellular-free calcium concentration and large-amplitude currents, a deficit that is not restored by the expression of the α5SNP [14]. In addition, an *in vitro* study found the α5SNP induces a reduced response to nicotinic agonists when extracellular calcium is high [37]. It also suggests that the deficit in reactivity to nicotine of IPN neurons represents a constitutive predisposition factor to relapse to nicotine seeking.

The IPN has been previously involved in avoidance of aversive stimuli [38, 39], locomotor activity [40], nicotine withdrawal [41] and sensitization [42], and morphine-, methamphetamine-, and nicotine-SA [43–45]. The IPN is a primarily GABAergic (>95%) [12] brain nucleus that contains the majority of the α5 nAChR subunit in the rat brain (Figure 1C) and projects, among others, to the LH [46]. Glutamatergic axons from the LH target glutamatergic neurons in the medial division of the LHb [47]. Interestingly, both LH and LHb have been involved in relapse to cocaine [32, 48–50], heroin [31], and alcohol [51–53] seeking. In addition, a recent study showed that the specific LH to LHb projection is necessary for regulating voluntary ethanol consumption [54]. Along this line, modulating the activity of IPN neurons may represent a novel research area to impact relapse to drugs of abuse.

In our study, activation of α5-containing GABAergic projection neurons in the IPN may inhibit the activity of the LH-LHbm circuit. This suggests that, in WT rats, activation by nicotine of α5-containing GABAergic projection neurons from this structure acts as a "brake" to limit relapse to nicotine seeking and that this brake is being lifted by the presence of the rs16969968 polymorphism.

Considering that the majority of nAChR α5 subunits are present in the IPN of the rat's brain, the development of a class of therapeutic compounds designed to specifically enhance the activity of α5*nAChRs, such as positive allosteric modulators, may represent a novel personalized strategy with high specificity to prevent relapse to tobacco smoking in populations carrying the rs16969968 polymorphism.

STAR★METHODS

Detailed methods are provided in the online version of this paper and include the following:

- KEY RESOURCES TABLE
- CONTACT FOR REAGENT AND RESOURCE SHARING
- EXPERIMENTAL MODEL AND SUBJECT DETAILS
  - Rats
- METHOD DETAILS
  - Creation of the α5KO and A5SNP rats
  - Immunoprecipitation
  - *In vivo* electrophysiological recordings
  - *Ex vivo* whole-cell patch clamp recordings
  - Nicotine self-administration
  - First self-administration experiment
  - Second self-administration experiment
  - c-Fos Immunofluorescence
- QUANTIFICATION AND STATISTICAL ANALYSIS
  - Immunoprecipitation
  - *In vivo* Electrophysiological data
  - *Ex vivo* whole-cell patch clamp recordings of IPN neurons
  - Nicotine self-administration
  - c-Fos counting

SUPPLEMENTAL INFORMATION

Supplemental Information includes five figures and can be found with this article online at https://doi.org/10.1016/j.cub.2018.08.044.

ACKNOWLEDGMENTS

We thank F. Marti for his help with the electrophysiological data analysis and David Godefroy for imaging using the nanozoomer (Institut de la Vision platform). This work was supported by the Institut Pasteur, Centre National de la Recherche Scientifique UMR 3571 and 8246, the programs PasteurInnov 2012 and PasteurInnov 2013, the Fondation de la Recherche Médicale (FRM) (grants SPF20140129365 and DPA20140629803 to U.M.), the Agence Nationale de la Recherche (ANR), ANR Neuroscience and ANR BLANC, Laboratoire d'Excellence LABEX BIO-PSY by the FP7 ERANET program NICO-GENE grant agreement convention ANR no. 2010-NEUR-004-01, the European Commission FP7 RTD Project HEALTH-2009-Neurocyp.08-202088 grant 242167, and French National Cancer Institute grant CANCEROPOLE IDF 2016-1-TABAC-01-IP-1 MASKOS (all to U.M.). This work was also supported by the ANR-JCJC Nicopto, a NARSAD Young Investigator Grant from the Brain and Behavior Research Foundation, and the Medisite Foundation to A.M. R.D.C. was supported by a Ph.D. fellowship from the DIM Cerveau and Pensee program of the Region Ile-de-France. The laboratories of U.M. and P.F. are part of the École des Neurosciences de Paris Ile-de-France RTRA network. U.M. and P.F. are members of the LABEX BIO-PSY. As such, this work was supported by French state funds managed

by the ANR within the Investissements d'Avenir programme under reference ANR-11-IDEX-0004-02.

AUTHOR CONTRIBUTIONS

B.F. designed the study; performed the behavioral experiments, the molecular work to create the transgenic rats, the immunofluorescence experiments, and c-Fos quantification; and wrote the manuscript. P.S. performed the immunoprecipitation experiments. F.L. supervised the experiments leading to the creation of the transgenic rats. C.M. performed the *in vivo* electrophysiology experiments. S.P. supervised the molecular work and participated in the writing of the manuscript. S.M. and R.D.C. performed the *ex vivo* electrophysiology of IPN neurons experiments. M.B. managed the rat colony and participated in the immunofluorescence experiments and in the writing of the manuscript. A.H. and L.T. performed the *ex vivo* electrophysiology of VTA neurons experiments (supervised by B.L.). A.M. supervised the *ex vivo* electrophysiology of IPN neurons experiments and participated in the writing of the manuscript. P.F. supervised the *in vivo* electrophysiology experiments and participated in the writing of the manuscript. U.M. supervised the study and participated in the writing of the manuscript.

DECLARATION OF INTERESTS

The authors declare no competing interests.

Received: May 9, 2018
Revised: July 9, 2018
Accepted: August 20, 2018
Published: October 4, 2018

REFERENCES

1. Peto, R., Lopez, A.D., Boreham, J., Thun, M., Heath, C., Jr., and Doll, R. (1996). Mortality from smoking worldwide. Br. Med. Bull. *52*, 12–21.
2. Changeux, J.P. (2010). Nicotine addiction and nicotinic receptors: lessons from genetically modified mice. Nat. Rev. Neurosci. *11*, 389–401.
3. Gotti, C., Zoli, M., and Clementi, F. (2006). Brain nicotinic acetylcholine receptors: native subtypes and their relevance. Trends Pharmacol. Sci. *27*, 482–491.
4. True, W.R., Heath, A.C., Scherrer, J.F., Waterman, B., Goldberg, J., Lin, N., Eisen, S.A., Lyons, M.J., and Tsuang, M.T. (1997). Genetic and environmental contributions to smoking. Addiction *92*, 1277–1287.
5. Bierut, L.J., Madden, P.A., Breslau, N., Johnson, E.O., Hatsukami, D., Pomerleau, O.F., Swan, G.E., Rutter, J., Bertelsen, S., Fox, L., et al. (2007). Novel genes identified in a high-density genome wide association study for nicotine dependence. Hum. Mol. Genet. *16*, 24–35.
6. Bierut, L.J., Stitzel, J.A., Wang, J.C., Hinrichs, A.L., Grucza, R.A., Xuei, X., Saccone, N.L., Saccone, S.F., Bertelsen, S., Fox, L., et al. (2008). Variants in nicotinic receptors and risk for nicotine dependence. Am. J. Psychiatry *165*, 1163–1171.
7. Sherva, R., Wilhelmsen, K., Pomerleau, C.S., Chasse, S.A., Rice, J.P., Snedecor, S.M., Bierut, L.J., Neuman, R.J., and Pomerleau, O.F. (2008). Association of a single nucleotide polymorphism in neuronal acetylcholine receptor subunit alpha 5 (CHRNA5) with smoking status and with 'pleasurable buzz' during early experimentation with smoking. Addiction *103*, 1544–1552.
8. Chen, L.S., Hung, R.J., Baker, T., Horton, A., Culverhouse, R., Saccone, N., Cheng, I., Deng, B., Han, Y., Hansen, H.M., et al. (2015). CHRNA5 risk variant predicts delayed smoking cessation and earlier lung cancer diagnosis–a meta-analysis. J. Natl. Cancer Inst. *107*, djv100.
9. Saccone, S.F., Hinrichs, A.L., Saccone, N.L., Chase, G.A., Konvicka, K., Madden, P.A., Breslau, N., Johnson, E.O., Hatsukami, D., Pomerleau, O., et al. (2007). Cholinergic nicotinic receptor genes implicated in a nicotine dependence association study targeting 348 candidate genes with 3713 SNPs. Hum. Mol. Genet. *16*, 36–49.
10. Jensen, K.P., DeVito, E.E., Herman, A.I., Valentine, G.W., Gelernter, J., and Sofuoglu, M. (2015). A CHRNA5 smoking risk variant decreases the aversive effects of nicotine in humans. Neuropsychopharmacology *40*, 2813–2821.
11. Wada, E., McKinnon, D., Heinemann, S., Patrick, J., and Swanson, L.W. (1990). The distribution of mRNA encoded by a new member of the neuronal nicotinic acetylcholine receptor gene family (alpha 5) in the rat central nervous system. Brain Res. *526*, 45–53.
12. Hsu, Y.W., Tempest, L., Quina, L.A., Wei, A.D., Zeng, H., and Turner, E.E. (2013). Medial habenula output circuit mediated by α5 nicotinic receptor-expressing GABAergic neurons in the interpeduncular nucleus. J. Neurosci. *33*, 18022–18035.
13. Kuryatov, A., Berrettini, W., and Lindstrom, J. (2011). Acetylcholine receptor (AChR) α5 subunit variant associated with risk for nicotine dependence and lung cancer reduces $(\alpha4\beta2)_2\alpha5$ AChR function. Mol. Pharmacol. *79*, 119–125.
14. Sciaccaluga, M., Moriconi, C., Martinello, K., Catalano, M., Bermudez, I., Stitzel, J.A., Maskos, U., and Fucile, S. (2015). Crucial role of nicotinic α5 subunit variants for Ca2+ fluxes in ventral midbrain neurons. FASEB J. *29*, 3389–3398.
15. Deflorio, C., Blanchard, S., Carisi, M.C., Bohl, D., and Maskos, U. (2017). Human polymorphisms in nicotinic receptors: a functional analysis in iPS-derived dopaminergic neurons. FASEB J. *31*, 828–839.
16. Fowler, C.D., Lu, Q., Johnson, P.M., Marks, M.J., and Kenny, P.J. (2011). Habenular α5 nicotinic receptor subunit signalling controls nicotine intake. Nature *471*, 597–601.
17. Morel, C., Fattore, L., Pons, S., Hay, Y.A., Marti, F., Lambolez, B., De Biasi, M., Lathrop, M., Fratta, W., Maskos, U., and Faure, P. (2014). Nicotine consumption is regulated by a human polymorphism in dopamine neurons. Mol. Psychiatry *19*, 930–936.
18. Parker, C.C., Chen, H., Flagel, S.B., Geurts, A.M., Richards, J.B., Robinson, T.E., Solberg Woods, L.C., and Palmer, A.A. (2014). Rats are the smart choice: rationale for a renewed focus on rats in behavioral genetics. Neuropharmacology *76 Pt B*, 250–258.
19. Kim, H., and Kim, J.S. (2014). A guide to genome engineering with programmable nucleases. Nat. Rev. Genet. *15*, 321–334.
20. Mani, M., Smith, J., Kandavelou, K., Berg, J.M., and Chandrasegaran, S. (2005). Binding of two zinc finger nuclease monomers to two specific sites is required for effective double-strand DNA cleavage. Biochem. Biophys. Res. Commun. *334*, 1191–1197.
21. Sander, J.D., and Joung, J.K. (2014). CRISPR-Cas systems for editing, regulating and targeting genomes. Nat. Biotechnol. *32*, 347–355.
22. Mashimo, T. (2014). Gene targeting technologies in rats: zinc finger nucleases, transcription activator-like effector nucleases, and clustered regularly interspaced short palindromic repeats. Dev. Growth Differ. *56*, 46–52.
23. Shaham, Y., Shalev, U., Lu, L., de Wit, H., and Stewart, J. (2003). The reinstatement model of drug relapse: history, methodology and major findings. Psychopharmacology (Berl.) *168*, 3–20.
24. Falvella, F.S., Alberio, T., Noci, S., Santambrogio, L., Nosotti, M., Incarbone, M., Pastorino, U., Fasano, M., and Dragani, T.A. (2013). Multiple isoforms and differential allelic expression of CHRNA5 in lung tissue and lung adenocarcinoma. Carcinogenesis *34*, 1281–1285.
25. Goodwin, A.K., Hiranita, T., and Paule, M.G. (2015). The reinforcing effects of nicotine in humans and nonhuman primates: a review of intravenous self-administration evidence and future directions for research. Nicotine Tob. Res. *17*, 1297–1310.
26. Donny, E.C., Caggiula, A.R., Mielke, M.M., Booth, S., Gharib, M.A., Hoffman, A., Maldovan, V., Shupenko, C., and McCallum, S.E. (1999). Nicotine self-administration in rats on a progressive ratio schedule of reinforcement. Psychopharmacology (Berl.) *147*, 135–142.
27. Paterson, N.E., and Markou, A. (2005). The metabotropic glutamate receptor 5 antagonist MPEP decreased break points for nicotine, cocaine and food in rats. Psychopharmacology (Berl.) *179*, 255–261.

28. Di Chiara, G., and Bassareo, V. (2007). Reward system and addiction: what dopamine does and doesn't do. Curr. Opin. Pharmacol. *7*, 69–76.
29. Subramaniyan, M., and Dani, J.A. (2015). Dopaminergic and cholinergic learning mechanisms in nicotine addiction. Ann. N Y Acad. Sci. *1349*, 46–63.
30. Hoffman, G.E., Lee, W.S., Smith, M.S., Abbud, R., Roberts, M.M., Robinson, A.G., and Verbalis, J.G. (1993). c-Fos and Fos-related antigens as markers for neuronal activity: perspectives from neuroendocrine systems. NIDA Res. Monogr. *125*, 117–133.
31. Zhang, F., Zhou, W., Liu, H., Zhu, H., Tang, S., Lai, M., and Yang, G. (2005). Increased c-Fos expression in the medial part of the lateral habenula during cue-evoked heroin-seeking in rats. Neurosci. Lett. *386*, 133–137.
32. Kallupi, M., de Guglielmo, G., Cannella, N., Li, H.W., Caló, G., Guerrini, R., Ubaldi, M., Renger, J.J., Uebele, V.N., and Ciccocioppo, R. (2013). Hypothalamic neuropeptide S receptor blockade decreases discriminative cue-induced reinstatement of cocaine seeking in the rat. Psychopharmacology (Berl.) *226*, 347–355.
33. Besson, M., Guiducci, S., Granon, S., Guilloux, J.P., Guiard, B., Repérant, C., Faure, P., Pons, S., Cannazza, G., Zoli, M., et al. (2016). Alterations in alpha5* nicotinic acetylcholine receptors result in midbrain- and hippocampus-dependent behavioural and neural impairments. Psychopharmacology (Berl.) *233*, 3297–3314.
34. Matta, S.G., Balfour, D.J., Benowitz, N.L., Boyd, R.T., Buccafusco, J.J., Caggiula, A.R., Craig, C.R., Collins, A.C., Damaj, M.I., Donny, E.C., et al. (2007). Guidelines on nicotine dose selection for in vivo research. Psychopharmacology (Berl.) *190*, 269–319.
35. Jackson, K.J., Marks, M.J., Vann, R.E., Chen, X., Gamage, T.F., Warner, J.A., and Damaj, M.I. (2010). Role of alpha5 nicotinic acetylcholine receptors in pharmacological and behavioral effects of nicotine in mice. J. Pharmacol. Exp. Ther. *334*, 137–146.
36. Frahm, S., Slimak, M.A., Ferrarese, L., Santos-Torres, J., Antolin-Fontes, B., Auer, S., Filkin, S., Pons, S., Fontaine, J.F., Tsetlin, V., et al. (2011). Aversion to nicotine is regulated by the balanced activity of β4 and α5 nicotinic receptor subunits in the medial habenula. Neuron *70*, 522–535.
37. Tammimäki, A., Herder, P., Li, P., Esch, C., Laughlin, J.R., Akk, G., and Stitzel, J.A. (2012). Impact of human D398N single nucleotide polymorphism on intracellular calcium response mediated by α3β4α5 nicotinic acetylcholine receptors. Neuropharmacology *63*, 1002–1011.
38. Wirtshafter, D. (1981). The role of interpeduncular connections with the tegmentum in avoidance learning. Physiol. Behav. *26*, 985–989.
39. Hammer, K.H., and Klingberg, F. (1990). Active avoidance is permanently abolished after lesions of the nucleus interpeduncularis in rat. Biomed. Biochim. Acta *49*, 489–497.
40. Thornton, E.W., Murray, M., Connors-Eckenrode, T., and Haun, F. (1994). Dissociation of behavioral changes in rats resulting from lesions of the habenula versus fasciculus retroflexus and their possible anatomical substrates. Behav. Neurosci. *108*, 1150–1162.
41. Salas, R., Sturm, R., Boulter, J., and De Biasi, M. (2009). Nicotinic receptors in the habenulo-interpeduncular system are necessary for nicotine withdrawal in mice. J. Neurosci. *29*, 3014–3018.
42. Eggan, B.L., and McCallum, S.E. (2017). α3β4 nicotinic receptors in the medial habenula and substance P transmission in the interpeduncular nucleus modulate nicotine sensitization. Behav. Brain Res. *316*, 94–103.
43. Glick, S.D., Ramirez, R.L., Livi, J.M., and Maisonneuve, I.M. (2006). 18-methoxycoronaridine acts in the medial habenula and/or interpeduncular nucleus to decrease morphine self-administration in rats. Eur. J. Pharmacol. *537*, 94–98.
44. Glick, S.D., Sell, E.M., and Maisonneuve, I.M. (2008). Brain regions mediating alpha3beta4 nicotinic antagonist effects of 18-MC on methamphetamine and sucrose self-administration. Eur. J. Pharmacol. *599*, 91–95.
45. Glick, S.D., Sell, E.M., McCallum, S.E., and Maisonneuve, I.M. (2011). Brain regions mediating α3β4 nicotinic antagonist effects of 18-MC on nicotine self-administration. Eur. J. Pharmacol. *669*, 71–75.
46. Antolin-Fontes, B., Ables, J.L., Görlich, A., and Ibañez-Tallon, I. (2015). The habenulo-interpeduncular pathway in nicotine aversion and withdrawal. Neuropharmacology *96* (Pt B), 213–222.
47. Poller, W.C., Madai, V.I., Bernard, R., Laube, G., and Veh, R.W. (2013). A glutamatergic projection from the lateral hypothalamus targets VTA-projecting neurons in the lateral habenula of the rat. Brain Res. *1507*, 45–60.
48. Meye, F.J., Soiza-Reilly, M., Smit, T., Diana, M.A., Schwarz, M.K., and Mameli, M. (2016). Shifted pallidal co-release of GABA and glutamate in habenula drives cocaine withdrawal and relapse. Nat. Neurosci. *19*, 1019–1024.
49. Gill, M.J., Ghee, S.M., Harper, S.M., and See, R.E. (2013). Inactivation of the lateral habenula reduces anxiogenic behavior and cocaine seeking under conditions of heightened stress. Pharmacol. Biochem. Behav. *111*, 24–29.
50. Friedman, A., Lax, E., Dikshtein, Y., Abraham, L., Flaumenhaft, Y., Sudai, E., Ben-Tzion, M., Ami-Ad, L., Yaka, R., and Yadid, G. (2010). Electrical stimulation of the lateral habenula produces enduring inhibitory effect on cocaine seeking behavior. Neuropharmacology *59*, 452–459.
51. Haack, A.K., Sheth, C., Schwager, A.L., Sinclair, M.S., Tandon, S., and Taha, S.A. (2014). Lesions of the lateral habenula increase voluntary ethanol consumption and operant self-administration, block yohimbine-induced reinstatement of ethanol seeking, and attenuate ethanol-induced conditioned taste aversion. PLoS ONE *9*, e92701.
52. Marchant, N.J., Rabei, R., Kaganovsky, K., Caprioli, D., Bossert, J.M., Bonci, A., and Shaham, Y. (2014). A critical role of lateral hypothalamus in context-induced relapse to alcohol seeking after punishment-imposed abstinence. J. Neurosci. *34*, 7447–7457.
53. Khoo, S.Y., Gibson, G.D., Prasad, A.A., and McNally, G.P. (2017). How contexts promote and prevent relapse to drug seeking. Genes Brain Behav. *16*, 185–204.
54. Sheth, C., Furlong, T.M., Keefe, K.A., and Taha, S.A. (2017). The lateral hypothalamus to lateral habenula projection, but not the ventral pallidum to lateral habenula projection, regulates voluntary ethanol consumption. Behav. Brain Res. *328*, 195–208.
55. David, R., Ciuraszkiewicz, A., Simeone, X., Orr-Urtreger, A., Papke, R.L., McIntosh, J.M., Huck, S., and Scholze, P. (2010). Biochemical and functional properties of distinct nicotinic acetylcholine receptors in the superior cervical ganglion of mice with targeted deletions of nAChR subunit genes. Eur. J. Neurosci. *31*, 978–993.
56. Scholze, P., Ciuraszkiewicz, A., Groessl, F., Orr-Urtreger, A., McIntosh, J.M., and Huck, S. (2011). α4β2 nicotinic acetylcholine receptors in the early postnatal mouse superior cervical ganglion. Dev. Neurobiol. *71*, 390–399.
57. Beiranvand, F., Zlabinger, C., Orr-Urtreger, A., Ristl, R., Huck, S., and Scholze, P. (2014). Nicotinic acetylcholine receptors control acetylcholine and noradrenaline release in the rodent habenulo-interpeduncular complex. Br. J. Pharmacol. *171*, 5209–5224.
58. Forget, B., Coen, K.M., and Le Foll, B. (2009). Inhibition of fatty acid amide hydrolase reduces reinstatement of nicotine seeking but not break point for nicotine self-administration–comparison with CB(1) receptor blockade. Psychopharmacology (Berl.) *205*, 613–624.
59. Forget, B., Pushparaj, A., and Le Foll, B. (2010). Granular insular cortex inactivation as a novel therapeutic strategy for nicotine addiction. Biol. Psychiatry *68*, 265–271.
60. Forget, B., Wertheim, C., Mascia, P., Pushparaj, A., Goldberg, S.R., and Le Foll, B. (2010). Noradrenergic alpha1 receptors as a novel target for the treatment of nicotine addiction. Neuropsychopharmacology *35*, 1751–1760.

Distinct dopamine circuits transmit the reinforcing and anxiogenic effects of nicotine

Authors

Nguyen C[1], Mondoloni S[1], Centeno I[1], Durand-de Cuttoli R[1], Tolu S[1], Valverde S[1], Le Borgne T[1], Hannesse B[1], Pons S[2], Maskos U[2], Dalkara D[3], Hardelin JP[1], Mourot A[1], Marti F[1#*] & Faure P[1#*]

Affiliations

[1] Sorbonne Université, Inserm, CNRS, Neuroscience Paris Seine - Institut de biologie Paris Seine (NPS - IBPS), 75005 Paris, France.

[2] Institut Pasteur, Unité Neurobiologie intégrative des systèmes cholinergiques, Département de neuroscience, 75724 Paris cedex, France.

[3] Sorbonne Université, Inserm, CNRS, Institut de la Vision, Paris, France.

[#] equal contributions

[*] Correspondence to fabio.marti@upmc.fr, phfaure@gmail.com

Summary

Nicotine, the addictive component of tobacco, stimulates dopamine (DA) neurons of the ventral tegmental area (VTA) to establish and maintain reinforcement. Nicotine also induces negative emotional states such as anxiety, yet through an unknown circuitry. Here we show that nicotine at reinforcing doses drives opposite functional responses on two distinct populations of VTA DA neurons with anatomically segregated projections: it activates those that project to the nucleus accumbens (NAc) while it inhibits those that project to the amygdala nuclei (Amg). We further show that nicotine, by acting on β2 subunit-containing nicotinic acetylcholine receptors of the VTA, mediates both reinforcement and anxiety. Finally, using optogenetic experiments we dissociate the roles of the VTA-NAc excitation and VTA-Amg inhibition in reinforcement and anxiety-like behavior, respectively. We thus propose that the positive and negative behavioral outcomes of nicotine consumption involve distinct subpopulations of VTA DA neurons with opposite responses to nicotine.

Keywords

nicotinic acetylcholine receptors; dopamine circuits; addiction; juxtacellular recordings; optogenetics; amygdala; nucleus accumbens; ventral tegmental area

Introduction

Nicotine is the principal addictive component that drives continued tobacco use. The initiation of addiction involves the mesocorticolimbic dopamine (DA) system, which contributes to the processing of rewarding stimuli during the overall shaping of successful behaviors (Schultz, 2007). It has been hypothesized that addictive drugs such as nicotine hijack the same mechanisms as reinforcement learning, leading to an overvaluation of the drug reward at the expense of natural rewards. While drug-induced reinforcement learning generally involves an increase in extracellular DA concentration in the nucleus accumbens (NAc), the underlying molecular and cellular mechanisms are drug dependent (Changeux, 2010; Di Chiara and Imperato, 1988; Luscher, 2016). Nicotine, for instance, exerts its reinforcing effects through the direct activation of nicotinic acetylcholine receptors (nAChRs), a family of pentameric ligand-gated ion channels (Changeux et al., 1998), on midbrain DA and GABA neurons, thus increasing the activity of both neuronal populations (Maskos et al., 2005; Morel et al., 2014; Tolu et al., 2013). Cell type-specific optogenetic manipulations have confirmed that DA cell activation is sufficient to drive the transition toward addiction, and established causal links between DA neuron activation and drug-adaptive behaviors (Pascoli et al., 2015). However, such view does not take into account the heterogeneity of midbrain DA neurons and the possibility that different messages can be transmitted in parallel from DA neurons of the ventral tegmental area (VTA). Indeed, VTA DA neurons belong to anatomically distinct circuits, differ in their molecular properties, and show diverse responses to external stimuli (Lammel et al., 2008; Poulin et al., 2018). DA neurons not only transmit signals related to salience and reward, but also to aversive stimuli (Brischoux et al., 2009; de Jong et al., 2019), including the negative effects of nicotine at high doses (Grieder et al., 2019; 2010). However, how DA neurons simultaneously transmit opposing signals in response to the same stimuli remains unclear. Whereas the vast majority of research teams that have examined nicotine-evoked responses report a homogenous activation of DA neurons and an increase in DA release in their projection areas (Di Chiara and Imperato, 1988; Grenhoff et al., 1986; Mansvelder and McGehee, 2000; Maskos et al., 2005; Picciotto et al., 1998; Zhao-Shea et al., 2011), other reports suggested that DA neuron responses to nicotine are more heterogeneous than previously thought (Eddine et al., 2015; Mameli-Engvall et al., 2006; Zhao-Shea et al., 2011). Therefore, a key issue is how the multiple effects of nicotine map onto the DA cell diversity, and whether nAChRs or other features can define different neuronal subpopulations that, through their response to nicotine, would influence specific behaviors.

Results

DA neurons in the VTA display opposite responses to acute nicotine injection

We performed single-cell electrophysiological recordings on anaesthetized mice, using an intravenous (IV) injection of a reinforcing dose of nicotine (30 µg/kg) (Morel et al., 2014), to record the responses of VTA DA neurons (n = 245). These neurons were first identified during the recording based on their electrophysiological properties (i.e., firing rate and action potential width (Mameli-Engvall et al., 2006; Ungless and Grace, 2012)), and then filled with neurobiotin by the juxtacellular labeling technique (Eddine et al., 2015; Pinault, 1996). All neurons were confirmed as DA neurons *post hoc* by immunofluorescence co-labeling with tyrosine hydroxylase (TH) (Figure 1A). Acute nicotine injections induced a significant variation, either positive or negative, of DA neuron firing rates (Figure 1B, left). Among the 245 DA neurons identified, some were activated (n = 155) whereas others were inhibited (n = 90) by the nicotine injection

compared to the control saline injection, as previously reported (Eddine et al., 2015). The amplitudes of nicotine-induced activation and inhibition were similar, at about ± 35 % from baseline (Figure 1B, right). We first sought to determine whether the opposing responses to nicotine injection between these DA neuron populations were associated with a difference in their spontaneous activity. The spontaneous activity of VTA DA neurons is characterized by their firing rate and the percentage of spikes within a burst (%SWB) (Mameli-Engvall et al., 2006). Bursts are classically identified as discrete events consisting of a sequence of spikes with (i) burst onset defined by two consecutive spikes within an interval < 80 ms and (ii) burst termination defined by an inter-spike interval > 160 ms (Grace and Bunney, 1984a; Ungless and Grace, 2012). We found that DA neurons activated or inhibited by the nicotine injection had similar firing rates (Δ = 0.3 Hz, p = 0.054), however the inhibited neurons showed more bursting activity than the activated ones (Δ = 5.1 %, p = 0.04) (Figure 1C, left). An analysis of the distribution of burst time intervals also highlighted different profiles in the distribution of interspike intervals depending on the burst length (Figure 1C, right). Other parameters describing cell spontaneous activity (e.g. coefficient of variation, burst length, …) were analyzed, but none of them revealed a difference between activated and inhibited DA neurons (not shown). We thus observed small differences in bursting activity between activated and inhibited DA neurons, but we were not able to predict their nicotine-evoked responses based on the analysis of their spontaneous activity, either by traditional classification procedures or by machine learning (Figure S1 A - C). We next asked whether these two populations are anatomically segregated. Neurobiotin-filled cell bodies of each recorded neuron were positioned onto slices of the Mouse Brain Atlas (Paxinos and Franklin, 2004) (Figure S1 D) to study their anatomical location. As illustrated by a single atlas plate schematic (bregma - 3.3 mm), anatomical coordinates suggested that the inhibited neurons were located more medially within the VTA than the activated neurons, independently of their antero-posterior or dorso-ventral positions (Figure 1D).

The two subpopulations of DA neurons in the VTA, activated or inhibited by nicotine injection, have distinct axonal projections to the nucleus accumbens or the amygdala

The DA system is heterogeneous, and is increasingly thought about in terms of anatomically and functionally distinct subnetworks (Watabe-Uchida et al., 2012). DA neurons in the VTA have been reported to project to different terminal regions based on their localization along the mediolateral axis (Beier et al., 2019; 2015; Lammel et al., 2008), thus we next investigated whether these two subpopulations belong to anatomically distinct dopamine circuits by probing the nicotine-evoked responses of DA neurons with identified projection sites. To do so, green retrobeads (RB), a retrograde tracer, were injected either in the nucleus accumbens (NAc: shell and core) or in the amygdala nuclei (Amg: basolateral and central amygdala) (Figure S2.1). Two weeks later, spontaneous and nicotine-evoked activity of VTA DA neurons were recorded *in vivo* in anesthetized mice, and then all neurons were labeled with neurobiotin. Triple labeling immunofluorescence allowed us to confirm *post hoc* the DA nature (TH+), projection site (RB+ / RB-), and position (NB+) of the recorded neurons (Figure 2A). We first noted that, in line with previous reports (Lammel et al., 2008), Amg-projecting DA neurons are located more medially in the VTA than NAc-projecting DA neurons (Figure S2.1). We identified 32 nicotine-activated and 17 nicotine-inhibited cells in mice with RB injected in the NAc, and 26 nicotine-activated and 26 nicotine-inhibited cells in mice with RB injected in the Amg (Figure 2B, E). For mice with RB injection in the NAc, 93% (28/30) of NAc-projecting VTA DA neurons (RB+, TH+) were activated by a nicotine injection, while 7% (2/30) of neurons were inhibited. In contrast, in these mice 79% (15/19) of DA neurons

without evidence for projection to the NAc (RB-, TH+) were inhibited by a nicotine injection, and only 21% (4/19) of RB- neurons were activated (Figure 2C). For mice with RB injection in the Amg, 86% (19/22) of Amg-projecting VTA DA neurons (RB+, TH+) were inhibited by a nicotine injection, while 14% (3/22) were activated. Whereas, in these mice, DA neurons without evidence for projection to the Amg (RB-, TH+) were mainly activated by a nicotine injection (77%, 23/30), with 23% (7/30) of neurons inhibited (Figure 2E, F). Overall, these results indicate that the majority of VTA DA neurons activated by nicotine injection project to the NAc, whereas the majority of VTA DA neurons inhibited by nicotine project instead to the Amg. We next took advantage of this anatomical distinction to analyze their respective electrophysiological properties in *ex vivo* patch-clamp recordings on coronal VTA slices with NAc-projecting DA cells or Amg-projecting DA cells labeled with RB (Figure S2.2). Amg-projecting DA neurons demonstrated higher excitability (Figure S2.2B) than NAc-projecting DA neurons, but no difference in nicotine-evoked currents was found between these two populations (Figure S2.2D). These results indicate that these two VTA DA cell populations have different membrane properties, but do not markedly differ in the expression or function of nAChRs.

The anxiogenic effect of nicotine injection involves β2 subunit-containing nAChRs in the VTA

We next asked whether these two distinct dopamine sub-circuits are associated with different behavioral outcomes after an acute injection of nicotine. Nicotine is known to have rewarding properties, through the activation of VTA DA neurons (Durand-de Cuttoli et al., 2018; Maskos et al., 2005; Tolu et al., 2013). Nicotine can also induce negative outcomes such as anxiety-like behaviors and stress-induced depressive-like states (Kutlu and Gould, 2015; Morel et al., 2017; Picciotto and Mineur, 2013). However, whether these negative effects are mediated by VTA DA neurons is unknown. We thus asked whether the anxiogenic effect of nicotine is mediated by VTA DA neurons, by analyzing mouse behavior in an elevated-O-maze (EOM). First, we found that mice injected with nicotine (intra-peritoneal, IP, 0.5 mg/kg) spent less time in the open arms of the EOM when compared to mice injected with saline, indicating that nicotine triggers anxiety-like behavior in mice (Figure 3A and Figure S3.1 for individual data). This anxiety-like phenotype was not related to a noticeable nicotine effect on locomotor activity (Figure S3.1). To provide evidence for a specific role of VTA neuron response to nicotine in this anxiogenic effect, we then locally infused nicotine into the VTA by a fixed implanted cannula, and found that, just as observed with the IP nicotine injection, these mice spent less time in the open arms of the EOM than those injected with saline (Figure 3B and Figure S3.1 for individual data). Local nicotine infusion in the VTA was therefore sufficient to trigger such anxiogenic effect. Finally, as nicotine-evoked responses have been shown to be mainly mediated by β2-containing nAChRs (β2*nAChRs) expressed on the soma of both DA and GABA neurons of the VTA (Tolu et al., 2013), we next assessed the role of β2*nAChRs within the VTA in mediating the anxiogenic effects of nicotine by using knock-out mice deleted for the nAChR β2 subunit ($\beta2^{-/-}$ mice). Electrophysiological recordings of VTA DA neurons in $\beta2^{-/-}$ mice demonstrated neither excitatory nor inhibitory responses to nicotine injection. In contrast, lentiviral re-expression of the β2 subunit restricted to the VTA of $\beta2^{-/-}$ mice ($\beta2^{-/-}$Vec mice), restored both excitatory and inhibitory responses to nicotine (Figure 3C). Finally, we found that $\beta2^{-/-}$ mice injected or not with GFP expressing virus (see Figure S3F) were impervious to the anxiogenic effect of nicotine in the EOM, as nicotine did not reduce the time spent by $\beta2^{-/-}$ mice in the open arms, but that this effect could be restored by re-expression of the β2 subunit within the VTA ($\beta2^{-/-}$Vec, Figure 3D). Together, these results indicate that both the activation or inhibition of VTA DA neurons by nicotine, as well as the anxiogenic effects of nicotine in the

EOM, require signaling through β2*nAChRs in the VTA. However, the present data do not allow us to conclude whether the anxiogenic effect of nicotine requires the activation of VTA DA neurons, their inhibition, or both types of response.

The two projection pathways of DA neurons of the VTA underlie opposite functions in reinforcement and anxiety

To dissociate whether nicotine-evoked activation or inhibition of VTA DA neurons is necessary for the behavioral effects of nicotine, one would ideally need to isolate these responses in DA neurons, as well as in VTA GABA neurons, which also express nAChRs (Grieder et al., 2019; Tolu et al., 2013). Because activation and inhibition by nicotine are concomitant and not easily isolable from one another, and because the responses of VTA DA and GABA neurons to nicotine are also tightly linked (Tolu et al., 2013), we decided to mimic each response separately with an optogenetic approach. We used a calcium translocating channelrhodopsin (CatCh (Kleinlogel et al., 2011) for activation and a red-shifted cruxhalorhodopsin (Jaws (Chuong et al., 2014)) for inhibition (Figure S4.1). Dopamine transporter (DAT)-Cre mice, in which Cre recombinase expression is restricted to DA neurons without disrupting endogenous DAT expression (Turiault et al., 2007; Zhuang et al., 2005), were bilaterally injected in the VTA with CatCh (AAV5-flox-EF1a-hCatCh-YFP), Jaws (pXR5-CAG-flex-Jaws-eGFP), or a control enhanced yellow fluorescent protein (eYFP) with no opsin (AAV5-flox-EF1a-YFP , Figure S4.2A-B), and optical fibers were implanted either in the Basolateral Amg (BLA, Figure S4.2C) or in the NAc lateral shell (NAcLSh, Figure S4.2D) of these mice to restrict the effects of optogenetic stimulation to DA terminals within these regions.

We first examined the effects of these manipulations in the EOM test. Light-evoked inhibition of DA neuron terminals in the BLA reduced the percentage of time spent by Jaws-expressing mice in the open arms of the EOM, while no effect of the light stimulation was detected in control mice expressing only eYFP (Figure 4A and Figure S4.3A for individual data). Light-evoked activation of DA terminals in the BLA showed the opposite effect, increasing the percentage of time spent by CatCh-expressing mice in the open arms of the EOM compared to mice expressing eYFP (Figure 4B and Figure S4.3B for individual data). In contrast, light-evoked activation of DA neuron terminals in the NAcLSh of CatCh-expressing mice had no effect on the time spent in the open arms of the EOM compared to control mice expressing eYFP (Figure 4C and Figure S4.3C for individual data), and there was no noticeable effect of the light-stimulation on locomotor activity in any of these groups of DAT-Cre mice (Figure S4.3D-F). To determine whether the anxiogenic effect observed during inhibition of DA neuron terminals in the BLA was specific to the BLA nuclei, we compared groups of WT mice injected with either Jaws or GFP in the VTA and implanted with bilateral optical-fibers either in the BLA or in the central amygdala (CeA), which both receive DA input (Figure S4.3). We found that inhibiting VTA neuron terminals decreased the percentage of time spent in the open arms of the EOM when optical fibers were implanted in the BLA, but not when they were implanted in the CeA (Figure S4.4). Finally, to directly link nicotine-evoked inhibition of DA neurons to its anxiogenic effect, we reasoned that an optogenetic activation of the BLA-projecting terminals of VTA DA neurons would counteract the nicotine-evoked inhibition of this pathway, and should therefore abolish the anxiogenic effect of the drug. Thus, DAT-Cre mice expressing CatCh in the VTA were injected with IP nicotine one minute before the EOM test, and received light stimulation in the BLA throughout the 9-minute test. Light-evoked activation of BLA DA terminals during the EOM abolished the anxiogenic effect of nicotine injection

in CatCh expressing mice when compared to eYFP expressing controls, which decreased the percentage of their time spent in the open arms after IP nicotine injection (Figure 4D).

We next investigated the effects of activating and inhibiting these two pathways on reinforcement using an online place preference paradigm (OPP). Activation of DA neuron terminals in the NAcLSh increased the preference score (percentage of time in ON – percentage of time in OFF) in mice expressing CatCh, indicating a rewarding effect of stimulating the VTA-NAcLSh pathway (Figure 4E). Light-evoked inhibition of DA neuron terminals in the BLA, however, reduced the preference score for the compartment where animals were photo-stimulated, and activation of these terminals showed no effect (Figure 4E).
Together, these results argue for a functional dissociation of these two pathways: inhibition of Amg-projecting DA neurons evokes anxiogenic effects, while activation of NAc-projecting DA neurons mediates reward but has no effect on anxiety-like behavior. Furthermore, we show that the VTA-BLA DA pathway is the substrate for the anxiogenic effect of nicotine.

Discussion

The VTA had long been perceived as a structure that broadly disseminates DA in the brain, with the different time courses of DA activity providing a phenomenological account for the functional involvement of DA neurons in different behavioral and neural processes (Schultz 2007). This temporal account of DA neuron function was gradually replaced or extended by the notion that the DA system, in particular the VTA, is divided into subpopulations of DA neurons, each associated with distinct appetitive, aversive, or attentional behaviors (Lammel et al., 2012). However, we are only beginning to appreciate how the functional activation/inactivation dynamics within these subpopulations impact behavioral and neural processes. Here, we show that activation and inhibition of VTA DA neurons appear concurrently as a consequence of nicotine injection. Furthermore, our results demonstrate that these activation/inhibition processes correspond to two anatomically and functionally distinct circuits, which mediate contrasting behavioral effects.

VTA DA neurons are known to be heterogeneous in their axonal projections, electrophysiological properties, and in several molecular features. They show for example striking differences in their expression of hyperpolarization-activated cyclic nucleotide-gated cation channels (HCN), the dopamine transporter (DAT), the dopamine receptor D2R, or vesicular glutamate transporters (VGLUTs) (Lammel et al., 2008; Margolis et al., 2008; Morales and Margolis, 2017). However, the role and the functional consequences of VTA DA neuron heterogeneity in behavior remain poorly understood. Here, we have demonstrated that nicotine evokes opposite responses in two distinct subpopulations of VTA DA neurons, those that project their axons to the NAc are activated by nicotine, while those that project to the Amg are inhibited. In addition to their functional and anatomical segregation, we found that these subpopulations display different bursting activities *in vivo*, and different excitabilities *in vitro*. However, they cannot be distinguished solely on the basis of their spontaneous firing pattern in anesthetized mice. Are there specific differences between these two neuronal populations, beside their projection sites, that would underlie their opposing responses to nicotine injection? NAc-projecting DA neurons exhibit smaller I_h currents than BLA-projecting DA neurons, but have similar input resistances and capacitances (Ford et al., 2006), and similar expressions of DAT, D2R and TH (Su et al., 2019). We have previously reported that activated and inhibited DA cells react similarly to D2R agonist or antagonist injection *in vivo*, which is

also consistent with similar D2R expression levels in the two neuronal populations (Eddine et al., 2015). Finally, there is no clear variation in nicotine-evoked currents in Amg or NAc-projecting DA cells, suggesting that nAChR expression does not differ markedly between these populations. Overall, we did not find striking evidence of intrinsic differences between NAc-projecting or Amg-projecting VTA DA neurons that could explain their differences in the nicotine-evoked responses. While differences may exist, it is also possible that the emergence of either nicotine-evoked activation or inhibition of these neurons arises from network dynamic. Within the VTA, nicotine directly activates both DA and GABA neurons, as they each express nAChRs (Klink et al., 2001; Tolu et al., 2013). In particular, β2*nAChRs of the VTA are key mediators of the positive reinforcing effects of nicotine, as previously shown by re-expressing β2 locally in the VTA of $\beta2^{-/-}$ mice (Maskos et al., 2005; Tolu et al., 2013), or by rendering β2*nAChRs insensitive to nicotine using light (Durand-de Cuttoli et al., 2018). Here, we show that β2*nAChRs of VTA neurons are also required to evoke the inhibition of the VTA-Amg DA neuron subpopulation after systemic nicotine injection. Therefore, nicotine acting through β2*nAChRs activates VTA GABAergic interneurons and DA neurons that project to the NAc, while simultaneously inhibiting DA neurons projecting to the Amg. Several independent mechanisms may explain the inhibitory effect of nicotine on this subpopulation. These include (1) the activation of GABAergic interneurons that would, in turn, inhibit specifically this VTA DA neuron subpopulation; (2) inhibition through local DA release (Eddine et al., 2015), even though no difference in D2R-mediated inhibitory postsynaptic currents or in DA reuptake between NAc-projecting and BLA-projecting DA neurons has been reported (Ford et al., 2006); or (3) feedback inhibition. Indeed, subpopulations of DA neurons are embedded within distinct inhibitory networks resulting in specific feedback loops between VTA and NAc subregions (de Jong et al., 2019). NAc-projecting DA neurons could therefore inhibit DA neurons projecting to the Amg through an as yet unknown striatal relay.

Nicotine is highly reinforcing, but also generates aversive and anxiogenic effects at various doses (Balerio et al., 2006; Kutlu and Gould, 2015; Picciotto and Mineur, 2013; Wolfman et al., 2018). Thus, depending on the context, the exact same dose of nicotine can trigger anxiety and/or reinforcement. Aversion for high doses of nicotine and anxiety associated with nicotine withdrawal have been attributed to nicotinic and glutamatergic signaling in the habenulo-interpeduncular axis (Fowler et al., 2011; Frahm et al., 2011; Molas et al., 2017; Zhao-Shea et al., 2013). There is also evidence that nAChRs of neurons located in the Amg modulate depressive-like states (Mineur et al., 2016). However, a role for DA in aversion has also been proposed. D1R and D2R antagonists prevent conditioned-place aversion induced by an acute high-dose nicotine injection (Grieder et al., 2012), and β2*nAChRs were shown to be necessary for both the aversive and rewarding effects of nicotine using a subunit re-expression strategy in VTA DA and GABAergic neurons of $\beta2^{-/-}$ mice (Grieder et al., 2019). However, the mechanism underlying these opposite effects of the drug has not yet been established. Here, we show that activation of β2*nAChRs of VTA neurons is necessary for nicotine to inhibit Amg-projecting DA neurons and induce anxiety-like behavior. This indicates that DA signaling is critically involved in the acute anxiogenic effect of nicotine and could also mediate aversion to nicotine. Moreover, injections of nicotine at the doses used in this study are known to be rewarding in different paradigms in mice, which has been attributed to VTA DA neuron activation (Durand-de Cuttoli et al., 2018; Maskos et al., 2005; Tolu et al., 2013). Overall, our study shows that the same intake of nicotine can induce a rewarding effect by activating the VTA-NAc dopamine pathway, and simultaneously signal a negative emotional state by inhibiting the VTA-Amg dopamine pathway.

Our findings emphasize the complex role of the DA system in not only positive but also negative motivational processes, and promote a more nuanced view of the effects of reinforcing doses of nicotine on VTA DA neurons. Opposing responses of DA neurons to drug exposure have also been observed with cocaine (Mejias-Aponte et al., 2015), ethanol (Doyon et al., 2013), and morphine (Margolis et al., 2014). Notably, the inhibition induced by opioids differs in BLA-projecting and NAc-projecting VTA DA neurons (Ford et al., 2006), suggesting that the behavioral effects of opioid drugs could also result from a specific pattern of inhibition in these two pathways. Since our results demonstrate that both rewarding and anxiogenic messages occur simultaneously upon nicotine exposure, and are conveyed by distinct subpopulations of VTA DA neurons, the question then arises as to how the concurrent engagement of two circuits with opposing messages could compete to produce nicotine reinforcement, and whether an imbalance between the two would lead to addiction. Indeed, this question may prove critical when it comes to medical strategies aimed at smoking cessation. While the optogenetic strategies used in this study are well suited to mimic the individual effects of a drug that also produces strong and synchronized neuronal activity, the translational value of these effects is perhaps not to be sought in the specific activation or inhibition of a given neuronal pathway, but rather in the functional imbalance that this creates between the target structures of VTA neurons. Nevertheless, a detailed understanding of the multiple pathways engaged in nicotine-evoked responses and of their respective behavioral contributions can still help us understand the mechanisms leading to nicotine addiction. In this respect, the activation and inhibition processes which appear in VTA DA neurons as a consequence of systemic nicotine injection call for further mechanistic studies, but we show that they correspond to discrete neuronal circuits and that they mediate distinct behavioral effects, both of which are relevant to the understanding of addiction.

Acknowledgements:
We thank Lauren Reynolds for critical reading of the manuscript. We are grateful to France Lam and the imaging platform facility (IBPS), the animal facilities (IBPS), Victor Gorgievski for behavioral data acquisition. We are grateful to Mélissa Desrosiers, Camille Robert and Paris Vision Institute AAV production facility for viral production and purification.
This work was supported by the Centre National de la Recherche Scientifique CNRS UMR 8246, INSERM U1130, the Foundation for Medical Research (FRM, Equipe FRM DEQ2013326488 to P.F), FRM FDT201904008060 (to SM), the French National Cancer Institute Grant TABAC-16-022 et TABAC-19-020 (to P.F.), French state funds managed by the ANR (ANR-16 Nicostress to PF, ANR-19 Vampire to FM), The LabEx Bio-Psy (to P.F and Doctoral Fellowship to CNG). PF and UM are members of LabEx Bio-Psy.

Author contributions:
C.N., F.M. and P.F. designed the study. C.N., F.M. and P.F. analyzed the data. C.N. and F.M. performed *in vivo* electrophysiological recordings. S.T. and S.V. contributed to *in vivo* electrophysiological recordings. S.M. performed *ex vivo* patch-clamp recordings and data analyses. T.L.B. contributed to *in vivo* electrophysiological data analyses. C.N. performed injections, fiber and cannula implantations. C.N. and I.C performed behavioral experiments. S.M. and B.H. contributed to behavioral experiments. R.D.C and A.M contributed to optogenetic experiments. C.N and S.M. performed immunostaining experiments. D.D., S.P. and U.M. provided viruses. U.M. provided ACNB2 KO mice. C.N., J.P.H., A.M., F.M. and P.F. wrote the manuscript.

Declaration of interests: Authors declare no competing financial interests.

Figure Legends

Figure 1: Nicotine evoked opposite responses in DA neurons of the VTA

(A) Intravenous (IV) injections of nicotine (Nic, 30 µg/kg) induce activation and inhibition of distinct VTA DA cells. Post-recording identification of neurobiotin (NB)-labeled VTA DA neurons by immunofluorescence (TH = tyrosine hydroxylase, NB = streptavidin-AMCA against neurobiotin). **(B)** *Left*: Cumulative distribution of responses after IV injection of either saline (Sal, grey, n = 233) or nicotine (Nic, black, n = 245) (Kolmogorov-Smirnov test *** $p < 0.001$). *Center*: Time course for the average change in firing frequency upon nicotine injection for activated (red, n = 155) and inhibited (blue, n = 90) VTA DA neurons. *Right*: Average amplitude of the nicotine response for activated (red, mean = 33.75 $\pm$ 52 %) and inhibited DA neurons (blue, mean = -35.42 $\pm$ -2 %), compared to saline injection (grey, n = 147 and 86, respectively) (Wilcoxon test *** $p < 0.001$). **(C)** Analysis of the spontaneous activity of NB-labeled DA neurons that were either activated (red) or inhibited (blue) by the nicotine injection. *Left*: Basal firing rates between activated and inhibited neurons were not statistically different (Wilcoxon test $p = 0.054$) but nicotine-inhibited neurons displayed higher percentage of spikes-within-burst (%SWB) than activated ones. (Wilcoxon test * $p = 0.04$). *Right:* Interval between SWB (in ms) as a function of the length of the burst (from two to six action potentials). **D)** Localization of NB-labeled, nicotine-activated and -inhibited DA neurons, positioned on the Paxinos atlas at bregma - 3.3 mm. Nicotine-inhibited neurons had a more medial distribution in the VTA than the nicotine-activated subpopulation (Wilcoxon test *** $p < 0.001$), but neither antero-posterior (Wilcoxon test $p = 0.4$) nor dorso-ventral (Wilcoxon test $p = 0.5$) differences in their distribution were observed.

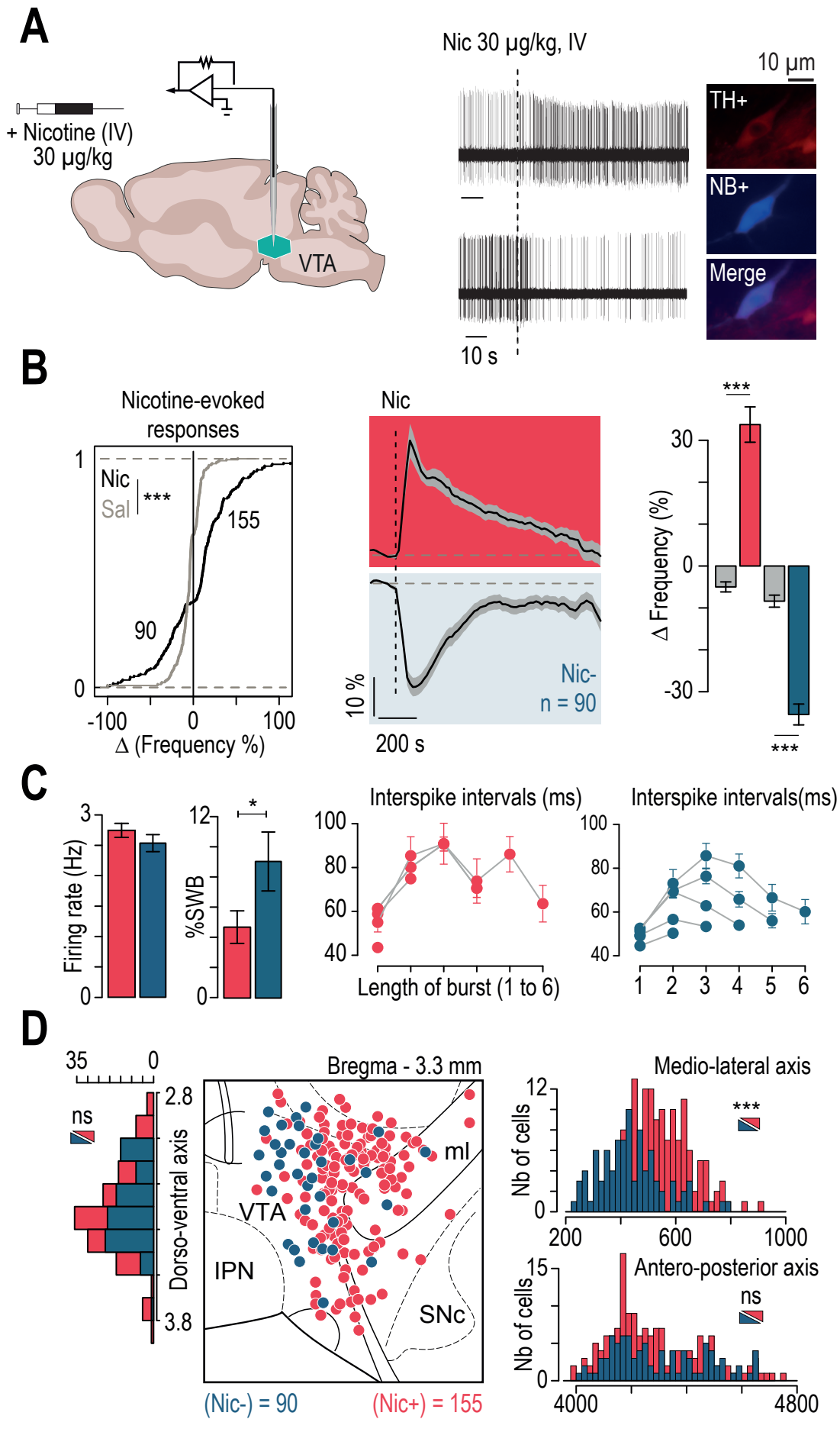
A
+ Nicotine (IV)
30 µg/kg
VTA
Nic 30 µg/kg, IV
10 s
10 µm
TH+
NB+
Merge
B
Nicotine-evoked responses
Nic
Sal
***
155
90
1
0
-100
0
100
Δ (Frequency %)
Nic
10 %
200 s
Nic-
n = 90
***
30
0
-30
Δ Frequency (%)
***
C
Firing rate (Hz)
3
0
%SWB
12
0
*
Interspike intervals (ms)
100
80
60
40
Length of burst (1 to 6)
Interspike intervals(ms)
1 2 3 4 5 6
D
35
0
ns
2.8
3.8
Dorso-ventral axis
Bregma - 3.3 mm
ml
VTA
IPN
SNc
(Nic-) = 90
(Nic+) = 155
Medio-lateral axis
Nb of cells
12
0
***
200
600
1000
Antero-posterior axis
15
0
ns
4000
4800

Figure 1

Figure 2: Nicotine evoked opposite responses in VTA DA neurons that project to the NAc or to the Amg

(A) Retrobeads (RB) were injected in the NAc, and VTA DA neuron responses to an IV nicotine injection were recorded *in vivo,* and labeled with neurobiotin. DA neurons that project to the NAc were identified *post-hoc* by immunofluorescent co-labeling of TH, NB and RB. **(B)** Localization of NB-labeled DA neurons (NB+ TH+, n = 49) following RB injection (●RB+, ○ RB-) into the NAc. Red and blue colors denote nicotine-activated neurons (Nic+) and -inhibited neurons (Nic-), respectively. (RB+ Nic+, n = 28; RB+ Nic-, n = 2; RB- Nic+, n = 4; RB- Nic-, n = 15). **(C)** *Top:* Percentage and number of Nic+ (red) and Nic- (blue) cells among NAc-projecting DA neurons (RB+). Mean change in firing frequency of NAc-projecting DA neurons in response to an IV injection of nicotine (red) or saline (black). *Bottom*: Percentage and number of Nic+ (red) and Nic- (blue) cells in non RB-labeled neurons (RB-). Mean change in firing frequency of RB- DA neurons in response to an IV injection of nicotine (red) or saline (black). **(D)** In separate experiments, RBs were injected in the Amg, and two weeks later VTA DA neuron responses to an IV Nic injection were recorded *in vivo,* and neurons were subsequently labeled with neurobiotin. Amg-projecting DA neurons were identified *post hoc* by immunofluorescent co-labeling of TH, NB and RB. **(E)** Localization of NB-labeled DA neurons (NB+ TH+, n = 52) following RB injection into the Amg. (RB+ Nic+, n = 3; RB+ Nic-, n = 19; RB- Nic+, n = 23; RB- Nic-, n = 7). **(F)** *Top:* Same than (C) for AMg-projecting DA neurons. *Bottom:* Same than (C) for non RB-labeled neurons when RB were injected in the AMg

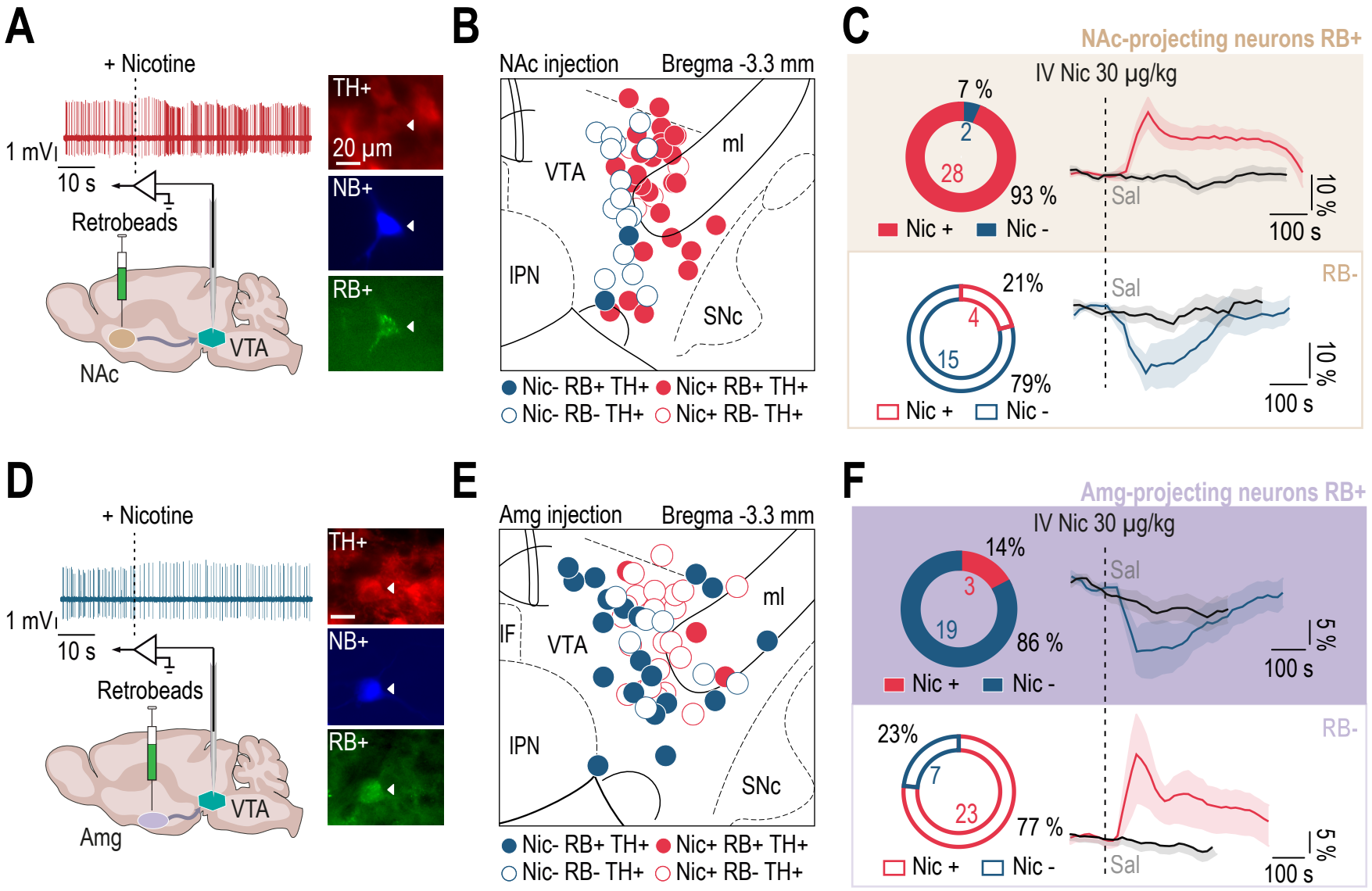
A
+ Nicotine
1 mV
10 s
Retrobeads
NAc
VTA
TH+
20 µm
NB+
RB+
B
NAc injection
Bregma -3.3 mm
VTA
ml
IPN
SNc
Nic- RB+ TH+
Nic+ RB+ TH+
Nic- RB- TH+
Nic+ RB- TH+
C
NAc-projecting neurons RB+
IV Nic 30 µg/kg
7 %
2
28
93 %
Nic +
Nic -
Sal
10 %
100 s
RB-
21%
4
15
79%
D
+ Nicotine
1 mV
10 s
Retrobeads
Amg
VTA
TH+
NB+
RB+
E
Amg injection
Bregma -3.3 mm
IF
VTA
ml
IPN
SNc
Nic- RB+ TH+
Nic+ RB+ TH+
Nic- RB- TH+
Nic+ RB- TH+
F
Amg-projecting neurons RB+
IV Nic 30 µg/kg
14%
3
19
86 %
Nic +
Nic -
Sal
5 %
100 s
RB-
23%
7
23
77 %
Nic +
Nic -
Sal
5 %
100 s

Figure 2

Figure 3: β2 subunit-containing nAChRs mediated both VTA DA neuron responses to nicotine injection and nicotine-induced anxiogenic effects.

(A) Nicotine (Nic, 0.5 mg/kg) or saline (Sal) were injected intraperitoneally (IP) 1 minute before the 9-minute elevated O-maze (EOM) test. In wild-type (WT) mice (n = 21), nicotine injection decreased the time spent in the open arms of the EOM compared to the group injected with Sal (n = 23) (two-way RM ANOVA main effect of time $F_{(2,84)} = 3.84$, * p = 0.025, treatment x time interaction $F_{(2,84)} = 5.37$, ** p = 0.006; *post hoc* Wilcoxon test with Bonferroni corrections * p (3 vs 9 minutes) = 0.03, p (3 vs 6 minutes) = 0.1, p (6 vs 9') = 0.2; *post hoc* Wilcoxon test Sal vs Nic at 9 minutes *** p < 0.001). **(B)** Same than (A) for intracranial infusion of either Sal (n=6) or Nic (100 ng in 100 nl infusion over 1 minute before the test, n=7) (two-way RM ANOVA main effect of time $F_{(2,22)} = 12.48$, *** p < 0.001, treatment x time interaction $F_{(2,22)} = 9.66$, *** p < 0.001; *post hoc* Student's t-test with Bonferroni corrections: *** p (3 vs 9 minutes) < 0.001, * p (3 vs 6 minutes) = 0.03, * p (6 vs 9 minutes) = 0.02; *post hoc* Student's t-test Sal vs Nic at 9 minutes, p = 0.054). **(C)** *Left*: Juxtacellular recording traces of VTA DA neurons in mice deleted for the β2 nAChR subunit ($\beta2^{-/-}$) and $\beta2^{-/-}$Vec mice. Mean firing frequency variation indicated no nicotine-evoked responses in VTA DA neurons of $\beta2^{-/-}$ mice (n = 46 cells from 12 mice), and that responses were restored in $\beta2^{-/-}$Vec mice (nicotine-evoked : activation Δ+, n = 51 cells from 18 mice ; and inhibition Δ-, n = 39 cells from 19 mice). *Right*: Immunofluorescence for TH and GFP on $\beta2^{-/-}$Vec mice. Cumulative distribution of nicotine-evoked response amplitude of VTA DA neurons in $\beta2^{-/-}$ mice (n = 46 cells from 12 mice, grey) and $\beta2^{-/-}$Vec mice (n = 90 cells from 24 mice, black) (Kolmogorov-Smirnov test ** p = 0.008). Bar plots show the maximum firing variation induced by nicotine (filled bars) and saline (unfilled bars) in the two groups. Nicotine injection did not alter the firing frequency of VTA DA neurons in $\beta2^{-/-}$ mice, but induced a significant increase (mean 12.45 ± 13.37) or decrease (mean -13.16 ± 16.31) in $\beta2^{-/-}$Vec mice compared to saline or $\beta2^{-/-}$ mice (Wilcoxon paired tests with Bonferroni corrections *** p < 0.001 and ** p = 0.005) **(D)** IP nicotine injection (0.5 mg/kg) in the EOM, for a control group (n = 23, brown) of $\beta2^{-/-}$ mice in which some were injected in the VTA with GFP (n = 6/23) and for $\beta2^{-/-}$Vec mice (n = 18, green). Re-expression of β2 subunit in the VTA restored the nicotine-evoked anxiogenic effects in the EOM, which were absent in the $\beta2^{-/-}$GFP mice (two-way RM ANOVA main effect of time $F_{(2,78)} = 6.87$, ** p = 0.002, treatment x time interaction $F_{(2,78)} = 3.43$, * p = 0.04; *post hoc* Student's t-test with Bonferroni corrections ** p < 0.01 and * p < 0.05).

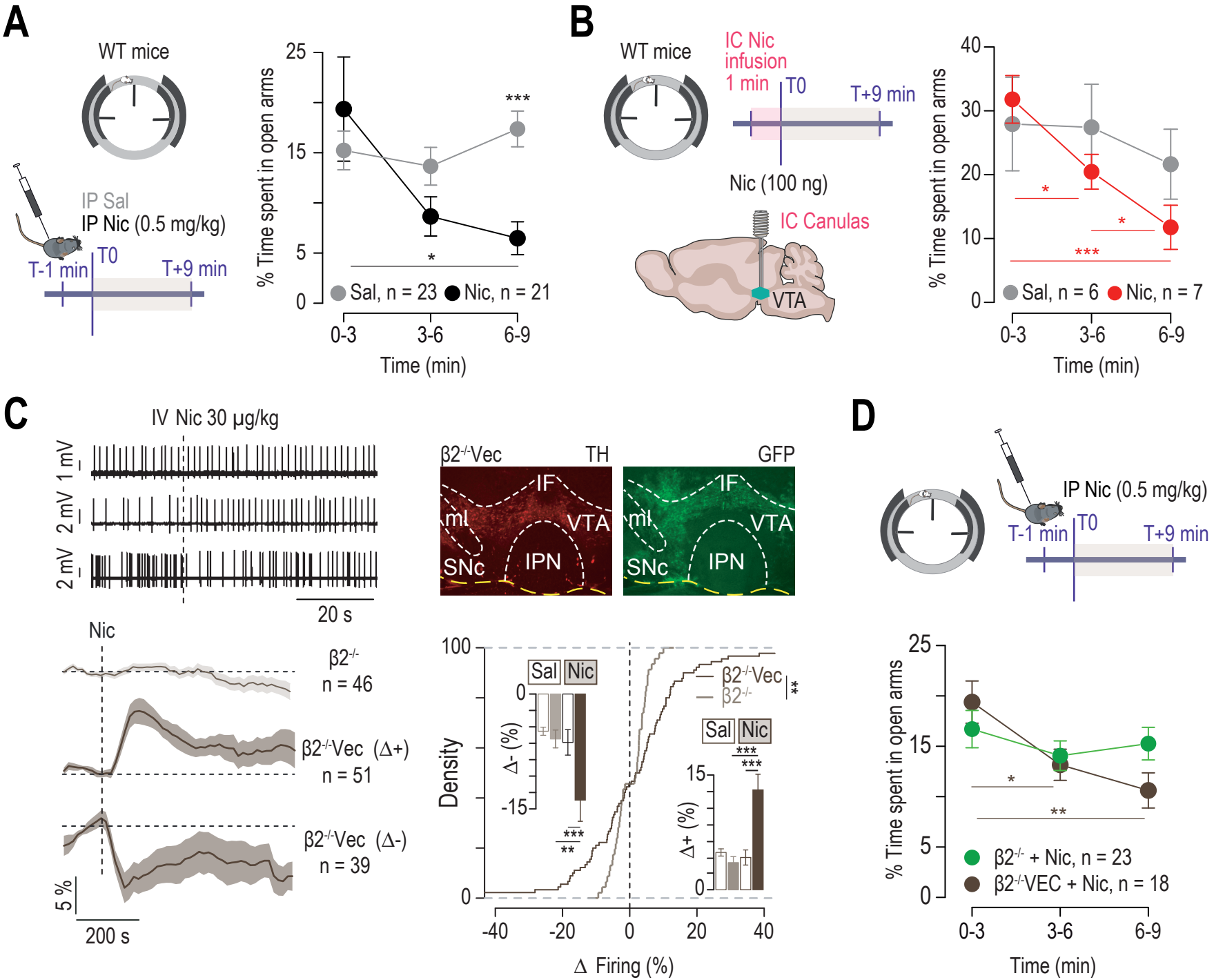
A
WT mice
IP Sal
IP Nic (0.5 mg/kg)
T-1 min
T0
T+9 min
% Time spent in open arms
Sal, n = 23
Nic, n = 21
0-3
3-6
6-9
Time (min)
B
WT mice
IC Nic infusion 1 min
T0
T+9 min
Nic (100 ng)
IC Canulas
VTA
% Time spent in open arms
Sal, n = 6
Nic, n = 7
Time (min)
C
IV Nic 30 µg/kg
1 mV
2 mV
2 mV
20 s
Nic
β2-/-
n = 46
β2-/-Vec (Δ+)
n = 51
β2-/-Vec (Δ-)
n = 39
5 %
200 s
β2-/-Vec
TH
GFP
IF
ml
VTA
SNc
IPN
Density
Sal
Nic
β2-/-Vec
β2-/-
Δ- (%)
Δ+ (%)
Δ Firing (%)
D
IP Nic (0.5 mg/kg)
T-1 min
T0
T+9 min
% Time spent in open arms
β2-/- + Nic, n = 23
β2-/-VEC + Nic, n = 18
Time (min)

Figure 3

Figure 4: Selective optogenetic manipulation of VTA-BLA and VTA-NAcLSh pathways highlights the opposite effects of nicotine injection on VTA DA neurons.

(A) Percentage of time spent in the EOM open arms for Jaws (orange, n = 18) and YFP control (green, n = 19) groups stimulated continuously at 520 nm over a 5-minute period (ON) in the BLA (two-way RM ANOVA time x opsin interaction $F_{(2,70)} = 3.32$, * p = 0.04 ; *post hoc* Student's t-test Jaws vs YFP: * p(ON) = 0.038 ; *post hoc* Student's t-test with Bonferroni corrections Jaws * p (5 vs 10 minutes) = 0.01, * p (10 vs 15 minutes) = 0.02) (**B)** Same for CatCh (blue, n = 18) and YFP control (green, n = 19) groups stimulated at 470 nm over a 5-minute period (ON) at 10 Hz, 5 ms-pulse in the BLA (Two-way ANOVA main effect of time $F_{(2,70)} = 4.41$, * p = 0.016, time x opsin interaction $F_{(2,70)} = 4.43$, * p = 0.015; *post hoc* Student's t-test YFP vs CatCh ** p(ON) = 0.009, *post hoc* Student's t-test with Bonferroni corrections CatCh ** p (5 vs 10 minutes) = 0.001; * p (10 vs 15 minutes) = 0.01) (**C**) Same for CatCh (blue, n = 13) and control YFP (green, n = 14) groups stimulated at 470 nm over a 5-minute period (ON) at 10 Hz, 5 ms-pulse in the NAcLSh. **(D)** Same for CatCh (blue, n = 13) and YFP (green, n = 9) groups stimulated in the BLA throughout the test at 10 Hz, 5-ms light-pulse, after all receiving a nicotine IP injection (CatCh vs YFP: two-way RM ANOVA main effect of time $F_{(2,40)} = 4.92$, * p = 0.01, time x opsin interaction $F_{(2,40)} = 3.74$, * p = 0.03; *post hoc* Student's t-test YFP vs CatCh at 9 minutes ** p = 0.006; one-way RM ANOVA YFP: $F_{(2,16)} = 5.77$, * p = 0.01; CatCh: $F_{(2,24)} = 1.59$, p = 0.6). **(E)** Preference score in 20min-online place preference test (OPP) defined by the % of time spent in the compartment where the animals are photo-stimulated compared to the compartment where they are not (ON-OFF). (*Top-down*) Optical inhibition of the VTA-BLA pathway (orange, n = 17) induced online place avoidance compared to the control group (YFP in green, n = 20). Mice with optical activation of the VTA-BLA pathway (blue, n = 12) did not display any difference compared to the control group (YFP in green, n = 13). Optical activation of the VTA-NAcLSh pathway (blue, n = 13) induced online place preference compared to the control group (YFP in green, n = 14). (Student's t-test * p < 0.05**)**

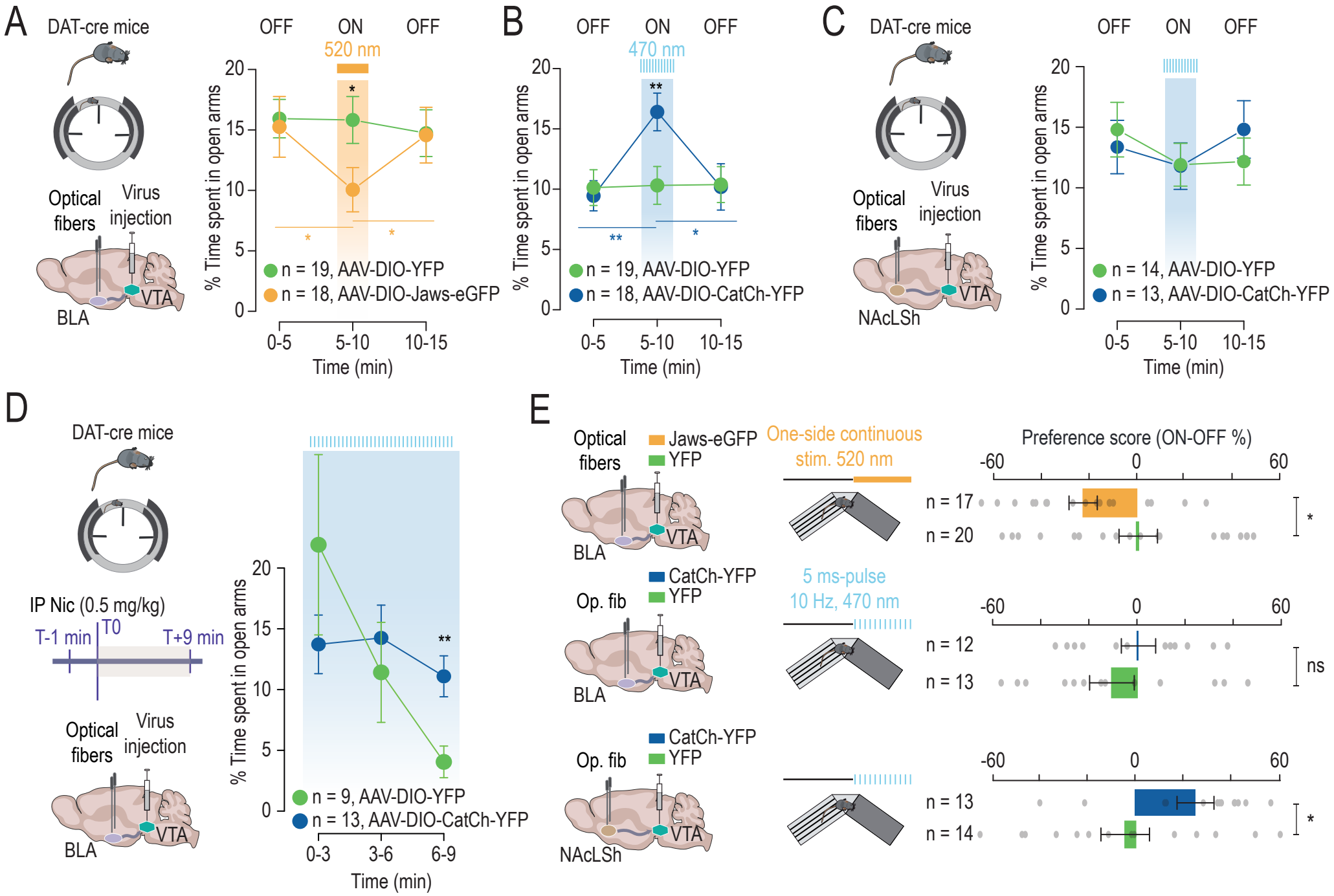
A
DAT-cre mice
Optical fibers
Virus injection
VTA
BLA
OFF
ON
OFF
520 nm
% Time spent in open arms
n = 19, AAV-DIO-YFP
n = 18, AAV-DIO-Jaws-eGFP
0-5
5-10
10-15
Time (min)
B
OFF
ON
OFF
470 nm
% Time spent in open arms
n = 19, AAV-DIO-YFP
n = 18, AAV-DIO-CatCh-YFP
0-5
5-10
10-15
Time (min)
C
DAT-cre mice
Optical fibers
Virus injection
VTA
NAcLSh
OFF
ON
OFF
% Time spent in open arms
n = 14, AAV-DIO-YFP
n = 13, AAV-DIO-CatCh-YFP
0-5
5-10
10-15
Time (min)
D
DAT-cre mice
IP Nic (0.5 mg/kg)
T-1 min
T0
T+9 min
Optical fibers
Virus injection
VTA
BLA
% Time spent in open arms
n = 9, AAV-DIO-YFP
n = 13, AAV-DIO-CatCh-YFP
0-3
3-6
6-9
Time (min)
E
Optical fibers
Jaws-eGFP
YFP
VTA
BLA
One-side continuous stim. 520 nm
Preference score (ON-OFF %)
n = 17
n = 20
CatCh-YFP
YFP
Op. fib
5 ms-pulse 10 Hz, 470 nm
n = 12
n = 13
ns
CatCh-YFP
YFP
Op. fib
NAcLSh
n = 13
n = 14

Figure 4

Supplementary Figures

Figure S1

(A-B) Principal component analysis (PCA) of the spontaneous activity of VTA DA neurons labeled in vivo after juxtacellular recordings. First (axis Dim 1) and second (axis Dim 2) components are represented. Based on their basal activity, neurons are distributed in 4 clusters (cluster 1, n = 77; cluster 2, n = 132; cluster 3, n = 28; cluster 4, n = 7) (**A**), with nicotine-activated (in red, n = 154) and nicotine-inhibited (in blue, n = 90) neurons found in each of these clusters (**B**). **(C)** Mean firing frequency (Hz) as a function of percentage of spikes within a burst (%SWB) for the 4 clusters found with the PCA analysis, with the existence of nicotine-activated (cluster 1, n = 52; cluster 2, n = 85; cluster 3, n = 15; cluster 4, n = 2) and nicotine-inhibited (cluster 1, n = 25; cluster 2, n = 47; cluster 3, n = 13; cluster 4, n = 5) DA neurons in all of them. **(D)** Localization of VTA DA neurons labeled *in vivo* after juxtacellular recordings. Neurons are color-coded according to their responses to nicotine injection (activated in red, n = 155 and inhibited in blue, n = 90), and positioned according to the antero-posterior axis on the Paxinos atlas from Bregma -2.8 to -3.8 mm.

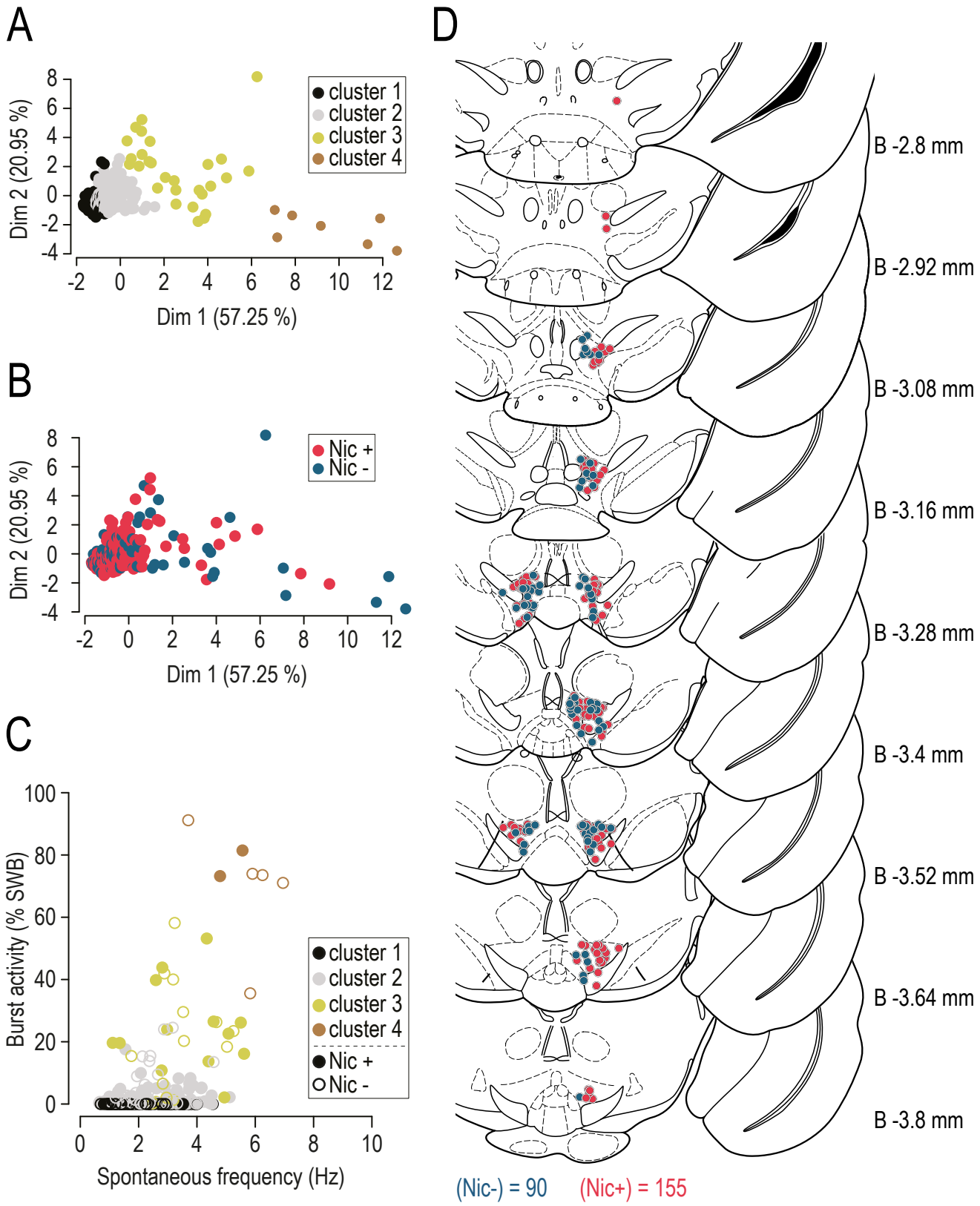
A
Dim 2 (20.95 %)
Dim 1 (57.25 %)
cluster 1
cluster 2
cluster 3
cluster 4
B
Dim 2 (20.95 %)
Dim 1 (57.25 %)
Nic +
Nic -
C
Burst activity (% SWB)
Spontaneous frequency (Hz)
cluster 1
cluster 2
cluster 3
cluster 4
Nic +
Nic -
D
B -2.8 mm
B -2.92 mm
B -3.08 mm
B -3.16 mm
B -3.28 mm
B -3.4 mm
B -3.52 mm
B -3.64 mm
B -3.8 mm
(Nic-) = 90
(Nic+) = 155

Figure S1

Figure S2.1:

(A, B) Examples of NAc-injection sites **(A)** and Amg-injection sites **(B)** with retrobead (RB) tracer (in yellow) reported onto Paxinos atlas slices. **(C, D)** Examples of immunohistofluorescence analysis of VTA slices (TH+, red) revealing neuronal soma containing RB (RB+, green), after injection of the retrobeads into the NAc **(C)** or into the Amg **(D)**. **(E) A** Paxinos atlas slice at 3.3 mm from bregma onto which Neurobiotin-filled cell bodies of each recorded neuron were positioned. **(F)** Analysis of the medio-lateral distribution of recorded DA neurons of the VTA (shown as density) projecting either to the NAc (n = 30, gold) or to the Amg (n = 22, purple) revealed that Amg-projecting neurons are located more medially in the VTA than NAc-projecting neurons (Wilcoxon test, *** $p < 0.001$).

IF: *interfascicular nucleus*; IPN: *interpeduncular nucleus*; ml: *medial lemniscus*; SNc: *substantia nigra pars compacta*

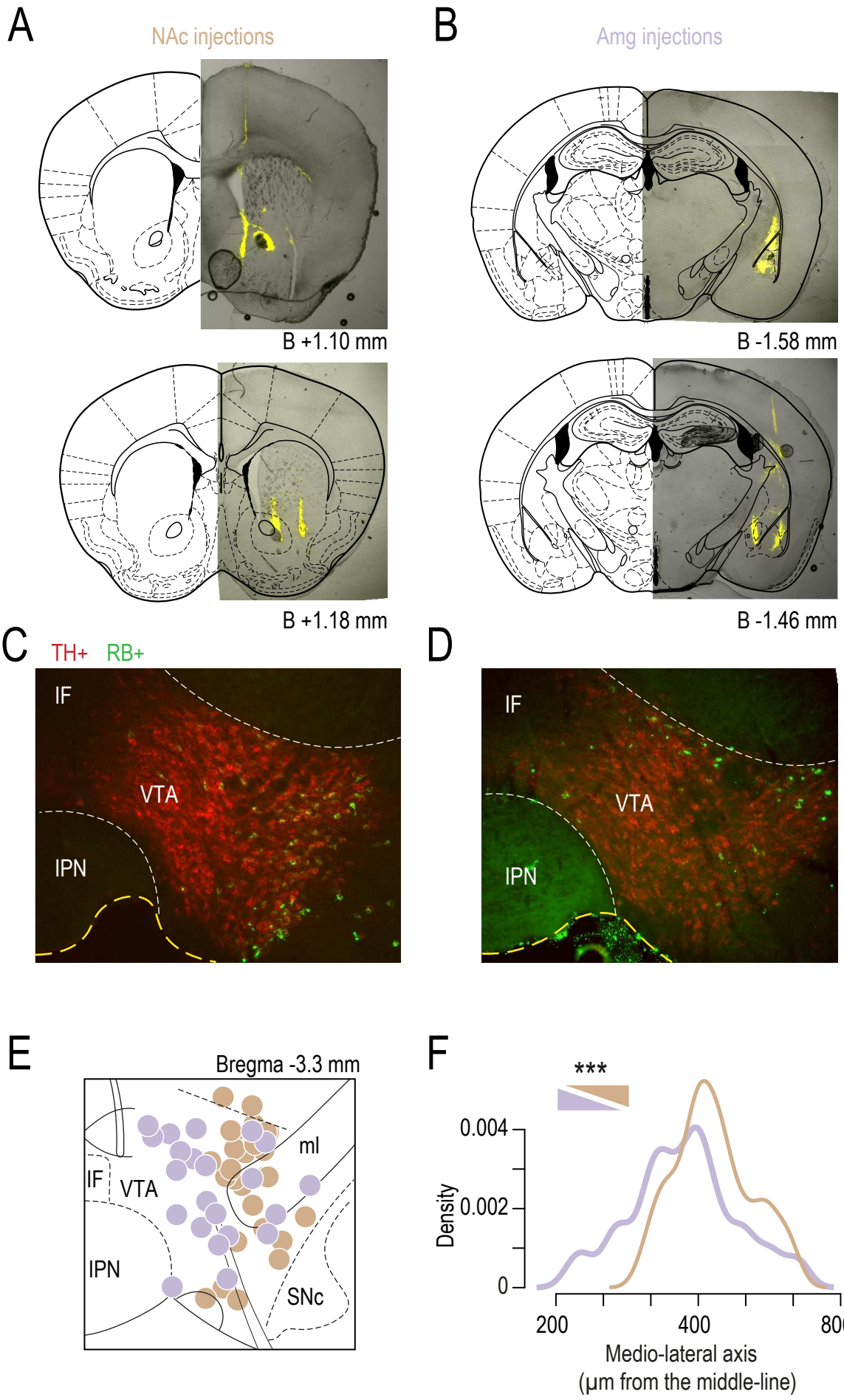
A
NAc injections
B +1.10 mm
B +1.18 mm
B
Amg injections
B -1.58 mm
B -1.46 mm
C
TH+ RB+
IF
VTA
IPN
D
IF
VTA
IPN
E
Bregma -3.3 mm
IF
VTA
IPN
ml
SNc
F
***
0.004
0.002
0
Density
200
400
800
Medio-lateral axis
(µm from the middle-line)

Figure S2.1

Figure S2.2

(A) Immunohistofluorescence analysis of a NAc-projecting neurons of the VTA labeled (neurobiotin, NB+) after patch-clamp recording: confirmed as DA (TH+) and NAc-projecting (retrobeads, RB+). **(B)** Immunohistofluorescence analysis of an Amg-projecting neuron of the VTA labeled (NB+) after patch-clamp recording: confirmed as DA (TH+) and Amg-projecting (RB+). **(C)** Firing of NAc-projecting and Amg-projecting DA neurons of the VTA after injection of currents (20, 60 and 100 pA). **(D)** Higher excitability of Amg-projecting (n = 17, purple) compared to NAc-projecting DA neurons (n = 16, gold) (two-way RM ANOVA main effect phenotype $F_{(1,26)} = 4.96$, * $p = 0.035$, current $F_{(4,104)} = 15.97$, *** $p < 0.001$, current x phenotype interaction $F_{(4,104)} = 13.78$, *** $p < 0.001$). **(E)** Nicotine-evoked currents (local puff 100 µM) in RB+-identified, NAc- or Amg-projecting VTA DA neurons recorded in brain slices (whole-cell voltage-clamp mode -60 mV). **(F)** Mean currents evoked by nicotine in either NAc-projecting (n = 16, gold, 33.0 ± 19.8 pA) or Amg-projecting (n = 17, purple, 22.4 ± 13.3 pA) VTA DA neurons are not statistically different (Student's t-test $p = 0.08$).

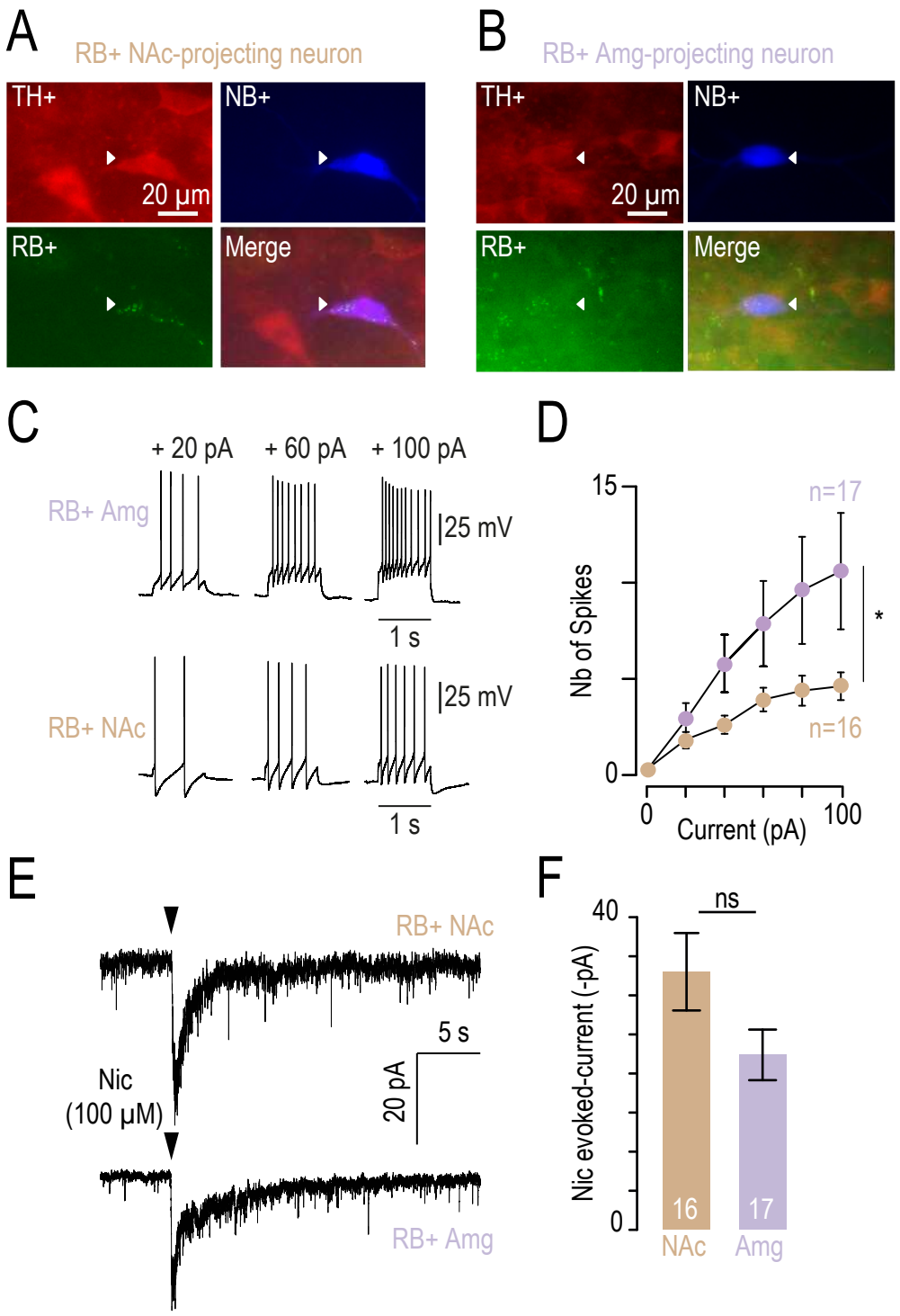
A
RB+ NAc-projecting neuron
TH+
NB+
20 µm
RB+
Merge
B
RB+ Amg-projecting neuron
TH+
NB+
20 µm
RB+
Merge
C
+ 20 pA
+ 60 pA
+ 100 pA
RB+ Amg
25 mV
1 s
RB+ NAc
25 mV
1 s
D
15
0
Nb of Spikes
n=17
n=16
*
0
Current (pA)
100
E
RB+ NAc
5 s
Nic
(100 µM)
20 pA
RB+ Amg
F
40
0
Nic evoked-current (-pA)
ns
16
17
NAc
Amg

Figure S2.2

Figure S3

(A) Locomotor activity, measured in a square open field (OF), of mice receiving an intraperitoneal (IP) injection of either saline (IP Sal, grey, n = 11) or nicotine (IP Nic 0.5 mg/kg, black, n = 7). Mice did not display any statistically significant difference in the distance traveled over time (pooled each 3 minutes, two way RM ANOVA no time, no treatment or interaction effect $p > 0.05$) or in the total distance traveled during 9 minutes (presented as bar plot, Student's t-test $p > 0.05$) **(B)** EOM detailed for WT mice tested with Sal (grey, n = 23) or Nic (black, n = 21) (one-way RM ANOVA Nic: $F_{(2,40)} = 5.18$, ** $p = 0.01$; Sal: $F_{(2,44)} = 1.65$, $p = 0.2$) after IP injection. **(C)** Example of *post hoc* verification of intracranial guide cannula implantations in WT mice. Bilateral injection cannulas (0.5 µm longer than the guide cannulas) are inserted on the day of the experiment, for local infusion into the VTA. TH labeling is shown in yellow. **(D)** Detailed scores of wild-type mice in the EOM after intracranial infusion of Sal (grey, n = 6) or Nic (red, n = 7) 1 mg/mL (one-way RM ANOVA Nic: $F_{(2,12)} = 26.11$, *** $p < .001$; Sal: $F_{(2,10)} = 0.01$, $p = 0.99$) 1 minute before the test. **(E)** Schematic of β2 subunit re-expression by lentiviral vectorization in the VTA of $\beta2^{-/-}$ mice. Lentivirus encoding either pGK-β2-IRES-GFP ($\beta2^{-/-}$Vec) or pGK-GFP ($\beta2^{-/-}$GFP) as a control were injected into the VTA. Example of immunohistofluorescence analysis of a $\beta2^{-/-}$Vec mouse brain labeled for TH (red) and GFP (green). **(F)** $\beta2^{-/-}$GFP (n = 6, green) and $\beta2^{-/-}$ mice (n = 17, grey) did not diplay difference in time spent in the EOM (two-way RM ANOVA no time, no treatment or interaction effect $p > 0.05$). **(G)** Detailed scores in the EOM for $\beta2^{-/-}$ mice (n = 23, green) and $\beta2^{-/-}$Vec mice (n = 18, brown), after IP injection of Nic 0.5 mg/kg (one-way RM ANOVA $\beta2^{-/-}$Vec: $F_{(2,34)} = 8.65$, *** $p < 0.001$; $\beta2^{-/-}$: $F_{(2,44)} = 1.08$, $p = 0.3$) 1 minute before the test.

Mean scores are represented in bold and color, and individual scores with empty grey dots.

IF: *interfascicular nucleus* ; IPN : *interpeduncular nucleus* ; SNc : *substantia nigra pars compacta ;* ml : *medial lemniscus* ; SNc : *substantia nigra pars compacta.*

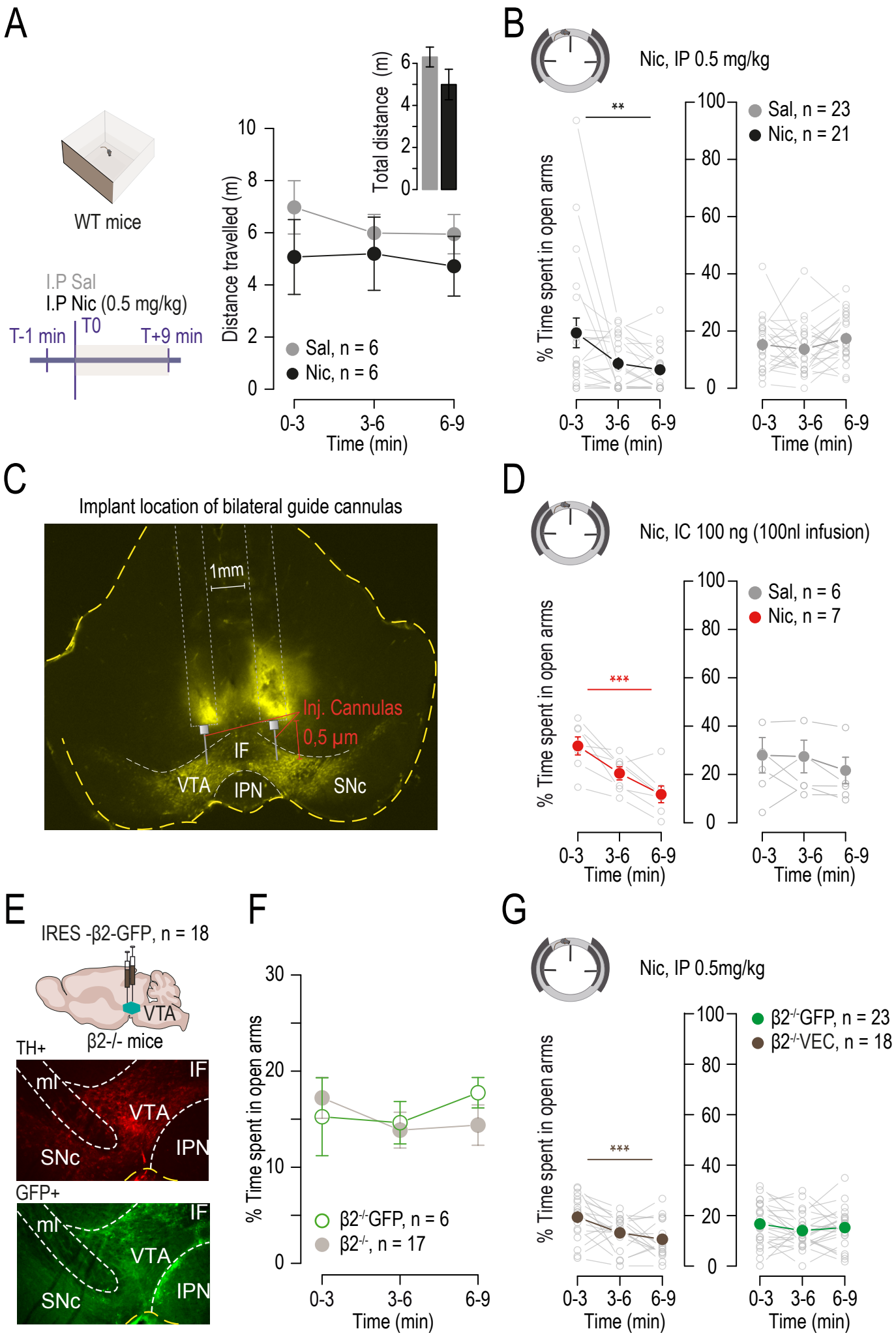
A
WT mice
I.P Sal
I.P Nic (0.5 mg/kg)
T-1 min
T0
T+9 min
Distance travelled (m)
Total distance (m)
Sal, n = 6
Nic, n = 6
0-3
3-6
6-9
Time (min)
B
Nic, IP 0.5 mg/kg
**
% Time spent in open arms
Sal, n = 23
Nic, n = 21
C
Implant location of bilateral guide cannulas
1mm
Inj. Cannulas
0,5 µm
IF
VTA
IPN
SNc
D
Nic, IC 100 ng (100nl infusion)
***
Sal, n = 6
Nic, n = 7
E
IRES -β2-GFP, n = 18
VTA
β2-/- mice
TH+
GFP+
ml
F
% Time spent in open arms
β2-/-GFP, n = 6
β2-/-, n = 17
G
Nic, IP 0.5mg/kg
β2-/-GFP, n = 23
β2-/-VEC, n = 18

Figure S3

Figure S4.1

(A) Immunohistofluorescence analysis of VTA DA neurons after patch-clamp recordings in mice injected with AAV-Ef1α-DIO-Jaws-eGFP into the VTA. Neurobiotin (NB, blue), tyrosine hydroxylase (TH, red), YFP (green). **(B)** Example of a recording trace of a VTA DA neuron during continuous light stimulation (20 s, 520 nm) and raster plot of action potential showing light-induced inhibition in Jaws-expressing DA neurons (n = 7). **(C)** Immunohistochemistry of VTA DA neurons (NB, blue; TH, red; YFP, green) after patch-clamp recording in mice injected with AAV-DIO-CatCh-YFP into VTA. **(D)** Example of recording trace of a DA neuron of the VTA during light stimulation (10 Hz, 5-ms pulse, 470 nm) and light-evoked inward current in DA neurons expressing CatCh. Mean light-evoked current in seven DA neurons.

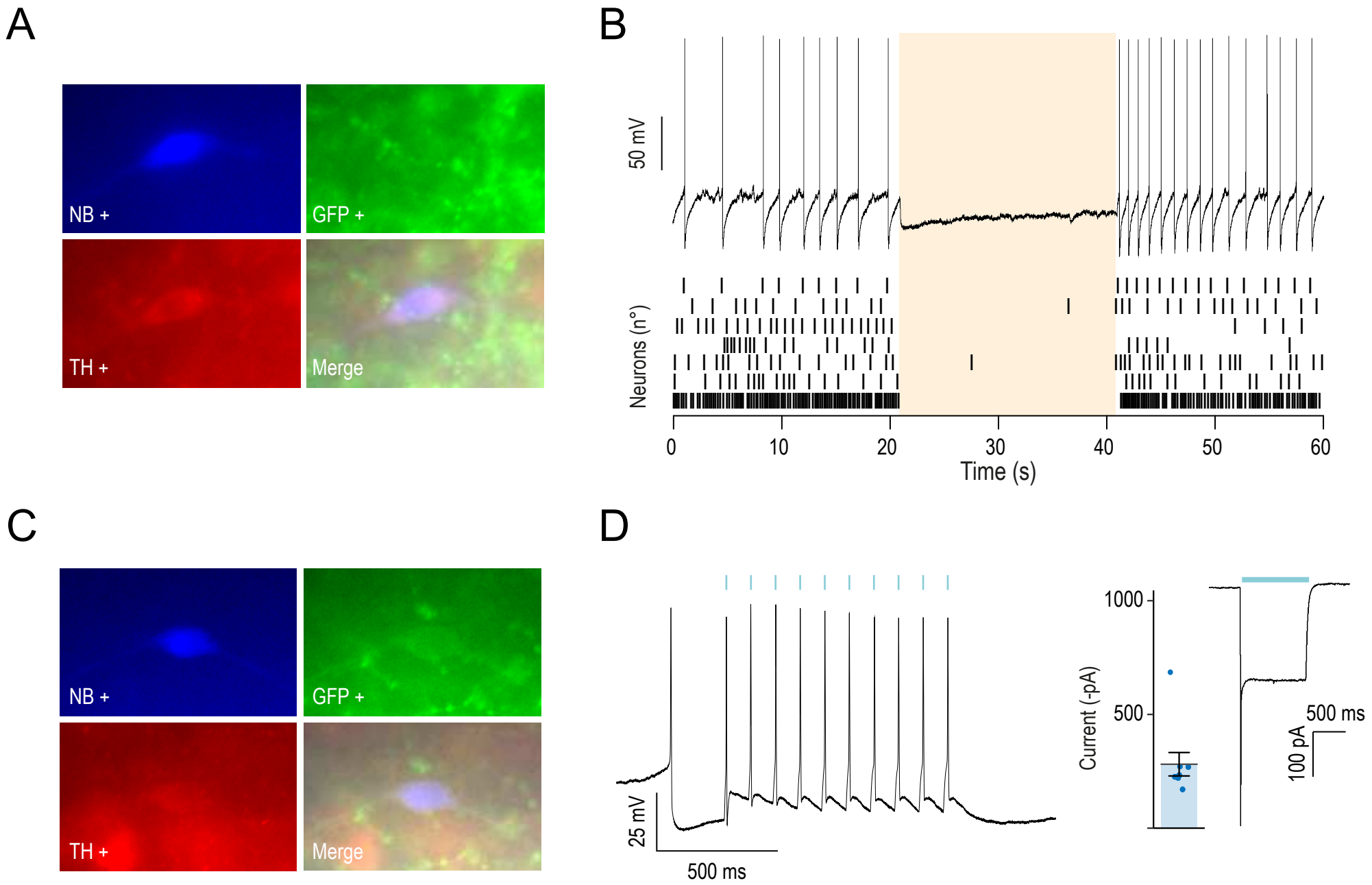
A
NB +
GFP +
TH +
Merge
B
50 mV
Neurons (n°)
0
10
20
30
40
50
60
Time (s)
C
NB +
GFP +
TH +
Merge
D
25 mV
500 ms
1000
500
Current (-pA)
500 ms
100 pA

Figure S4.1

Figure S4.2

(A) Immunohistofluorescence analysis of VTA slices after AAV-DIO-Jaws-eGFP and AAV-DIO-YFP injections into VTA. **(B)** Immunohistofluorescence analysis of VTA slices after AAV-Ef1α-DIO-hCatCh-YFP and AAV-Ef1α-DIO-YFP injections into the VTA. **(C)** Example of *post-hoc* verification of the fiber implantation into the basolateral Amg (BLA) of mice used in optogenetic experiments, injected either with AAV-Ef1α-DIO-Jaws-eGFP (orange dots indicate the location of one hemisphere fiber tip that was verified, n = 13, left side of the slices) and its YFP control (green dots, n = 10, left side of the slices) or with AAV-Ef1α-DIO-hCatCh-YFP (blue dots, n = 16, right side of the slices) and its YFP control (green dots, n = 11, right side of the slices). The optical fibers were positioned onto Paxinos atlas slices from bregma -1.22 to -1.82 mm. **(D)** *Post-hoc* verification of the fiber implantation into the NAc lateral shell (NAcLSh) of mice used in optogenetic experiments, injected either with AAV-Ef1α-DIO-hCatCh-YFP (blue dots, n = 13, left of the slices) and its YFP control (green dots, n = 14, right of the slices). The optical fibers were positioned onto Paxinos atlas slices from bregma + 0.86 to + 1.70 mm.

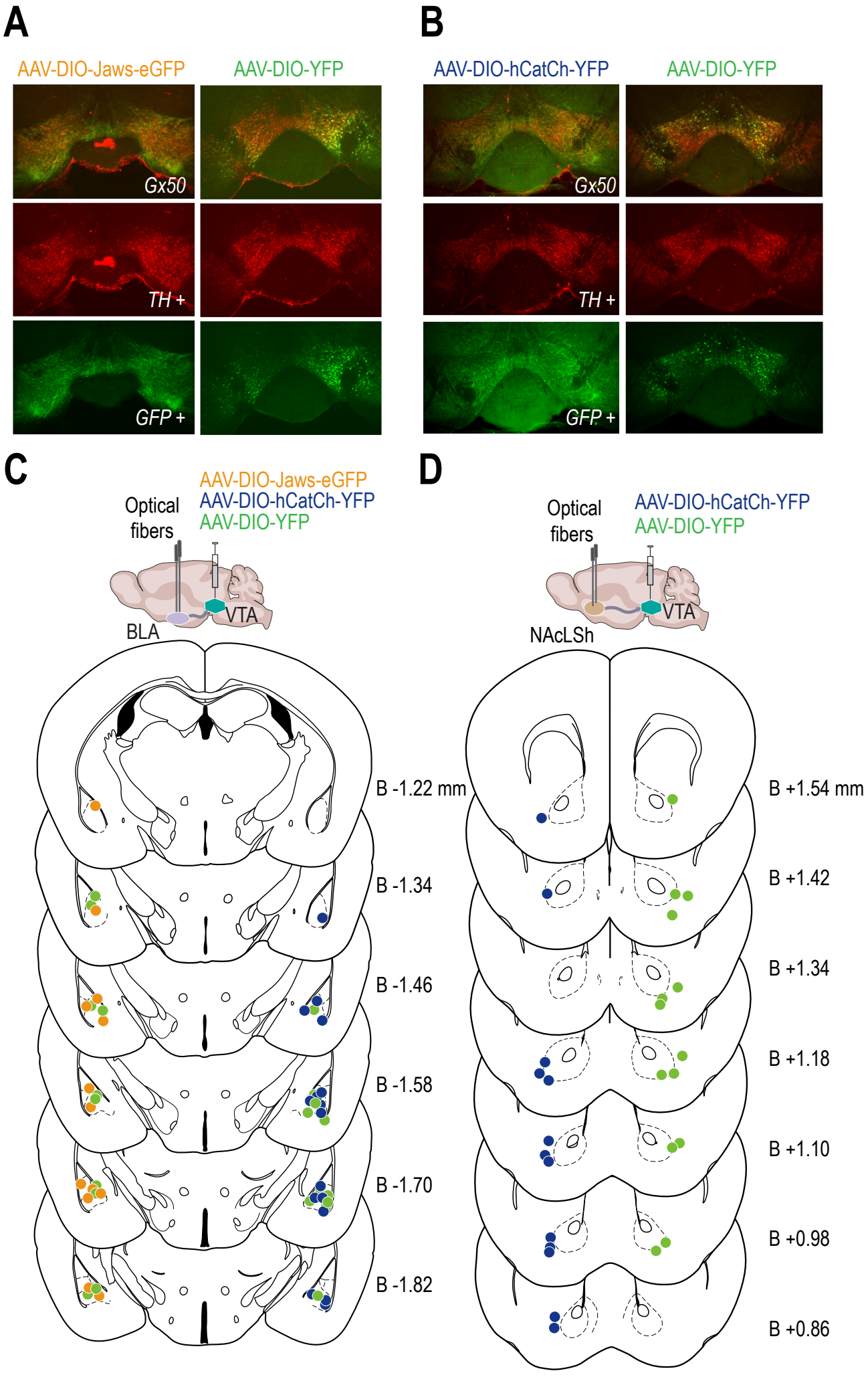
A
AAV-DIO-Jaws-eGFP
AAV-DIO-YFP
Gx50
TH +
GFP +
B
AAV-DIO-hCatCh-YFP
AAV-DIO-YFP
Gx50
TH +
GFP +
C
AAV-DIO-Jaws-eGFP
AAV-DIO-hCatCh-YFP
AAV-DIO-YFP
Optical fibers
VTA
BLA
B -1.22 mm
B -1.34
B -1.46
B -1.58
B -1.70
B -1.82
D
Optical fibers
AAV-DIO-hCatCh-YFP
AAV-DIO-YFP
VTA
NAcLSh
B +1.54 mm
B +1.42
B +1.34
B +1.18
B +1.10
B +0.98
B +0.86

Figure S4.2

Figure S4.3

(A) Time spent in open arms of the EOM by mice injected with AAV-Ef1α-DIO-Jaws-eGFP (n = 18, orange, one-way RM ANOVA $F_{(2,34)} = 5.28$, ** p = 0.01) and AAV-Ef1α-DIO-YFP (n = 19, green, one-way RM ANOVA $F_{(2,36)} = 0.32$, p = 0.7) in the VTA , with (ON) or without (OFF) light-evoked inhibition of DA axon terminals in the BLA (the test lasts 15 minutes, with continuous photostimulation at 520 nm during a 5-minute ON period). **(B)** Time spent in open arms of the EOM by mice injected with AAV-Ef1α-DIO-hCatCh-YFP (n = 18, blue, one-way RM ANOVA $F_{(2,34)} = 9.27$, *** p < 0.001) and AAV-Ef1α-DIO-YFP (n = 19, green, one-way ANOVA $F_{(2,36)} = 0.01$, p = 0.99) in the VTA , with (ON) or without (OFF) light-evoked activation of DA axon terminals in the BLA (10 Hz photostimulation at 470 nm, 5-ms pulse, during a 5-minute ON period). **(C)** Time spent in open arms of the EOM by mice injected with AAV-Ef1α-DIO-hCatCh-YFP (n = 13, blue, one-way RM ANOVA $F_{(2,24)} = 0.61$, p = 0.55) and AAV-Ef1α-DIO-YFP (n = 14, green, one-way RM ANOVA $F_{(2,26)} = 1.47$, p = 0.25) in the VTA , during (ON) or out (OFF) light-evoked activation of DA axon terminals in the NAcLSh (10 Hz photostimulation at 470 nm, 5-ms pulses, during a 5-minute ON period). **(D)** A square open field (OF) paradigm was conducted in the three paired groups of animals to assess their locomotor activities: Jaws- and YFP-injected mice implanted in the Amg (two-way RM ANOVA, main effect epoch $F_{(2,76)} = 44.27$, *** p < 0.001, no opsin or interaction effect) ; **(E)** CatCh- and YFP-injected mice implanted in the BLA (two-way RM ANOVA, main effect epoch $F_{(2,42)} = 25.17$, *** p < 0.001, no opsin or interaction effect) ; **(F)** and CatCh- and GFP-injected mice implanted in the NAcLSh (two-way RM ANOVA, main effect epoch $F_{(2,50)} = 14.27$, ***p < 0.001, epoch x opsin interaction $F_{(2,50)} = 4$, * p = 0.02, *post hoc* Wilcoxon test YFP vs CatCh at 5 minutes * p = 0.04). Animals showed no difference in terms of locomotor activity between groups or as a function of the stimulation period within a group.
Mean scores are represented in bold and color, and individual scores in grey

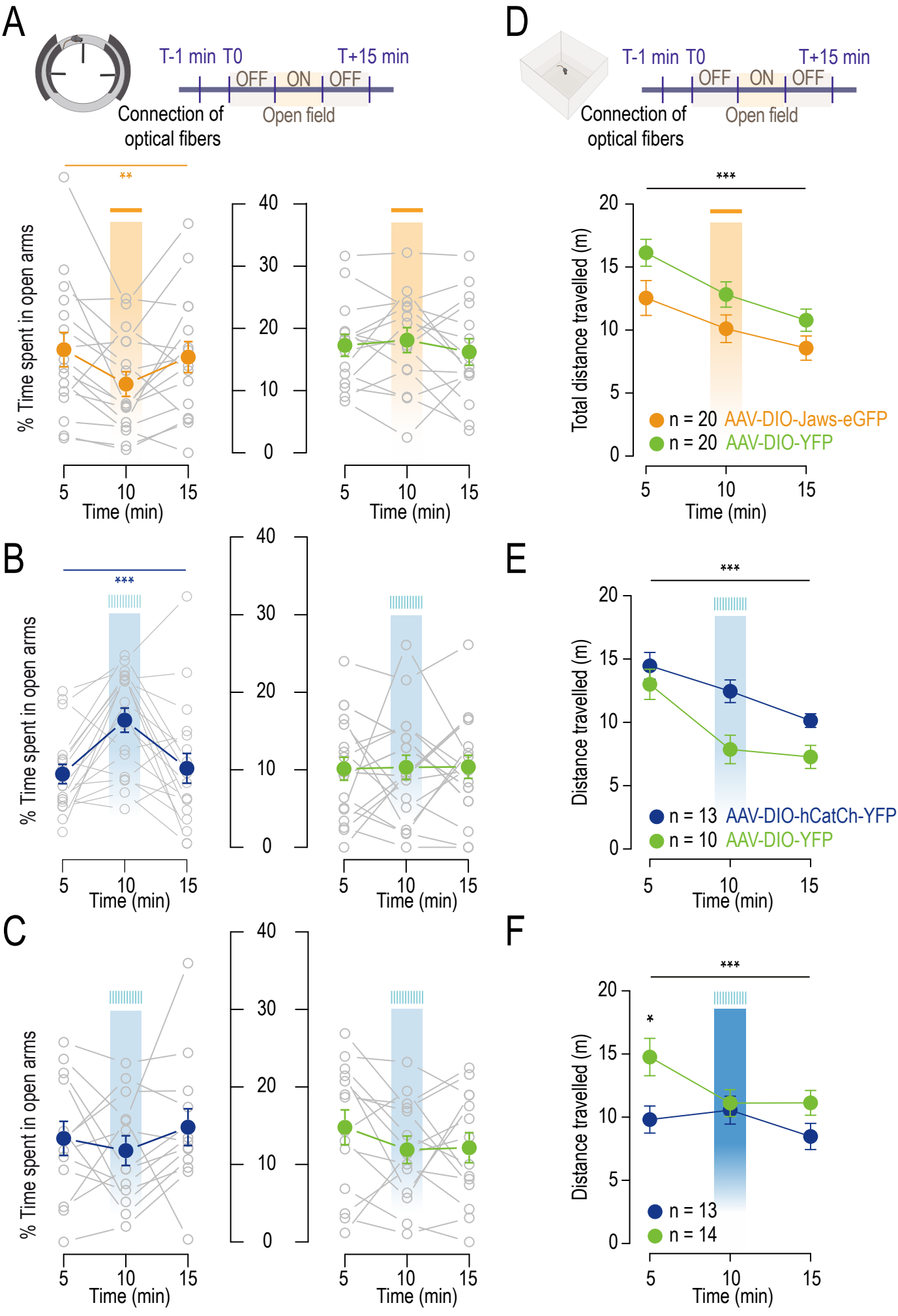
A
T-1 min T0
OFF
ON
OFF
T+15 min
Connection of optical fibers
Open field
D
T-1 min T0
OFF
ON
OFF
T+15 min
Connection of optical fibers
Open field
**
% Time spent in open arms
40
30
20
10
0
5
10
15
Time (min)
***
Total distance travelled (m)
20
15
10
5
0
n = 20 AAV-DIO-Jaws-eGFP
n = 20 AAV-DIO-YFP
B
***
% Time spent in open arms
Time (min)
E
***
Distance travelled (m)
n = 13 AAV-DIO-hCatCh-YFP
n = 10 AAV-DIO-YFP
C
% Time spent in open arms
Time (min)
F
***
*
Distance travelled (m)
n = 13
n = 14
Time (min)

Figure S4.3

Figure S4.4

(A) (*Left*) Representative immunohistofluorescence analysis of VTA slices for Jaws expression (GFP: green labeling, TH: red labeling). (*Right*) Optical fibers were implanted in the basolateral Amg (BLA, bregma -1.61; lateral 3.18; ventral 4.7 mm) of wild-type (WT) mice injected either with AAV-CAG-Jaws-GFP (orange dots represent the location of one hemisphere fiber tip that was verified, n = 7) or with AAV-CAG-GFP control (green dots, n = 3) into the VTA. **(B)** Mice implanted in the BLA were tested for any difference in locomotor activity between groups in the open field (OF). The test lasted 15 minutes and consisted of a 5-minute period of photostimulation (continuous at 520 nm) in between two non-stimulation periods (OFF-ON-OFF). During both OFF- and ON-periods, the groups did not present any statistically significant difference in the distance traveled in the OF (two-way RM ANOVA main effect epoch $F_{(2,44)}$ = 5.89, ** p = 0.005, no opsin or interaction effect). **(C)** Inhibiting BLA axon terminals by photostimulation of inhibitory opsin Jaws during the EOM task induced a decrease in the time spent by the mice in the open arms compared to the control group (two-way RM ANOVA, epoch x opsin interaction $F_{(2,42)}$ = 3.44, * p = 0.04, *post hoc* Student's t-test p (ON Jaws vs GFP) = 0.056). **(D)** (*Left*) Representative immunohistofluorescence analysis of VTA slices for Jaws expression (GFP: green, TH: red). (*Right*) Positions of optical fibers on one hemisphere implanted in the central amygdala (CeA) of another group of WT mice injected with either AAV-CAG-Jaws-GFP GFP (n=7, orange dots) or with AAV-CAG-GFP (n=7, green) into the VTA. **(E)** Inhibiting CeA terminals by photostimulation did not produce any statistically significant difference in locomotor activity in the OF test between the Jaws- and GFP-expressing groups (two-way RM ANOVA main effect epoch $F_{(2,32)}$ = 23.11, *** p < 0.001, epoch x opsin interaction $F_{(2,32)}$ = 3.8, * p = 0.03, no opsin effect). **(F)** The two groups did not display any difference in time spend in the open arm of the EOM test either (two-way RM ANOVA, epoch x opsin interaction $F_{(2,32)}$ = 3.67, * p = 0.04). *Post-hoc Student's t test with Bonferroni corrections. *** p < 0.001, ** p < 0.01 and * p < 0.05*

IF: *interfascicular nucleus* ; IPN: *interpeduncular nucleus* ; ml: *medial lemniscus* ; SNc: *substantia nigra pars compacta*

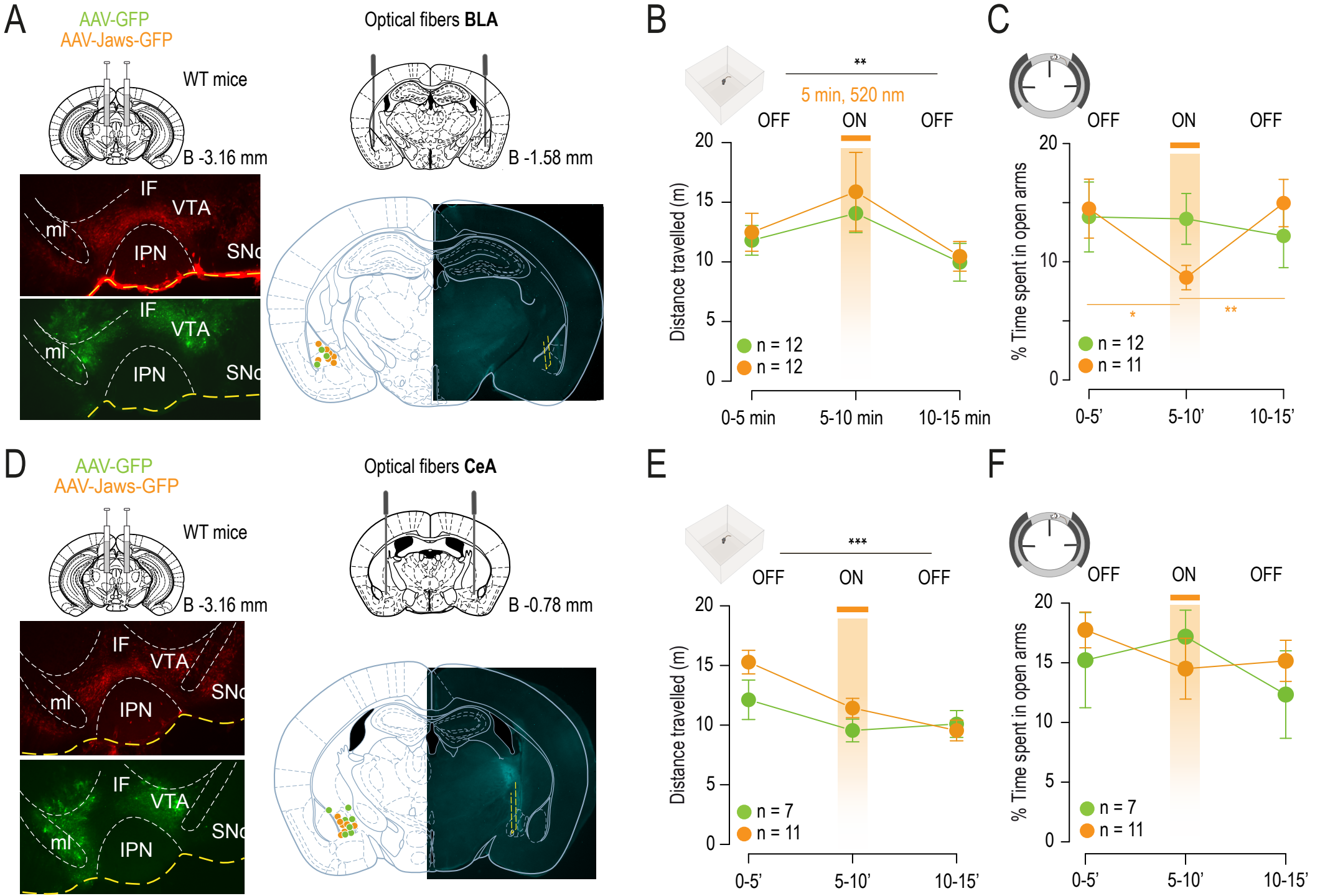
A
AAV-GFP
AAV-Jaws-GFP
WT mice
B -3.16 mm
Optical fibers BLA
B -1.58 mm
IF
VTA
ml
IPN
SNc
B
**
5 min, 520 nm
OFF
ON
OFF
Distance travelled (m)
n = 12
n = 12
0-5 min
5-10 min
10-15 min
C
% Time spent in open arms
n = 12
n = 11
*
**
0-5'
5-10'
10-15'
D
AAV-GFP
AAV-Jaws-GFP
WT mice
B -3.16 mm
Optical fibers CeA
B -0.78 mm
E
***
n = 7
n = 11
F
n = 7
n = 11

Figure S4.4

STAR Methods

LEAD CONTACT

Further information and requests for resources and reagents should be directed to and will be fulfilled by the Lead Contact, Philippe Faure (phfaure@gmail.com).

MATERIALS AVAILABILITY

This study did not generate new unique reagents.

DATA AND CODE AVAILABILITY

All the data are available from the corresponding authors upon request.

EXPERIMENTAL MODEL AND SUBJECT DETAILS

Wild-type C57Bl/6Rj (Janvier Labs, France), ACNB2 KO ($\beta2^{-/-}$) and DAT^{iCRE} (DAT-Cre) male mice, weighing 25-35 grams, were used in this study. $\beta2^{-/-}$ mice were generated using standard homologous recombination procedures. Founders were backcrossed onto a C57BL/6J background for a least 20 generations and bred on site. DAT^{iCRE} mice were provided by François Tronche's team (IBPS Paris, France). They were bred on site and genotyped as described (Turiault et al., 2007).
Mice were kept in an animal facility where temperature (20 ± 1°C) and humidity were automatically monitored, and a circadian light-dark cycle of 12/12 hours was maintained. All experiments were performed on 8-to-16-week-old mice. All experiments were performed in accordance with the recommendations for animal experiments issued by the European Commission directives 219/1990, 220/1990 and 2010/63, and approved by Sorbonne University.

METHOD DETAILS

AAV production

AAV vectors were produced as previously described (Khabou et al., 2018) using the co-transfection method, and purified by iodixanol gradient ultracentrifugation (Choi et al., 2007). AAV vector stocks were titrated by quantitative PCR (qPCR) (Aurnhammer et al., 2012) using SYBR Green (Thermo Fischer Scientific). Lentiviruses were prepared as previously described (Maskos et al., 2005; Tolu et al., 2013), with a titer of either 380 ng of p24 protein per µl or 764 ng/µl for the AChR β2-expressing vector, and 150 ng of p24 protein per µl or 361 mg per 2 µl for GFP-expressing vector.

Drugs

The solution of nicotine (Nic) used for all experiments is a nicotine hydrogen tartrate salt (Sigma-Aldrich, USA). For juxtacellular recordings, we performed an intravenous injection of nicotine at a dose of 30 µg/kg (4.16 mg/kg, free base) or saline water (H_2O with 0.9 % NaCl). For the behavioral test, in elevated O-maze (EOM) or open-field (OF), mice were injected intra-peritoneally with nicotine at 0.5 mg/kg 1-minute prior to the test. For intra-cranial (IC) experiments in EOM, saline solution or 100ng of Nic tartrate were

infused in 100 nl/injection over 1 minute before the beginning of the test. All solutions were prepared in the laboratory.

Retrobeads injection

Green fluorescent retrobeads (RB) tracers (LumaFluor Inc., Naples, FL) were injected (200 nl per site, 0.1 µl/min) in wild-type (WT) animals either in the NAc (NAc lateral shell NAcLatSh : bregma + 1.45 mm; lateral 1.75 mm; ventral 4.0 mm ; NAc medial shell : bregma + 1.78 mm; lateral 0.45 mm; ventral 4.1 mm ; NAc core : bregma 1.55 mm; lateral 1.0 mm; ventral 4.0 mm) or in the Amg (BLA : bregma - 1.61 mm; lateral 3.18 mm; ventral 4.7 mm ; CeA : bregma - 0.78 mm; lateral 2.3 mm; ventral 4.8 mm) with a 10 µl Hamilton syringe (Hamilton) coupled with a polyethylene tubing to a 36G injection cannula (Phymep). Note that these empirically derived stereotaxic coordinates do not precisely match those given in the mouse brain atlas (Paxinos and Franklin, 2004), which we used as references for the injection-site images. To enable retrograde transport of the RB into the somas of midbrain DA neurons, we waited for an adequate time to perform the electrophysiology experiments, depending on the injection zone: 3 weeks after NAc injection and 2 weeks after Amg injection.

Virus injection and optogenetics experiments

DAT^{iCRE} mice were anesthetized (Isoflurane 1%) and IC injection was performed into the VTA (coordinates bregma: + 3.1 mm; lateral: 0.5 mm; ventral: 4.5 mm) with 0.5 µl of an adeno-associated virus (AAV5.EF1α.DIO.CatCh.YFP $2.46e^{12}$ or $6.53e^{14}$ ng/µL, AAV5.EF1α.DIO.Jaws.eGFP $1.16e^{14}$ ng/µL diluted at 1:10, AAV5.EF1α.DIO.YFP $6.89e^{14}$ or $9.10e^{13}$ ng/µL). A double-floxed inverse open reading frame (DIO) allowed restraining the expression of CatCh (Ca^{2+} translocating channelrhodopsin) or Jaws (red-shifted cruxhalorhodopsin) to VTA DA neurons. Optical fibers (200 µm core, NA = 0.39, Thor Labs) coupled to a ferule (1.25 mm) were implanted bilaterally in the different target sites of the VTA (coordinates for BLA implantation: bregma: - 1.6 mm; lateral: 3.18 mm; ventral: 4.5 mm) (coordinates for NAc LatSh implantation: bregma: + 1.5 mm; lateral: 1.55 mm; ventral: 3.95 mm), and fixed to the skull with dental cement (SuperBond, Sun medical). An ultra-high-power LED coupled to a patch cord (500 µm core, NA = 0.5, Prizmatix) was used for optical stimulation (output intensity of 10 mW). Optical stimulation was delivered at a frequency of 10 Hz, 5 ms-pulse at 470 nm (Prizmatix LED) for activating stimulation, and with a continuous stimulation at 520 nm (Prizmatix LED) for inhibiting stimulation.

Optogenetic experiment performed on WT mice were conducted in the same manner as described above. Viruses were bilaterally injected into the VTA at the same coordinates as previously.

The first experiments were conducted on the animals at least 4 weeks after virus injection, to allow the construct to expressed by target cells. The optical stimulation cable was plugged onto the ferule during all experimental sessions to prepare the animals and control for latent experimental effects.

To perform non-specific optogenetic stimulation of different subnuclei of the amygdala (Amg), either AAV2-CAG-Jaws-GFP (1.45 e-12 ng/µL) or AAV2-7m8-CAG-GFP (5.70 e-12 ng/µL) were injected bilaterally into the VTA of distinct groups of wild-type (WT) mice as described in Methods. Bilateral optical fibers were implanted in those mice either in the basolateral amygdala (BLA, bregma: -1.6 mm; lateral: 3.18 mm; ventral: 4.5 mm) or in the central amygdala (CeA, bregma: -0.78 mm; lateral: 2.3 mm; ventral: 4.8 mm).

Intracranial infusion

Bilateral guide cannulae (Bilaney) were implanted in the VTA (bregma: + 3.1 mm; lateral: 0.5 mm; ventral: 4.3 mm) of mice under anaesthesia (Isoflurane 3% induction and 1.5% maintenance) in order to allow local infusion of drugs prior to the EOM experiment. Before each experiment session, a double injection cannulae (4.5 mm length, 1 mm interval) was inserted into the implanted bilateral guide cannulae (length under pedestal 4.0 mm), 0.5 mm beyond the tip of the guide cannula. The injection cannula was connected to a multi-syringe pump (Univentor) that allowed saline or nicotine injection over 1 min (100 ng in 100 nl/injection).

***In vivo* electrophysiology**

Mice were deeply anaesthetized with chloral hydrate (8%), 400 mg/kg I.P., supplemented as required to maintain optimal anesthesia throughout the experiment. The scalp was opened and a hole was drilled in the skull above the location of the VTA. Intravenous administration of drugs was carried out through a catheter into the saphenous vein of the animal. Extracellular recording electrodes were constructed from 1.5 mm O.D. / 1.17 mm I.D. borosilicate glass tubing (Harvard Apparatus) using a vertical electrode puller (Narishige). The tip was broken straight and clean under microscopic control to obtain a diameter of about 1 µm. The electrodes were filled with a 0.5% NaCl solution containing 1.5% of neurobiotin® tracer (VECTOR laboratories) yielding impedances of 6-9 MΩ. Electrical signals were amplified by a high-impedance amplifier (Axon Instruments) and monitored audibly through an audio monitor (A.M. Systems Inc.). The signal was digitized, sampled at 25 kHz, and recorded on a computer using Spike2 software (Cambridge Electronic Design) for later analysis. The electrophysiological activity was sampled in the central region of the VTA (coordinates: between 3.1 to 4 mm posterior to bregma, 0.3 to 0.7 mm lateral to midline, and 4 to 4.8 mm below brain surface). Individual electrode tracks were separated from one another by at least 0.1 mm in the horizontal plane. Spontaneously active DA neurons were identified based on previously established electrophysiological criteria (Grace and Bunney, 1984b; 1984a; Ungless and Grace, 2012).

After recording, nicotine-responsive cells were labelled by electroporation of their membrane. To do so, successive currents squares were applied until the membrane breaks in order to fill their soma with neurobiotin contained into the glass pipet (Pinault 1996). To be able to establish correspondence between neurons responses and their localization in the VTA, we labeled one type of response per mouse: solely activated neurons or solely inhibited neurons, with a limited number of cells per brain (1 to 4 neurons maximum, 2 by hemisphere), always with the same concern of localization of neurons in the VTA.

***Ex vivo* patch-clamp recordings**

For a functional verification of CatCh or Jaws expression, the same virus as described above was injected into 7-9 week-old male DAT^{iCRE} mice. For the characterization of NAc-projecting and Amg-projecting neurons, green retrobead tracers (Lumafluor) were injected into 7-9 weeks old male WT mice. After 4 weeks (for DAT-Cre) or 2 weeks (for WT), mice were deeply anesthetized by an intraperitoneal injection of a mix of ketamine (150 mg/kg Imalgene® 1000, Merial) and xylazine (60 mg/kg, Rompun® 2%, Bayer). Coronal midbrain sections (250 µm) were sliced with a Compresstome (VF-200, Precisionary Instruments) after intracardial perfusion of cold (4°C) sucrose-based artificial cerebrospinal fluid (SB-aCSF) containing (in mM): 125 NaCl, 2.5 KCl, 1.25 NaH_2PO_4, 5.9 $MgCl_2$, 26 $NaHCO_3$, 25 sucrose, 2.5 glucose, 1 kynurenate (pH 7.2, 325 mOsm). After 10 to 60 minutes at 35°C for recovery, slices were transferred into oxygenated aCSF containing (in mM): 125 NaCl, 2.5 KCl, 1.25 NaH_2PO_4, 2 $CaCl_2$, 1 $MgCl_2$, 26 $NaHCO_3$, 15 sucrose, 10 glucose (pH 7.2, 325 mOsm) at room temperature for the rest of the

day, and individually transferred to a recording chamber continuously perfused at 2 mL/minute with oxygenated aCSF. Patch pipettes (4-8 MΩ) were pulled from thin wall borosilicate glass (G150TF-3, Warner Instruments) with a micropipette puller (P-87, Sutter Instruments, Novato, CA) and filled with a potassium gluconate-based intracellular solution containing either (in mM): 116 K-gluconate, 20 HEPES, 0.5 EGTA, 6 KCl, 2 NaCl, 4 ATP, 0.3 GTP, and biocytin 2 mg/mL (pH adjusted to 7.2). Neurons were visualized using an upright microscope coupled with a Dodt contrast lens, and illuminated with a white light source (Scientifica). A 460 nm LED (pE-2, Cooled) was used for visualizing GFP, YFP- or RB positive cells (using a bandpass filter cube, AHF). Whole-cell recordings were performed using a patch-clamp amplifier (Axoclamp 200B, Molecular Devices) connected to a Digidata (1550 LowNoise acquisition system, Molecular Devices). Signals were low-pass filtered (Bessel, 2 kHz) and collected at 10 kHz using the data acquisition software pClamp 10.5 (Molecular Devices). Optical stimulation was applied through the microscope with two LEDs (460 nm and 525 nm, pE-2, CoolLED). To characterize CatCh expression, a 1 s continuous photostimulation was used to evoke currents in voltage-clamp mode (-60 mV), and a 10 Hz - 5 ms/pulse photostimulation was used to drive neuronal firing in current-clamp mode. Regarding Jaws expression, continuous photostimulation (20 sec) was used in current-clamp (-60 mV). To record nicotinic currents from RB+ DA neurons of the VTA, local puffs (500 ms) of nicotine tartrate (100 µM in aCSF) were applied with a glass pipette (2-3 µm diameter) positioned 20 to 30 µm away from the soma and connected to a picospritzer (World Precision Instruments, adjusted to ~2 psi). All electrophysiological recordings were extracted using Clampfit (Molecular Devices) and analyzed with R.

Immunostaining

After euthanasia, brains were rapidly removed and fixed in 4% paraformaldehyde. After a period of at least three days of fixation at 4°C, serial 60-µm sections were cut from the midbrain with a vibratome. Immunostaining experiments were performed as follows: free-floating VTA brain sections were incubated for 1 hour at 4°C in a blocking solution of phosphate-buffered saline (PBS) containing 3% bovine serum albumin (BSA, Sigma; A4503) (vol/vol) and 0.2% Triton X-100 (vol/vol), and then incubated overnight at 4 °C with a mouse anti-tyrosine hydroxylase antibody (anti-TH, Sigma, T1299) and a chicken anti-eYFP antibody (Life technologies Molecular Probes, A-6455), both at 1:500 dilution, in PBS containing 1.5% BSA and 0.2% Triton X-100. The following day, sections were rinsed with PBS, and then incubated for 3 hours at 22-25 °C with Cy3-conjugated anti-mouse and Alexa488-conjugated anti-chicken secondary antibodies (Jackson ImmunoResearch, 715-165-150 and 711-225-152) at 1:500 and 1:1000 dilution in a solution of 1.5% BSA in PBS, respectively. After three rinses in PBS, slices were wet-mounted using Prolong Gold Antifade Reagent (Invitrogen, P36930). Microscopy was carried out with a fluorescent microscope, and images captured using a camera and analyzed with ImageJ.

In the case of electrophysiological recordings, the recorded neurons were identified by immunohisto-fluorescence as described above, with the addition of 1:200 AMCA-conjugated streptavidin (Jackson ImmunoResearch) in the solution. Immunoreactivity for both TH and neurobiotin (NB) allowed us to confirm the neurochemical phenotype of DA neurons in the VTA (TH+ NB+).

In the case of optogenetic experiments on DAT^{iCRE} mice, identification of the transfected neurons by immunohistofluorescence was performed as described above, with the addition of chicken-anti-eYFP primary antibody (1:500, ab13970, Abcam) in the solution. A goat-anti-chicken AlexaFluor 488 (1:500, Life Technologies) was then used as secondary antibody. Immunoreactivity for TH, YFP and

neurobiotin/biocytin allowed us to confirm the neurochemical phenotype of DA neurons in the VTA (TH+ NB+) and the transfection success (YFP+).

Images acquisition

All immunohistochemical slices were imaged by acquisition on a Leica DMR epi-fluorescent microscope, under identical conditions of magnification, illumination and exposure (using photometrics coolsnap camera). Images were captured in gray level using MetaView software (Universal Imaging Corporation, Ropper Scientific, France) and colored post-acquisition on ImageJ software.

Elevated O-maze test

All behavioral tests were conducted during the light period of the animal cycle (between 1:00 and 7:00PM). The raw data for behavioral experiments were acquired as the time spent by animals in the different zones of the environments. The animals were detected in their body center using a 2D USB camera, connected to Anymaze software for acquisition.

The elevated O-maze (EOM) apparatus consists of two open (stressful) and two enclosed (protecting) elevated arms that together form a zero or circle (diameter of 50 cm, height of 58 cm, 10 cm-wide circular platform). Time spent in exploring enclosed versus open arms indicates then the anxiety level of the animal.

The first EOM experiment assess the effect of acute Nic injection (0.5mg/kg) on WT animals. The test lasts 10 minutes. Animals are injected 1-min prior the test and then put in the EOM for 9 min.

For intra-cranial infusion of Nic in the second experiment of EOM, animals received Nic (100ng/infusion) over 1-min prior the test. It lasted for 9 min as described above.

Finally, optogenetic experiments in EOM lasted for 15 minutes, with alternance of 5min-period of stimulation and non-stimulation (OFF-ON-OFF). When nicotine was injected in mice, the EOM test lasted for 9 min with the same protocol as described above.

Online place preference test

The online place preference (OPP) protocols were performed in a Y-maze apparatus (Imetronic, Pessac, France), using only two arms of the Y-maze as two distinct compartments (the third arm was closed by a door and not available to the animal). The chamber in between is an equilateral triangle (side of 11 cm) used as a neutral compartment, where the animal was never photo-stimulated. Each arm of the maze measured 25 cm × 12 cm. The first arm displayed black and white stripes with smooth walls and floor, whereas the other arm displayed uniform-gray rough walls and floor. Choices of the compartment where the animals will be stimulated were counterbalanced across animals in the same test and YFP-control groups.

The OPP test consisted of a 20 minute-session where animals can freely navigate between the compartments but were photo-stimulated only in one of the two compartments.

Implanted bilateral fibers were connected with a bilateral fiber (diameter of 400 µm, NA = 0.39, Thorlabs) attached to a rotor connecting the 470 nm- or 520 nm-LED (Prizmatix) with a fiber of diameter 500 µm and NA = 0.5 (Thorlabs). LED output was controlled using a Master-8 pulse stimulator (A.M.P.I., Jerus) which delivered a discontinuous stimulation of 5-ms light flashes at 10 Hz frequency and 470 nm wavelength (for CatCh experiments), or a continuous stimulation at 520 nm (for Jaws experiments). Naive mice were connected and placed at the center of the neutral compartment before starting the recording.

The time spent in the neutral compartment is not taken into account in the result. The results are presented as preference score which is the difference of time spent between the stimulated compartment over the non stimulated compartment.

Open field paradigm

The Open field (OF) is a square enclosure of 50 cm x 50 cm where animals can move freely. Animal displacements were quantified by comparing the time spent in the center versus the periphery of the square. When nicotine was injected to WT mice in the OF test (IP injection of nicotine tartrate at 0.5 mg/kg, 0.1 mL/10 g, 1 minute prior to the test), animals were placed in the center of the OF for a 9-minute test duration, freely moving inside the enclosure. Regarding the optogenetic experiments conducted in the OF, animals were placed in the maze for 15 minutes, while alternating between OFF, ON and OFF optical stimulations of 5-minute periods.

QUANTIFICATION AND STATISTICAL ANALYSIS

Measurement of neuronal activity

Timestamps of action potentials were extracted in Spike 2 and analyzed using R, a language and environment for statistical computing (Team, 2005, http://www.r-project.org). Spontaneous activity of DA cell firing *in vivo* was analyzed with respect to the average firing frequency (in Hz) and the percentage of spikes-within-burst (%SWB = number of spikes within burst divided by total number of spikes in a given window). Neuronal basal activity was defined on at least three-minute recording.

Classification analysis and machine learning

To determine whether the spontaneous activity of *in vivo*-labeled, VTA DA neurons could predict their nicotine-evoked responses (activation or inhibition), we analyzed 8 variables that characterize the firing patterns: the mean firing frequency, the standard deviation and coefficient of variation of the firing frequency estimated on sliding windows, the percentage of spikes within bursts, the bursting frequency, the mean number of spikes in a burst, the fraction of time spent in bursting activity, and the burst length. Firing frequency and burst activity are quantified as described in the materials and methods section. Principal component analysis (PCA) and hierarchical clustering on principle components (HCPC) were conducted using R package FactoMineR. PCA and clustering distinguished 4 clusters that did not match with the nicotine-evoked responses. We then used the R package RandomForest to test for a prediction of nicotine-evoked responses from spontaneous cell activity. We determined that 5000 was the optimal number of trees in the forest and that 2 was the best number of variables randomly sampled as candidates at each split.

Method for classifying VTA DA neurons subpopulations in response to nicotine

Subpopulations of DA neurons were automatically classified using variation of firing frequency and the following routine: considering the maximal variation from a short baseline (3 minutes before injection), within 3 minutes after injection, neurons displaying an increase in firing frequency were defined as ‘‘activated’’, and neurons displaying a decrease in firing frequency were defined as ‘‘inhibited’’ (up or below zero in the cumulative distribution of responses to nicotine). In $\beta2^{-/-}$ mice, VTA DA neurons did not show a clear change of their firing rate after nicotine injection (i.e., less than 5% of variation from baseline),

and therefore were considered as a unique population to represent the mean response variation in Figure 3B.

Quantification of nicotine responses

Firing frequency was quantified on overlapping 60-second windows shifted by 15 seconds time steps. For each neuron, firing frequency was rescaled as a percentage of its baseline value averaged during 3 minutes before nicotine injection. The responses to nicotine were thus presented as a percentage of variation from baseline (mean ± S.E.M.). The effect of nicotine was assessed by comparison of the maximum of firing frequency variation induced by nicotine and saline injection. For activated (respectively inhibited) neurons, the maximal (respectively minimal) value of the firing frequency was measured within the response period (3 minutes) that followed nicotine or saline injection. The results were presented as mean ± S.E.M. of the difference of maximum variation after nicotine or saline.

Quantification of juxtacellular labeling

A total number of 245 neurons have been recorded and labeled for Figure 1. Those 245 neurons were used in Figure 1B-D. Among them, 101 neurons were shown in Figure 2B and E, containing 49 neurons labeled in NAc-RB injected mice and 52 in Amg-RB injected mice. The locations of the labeled neurons were manually placed on sections of the Paxinos atlas georeferenced in a 2D grid using adobe illustrator rules. The medio-lateral and dorso-ventral coordinates of the location of each neuron were extracted from the grid pattern and the antero-posterior coordinates were estimated from the section of the Paxinos atlas on which the neurons were placed. These three coordinates were used to make density histograms of location for nicotine-activated and nicotine-inhibited DA neurons or NAc-projecting and Amg-projecting DA neurons.

Statistics: Figure by Figure

All statistical analyses were done using the R software with home-made routines. Results are plotted as a mean ± S.E.M. The total number (n) of observations in each group and the statistics used are indicated in the figures directly or in the figure legends. Classically comparisons between means were performed using parametric tests as Student's t-test, or two-way ANOVA for comparing two groups when parameters followed a normal distribution (Shapiro-Wilk normality test $p > 0.05$), or Wilcoxon non-parametric test as when the distribution was skewed. Bonferroni *post hoc* analysis was applied, when necessary, to compare means. $P > 0.05$ was considered not to be statistically significant. Statistical significance was set at $p < 0.05$ (*), $p < 0.01$ (**), or $p < 0.001$ (***).

Figure 1: Kolmogorov-Smirnov test was used to compare the responses of VTA DA neurons to saline or nicotine injection. Wilcoxon tests were used to demonstrate a significant increase or decrease of firing frequency induced by nicotine injection compared to saline injection (B). Wilcoxon test was used to compared coordinates of nicotine-inhibited and nicotine-activated recorded neurons (C).

Figure 3: For behavior (A-C), over time effect of nicotine or saline injection (IP and IC) on the time spent by the mice in the open arms of the EOM was first tested with one-way repeated measures ANOVA for each group of mice (shown in Figure S3.1B-D-G). Two-way repeated measures ANOVA (time/treatment or time/genotype) were used to compare the difference between the groups. In case of significant interaction effect between factors, Wilcoxon or Student's t-test with Bonferroni corrections were used for

intra- and inter-group *post hoc* analysis (as indicated in the figure). For electrophysiology (B), Kolmogorov-Smirnov test was used to compare responses to nicotine of DA neurons in $\beta2^{-/-}$ mice and $\beta2^{-/-}$Vec mice. Wilcoxon tests with Bonferroni corrections are used to demonstrate a significant increase or decrease of firing frequency induced by IV nicotine injection in β2Vec mice compared to saline and nicotine injections in $\beta2^{-/-}$ mice.

Figure 4: For EOM experiments (A-C), effect of light was first tested with one-way repeated measures ANOVA for each group of mice (shown in Figure S4.3A-B-C). Two-way repeated measures ANOVA (epoch/opsin) were used to compare the difference between the groups. In case of significant interaction effect between factors, Wilcoxon or Student's t-test with Bonferroni corrections were used for intra- and inter-group *post hoc* analysis (as indicated in the figure). For EOM experiment under nicotine (D), over time effect of nicotine injection on the time spent by the mice in the open arms of the O-maze was first tested with one-way repeated measures ANOVA for each group. Two-way repeated measures ANOVA (epoch/opsin) were used to compare the difference between the groups. In case of significant interaction effect between factor, Wilcoxon or Student's t-test with Bonferroni corrections were used for intra- and inter- group *post hoc* analysis (as indicated in the figure). For OPP experiments (E), preference score between group were compared with Student's t-test.

Figure S2.1: See section "Classification analysis and machine learning".

Figure S2.1: Two-way repeated measures ANOVA (current, phenotype) was used to compare neuronal excitability (Fig. S2.1D). Wilcoxon test was used to compared coordinates of nicotine-inhibited and nicotine-activated recorded neurons (Fig. S2.1F).

Figure S2.2: Wilcoxon test was used to compare nicotine-evoked currents (Fig. S2.2F).

Figure S3: Two-way repeated measures ANOVA (time, treatment) was used to compare the distance traveled by mice in the OF after nicotine or saline injection (Fig. S3A). One-way repeated measures ANOVA were used to test the overtime effect of saline or nicotine intraperitoneal injection, or intracranial infusion, or the time spent by mice in the open arms of the EOM (Fig. S3B, D, G). Two-way repeated measures ANOVA (time, genotype) was used to compare the time spent in the open arms of the EOM after nicotine injection between groups (Fig. S3F). In case of a significant interaction effect between factors, Wilcoxon or Student's t-test with Bonferroni corrections were used for intra- and inter-group *post hoc* analysis.

Figure S4.3: For anxiety measurements, one-way repeated measures ANOVA were used to test the light effect on the time spent in the open arms of the EOM (Fig. 4.3A-C). For locomotor activity, two-way repeated measures ANOVA (epoch, opsin) were used to compare the difference of light effect on the distance traveled by the mice between the groups (Fig. 4.3D-F). In case of a significant interaction effect between factors, Wilcoxon or Student's t-test with Bonferroni corrections were used for intra- and inter-group *post hoc* analysis (as indicated in the figure).

Figure S4.4: EOM experiments (C-F) and locomotor activity (C-F) were analyzed as previously described for Fig.S4.3.

References

Aurnhammer, C., Haase, M., Muether, N., Hausl, M., Rauschhuber, C., Huber, I., Nitschko, H., Busch, U., Sing, A., Ehrhardt, A., et al. (2012). Universal real-time PCR for the detection and quantification of adeno-associated virus serotype 2-derived inverted terminal repeat sequences. Hum Gene Ther Methods *23*, 18–28.

Balerio, G.N., Aso, E., and Maldonado, R. (2006). Role of the cannabinoid system in the effects induced by nicotine on anxiety-like behaviour in mice. Psychopharmacology *184*, 504–513.

Beier, K.T., Gao, X.J., Xie, S., DeLoach, K.E., Malenka, R.C., and Luo, L. (2019). Topological Organization of Ventral Tegmental Area Connectivity Revealed by Viral-Genetic Dissection of Input-Output Relations. CellReports *26*, 159–167.e6.

Beier, K.T., Steinberg, E.E., DeLoach, K.E., Xie, S., Miyamichi, K., Schwarz, L., Gao, X.J., Kremer, E.J., Malenka, R.C., and Luo, L. (2015). Circuit Architecture of VTA Dopamine Neurons Revealed by Systematic Input-Output Mapping. Cell *162*, 622–634.

Brischoux, F., Chakraborty, S., Brierley, D.I., and Ungless, M.A. (2009). Phasic excitation of dopamine neurons in ventral VTA by noxious stimuli. Proc Natl Acad Sci USA *106*, 4894–4899.

Changeux, J.-P., Bertrand, D., Corringer, P.J., Dehaene, S., Edelstein, S., Léna, C., Le Novère, N., Marubio, L., Picciotto, M., and Zoli, M. (1998). Brain nicotinic receptors: structure and regulation, role in learning and reinforcement. Brain Res Brain Res Rev *26*, 198–216.

Changeux, J.-P. (2010). Nicotine addiction and nicotinic receptors: lessons from genetically modified mice. Nat Rev Neurosci *11*, 389–401.

Choi, V.W., Asokan, A., Haberman, R.A., and Samulski, R.J. (2007). Production of recombinant adeno-associated viral vectors. Curr Protoc Hum Genet *Chapter 12*, Unit12.9–12.9.21.

Chuong, A.S., Miri, M.L., Busskamp, V., Matthews, G.A.C., Acker, L.C., Sørensen, A.T., Young, A., Klapoetke, N.C., Henninger, M.A., Kodandaramaiah, S.B., et al. (2014). Noninvasive optical inhibition with a red-shifted microbial rhodopsin. (Nature Publishing Group).

de Jong, J.W., Afjei, S.A., Pollak Dorocic, I., Peck, J.R., Liu, C., Kim, C.K., Tian, L., Deisseroth, K., and Lammel, S. (2019). A Neural Circuit Mechanism for Encoding Aversive Stimuli in the Mesolimbic Dopamine System. Neuron *101*, 133–151.e137.

Di Chiara, G., and Imperato, A. (1988). Drugs abused by humans preferentially increase synaptic dopamine concentrations in the mesolimbic system of freely moving rats. Proc Natl Acad Sci USA *85*, 5274–5278.

Doyon, W.M., Dong, Y., Ostroumov, A., Thomas, A.M., Zhang, T.A., and Dani, J.A. (2013). Nicotine Decreases Ethanol-Induced Dopamine Signaling and Increases Self-Administrationvia Stress Hormones. Neuron 1–11.

Durand-de Cuttoli, R., Mondoloni, S., Marti, F., Lemoine, D., Nguyen, C., Naudé, J., d'Izarny-Gargas, T., Pons, S., Maskos, U., Trauner, D., et al. (2018). Manipulating midbrain dopamine neurons and reward-related behaviors with light-controllable nicotinic acetylcholine receptors. eLife *7*, 15991.

888 Eddine, R., Valverde, S., Tolu, S., Dautan, D., Hay, A., Morel, C., Cui, Y., Lambolez, B., Venance, L.,
889 Marti, F., et al. (2015). A concurrent excitation and inhibition of dopaminergic subpopulations in
890 response to nicotine. Sci. Rep. *5*, 8184.

891 Ford, C.P., Mark, G.P., and Williams, J.T. (2006). Properties and opioid inhibition of mesolimbic
892 dopamine neurons vary according to target location. Journal of Neuroscience *26*, 2788–2797.

893 Fowler, C.D., Lu, Q., Johnson, P.M., Marks, M.J., and Kenny, P.J. (2011). Habenular α5 nicotinic
894 receptor subunit signalling controls nicotine intake. Nature *471*, 597–601.

895 Frahm, S., Ślimak, M.A., Ferrarese, L., Santos-Torres, J., Antolin-Fontes, B., Auer, S., Filkin, S., Pons,
896 S., Fontaine, J.-F., Tsetlin, V., et al. (2011). Aversion to Nicotine Is Regulated by the Balanced Activity
897 of β4 and α5 Nicotinic Receptor Subunits in the Medial Habenula. Neuron *70*, 522–535.

898 Grace, A.A., and Bunney, B.S. (1984a). The control of firing pattern in nigral dopamine neurons: burst
899 firing. J Neurosci *4*, 2877–2890.

900 Grace, A.A., and Bunney, B.S. (1984b). The control of firing pattern in nigral dopamine neurons: single
901 spike firing. J Neurosci *4*, 2866–2876.

902 Grenhoff, J., Aston-Jones, G., and Svensson, T.H. (1986). Nicotinic effects on the firing pattern of
903 midbrain dopamine neurons. Acta Physiol. Scand. *128*, 351–358.

904 Grieder, T.E., George, O., and Tan, H. (2012). Phasic D1 and tonic D2 dopamine receptor signaling
905 double dissociate the motivational effects of acute nicotine and chronic nicotine withdrawal.

906 Grieder, T.E., Besson, M., Maal-Bared, G., Pons, S., Maskos, U., and van der Kooy, D. (2019). β2*
907 nAChRs on VTA dopamine and GABA neurons separately mediate nicotine aversion and reward. Proc
908 Natl Acad Sci USA *116*, 25968–25973.

909 Grieder, T.E., Sellings, L.H., Vargas-Perez, H., Ting-A-Kee, R., Siu, E.C., Tyndale, R.F., and van der
910 Kooy, D. (2010). Dopaminergic signaling mediates the motivational response underlying the opponent
911 process to chronic but not acute nicotine. Neuropsychopharmacology *35*, 943–954.

912 Khabou, H., Garita-Hernandez, M., Chaffiol, A., Reichman, S., Jaillard, C., Brazhnikova, E., Bertin, S.,
913 Forster, V., Desrosiers, M., Winckler, C., et al. (2018). Noninvasive gene delivery to foveal cones for
914 vision restoration. JCI Insight *3*.

915 Kleinlogel, S., Feldbauer, K., Dempski, R.E., Fotis, H., Wood, P.G., Bamann, C., and Bamberg, E.
916 (2011). Ultra light-sensitive and fast neuronal activation with the Ca^{2}+-permeable channelrhodopsin
917 CatCh. Nature Neuroscience *14*, 513–518.

918 Klink, R., de Kerchove d'Exaerde, A., Zoli, M., and Changeux, J.P. (2001). Molecular and physiological
919 diversity of nicotinic acetylcholine receptors in the midbrain dopaminergic nuclei. J Neurosci *21*, 1452–
920 1463.

921 Kutlu, M.G., and Gould, T.J. (2015). Nicotine Modulation of Fear Memories and Anxiety: Implications for
922 Learning and Anxiety Disorders. Biochem Pharmacol 1–58.

923 Lammel, S., Hetzel, A., Häckel, O., Jones, I., Liss, B., and Roeper, J. (2008). Unique properties of
924 mesoprefrontal neurons within a dual mesocorticolimbic dopamine system. Neuron *57*, 760–773.

Lammel, S., Lim, B.K., Ran, C., Huang, K.W., Betley, M.J., Tye, K.M., Deisseroth, K., and Malenka, R.C. (2012). Input-specific control of reward and aversion in the ventral tegmental area. Nature *491*, 212–217.

Luscher, C. (2016). The Emergence of a Circuit Model for Addiction. Annu Rev Neurosci *39*, annurev–neuro–070815–013920.

Mameli-Engvall, M., Evrard, A., Pons, S., Maskos, U., Svensson, T.H., Changeux, J.-P., and Faure, P. (2006). Hierarchical control of dopamine neuron-firing patterns by nicotinic receptors. Neuron *50*, 911–921.

Mansvelder, H.D., and McGehee, D.S. (2000). Long-term potentiation of excitatory inputs to brain reward areas by nicotine. Neuron *27*, 349–357.

Margolis, E.B., Hjelmstad, G.O., Fujita, W., and Fields, H.L. (2014). Direct bidirectional μ-opioid control of midbrain dopamine neurons. Journal of Neuroscience *34*, 14707–14716.

Margolis, E.B., Mitchell, J.M., Ishikawa, J., Hjelmstad, G.O., and Fields, H.L. (2008). Midbrain dopamine neurons: projection target determines action potential duration and dopamine D(2) receptor inhibition. Journal of Neuroscience *28*, 8908–8913.

Maskos, U., Molles, B.E., Pons, S., Besson, M., Guiard, B.P., Guilloux, J.-P., Evrard, A., Cazala, P., Cormier, A., Mameli-Engvall, M., et al. (2005). Nicotine reinforcement and cognition restored by targeted expression of nicotinic receptors. Nature *436*, 103–107.

Mejias-Aponte, C.A., Ye, C., Bonci, A., Kiyatkin, E.A., and Morales, M. (2015). A Subpopulation of Neurochemically-Identified Ventral Tegmental Area Dopamine Neurons Is Excited by Intravenous Cocaine. J Neurosci *35*, 1965–1978.

Mineur, Y.S., Fote, G.M., Blakeman, S., Cahuzac, E.L.M., Newbold, S.A., and Picciotto, M.R. (2016). Multiple Nicotinic Acetylcholine Receptor Subtypes in the Mouse Amygdala Regulate Affective Behaviors and Response to Social Stress. Neuropsychopharmacology *41*, 1579–1587.

Molas, S., DeGroot, S.R., Zhao-Shea, R., and Tapper, A.R. (2017). Anxiety and Nicotine Dependence: Emerging Role of the Habenulo-Interpeduncular Axis. Trends Pharmacol Sci *38*, 169–180.

Morales, M., and Margolis, E.B. (2017). Ventral tegmental area: cellular heterogeneity, connectivity and behaviour. Nat Rev Neurosci *18*, 73–85.

Morel, C., Fattore, L., Pons, S., Hay, Y.A., Marti, F., Lambolez, B., De Biasi, M., Lathrop, M., Fratta, W., Maskos, U., et al. (2014). Nicotine consumption is regulated by a human polymorphism in dopamine neurons. Mol Psychiatry *19*, 930–936.

Morel, C., Fernandez, S.P., Pantouli, F., Meye, F.J., Marti, F., Tolu, S., Parnaudeau, S., Marie, H., Tronche, F., Maskos, U., et al. (2017). Nicotinic receptors mediate stress-nicotine detrimental interplay via dopamine cells' activity. Mol Psychiatry *23*, 1597–1605.

Pascoli, V., Terrier, J., Hiver, A., and Lüscher, C. (2015). Sufficiency of Mesolimbic Dopamine Neuron Stimulation for the Progression to Addiction. Neuron *88*, 1054–1066.

Paxinos, G., and Franklin, K.B.J. (2004). The Mouse Brain in Stereotaxic Coordinates (Gulf Professional Publishing).

963 Picciotto, M.R., Zoli, M., Rimondini, R., Léna, C., Marubio, L.M., Pich, E.M., Fuxe, K., and Changeux,
964 J.P. (1998). Acetylcholine receptors containing the beta2 subunit are involved in the reinforcing
965 properties of nicotine. Nature *391*, 173–177.

966 Picciotto, M.R., and Mineur, Y.S. (2013). Molecules and circuits involved in nicotine addiction: The many
967 faces of smoking. Neuropharmacology.

968 Pinault, D. (1996). A novel single-cell staining procedure performed in vivo under electrophysiological
969 control: morpho-functional features of juxtacellularly labeled thalamic cells and other central neurons
970 with biocytin or Neurobiotin. J. Neurosci. Methods *65*, 113–136.

971 Poulin, J.-F., Caronia, G., Hofer, C., Cui, Q., Helm, B., Ramakrishnan, C., Chan, C.S., Dombeck, D.A.,
972 Deisseroth, K., and Awatramani, R. (2018). Mapping projections of molecularly defined dopamine
973 neuron subtypes using intersectional genetic approaches. Nature Neuroscience *21*, 1–17.

974 Schultz, W. (2007). Multiple dopamine functions at different time courses. Annu Rev Neurosci *30*, 259–
975 288.

976 Su, M., Li, L., Wang, J., Sun, H., Zhang, L., Zhao, C., Xie, Y., Gamper, N., Du, X., and Zhang, H.
977 (2019). Kv7.4 Channel Contribute to Projection-Specific Auto-Inhibition of Dopamine Neurons in the
978 Ventral Tegmental Area. Front Cell Neurosci *13*, 557.

979 Tolu, S., Eddine, R., Marti, F., David, V., Graupner, M., Pons, S., Baudonnat, M., Husson, M., Besson,
980 M., Reperant, C., et al. (2013). Co-activation of VTA DA and GABA neurons mediates nicotine
981 reinforcement. Mol Psychiatry *18*, 382–393.

982 Turiault, M., Parnaudeau, S., Milet, A., Parlato, R., Rouzeau, J.-D., Lazar, M., and Tronche, F. (2007).
983 Analysis of dopamine transporter gene expression pattern -- generation of DAT-iCre transgenic mice.
984 Febs J. *274*, 3568–3577.

985 Ungless, M.A., and Grace, A.A. (2012). Are you or aren't you? Challenges associated with
986 physiologically identifying dopamine neurons. Tins *35*, 422–430.

987 Watabe-Uchida, M., Zhu, L., Ogawa, S.K., Vamanrao, A., and Uchida, N. (2012). Whole-Brain Mapping
988 of Direct Inputs to Midbrain Dopamine Neurons. Neuron *74*, 858–873.

989 Wolfman, S.L., Gill, D.F., Bogdanic, F., Long, K., Al-Hasani, R., McCall, J.G., Bruchas, M.R., and
990 McGehee, D.S. (2018). Nicotine aversion is mediated by GABAergic interpeduncular nucleus inputs to
991 laterodorsal tegmentum. Nature Communications *9*, 2710.

992 Zhao-Shea, R., Liu, L., Pang, X., Gardner, P.D., and Tapper, A.R. (2013). Activation of GABAergic
993 neurons in the interpeduncular nucleus triggers physical nicotine withdrawal symptoms. Curr Biol *23*,
994 2327–2335.

995 Zhao-Shea, R., Liu, L., Soll, L.G., Improgo, M.R., Meyers, E.E., McIntosh, J.M., Grady, S.R., Marks,
996 M.J., Gardner, P.D., and Tapper, A.R. (2011). Nicotine-mediated activation of dopaminergic neurons in
997 distinct regions of the ventral tegmental area. Neuropsychopharmacology *36*, 1021–1032.

998 Zhuang, X., Masson, J., Gingrich, J.A., Rayport, S., and Hen, R. (2005). Targeted gene expression in
999 dopamine and serotonin neurons of the mouse brain. J. Neurosci. Methods *143*, 27–32.